Viral Evasion of Cellular Stress responses

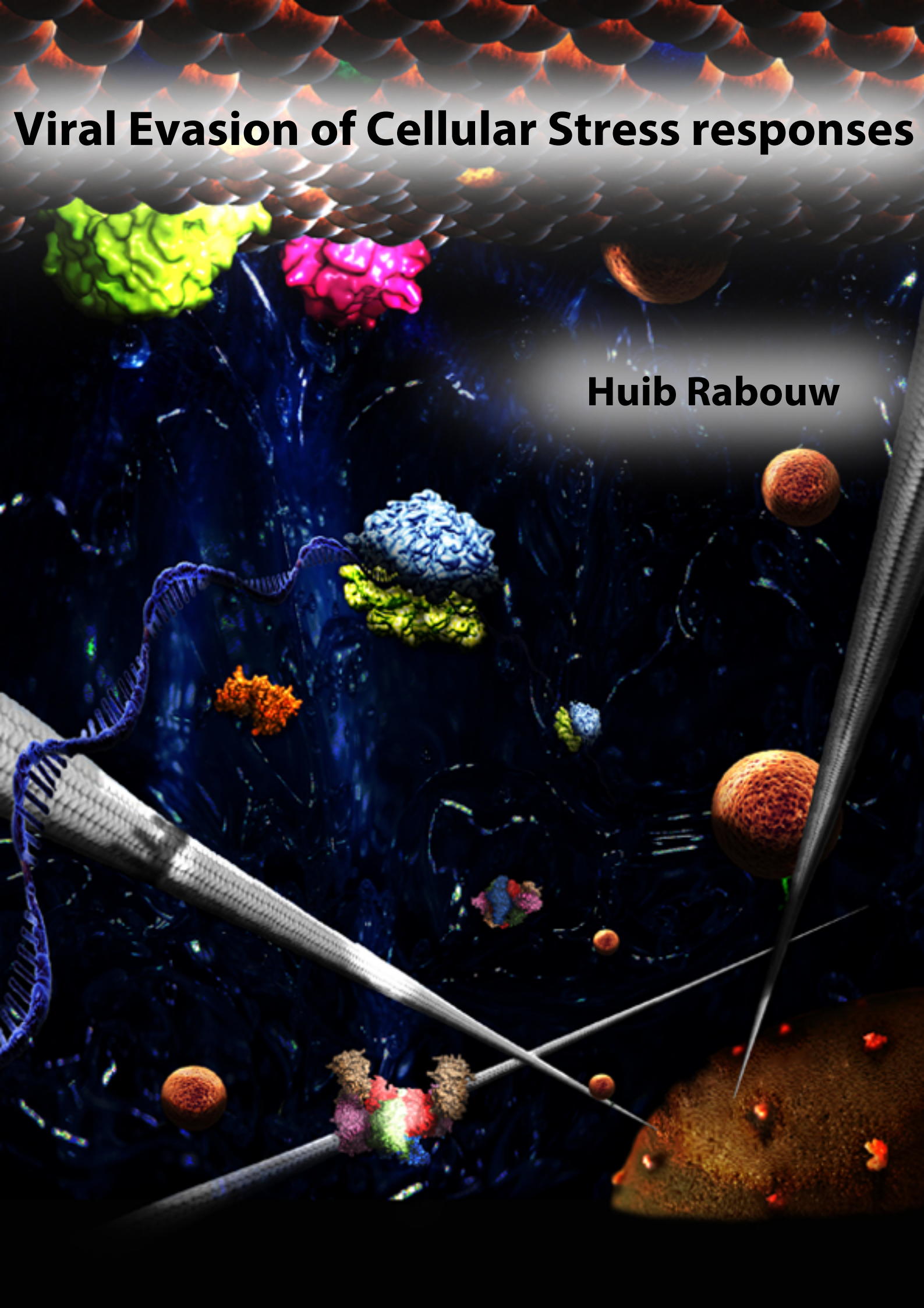

Huib Rabouw

Viral evasion of cellular stress responses

Huibert Hendrik Rabouw

Colofon

ISBN: 978-94-6375-758-4

Cover illustration: Huib Rabouw

Thesis lay-out: Huib Rabouw

Thesis Printing: Ridderprint - www.ridderprint.nl

Viral evasion of cellular stress responses

Het voorkomen van cellulaire stress reacties door virussen

(met een samenvatting in het Nederlands)

Proefschrift

ter verkrijging van de graad van doctor aan de
Universiteit Utrecht op gezag van de
rector magnificus, prof.dr. H.R.B.M. Kummeling,
ingevolge het besluit van het college voor promoties
in het openbaar te verdedigen op

dinsdag 4 februari 2020 des middags te 12.45 uur

door

Huibert Hendrik Rabouw

geboren op 14 mei 1990
te Gouda

Promotor:

Prof. dr. F.J.M. Van Kuppeveld

Copromotoren:

Dr. R.J. De Groot

Dr. M.A. Langereis

Table of Contents

Chapter 1

General Introduction

General introduction

Viruses are obligatory intracellular pathogens that depend on the host cell to produce new viral particles. For this, viruses redirect the cellular infrastructure and metabolism towards producing viral proteins and genetic material. To prevent viruses from spreading, every host cell is equipped with sensor mechanisms that detect, and respond to, virus infections. The best known antiviral response is the type I IFN pathway, which induces an antiviral state in the infected cell, as well as in neighboring uninfected cells. This thesis focusses on another antiviral pathway, the integrated stress response (ISR), which temporarily shuts down translation and thereby blocks the production of new viral proteins. Evolutionary pressure caused most viruses to develop mechanisms to circumvent ISR signaling. We set out to identify viral ISR antagonists and elucidate their mode of action. This way, we aim to acquire more knowledge about the interplay between viruses and cellular antiviral responses. The identification of viral proteins involved in evading antiviral responses may ultimately facilitate the development of attenuated recombinant viruses which could function as vaccine strains. Furthermore, we hope to gain additional insights into how translation is regulated by the ISR, as well as by what mechanisms the activity of the ISR may be modulated.

Translation is one of the most essential processes in life, as it generates the proteins that are key to virtually all biological activity. Translation encompasses an initiation step; the assembly of RNA and protein components required for translation, an elongation step; the formation of a polypeptide chain that will become a mature protein, and a termination step; the stop of translation when the protein is finished, and the disassembly of the translation complex. Translation initiation begins with the formation of ternary complexes (TCs), which consist of translation initiation factor 2 (eIF2) bound to a GTP molecule and an initiator tRNA (Met-tRNAi). The TC, together with translation initiation factors 1, 1A, 3, and 5, binds the 40S small ribosomal subunit to form the 43S pre-initiation complex. Meanwhile, translation initiation factors 4A, 4E, and 4G (together referred to as eIF4F) assemble at the cap structure of messenger RNA (mRNA) molecules. The 43S pre-initiation complex binds to eIF4F, and subsequently starts scanning along the mRNA for ATG start codons. Once a start codon is recognized by base-pairing with the UAC-anticodon within Met-tRNAi, the eIF2-bound GTP molecule is hydrolyzed to GDP, which lowers eIF2's affinity for Met-tRNAi by ~100 fold. This is the trigger for the release of eIF2•GDP and other translation initiation factors from the 40S ribosome. In the absence of translation initiation factors, the 60S large ribosomal subunit may bind to form the 80S ribosome, after which translation elongation commences. Translation elongation is a continuous repetition of three steps: (i) binding of the correct tRNA in the aminoacyl (A) site within the ribosome, (ii) transfer of the peptide chain from the previous tRNA onto the aminoacyl-tRNA in the A site, and (iii) repositioning of the tRNA

from the A site to the P site. The previous tRNA will simultaneously be transferred to the exit (E) site and leave the ribosome. Once an in-frame stop codon in the mRNA is recognized by the eukaryotic release factor eRF1, the peptide chain is released from the tRNA and the protein is finished.

Translation initiation is tightly regulated by several different pathways, such as the integrated stress response (ISR). The ISR comprises a complex network of sensor, mediator, and effector proteins, that together detect and respond to cellular stress. In mammalian cells, four different sensor proteins can be activated by a plethora of different stressors, via mechanisms that are often incompletely understood. Upon detection of their respective stressor, the ISR sensor proteins phosphorylate a conserved residue, S51, in the alpha subunit of translation initiation factor 2 (eIF2α). Phosphorylated eIF2 (p-eIF2) binds and sequesters the eIF2-specific guanidine exchange factor (GEF) eIF2B, thereby interfering with GDP/GTP exchange on native eIF2. As this is a crucial step in the recycling of eIF2•GDP into a TC, p-eIF2 effectively represses translation. Counterintuitively, under conditions of stress, a selection of mRNAs is more efficiently translated. The ensuing ISR-induced proteins have functions that help cells deal with stress situations, which will be addressed in more detail later in this introduction. Collectively, ISR-mediated inhibition of general translation conserves energy, and together with the enhanced synthesis of a subset of stress-related proteins, it alters the cells proteome to optimize the chances to restore cellular homeostasis.

ISR sensor proteins

Mammalian cells have four different ISR sensor proteins, Protein Kinase R (PKR), PKR-like ER-resident kinase (PERK), Heme Responsive Inhibitor (HRI), and General Control Non-derepressible 2 (GCN2) (Fig 1). These proteins differ in their activation domain, and thus in the types of stressors they respond to. Upon detection of their respective stressors, they activate by homodimerization and autophosphorylation, and subsequently phosphorylate eIF2 via a largely conserved eIF2α kinase domain. PKR activity is negatively affected by inhibitory sequences in its N-terminal domain, which encompasses two double-stranded RNA binding domains (dsRBDs) (1). Cytoplasmic dsRNAs, which are a danger signal that can indicate for example mitochondrial leakage or viral infections (2), bind these dsRBDs and lift the inhibitory effect, thus activating PKR. For efficient dimerization and subsequent activation, both dsRBDs of two separate PKR molecules interact with the same dsRNA (3). Consequently, PKR is inhibited by excessive amounts of dsRNA which cause separate PKR molecules to interact with different dsRNAs(4). Besides its ability to respond to dsRNA, PKR can also be activated independently of dsRNA, via interaction with PACT. An interaction of PKR with PACT, like an interaction

with dsRNA, causes structural rearrangements within PKR that prevent the NTD from interfering with the kinase function. PKR interaction with PACT depends on a double phosphorylation of PACT(5), which occurs under several types of stress conditions, via unknown mechanisms (6, 7). PERK is a transmembrane protein that has its activation domain in the ER lumen and its kinase domain in the cytoplasm. PERK is kept inactive through an interaction with the ER-resident chaperone BiP (8). When unfolded proteins accumulate in the ER, and BiP dissociates from PERK to assist in the correct folding of these proteins, PERK is activated, and phosphorylates eIF2α molecules. PERK is part of the so-called unfolded protein response (UPR) together with two other ER transmembrane proteins, IRE1 and ATF6, whose functions are aimed at restoring the folding capacity in the ER (9). GCN2 is activated upon detection of uncharged tRNAs (10), which may accumulate for example due to nutrient deprivation. By temporarily inhibiting translation through eIF2 phosphorylation, GCN2 mediates the conservation of energy when energy is scarce. GCN2 is also activated in response to several different other stressors, such as UV irradiation, H_2O_2 treatment, and even some viral RNA species (reviewed in (11)). It is entirely unclear how most of these triggers would cause uncharged tRNAs to accumulate, which suggests that GCN2 has multiple -thus far unexplained- mechanisms of activation. HRI (Heme-Regulated Inhibitor) was originally described as an inhibitor of translation in reticulocytes under conditions of low iron or heme (12). Its eIF2α kinase function is inhibited by heme binding, and consequently, HRI is activated when heme dissociates upon depletion. Additionally, HRI may be activated in response to several other stressors such as toxic heavy metal ions and heat shock (13, 14).

I SR mediator proteins

eIF2 is a heterotrimeric complex that binds GTP and a Met-tRNAi to form the Ternary Complex (TC). The TC and several other translation initiation factors bind the 40S ribosomal subunit to form the 43S pre-initiation complex, which subsequently associates to the eIF4F complex at the cap structure of mRNAs. After scanning and ATG start codon recognition, the eIF2-bound GTP is hydrolyzed to GDP and eIF2 is released from the ribosome, after which translation elongation commences. eIF2•GDP has low affinity for Met-tRNAi, so GDP/GTP exchange by the eIF2-specific guanine exchange factor (GEF) eIF2B is required for the recycling of eIF2 into new TCs to facilitate ongoing translation (15). In times of stress, when p-eIF2 accumulates due to activation of the eIF2 kinases, p-eIF2 interacts with eIF2B in a stable and unproductive manner, and thereby acts as an inhibitor of eIF2B function (16). Since eIF2B is present in low amounts within the cell, limited quantities of p-eIF2α can effectively deplete the cell's pool of active eIF2B (17). The intracellular concentrations of eIF2, p-eIF2, and eIF2B, and their affinities for one another together determine the rates of eIF2B-mediated TC formation (reviewed in (18)). The

direct consequence of ISR activity is a reduction in TC concentrations. The number of TCs remaining determines which mRNAs are being translated and how efficiently, and thereby also governs the overall effect of the ISR on cellular metabolism and survival. A schematic overview of the ISR with its sensors and mediators, as well as a brief summary of the ISR's effects, is given in Figure 2.

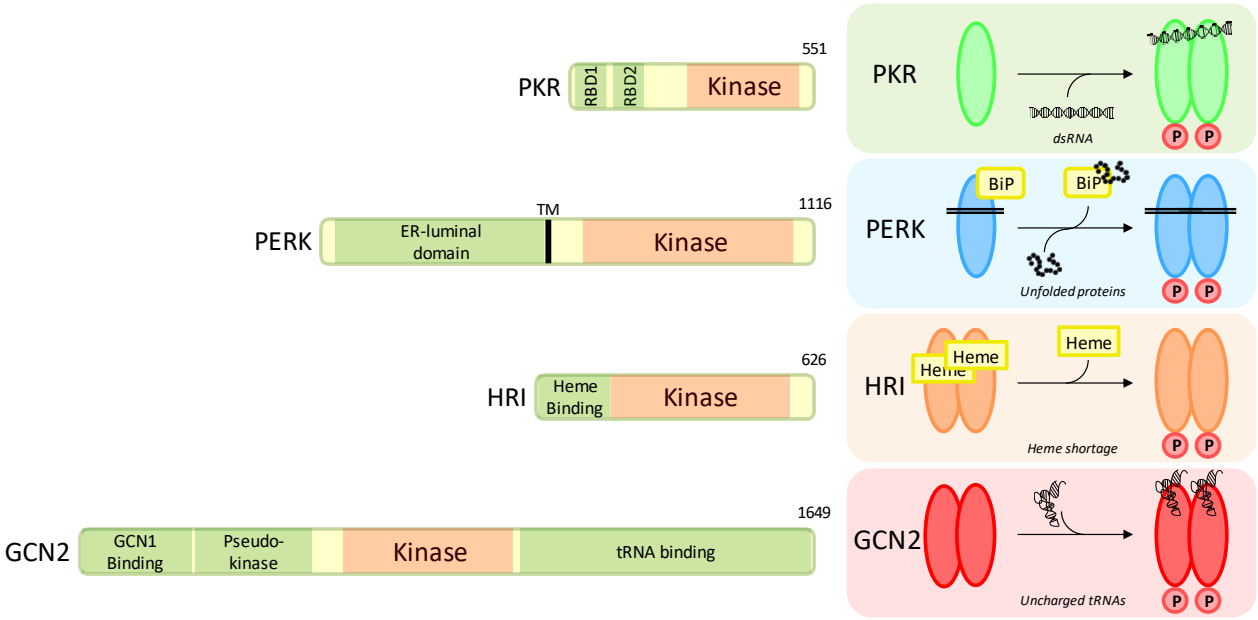

Figure 1. The four ISR-sensor proteins. *(left panel) Indicated in orange is the conserved eIF2α kinase-domain. Regions that are essential for activation are shown in green. (right panel) For each of the four ISR sensors, a schematic representation is given of the most well-studied mode of activation. Note that this is not a complete overview, since most ISR-sensor proteins may be activated via multiple routes.*

ISR effector proteins

ISR effector proteins are proteins whose synthesis escapes ISR-mediated repression, and that are instead upregulated in response to reduced TC availability. ATF4 is by far the most studied example of such protein, and is the key effector of the ISR (19). *ATF4* mRNA contains two ORFs, uORF1 and uORF2, upstream of the ATF4 ORF. ISR-mediated upregulation of ATF4 expression is based on continued scanning by the small ribosomal subunit after translation of the short uORF1, and subsequent re-initiation at a downstream ATG. However, translation initiation at uORF1 dissociates the TC, and start codons will go unrecognized until a new TC binds. Therefore, re-initiation is directly dependent on the timely recruitment of a new TC to the ribosome. Under resting conditions, when TC concentrations are high, a new TC will be bound rapidly and uORF2 will be translated, which overlaps with the ATF4 ORF and thus prevents ATF4 expression. In contrast, when TC concentrations become limiting, the scanning

ribosome may pass the uORF2 start codon before a new TC is recruited, in which case the ATG of the ATF4 ORF is used and ATF4 is expressed. Via this mechanism ATF4 is induced as TC concentrations drop, but ATF4 expression is repressed again at very low TC concentrations, since i) the total number of scanning ribosomes decreases with lower TC concentrations, and ii) scanning ribosomes might also skip the ATF4 start codon if TC reassociation takes too much time. A schematic overview of the regulation of *ATF4* mRNA translation under conditions of stress is given in figure 3. The lengths of the uORFs and the spacers in between determine the expression levels of ISR-upregulated proteins under conditions of limited TC availability (20). Since mRNAs encoding other ISR-effector proteins have different compositions in their regulatory element, each ISR-effector is likely affected differently by

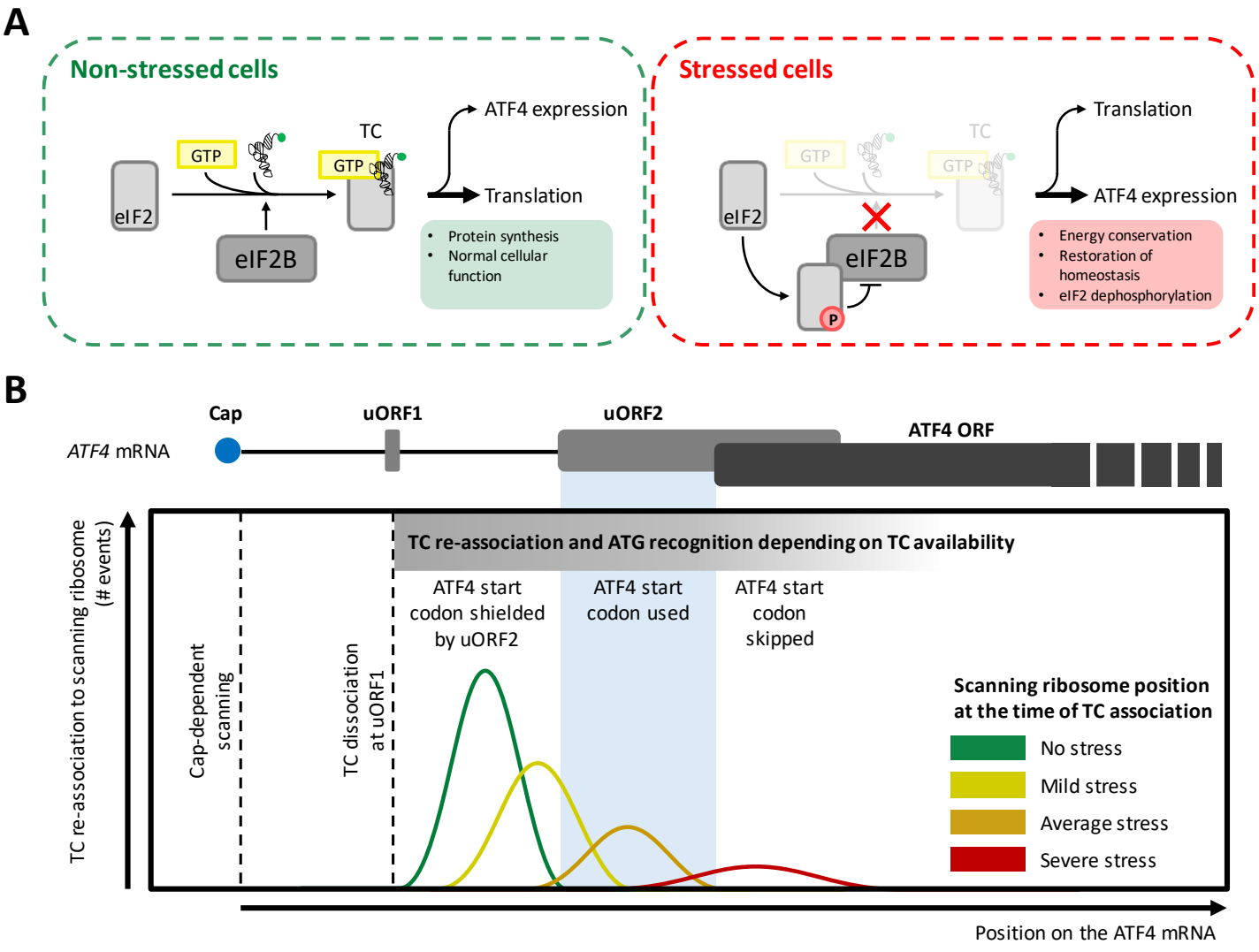

Figure 2. Schematic overview of the ISR and its regulation of ATF4 expression. *(A) In the absence of stress stimuli, native eIF2 is being recycled into eIF2•GTP•tRNAi ternary complexes (TCs) by the guanidine nucleotide exchange factor (GEF) eIF2B. Under stress conditions, when eIF2 is being phosphorylated, p-eIF2 stably interacts with eIF2B and prevents its GDP/GTP exchange activity on eIF2. The resulting reduced TC availability prevents global translation initiation, while inducing the expression of a set of ISR-effector proteins such as ATF4. (B) A representation of the ATF4 mRNA lay-out is shown in the top panel. This mRNA includes a small uORF1, and an uORF2 that overlaps with the ATF4 ORF. Translation of uORF1 displaces the TC from the scanning ribosome, which may subsequently re-initiate at a downstream start codon upon re-association of a new TC. The bottom panel shows a schematic overview of the TC re-association events in the absence of stress when TC concentrations are high, or under stress conditions with limited TC availability. At high TC levels, TC re-association to the scanning ribosome (shown on the y-axis) is rapid, and occurs primarily before the ribosome reaches the uORF2 start codon. As a consequence, uORF2 will be translated and ATF4 expression is blocked. Under conditions of stress, when TC concentrations become limiting, TC-reassociation will be slower and may occur at a time when the ribosome has already passed the uORF2 start codon. In this case, the ATF4 ORF start codon will be used and ATF4 is expressed. At very low TC concentrations however, the ribosome may skip both the uORF2 and ATF4 start codons and ATF4 expression is repressed. Thus, only TC-reassociation to scanning ribosomes located between the uORF2 and ATF4 start codons (indicated by the blue area) will trigger expression of ATF4. The total area under the curve within the blue shaded region represents the ATF4 expression level for each of the indicated stress conditions (green, no stress; yellow, mild stress; orange, average stress; red, severe stress).*

ISR activity. Consequently, the ISR-effector proteins induced in mildly stressed cells may substantially differ from those expressed in severely stressed cells.

An important reason why ATF4 is considered the key effector of the ISR, is that it is a transcriptional regulator for the expression of GADD34 and CHOP, which signal towards inactivation of the ISR and cell death, respectively (21–23). Therefore, ATF4 is considered a life-death switch that determines whether ISR activity should be reversed to resume normal protein synthesis, or whether cells should go into apoptosis. When stress conditions are temporal and/or mild, ISR-induced expression of GADD34 expression will accelerate eIF2 dephosphorylation by recruiting p-eIF2 and its phosphatase PP1. When stress conditions are severe or long-lived however, the increased CHOP expression will trigger apoptosis (23–25).

Despite the ISR's complexity, its effects can be summarized as follows: The ISR temporarily keeps cells alive in the face of stress conditions that would otherwise cause cell death, thus providing the necessary time to resolve the stress situation. If the stress is caused by a defect within the cell (e.g.

insufficient folding capacity in the ER to deal with the work-load), it focusses a cell's efforts towards solving the problem, thereby increasing the chance that balance can be restored. Under harsh stress conditions, either in duration or severity, the ISR signals towards apoptosis.

The ISR under normal and pathological conditions

The ISR is not only important under harmful stress conditions, but also plays a key role in normal cell biological processes such as differentiation, mitosis, survival, or apoptosis (26–29). Therefore, dysregulation in the ISR is involved in a wide variety of disorders, including respiratory, cardiovascular, neurological, and cancer-related problems (30–34). For this reason, modulation of the ISR is recognized as a potential therapeutic strategy that may beneficially impact ISR-associated disorders. Unfortunately, crude methods like systemically blocking PERK lead to adverse side-effects (35–37), since ISR activity is essential for the survival of specific cell types, in particular secretory cells with a high ER work-load (38, 39). This underlines the essential role of the ISR in normal cellular function, and suggests that a more subtle approach is warranted. The viability of ISR inhibition as basis for therapeutic strategies is demonstrated by experiments with the recently described small-molecule ISR inhibitor, ISRIB (40). ISRIB promotes the assembly of decameric (fully active) eIF2B complexes, thereby increasing the total eIF2B GEF activity and decreasing the cell's sensitivity to p-eIF2 (41–44). In vivo experiments in mice have shown that ISRIB, through its inhibition of ISR activity, alleviates the pathological consequences of a number of ISR-related defects, without apparent side-effects (29, 35, 40, 45–47).

Viruses and the ISR

Virus infections cause extensive changes in the intracellular environment and often activate at least one of the ISR sensors. Often, PKR is the primary ISR sensor of relevance in infected cells, as it may detect viral dsRNA replication intermediates which are formed during the life cycle of RNA viruses (48, 49). Alternatively, it may detect cellular dsRNAs that are released into the cytoplasm from mitochondria under conditions of stress(2). Also PERK may be activated during virus infections, as a consequence of virus-induced ER-stress (50–53), and even GCN2 has been reported to be activated by viral RNAs (54, 55). ISR activity may have a detrimental effect on cellular and viral translation and may thereby severely impair propagation of a wide variety of viruses. Viruses have therefore acquired proteins that suppress the ISR to optimize replication and production of progeny virus. This is often

achieved by interfering in the ISR signaling cascade to such effect that TC concentrations remain intact. Alternatively, some viral mRNAs contain specific structural elements, which alter its dependency on translation initiation factors (reviewed in (56, 57)). For example, a loop structure in alphavirus RNA (downstream loop; DLP) mediates translation in an eIF2-independent manner (58), and the dicistrovirus internal ribosomal entry site (IRES) renders viral translation independent of all translation initiation factors (59, 60).

Viral ISR antagonists

Most viruses are at least partially sensitive to ISR-mediated translational repression and encode specific ISR antagonists that prevent ISR signal transduction. These antagonists are classified based on which step in the ISR pathway they counteract. Class 1 antagonists prevent the first step in ISR signaling: the activation of the ISR sensor proteins. This activation process encompasses detection of the stressor, and homodimerization and autophosphorylation of the ISR-sensor. Thus, Class 1 antagonists can be defined as antagonists that prevent ISR-sensor autophosphorylation. Possible modes-of-action of Class 1 antagonists include the sequestration (e.g. Influenza NS1 (61)) or degradation (e.g. MHV nsp15 (62)) of ligands, blocking the interaction between ligand and sensor (e.g. HIV tat (63)), preventing eIF2 kinase dimerization (e.g. andesvirus N (64)), or blocking autophosphorylation activity. In most cases, Class 1 antagonists are PKR-specific, and bind either PKR itself or its ligand dsRNA. Also PERK-specific Class 1 antagonists have been described, such as HSV gB protein, that functions by directly interacting with PERK's ER-luminal domain to prevent its activation (65). Some Class 1 antagonists, such as HCMV pTRS1, are not specific to one ISR sensor protein, and target at least two by binding their (conserved) kinase domains (66). Class 2 antagonists do not counteract eIF2 kinase autophosphorylation but prevent the phosphorylation eIF2α. Many Class 2 antagonists are homologous to eIF2α and function as pseudo-substrates (e.g. swine pox virus C8L (67)). Other Class 2 antagonists, like RVFV NSs, actively induce the degradation of eIF2 kinases to repress eIF2 phosphorylation(68). Class 3 antagonists act downstream of eIF2 phosphorylation by inducing dephosphorylation of eIF2. These antagonists are typically homologous to the cellular protein GADD34, and have the same scaffolding function, bridging eIF2 and its phosphatase PP1 (e.g. TGEV protein 7 (69)). An extensive overview of the viral ISR antagonists described thus far is given in Table 1. In this thesis, we focus on evasion of the ISR by two distinct groups of positive strand RNA viruses, coronaviruses and picornaviruses.

Coronaviruses

Coronaviruses (CoVs) are categorized into four genera, α, β, γ, and δ, based on complete genome sequence comparisons. These CoVs infect a wide variety of hosts and are often host species specific. Thus far, six coronaviruses have been shown to infect humans, of which four (HKU1, OC43, 229E, and NL63) circulate globally and mediate mostly common cold-like symptoms. In a minor fraction of the infected individuals they may cause more severe symptoms like pneumonia, and bronchitis, as well as neurological or enteric complications. In 2002, severe acute respiratory syndrome (SARS) coronavirus jumped the species barrier into to human population (70), and has since infected more than 8000 individuals, with a mortality rate of ~10% (71). Luckily, this virus has been eliminated from the human population due to rapid implementation of control strategies. A decade later, middle-east respiratory syndrome (MERS) coronavirus was first reported to infect humans (72). This virus has an even higher mortality rate of ~35% (73), but the number of infected individuals is limited since MERS-CoV is (still) inefficiently transmitted between humans (74). These viruses are believed to originate from bat reservoirs, and to be transmitted to humans via intermediate hosts, such as dromedary camels for MERS-CoV and civet cats for SARS-CoV (75–77). Thus, SARS-CoV and MERS-CoV illustrate that coronaviruses have the potential to enter the human population and become a significant threat to human health.

CoVs have exceptionally large positive strand RNA genomes, which range from 26 kb to 32 kb in length. CoVs encode over 20 different proteins, from multiple different open reading frames. The 5’ ORF of approximately 20 kb encodes a polyprotein that is processed by viral proteases into non-structural proteins (nsps) involved in replication. The other ORFs encode either conserved, structural proteins (spike, envelope, membrane, and nucleocapsid), or accessory proteins with little or no conservation between virus species.

Accessory proteins are often non-essential but optimize virus propagation in a variety of different ways. The genes encoding these accessory proteins are thought to be obtained, adapted, and deleted, as CoVs accommodate to new host species (78). However, probably due to rapid and extensive adaptations, accessory proteins typically lack homology to cellular counterparts, which makes inferring their evolutionary origin, or even their current function, challenging. One way in which accessory proteins may promote virus propagation is by counteracting antiviral responses. Since coronavirus mRNAs are capped and poly-adenylated like cellular mRNAs, their translation is likely subject to

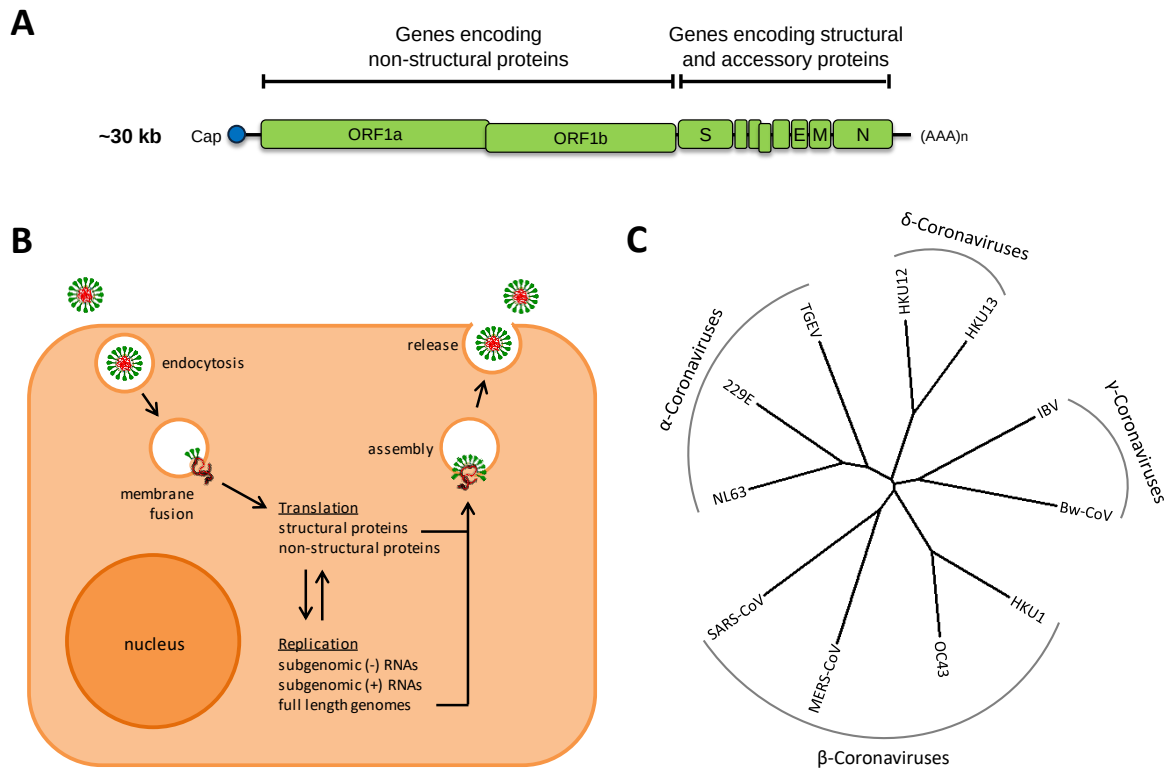

Figure 3. Simplified overview of the coronavirus genome composition, replication cycle, and phylogeny. *(A) Genome composition of a coronavirus. The coronavirus genome is capped and poly-adenylated, and has a length of around 30 kb. Coronaviruses encode a conserved set of non-structural proteins (nsps encoded by ORF1ab) and structural proteins (S, E, M, N). The remainder of the genes are non-essential accessory genes involved in optimization of virus replication. This particular example, MERS-CoV, encodes four accessory genes (p3, p4a, p4b, p5), but the number of accessory genes may widely vary between coronaviruses. (B) The coronavirus life cycle. Coronaviruses enter a cell via membrane fusion of the viral envelop with endosomal membranes. The genome is released into the cytosol and used as template to create subgenomic minus-strand and plus-strand RNAs, as well as full length genome copies. Translation of plus-strand subgenomic RNAs and full length genomes yields the viral proteins, which assist in replication as well as the formation and release of new membranous virus particles. (C) Phylogenetic analysis of a selection of coronaviruses from each of the major groups of coronaviruses (α, β, γ, and δ coronaviruses). Phylogenetic analysis was performed on full genome sequences aligned by MUSCLE, using the neighbour-joining method.*

inhibition by the ISR, and coronaviruses should benefit from preventing ISR activity. Indeed, the limited information available suggests that coronaviruses use several different strategies to interfere with the ISR. Mouse hepatitis virus (MHV) and human coronavirus 229E were shown to interfere with PKR activation, likely through the degradation of dsRNA by nsp15 (62, 79). IBV was suggested to counteract PKR activity using its nsp2 protein via an unknown mechanism (79). SARS-CoV induces PKR activation,

but prevents subsequent PKR-mediated eIF2α phosphorylation through an unknown mechanism (52). Transmissible gastroenteritis virus (TGEV) accessory protein 7 induces dephosphorylation of eIF2α by recruiting the eIF2α phosphatase PP1 (69).

Picornaviruses

The *Picornaviridae* encompasses a total of 47 genera that contain a plethora of pathogens impacting the health of humans and animals. These include the enteroviruses (e.g. poliovirus, cosackievirus, rhinovirus), parechoviruses (e.g. human parechovirus), hepatoviruses (e.g. hepatitis A virus), kobuviruses (e.g. aichivirus), aphthoviruses (e.g. foot-and-mouth disease virus), and cardioviruses (e.g. encephalomyocarditis virus). Picornaviruses are small, non-enveloped viruses with genome sizes ranging from 7,5-8 kb.

Picornavirus genomes are poly-adelynated but lack a 5' cap structure. Instead, translation of the viral RNA is initiated from an internal ribosomal entry site (IRES), of which several different types have been described (80). The picornavirus genome contains a single open reading frame which encodes a large polyprotein. This polyprotein is processed into the conserved structural proteins VP1-VP4, and non-structural proteins 2A-2C and 3A-3D. Additionally, several picornaviruses encode a leader (L) protein. These leader proteins are remarkably diverse throughout the picornavirus family, and are homologous only to L proteins encoded by viruses that belong to the same genus (81). These L proteins could be considered the picornavirus equivalent of the coronavirus accessory proteins, as they are often non-

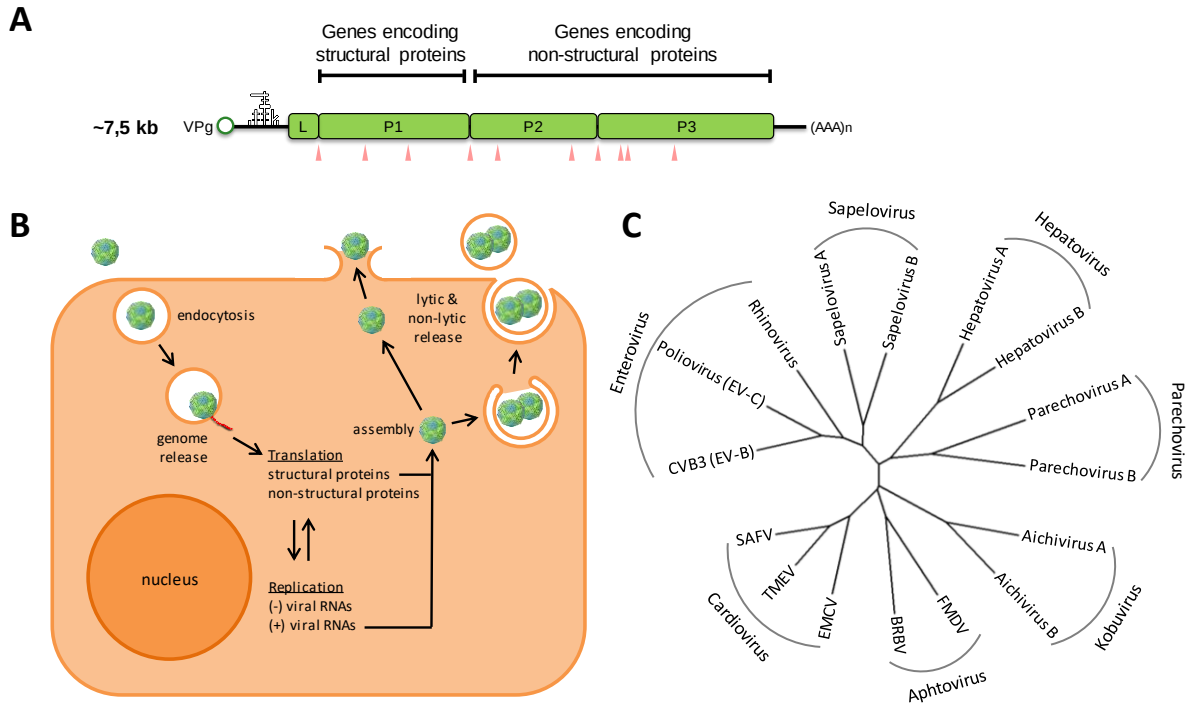

Figure 4. Simplified overview of the picornavirus genome composition, replication cycle, and phylogeny. *(A) Genome composition of a Picornavirus. The 5' end of the picornavirus genome is bound by viral protein 3B (often referred to as VPg), and its 3' end is poly-adenylated. Picornavirus translation is mediated by its 5' UTR which contains an IRES. Picornaviruses encode a large polyprotein which is proteolytically processed into the mature viral proteins by viral proteases (cleavage sites indicated by the arrowheads). Picornaviruses encode a conserved set of non-structural proteins (2A-2C encoded by P2, and 3A-3D encoded by P3) and structural proteins (VP1-VP4 encoded by P1). Several picornaviruses also encode a Leader protein as the N-terminal part of the polyprotein. (B) Picornaviruses release their genome through a pore in the endosomal membrane. The incoming viral RNA is directly used to create new viral proteins and subsequently to synthesize minus- and plus-strand copies. The structural proteins in combination with full-length plus-stranded genome copies are assembled into virions, which are shed from the host cell in a lytic as well as non-lytic manner. (C) Phylogenetic analysis of a selection of viruses from several of the major genera of the picornavirus family. Phylogenetic analysis was performed on full genome sequences aligned by MUSCLE, using the neighbour-joining method.*

essential but optimize virus replication in a variety of different ways, again including counteracting antiviral responses (82–84). Most, if not all, picornaviruses are at least partially or temporarily inhibited by ISR activity (85–88), and may benefit from ISR antagonists. There is some evidence suggesting that picornaviruses counteract the ISR, for example through degradation of PKR in poliovirus infected cells (89, 90), or by preventing PKR autophosphorylation in EMCV-infected cells (82).

Aim and Outline of the Thesis

For many viruses, efficient replication is contingent on the ability to evade antiviral responses such as the ISR. Yet, for most viruses it remains poorly understood by what mechanisms the ISR is suppressed. In this thesis we set out to identify new ISR antagonists encoded by picorna- and coronaviruses, and on the elucidation of their molecular mode of action. This will increase our knowledge about evasion mechanisms employed by viruses to protect themselves against antiviral responses. From a cell biological perspective, the study of viral ISR antagonists may also teach us more about how the ISR regulates translation, one of the core processes in life.

In **chapter 2**, we set out to investigate the function of an accessory protein (p4a) encoded by Middle-East Respiratory Syndrome coronavirus (MERS-CoV) as inhibitor of PKR-mediated ISR activation(91). We identify MERS-CoV p4a as a PKR-specific ISR antagonist that functions via dsRNA binding. Consistent with its mode of action of dsRNA sequestration, p4a also prevents the activation of another

dsRNA-activated antiviral pathway, the type I IFN induction pathway. While the mode of action of p4a was described before for several viral dsRNA binding proteins, p4a is the first coronavirus protein identified with this function.

In **chapter 3**, we assess the function of a small-molecule inhibitor of the ISR (ISRIB). Initially, we intended to use ISRIB to study the effects of the ISR during virus replication. We observed however, that ISRIB prevents ISR activation only early in infection, but failed to do so at later time points. Further investigation taught us that ISRIB prevents ISR activity only under conditions of mild stress, as defined by a limited level of eIF2 phosphorylation. High levels of p-eIF2 however may inhibit translation and enhance expression of ISR-induced proteins, even in the presence of ISRIB. ISRIB binds at the interface between two eIF2B pentamers to promote the assembly of full (decameric) eIF2B complexes. Since eIF2B has higher GEF activity when fully assembled, ISRIB boosts the total basal eIF2B GEF activity within a cell and thereby counteracts the effect of the ISR. This working mechanism is consistent with our finding that ISRIB only acts under mild stress. Since ISRIB does not prevent the sequestration of eIF2B by p-eIF2, high levels of p-eIF2 may still deplete a cell's pool of active eIF2B. In conclusion, ISRIB makes cells less sensitive rather than insensitive to ISR signaling, which may explain the apparent absence of side-effects of an ISRIB treatment *in vivo*.

In **chapter 4**, we investigated the function(s) of an accessory protein, AcP10, encoded by Beluga whale coronavirus. This protein drew our attention as bioinformatic analysis identified it as a uridine cytidine kinase (UCK), a function that has not been demonstrated for any RNA virus-encoded protein. We confirmed that AcP10 has UCK activity, but also observed it to have ISR antagonist activity independent of its UCK activity. This protein acts further downstream in the ISR pathway than p4a and does not affect activation of PKR or any of the other eIF2 kinases, nor their ability to phosphorylate eIF2. Instead, AcP10 prevents p-eIF2 from binding its target eIF2B, and thereby AcP10 ensures that eIF2B remains active even in the presence of p-eIF2. It does so via a direct interaction with eIF2B, likely at an area that overlaps the interaction site for p-eIF2, but not for native eIF2. Thus, AcP10 allows ongoing translation under conditions of severe stress. This mode-of-action was not previously described for any viral or host cell protein, and thus AcP10 is a prototype of an entirely novel class of ISR antagonists. In fact, unimpaired cellular translation in the presence of high concentrations of p-eIF2 had not previously been observed in eukaryotic cells, except in cells with genetic defects that disturb the p-eIF2•eIF2B interaction. We classified AcP10 as a Class 4 antagonist.

In **chapter 5**, we describe another Class 4 antagonist, the Leader protein encoded by the picornavirus Aichivirus (AiVL). We show that in AiV-infected cells, large amounts of cytoplasmic dsRNA accumulate, and eIF2 is efficiently being phosphorylated. However, (cellular) translation in intact and stress

granules do not form, indicating that AiV blocks the ISR directly downstream of p-eIF2. Recombinant AiV lacking a functional AiVL protein failed to rescue translation in the presence of p-eIF2, demonstrating that ISR antagonism in AiV-infected cells is mediated by AiVL. We determined that AiVL has a comparable function as AcP10 and binds eIF2B to prevent subsequent association of p-eIF2. Thereby, AiVL acts in a similar way as AcP10, rescuing translation in the presence of (high levels) of p-eIF2, irrespective of the eIF2 kinase involved. Yet, AiVL has no homology to AcP10. AcP10 and AiVL evolved independently, from an ancestral protein with uridine kinase activity, and from a pre-existing kobuvirus leader protein that lacked the ability to counteract the ISR, respectively. Taken together, we identify two independent examples of proteins with a highly similar, yet unprecedented mode of action. Thus, Class 4 ISR antagonists arose at least twice, in phylogenetically distinct virus families, by convergent evolution.

References

1. K. M. Vattem, K. A. Staschke, S. Zhu, R. C. Wek, Inhibitory sequences in the N-terminus of the double-stranded-RNA-dependent protein kinase, PKR, are important for regulating phosphorylation of eukaryotic initiation factor 2α (eIF2α). *Eur. J. Biochem.* **268**, 1143-53 (2001)

2. Y. Kim, *et al.*, PKR Senses Nuclear and Mitochondrial Signals by Interacting with Endogenous Double-Stranded RNAs. *Mol. Cell* **71**, 1051-1063 (2018)

3. P. A. Lemaire, E. Anderson, J. Lary, J. L. Cole, Mechanism of PKR Activation by dsRNA. *J. Mol. Biol.* **381**, 351-60 (2008)

4. J. Galabru, M. G. Katze, N. Robert, A. G. Hovanessian, The binding of double-stranded RNA and adenovirus VAI RNA to the interferon-induced protein kinase. *Eur. J. Biochem.* **178**, 581-9 (1989)

5. G. A. Peters, S. Li, G. C. Sen, Phosphorylation of specific serine residues in the PKR activation domain of PACT is essential for its ability to mediate apoptosis. *J. Biol. Chem.* **281**, 35129-36 (2006)

6. C. V. Patel, I. Handy, T. Goldsmith, R. C. Patel, PACT, a stress-modulated cellular activator of interferon-induced double-stranded RNA-activated protein kinase, PKR. *J. Biol. Chem.* **275**, 37993-8 (2000)

7. T. Ito, M. Yang, W. S. May, RAX, a cellular activator for double-stranded RNA-dependent protein kinase during stress signaling. *J. Biol. Chem.* **274**, 15427-32 (1999)

8. A. Bertolotti, Y. Zhang, L. M. Hendershot, H. P. Harding, D. Ron, Dynamic interaction of BiP and ER stress transducers in the unfolded-protein response. *Nat. Cell Biol.* **2**, 326-32 (2000)

9. P. Walter, D. Ron, The unfolded protein response: From stress pathway to homeostatic regulation. *Science.* **334**, 1081-6 (2011)

10. J. Dong, H. Qiu, M. Garcia-Barrio, J. Anderson, A. G. Hinnebusch, Uncharged tRNA activates GCN2 by displacing the protein kinase moiety from a bipartite tRNA-binding domain. *Mol. Cell* **6**, 269-79 (2000)

11. B. A. Castilho, *et al.*, Keeping the eIF2 alpha kinase Gcn2 in check. *Biochim. Biophys. Acta - Mol. Cell Res.* **1843**, 1948-68 (2014)

12. A. P. Han, *et al.*, Heme-regulated eIF2α kinase (HRI) is required for translational regulation and survival of erythroid precursors in iron deficiency. *EMBO J.* **20**, 6909-18 (2001)

13. R. L. Matts, J. R. Schatz, R. Hurst, R. Kagen, Toxic heavy metal ions activate the heme-regulated eukaryotic initiation factor-2α kinase by inhibiting the capacity of hemin-supplemented reticulocyte lysates to reduce disulfide bonds. *J. Biol. Chem.* **266**, 12695-702 (1991).

14. J. J. Chen, I. M. London, Regulation of protein synthesis by heme-regulated eIF-2α kinase. *Trends Biochem. Sci.* **20**, 105-8 (1995)

15. R. Panniers, E. C. Henshaw, A GDP/GTP exchange factor essential for eukaryotic initiation factor 2 cycling in Ehrlich ascites tumor cells and its regulation by eukaryotic initiation factor 2 phosphorylation. *J. Biol. Chem.* **258**, 7928-34 (1983)

16. a G. Rowlands, R. Panniers, E. C. Henshaw, The catalytic mechanism of guanine nucleotide exchange factor action and competitive inhibition by phosphorylated eukaryotic initiation factor 2. *J. Biol. Chem.* **263**, 5526-33 (1988)

17. A. Leroux, I. London, Regulation of protein synthesis by phosphorylation of eukaryotic initiation factor 2 alpha in intact reticulocytes and reticulocyte lysates. *PNAS* **79**, 2147–2151 (1982)

18. K. Pakos-Zebrucka, *et al.*, The integrated stress response. *EMBO Rep.* **17**, 1374–1395 (2016)

19. H. P. Harding, *et al.*, Regulated translation initiation controls stress-induced gene expression in mammalian cells. *Mol. Cell* **6**, 1099-108 (2000)

20. K. M. Vattem, R. C. Wek, Reinitiation involving upstream ORFs regulates ATF4 mRNA translation in mammalian cells. *PNAS.* **101**, 11269-74 (2004)

21. I. Novoa, H. Zeng, H. P. Harding, D. Ron, Feedback inhibition of the unfolded protein response by GADD34-mediated dephosphorylation of eIF2α. *J. Cell Biol.* **153**, 1011-22 (2001)

22. E. Kojima, *et al.*, The function of GADD34 is a recovery from a shutoff of protein synthesis induced by ER stress: elucidation by GADD34-deficient mice. *FASEB J.* **17**, 1573-5 (2003)

23. H. Zinszner, *et al.*, CHOP is implicated in programmed cell death in response to impaired function of the endoplasmic reticulum. *Genes Dev.* **12**, 982-95 (1998)

24. E. V. Maytin, M. Ubeda, J. C. Lin, J. F. Habener, Stress-inducible transcription factor CHOP/gadd153 induces apoptosis in mammalian cells via p38 kinase-dependent and -independent mechanisms. *Exp. Cell Res.* 267(2):193-204 (2001)

25. M. Matsumoto, M. Minami, K. Takeda, Y. Sakao, S. Akira, Ectopic expression of CHOP (GADD153) induces apoptosis in M1 myeloblastic leukemia cells. *FEBS Lett.* **395**, 143-7 (1996)

26. B. Datta, R. Datta, S. Mukherjee, Z. Zhang, Increased phosphorylation of eukaryotic initiation factor 2α at the G2/M boundary in human osteosarcoma cells correlates with deglycosylation of p67 and a decreased rate of protein synthesis. *Exp. Cell Res.* **250**, 223–230 (1999)

27. Y. Kim, *et al.*, PKR is activated by cellular dsRNAs during mitosis and acts as a mitotic regulator. *Genes Dev.* **28**, 1310–1322 (2014)

28. S. S. Cao, *et al.*, Phosphorylation of eif2α is dispensable for differentiation but required at a posttranscriptional level for paneth cell function and intestinal homeostasis in mice. *Inflamm. Bowel Dis.* **20**, 712–722 (2014)

29. C. Wang, *et al.*, Inhibiting the integrated stress response pathway prevents aberrant chondrocyte differentiation thereby alleviating chondrodysplasia. *Elife* **7,** pii: e37673. (2018)

30. E. F. A. Van't Wout, P. S. Hiemstra, S. J. Marciniak, The integrated stress response in lung disease. *Am. J. Respir. Cell Mol. Biol.* **50**, 1005-9 (2014)

31. D. Santos-Ribeiro, L. Godinas, C. Pilette, F. Perros, The integrated stress response system in cardiovascular disease. *Drug Discov. Today* **23**, 920–929 (2018)

32. D. J. McConkey, The integrated stress response and proteotoxicity in cancer therapy. *Biochem. Biophys. Res.*

Commun. **482**, 450-453 (2017)

33. J. A. Moreno, *et al.*, Sustained translational repression by eIF2α-P mediates prion neurodegeneration. *Nature* **485**, 507–511 (2012)

34. J. J. M. Hoozemans, *et al.*, The Unfolded Protein Response Is Activated in Pretangle Neurons in Alzheimer's Disease Hippocampus. *Am. J. Pathol.* **174**, 1241–1251 (2009)

35. M. Halliday, *et al.*, Partial restoration of protein synthesis rates by the small molecule ISRIB prevents neurodegeneration without pancreatic toxicity. *Cell Death Dis.* **6**, e1672 (2015)

36. J. A. Moreno, *et al.*, Oral treatment targeting the unfolded protein response prevents neurodegeneration and clinical disease in prion-infected mice. *Sci. Transl. Med.* **5**, 206ra138 (2013)

37. G. Mercado, *et al.*, Targeting PERK signaling with the small molecule GSK2606414 prevents neurodegeneration in a model of Parkinson's disease. *Neurobiol. Dis.* **112**, 136-148 (2018)

38. H. P. Harding, *et al.*, Diabetes mellitus and exocrine pancreatic dysfunction in Perk-/- mice reveals a role for translational control in secretory cell survival. *Mol. Cell* **7**, 1153–1163 (2001)

39. P. Zhang, *et al.*, The PERK Eukaryotic Initiation Factor 2 Kinase Is Required for the Development of the Skeletal System, Postnatal Growth, and the Function and Viability of the Pancreas. *Mol. Cell. Biol.* **22**, 3864-74 (2002)

40. C. Sidrauski, *et al.*, Pharmacological brake-release of mRNA translation enhances cognitive memory. *Elife* **2**, e00498 (2013)

41. C. Sidrauski, *et al.*, Pharmacological dimerization and activation of the exchange factor eIF2B antagonizes theintegrated stress response. *Elife* **4**, e07314 (2015)

42. Y. Sekine, *et al.*, Mutations in a translation initiation factor identify the target of a memory-enhancing compound. *Science.* **348**, 1027-30 (2015)

43. A. F. Zyryanova, *et al.*, Binding of ISRIB reveals a regulatory site in the nucleotide exchange factor eIF2B. *Science.* **359**, 1533-1536 (2018)

44. J. C. Tsai, *et al.*, Structure of the nucleotide exchange factor eIF2B reveals mechanism of memory-enhancing molecule. *Science.* **359**, pii: eaaq0939 (2018)

45. A. Chou, *et al.*, Inhibition of the integrated stress response reverses cognitive deficits after traumatic brain injury. *PNAS.* **114**, E6420-E6426 (2017)

46. H. G. Nguyen, *et al.*, Development of a stress response therapy targeting aggressive prostate cancer. *Sci. Transl. Med.* **10**, pii: eaar2036 (2018)

47. Y. L. Wong, *et al.*, The small molecule ISRIB rescues the stability and activity of vanishing white matter disease eIF2B mutant complexes. *Elife* **7**, pii: e32733 (2018)

48. K.-N. Son, Z. Liang, H. L. Lipton, Double-Stranded RNA Is Detected by Immunofluorescence Analysis in RNA and DNA Virus Infections, Including Those by Negative-Stranded RNA Viruses. *J. Virol.* **89**, 9383-92 (2015)

49. F. Weber, S. R. Paludan, S. B. Rasmussen, V. Wagner, R. Hartmann, Double-Stranded RNA Is Produced by Positive-Strand RNA Viruses and DNA Viruses but Not in Detectable Amounts by Negative-Strand RNA Viruses. *J. Virol.* **80**, 5059-64 (2006)

50. G. Cheng, Z. Feng, B. He, Herpes Simplex Virus 1 Infection Activates the Endoplasmic Reticulum Resident Kinase PERK and Mediates eIF-2 Dephosphorylation by the gamma(1)34.5 Protein. *J. Virol.* **79**, 1379-88 (2005)

51. D. Baltzis, *et al.*, Resistance to Vesicular Stomatitis Virus Infection Requires a Functional Cross Talk between the Eukaryotic Translation Initiation Factor 2 Kinases PERK and PKR. *J. Virol.* **78**, 12747-61 (2004)

52. V. Krähling, D. A. Stein, M. Spiegel, F. Weber, E. Mühlberger, Severe acute respiratory syndrome coronavirus triggers apoptosis via protein kinase R but is resistant to its antiviral activity. *J. Virol.* **83**, 2298–2309 (2009).

53. J. Song, *et al.*, Non-Structural Protein 2B of Human Rhinovirus 16 Activates Both PERK and ATF6 Rather Than IRE1 to Trigger ER Stress. *Viruses* **11**, pii: E133 (2019)

54. J. J. Berlanga, *et al.*, Antiviral effect of the mammalian translation initiation factor 2α kinase GCN2 against RNA viruses. *EMBO J.* **25**, 1730-40 (2006)

55. J. del Pino, *et al.*, GCN2 Has Inhibitory Effect on Human Immunodeficiency Virus-1 Protein Synthesis and Is Cleaved upon Viral Infection. *PLoS One* **7**, e47272 (2012)

56. K. M. Lee, C. J. Chen, S. R. Shih, Regulation Mechanisms of Viral IRES-Driven Translation. *Trends Microbiol.* **25**, 546-561 (2017)

57. L. Balvay, R. S. Rifo, E. P. Ricci, D. Decimo, T. Ohlmann, Structural and functional diversity of viral IRESes. *Biochim. Biophys. Acta - Gene Regul. Mech.* **1789**, 542-57 (2009)

58. I. Ventoso, *et al.*, Translational resistance of late alphavirus mRNA to eIF2α phosphorylation: A strategy to overcome the antiviral effect of protein kinase PKR. *Genes Dev.* **20**, 87-100 (2006)

59. N. Deniz, E. M. Lenarcic, D. M. Landry, S. R. Thompson, Translation initiation factors are not required for Dicistroviridae IRES function in vivo. *RNA* **15**, 932-46 (2009)

60. T. V. Pestova, C. U. T. Hellen, Translation elongation after assembly of ribosomes on the Cricket paralysis virus internal ribosomal entry site without initiation factors or initiator tRNA. *Genes Dev.* **17**, 181-6 (2003)

61. Y. Lu, M. Wambach, M. G. Katze, R. M. Krug, Binding of the Influenza Virus NS1 Protein to Double-Stranded RNA Inhibits the Activation of the Protein Kinase That Phosphorylates the eIF-2 Translation Initiation Factor. *Virology* **214**, 222–228 (1995)

62. E. Kindler, *et al.*, Early endonuclease-mediated evasion of RNA sensing ensures efficient coronavirus replication. *PLoS Pathog.* **13**, e1006195 (2017)

63. S. R. Brand, R. Kobayashi, M. B. Mathews, The Tat protein of human immunodeficiency virus type 1 is a substrate and inhibitor of the interferon-induced, virally activated protein kinase, PKR. *J. Biol. Chem.* **272**, 8388-95 (1997)

64. Z. Wang, M. A. Mir, Andes Virus Nucleocapsid Protein Interrupts Protein Kinase R Dimerization To Counteract Host

Interference in Viral Protein Synthesis. *J. Virol.* **89**, 1628-39 (2014)

65. M. Mulvey, C. Arias, I. Mohr, Maintenance of Endoplasmic Reticulum (ER) Homeostasis in Herpes Simplex Virus Type 1-Infected Cells through the Association of a Viral Glycoprotein with PERK, a Cellular ER Stress Sensor. *J. Virol.* **81**, 3377-90 (2007)

66. H. A. Vincent, B. Ziehr, N. J. Moorman, Mechanism of Protein Kinase R Inhibition by Human Cytomegalovirus pTRS1. *J. Virol.* **91**, 1–16 (2017).

67. M. Kawagishi-Kobayashi, C. Cao, J. Lu, K. Ozato, T. E. Dever, Pseudosubstrate inhibition of protein kinase PKR by swine pox virus C8L gene product. *Virology* **276**, 424-34 (2000)

68. M. Habjan, *et al.*, NSs Protein of Rift Valley Fever Virus Induces the Specific Degradation of the Double-Stranded RNA-Dependent Protein Kinase. *J. Virol.* **83**, 4365-75 (2009)

69. J. L. G. Cruz, *et al.*, Coronavirus gene 7 counteracts host defenses and modulates virus virulence. *PLoS Pathog.* **7** e1002090 (2011)

70. C. Drosten, *et al.*, Identification of a novel coronavirus in patients with severe acute respiratory syndrome. *N. Engl. J. Med.* **348**, 1967–76 (2003).

71. WHO | Severe Acute Respiratory Syndrome Coronavirus (SARS-CoV). *WHO*, https://www.who.int/csr/sars/country/table2004_04_ (2019)

72. A. M. Zaki, S. van Boheemen, T. M. Bestebroer, A. D. M. E. Osterhaus, R. A. M. Fouchier, Isolation of a Novel Coronavirus from a Man with Pneumonia in Saudi Arabia. *N. Engl. J. Med.* **367**, 1814-20 (2012)

73. WHO | Middle East Respiratory Syndrome Coronavirus (MERS-CoV) – Saudi Arabia. *WHO*, https://www.who.int/emergencies/mers-cov/en/ (2019)

74. Z. A. Memish, A. I. Zumla, R. F. Al-Hakeem, A. A. Al-Rabeeah, G. M. Stephens, Family Cluster of Middle East Respiratory Syndrome Coronavirus Infections. *N. Engl. J. Med.* **368**, 2487-94 (2013)

75. W. Li, *et al.*, Receptor and viral determinants of SARS-coronavirus adaptation to human ACE2. *EMBO J.* **24**, 1634–1643 (2005)

76. T. Briese, *et al.*, Dromedary Camels in Saudi Arabia Include Homologues of Human Isolates Revealed through Whole-Genome analysis etc. *MBio* **5**, 1–5 (2014)

77. M. T. Azhar EI, El-Kafrawy SA, Farraj SA, Hassan AM, Al-Saeed MS, Hashem AM, Evidence for Camel-to-Human Transmission of MERS Coronavirus. *New Engl. J. Med.* **370**, 2499–2505 (2014)

78. J. Min, *et al.*, Molecular evolution of the SARS coronavirus during the course of the SARS epidemic in China. *Science* **303**, 1666–1669 (2004)

79. X. Wang, *et al.*, Inhibition of protein kinase R activation and upregulation of GADD34 expression play a synergistic role in facilitating coronavirus replication by maintaining de novo protein synthesis in virus-infected cells. *J. Virol.* **83**, 12462–12472 (2009)

80. E. Martinez-Salas, R. Francisco-Velilla, J. Fernandez-Chamorro, A. M. Embarek, Insights into structural and mechanistic features of viral IRES elements. *Front. Microbiol.* **8**, 2629 (2018)

81. V. I. Agol, A. P. Gmyl, Viral security proteins: Counteracting host defences. *Nat. Rev. Microbiol.* **8**, 867-78 (2010)

82. L. J. Visser, *et al.*, FMDV leader protease cleaves G3BP1 and G3BP2 and inhibits stress granule formation. *J. Virol.* **93**, pii: e00922-18 (2019)

83. F. Borghese, T. Michiels, The Leader Protein of Cardioviruses Inhibits Stress Granule Assembly. *J. Virol.* **85**, 9614–9622 (2011).

84. S. V Hato, *et al.*, The mengovirus leader protein blocks interferon-alpha/beta gene transcription and inhibits activation of interferon regulatory factor 3. *Cell. Microbiol.* **9**, 2921–2930 (2007)

85. J. P. White, L. C. Reineke, R. E. Lloyd, Poliovirus Switches to an eIF2-Independent Mode of Translation during Infection. *J. Virol.* **85**, 8884–8893 (2011)

86. E. Welnowska, M. A. Sanz, N. Redondo, L. Carrasco, Translation of viral mRNA without active eIF2: The case of picornaviruses. *PLoS One* **6**, e22230 (2011)

87. N. Redondo, M. A. Sanz, E. Welnowska, L. Carrasco, Translation without eiF2 promoted by poliovirus 2A protease. *PLoS One* **6**, e25699 (2011)

88. T. R. Sweeney, I. S. Abaeva, T. V. Pestova, C. U. T. Hellen, The mechanism of translation initiation on type 1 picornavirus IRESs. *EMBO J.* **33**, 76-92 (2014)

89. T. L. Black, B. Safer, A. R. A. Hovanessian, M. G. Katze, The Cellular 68,000-Mr Protein Kinase Is Highly Autophosphorylated and Activated Yet Significantly Degraded during Poliovirus Infection: Implications for Translational Regulation. *J. Virol.* **63**, 2244-51 (1989)

90. Y.-H. Chang, K. S. Lau, R.-L. Kuo, J.-T. Horng, dsRNA Binding Domain of PKR Is Proteolytically Released by Enterovirus A71 to Facilitate Viral Replication. *Front. Cell. Infect. Microbiol.* **7**, 284 (2017)

91. H. H. Rabouw, *et al.*, Middle East Respiratory Coronavirus Accessory Protein 4a Inhibits PKR-Mediated Antiviral Stress Responses. *PLoS Pathog.* **12**, e1005982 (2016)

92. J. Poppers, M. Mulvey, D. Khoo, I. Mohr, Inhibition of PKR activation by the proline-rich RNA binding domain of the herpes simplex virus type 1 Us11 protein. *J. Virol.* **74**, 11215-21 (2000)

93. G. A. Peters, D. Khoo, I. Mohr, G. C. Sen, Inhibition of PACT-Mediated Activation of PKR by the Herpes Simplex Virus Type 1 Us11 Protein. *J. Virol.* **76**, 11054-64 (2002)

94. Y. Li, *et al.*, ICP34.5 protein of herpes simplex virus facilitates the initiation of protein translation by bridging eukaryotic initiation factor 2alpha (eIF2alpha) and protein phosphatase 1. *J. Biol. Chem.* **76**, 11054-64 (2011)

95. K. A. Cassady, Human Cytomegalovirus TRS1 and IRS1 Gene Products Block the Double-Stranded-RNA-Activated Host Protein Shutoff Response Induced by Herpes Simplex Virus Type 1 Infection. *J. Virol.* **79**, 8707-15 (2005)

96. B. Ziehr, H. A. Vincent, N. J. Moorman, Human Cytomegalovirus pTRS1 and pIRS1 Antagonize Protein Kinase R To

Facilitate Virus Replication. *J. Virol.* **90**, 3839-3848 (2016)

97. P. A. Clarke, N. A. Sharp, M. J. Clemens, Translational control by the Epstein-Barr virus small RNA EBER-1: Reversal of the double-stranded RNA-induced inhibition of protein synthesis in reticulocyte lysates. *Eur. J. Biochem.* **193**, 635-41 (1990)

98. J. Poppers, M. Mulvey, C. Perez, D. Khoo, I. Mohr, Identification of a Lytic-Cycle Epstein-Barr Virus Gene Product That Can Regulate PKR Activation. *J. Virol.* **77**, 228-36 (2003)

99. L. Burysek, P. M. Pitha, Latently Expressed Human Herpesvirus 8-Encoded Interferon Regulatory Factor 2 Inhibits Double-Stranded RNA-Activated Protein Kinase. *J. Virol.* **75**, 2345-52 (2002)

100. N. R. Sharma, V. Majerciak, M. J. Kruhlak, Z. M. Zheng, KSHV inhibits stress granule formation by viral ORF57 blocking PKR activation. *PLoS Pathog.* **13**, e1006677 (2017)

101. M. Esteban, *et al.*, The latency protein LANA2 from Kaposi's sarcoma-associated herpesvirus inhibits apoptosis induced by dsRNA-activated protein kinase but not RNase L activation. *J. Gen. Virol.* **84**, 1463-70 (2003)

102. R. S. Valchanova, M. Picard-Maureau, M. Budt, W. Brune, Murine Cytomegalovirus m142 and m143 Are both Required To Block Protein Kinase R-Mediated Shutdown of Protein Synthesis. *J. Virol.* **80**, 10181-90 (2006)

103. C. Peng, S. L. Haller, M. M. Rahman, G. McFadden, S. Rothenburg, Myxoma virus M156 is a specific inhibitor of rabbit PKR but contains a loss-of-function mutation in Australian virus isolates. *PNAS.* **113**, 3855-60 (2016)

104. M. M. Rahman, J. Liu, W. M. Chan, S. Rothenburg, G. McFadden, Myxoma Virus Protein M029 Is a Dual Function Immunomodulator that Inhibits PKR and Also Conscripts RHA/DHX9 to Promote Expanded Host Tropism and Viral Replication. *PLoS Pathog.* **9**, e1003465 (2013)

105. M. V Davies, H. W. Chang, B. L. Jacobs, R. J. Kaufman, The E3L and K3L vaccinia virus gene products stimulate translation through inhibition of the double-stranded RNA-dependent protein kinase by different mechanisms. *J. Virol.* **67**, 1688-92 (1993)

106. H. W. Chang, J. C. Watson, B. L. Jacobs, The E3L gene of vaccinia virus encodes an inhibitor of the interferon-induced, double-stranded RNA-dependent protein kinase. *PNAS.* **89**, 4825–4829 (1992)

107. A. C. Dar, F. Sicheri, X-ray crystal structure and functional analysis of vaccinia virus K3L reveals molecular determinants for PKR subversion and substrate recognition. *Mol. Cell* **10**, 295-305 (2002)

108. K. Carroll, O. Elroy-Stein, B. Moss, R. Jagus, Recombinant vaccinia virus K3L gene product prevents activation of double- stranded RNA-dependent, initiation factor 2α-specific protein kinase. *J. Biol. Chem.* **268**, 12837-42 (1993)

109. K. L. Willis, S. Patel, Y. Xiang, J. L. Shisler, The effect of the vaccinia K1 protein on the PKR-eIF2α pathway in RK13 and HeLa cells. *Virology* **394**, 73-81 (2009)

110. K. Childs, A. Moon, S. Goodbourn, L. K. Dixon, F. Zhang, The African Swine Fever Virus DP71L Protein Recruits the Protein Phosphatase 1 Catalytic Subunit To Dephosphorylate eIF2α and Inhibits CHOP Induction but Is Dispensable for These Activities during Virus Infection. *J. Virol.* **84**, 10681-9 (2010)

111. S. Kazemi, *et al.*, Control of Alpha Subunit of Eukaryotic Translation Initiation Factor 2 (eIF2) Phosphorylation by the Human Papillomavirus Type 18 E6 Oncoprotein: Implications for eIF2 -Dependent Gene Expression and Cell Death. *Mol. Cell. Biol.* **24**, 3415-29 (2004)

112. S. Rothenburg, V. G. Chinchar, T. E. Dever, Characterization of a ranavirus inhibitor of the antiviral protein kinase PKR. *BMC Microbiol.* **11**, 56 (2011)

113. J. J. Li, *et al.*, Baculovirus protein PK2 subverts eIF2α kinase function by mimicry of its kinase domain C-lobe. *PNAS.* **112**, E4364-73 (2015)

114. Z. Yue, A. J. Shatkin, Double-stranded RNA-dependent protein kinase (PKR) is regulated by reovirus structural proteins. *Virology* **234**, 364-71 (1997)

115. J. O. Langland, S. Pettiford, B. Jiang, B. L. Jacobs, Products of the porcine group C rotavirus NSP3 gene bind specifically to double-stranded RNA and inhibit activation of the interferon-induced protein kinase PKR. *J. Virol.* **68**, 3821-9 (1994)

116. M. E. Spurgeon, D. A. Ornelles, The Adenovirus E1B 55-Kilodalton and E4 Open Reading Frame 6 Proteins Limit Phosphorylation of eIF2 during the Late Phase of Infection. *J. Virol.* **83**, 9970-82 (2009)

117. J. Kitajewski, *et al.*, Adenovirus VAI RNA antagonizes the antiviral action of interferon by preventing activation of the interferon-induced eIF-2α kinase. *Cell* **45**, 195-200 (1986)

118. M. Gale, *et al.*, Control of PKR Protein Kinase by Hepatitis C Virus Nonstructural 5A Protein: Molecular Mechanisms of Kinase Regulation. *Mol. Cell. Biol.* **18**, 5208–5218 (1998)

119. D. R. Taylor, S. T. Shi, P. R. Romano, G. N. Barber, M. M. C. Lai, Inhibition of the interferon-inducible protein kinase PKR by HCV E2 protein. *Science.* **285**, 107-10 (1999)

120. N. Pavio, P. R. Romano, T. M. Graczyk, S. M. Feinstone, D. R. Taylor, Protein synthesis and endoplasmic reticulum stress can be modulated by the hepatitis C virus envelope protein E2 through the eukaryotic initiation factor 2 alpha kinase PERK. *J. Virol.* **77**, 3578-85 (2003)

121. P. A. Egan, Hepatitis C Virus Envelope Protein E1 Binds PERK and Represses the Unfolded Protein Response. *Open Virol. J.* **7**, 37-40 (2013)

122. J. Vyas, A. Elia, M. J. Clemens, Inhibition of the protein kinase PKR by the internal ribosome entry site of hepatitis C virus genomic RNA. *RNA* **9**, 858-70 (2003)

123. Y.-C. Tu, *et al.*, Blocking Double-Stranded RNA-Activated Protein Kinase PKR by Japanese Encephalitis Virus Nonstructural Protein 2A. *J. Virol.* **86**, 10347-58 (2012)

124. R. Cai, B. Carpick, R. F. Chun, K. T. Jeang, B. R. G. Williams, HIV-1 TAT inhibits PKR activity by both RNA-dependent and RNA- independent mechanisms. *Arch. Biochem. Biophys.* **373**, 361-7 (2000)

125. A. P. S. Rathore, M. L. Ng, S. G. Vasudevan, Differential unfolded protein response during Chikungunya and Sindbis virus infection: CHIKV nsP4 suppresses eIF2α phosphorylation. *Virol. J.* **10**, 36 (2013)

126. K. Takeuchi, T. Komatsu, Y. Kitagawa, K. Sada, B. Gotoh, Sendai Virus C Protein Plays a Role in Restricting PKR Activation by Limiting the Generation of Intracellular Double-Stranded RNA. *J. Virol.* **82**, 10102-10 (2008)

127. M. D. Gainey, P. J. Dillon, G. D. Parks, K. M. Clark, M. J. Manuse, Paramyxovirus-Induced Shutoff of Host and Viral Protein Synthesis: Role of the P and V Proteins in Limiting PKR Activation. *J. Virol.* **82**, 828-39 (2007)

128. K. Sharma, *et al.*, Influenza a virus nucleoprotein exploits Hsp40 to inhibit PKR activation. *PLoS One* **6**, e20215 (2011)

129. Z. Feng, M. Cerveny, Z. Yan, B. He, The VP35 protein of Ebola virus inhibits the antiviral effect mediated by double-stranded RNA-dependent protein kinase PKR. *J. Virol.* **81**, 182–192 (2007).

130. D. J. Groskreutz, E. C. Babor, M. M. Monick, S. M. Varga, G. W. Hunninghake, Respiratory syncytial virus limits α subunit of eukaryotic translation initiation factor 2 (eIF2α) phosphorylation to maintain translation and viral replication. *J. Biol. Chem.* **285**, 24023-31 (2010)

Table 1. Overview of viral ISR antagonists

Virus	Family	Genome	Protein	Target*	Class	Reference
Herpes Simplex Virus	Herpesviridae	dsDNA	US11	PKR	1	(92, 93)
			gB	PERK	1	(65)
			ICP34.5	PP1	3	(94)
Human Cytomegalovirus	Herpesviridae	dsDNA	TRS1	PKR & HRI	1	(66, 95, 96)
			IRS1	PKR	1	(95, 96)
Epstein-Barr Virus	Herpesviridae	dsDNA	EBER RNA	PKR	1	(97)
			Sm	PKR	1	(98)
Kaposi's Sarcoma-Associated Herpes Virus	Herpesviridae	dsDNA	vIRF-2	PKR	1	(99)
			ORF57	PKR	1	(100)
			LANA2	PKR	1 or 2†	(101)
Mouse Cytomegalovirus	Herpesviridae	dsDNA	m142, m143	PKR	1	(102)
Myxoma virus	Poxviridae	dsDNA	M156	PKR	2	(103)
			M029	PKR	1	(104)
Vaccinia Virus	Poxviridae	dsDNA	E3L	PKR	1	(105, 106)
			K3L	PKR	1 & 2‡	(105, 107, 108)
			K1	PKR	1	(109)
Swinepox	Poxviridae	dsDNA	C8L	PKR	2	(67)
African Swine Fever Virus	Asfarviridae	dsDNA	DP71L	PP1	3	(110)
Human Papillomavirus	Papillomaviridae	dsDNA	E6	PP1	3	(111)
Ranavirus	Iridoviridae	dsDNA	vIF2α	PKR	2	(112)
Baculovirus	Baculoviridae	dsDNA	PK2	PKR, HRI, & PERK	1	(113)
Reovirus	Reoviridae	dsRNA	Sigma3	PKR	1	(114)
Rotavirus	Reoviridae	dsRNA	Nsp3	PKR?	1	(115)
Adenovirus	Adenoviridae	dsRNA	E1B-55K, E4orf6	PKR	1	(116)
			VAI RNA	PKR	1	(117)
Hepatitis C Virus	Flaviviridae	Pos. RNA	NS5a	PKR	1	(118)
			E2	PKR & PERK	1	(119, 120)
			E1	PERK	1 or 2†	(121)
			IRES	PKR	1	(122)
Japanese Encephalitis Virus	Flaviviridae	Pos. RNA	Ns2a	PKR	1	(123)
Human Immunodeficiency Virus	Retroviridae	Pos. RNA	Tat	PKR	1 & 2‡	(63, 124)
Chikungunya Virus	Togaviridae	Pos. RNA	Nsp4	PERK	2	(125)

Transmissible Gastroenteritis Virus	**Coronaviridae**	**Pos. RNA**	**7**	**PP1**	**3**	(69)
Infectious Bronchitis Virus	**Coronaviridae**	**Pos. RNA**	**Nsp2**	**PKR**	**1**	(79)
Mouse Hepatitis Virus	**Coronaviridae**	**Pos. RNA**	**Nsp15**	**PKR**	**1**	(62)
Encephalomyocarditis Virus	**Picornaviridae**	**Pos. RNA**	**Leader**	**PKR**	**1**	(82)
Sendai virus	**Paramyxoviridae**	**Neg. RNA**	**C**	**PKR**	**1**	(126)
Simian Virus	**Paramyxoviridae**	**Neg. RNA**	**P, V**	**PKR**	**1**	(127)
Influenza A Virus	**Orthomyxoviridae**	**Neg. RNA**	**NS1**	**PKR**	**1**	(61)
			NP	**PKR**	**1**	(128)
Andes virus	**Hantaviridae**	**Neg. RNA**	**N**	**PKR**	**1**	(64)
Rift Valley Fever Virus	**Phenuiviridae**	**Neg. RNA**	**NSs**	**PKR**	**2**	(68)
Ebola Virus	**Filoviridae**	**Neg. RNA**	**VP35**	**PKR**	**1**	(129)
Respiratory Syncytial Virus	**Pneumoviridae**	**Neg. RNA**	**N**	**PKR**	**2**	(130)

* Listed are only the tested targets. Some antagonists may affect more proteins than shown in the table

† Distinction cannot be made based on available data

‡ These proteins function both as a Class 1 antagonist and Class 2 antagonist

Chapter 2

Middle East respiratory coronavirus accessory protein 4a inhibits PKR-mediated antiviral stress responses

Huib H. Rabouw[1], Martijn A. Langereis[1,#], Robert C.M. Knaap[2,#], Tim J. Dalebout[2], Javier Canton[3], Isabel Sola[3], Luis Enjuanes[3], Peter J. Bredenbeek[2], Marjolein Kikkert[2], Raoul J. de Groot[1], and Frank J.M. van Kuppeveld[1]

[1]Virology Division, Department of Infectious Diseases and Immunology, Faculty of Veterinary Medicine, Utrecht University, 3584 CL, Utrecht, The Netherlands

[2]Molecular Virology Laboratory, Department of Medical Microbiology, Leiden University Medical Center, 2333 ZA, Leiden, The Netherlands

[3]Department of Molecular and Cell Biology, National Center of Biotechnology (CNB-CSIC), Campus Universidad Autonoma de Madrid, Madrid, Spain

[#]*These authors contributed equally*

PLoS Pathogens ***12****, e1005982 (2016)*

Abstract

Middle East respiratory syndrome coronavirus (MERS-CoV) causes severe respiratory infections that can be life-threatening. To establish an infection and spread, MERS-CoV, like most other viruses, must navigate through an intricate network of antiviral host responses. Besides the well-known type I interferon (IFN-α/β) response, the protein kinase R (PKR)-mediated stress response is being recognized as an important innate response pathway. Upon detecting viral dsRNA, PKR phosphorylates eIF2α, leading to the inhibition of cellular and viral translation and the formation of stress granules (SGs), which are increasingly recognized as platforms for antiviral signaling pathways. It is unknown whether cellular infection by MERS-CoV activates the stress response pathway or whether the virus has evolved strategies to suppress this infection-limiting pathway. Here, we show that cellular infection with MERS-CoV does not lead to the formation of SGs. By transiently expressing the MERS-CoV accessory proteins individually, we identified a role of protein 4a (p4a) in preventing activation of the stress response pathway. Expression of MERS-CoV p4a impeded dsRNA-mediated PKR activation, thereby rescuing translation inhibition and preventing SG formation. In contrast, p4a failed to suppress stress response pathway activation that is independent of PKR and dsRNA. MERS-CoV p4a is a dsRNA binding protein. Mutation of the dsRNA binding motif in p4a disrupted its PKR antagonistic activity. By inserting p4a in a picornavirus lacking its natural PKR antagonist, we showed that p4a exerts PKR antagonistic activity also under infection conditions. However, a recombinant MERS-CoV deficient in p4a expression still suppressed SG formation, indicating the expression of at least one other stress response antagonist. This virus also suppressed the dsRNA-independent stress response pathway. Thus, MERS-CoV interferes with antiviral stress responses using at least two different mechanisms, with p4a suppressing the PKR-dependent stress response pathway, probably by sequestering dsRNA. MERS-CoV p4a represents the first coronavirus stress response antagonist described.

Summary

Human coronaviruses generally cause relatively mild respiratory disease. In the past 15 years, the world has witnessed the emergence of two coronaviruses with high mortality rates in humans; severe acute respiratory syndrome coronavirus (SARS-CoV) in 2002 and Middle East respiratory syndrome coronavirus (MERS-CoV) in 2012, both originating from animal reservoirs. Successful infection of a host not only depends on the presence of an appropriate receptor but also on the ability of a virus to evade innate antiviral host responses, which constitute the first line of defense against invading viruses. MERS-CoV has been reported to actively suppress the IFN-α/β response, but it is unknown whether it also interferes with another important innate antiviral response, the stress response pathway. Activation of this pathway by a kinase, PKR, curtails virus infection by shutting off cellular and viral protein synthesis. To date, no coronavirus protein has been recognized to suppress the stress response pathway. Here, we show that the accessory protein 4a of MERS-CoV is a potent stress antagonist that prevents PKR activation by sequestering its ligand, dsRNA. This finding furthers our understanding of the molecular mechanism used by MERS-CoV to evade infection-limiting antiviral host responses and may provide new avenues for therapeutic intervention.

Introduction

Innate antiviral responses represent the first line of defense against invading viral pathogens. Host cells are equipped with multiple mechanisms to detect and respond to non-self, pathogen-associated molecular patterns (PAMPs). One of these PAMPs, viral cytosolic RNA, can be detected by RIG-I-like receptors (RLRs), such as melanoma differentiation-associated protein 5 (MDA5) and retinoic acid inducible gene 1 (RIG-I). Upon recognition of viral, non-self RNA, signal transduction pathways are activated, which results in the expression of type I interferons (IFN-α/β), proinflammatory cytokines and chemokines. Secreted IFN-α/β triggers the transcription of interferon-stimulated genes (ISGs), both in infected as neighboring cells, and thereby implements an antiviral state that restricts virus propagation in the host.

Growing evidence points to an important role of the stress response pathway as an additional innate antiviral response (1, 2). One of the ISGs, protein kinase R (PKR), detects viral RNA in the cytoplasm, which induces its autophosphorylation and subsequent phosphorylation of the alpha subunit of eukaryotic translation initiation factor 2 (eIF2α). PKR mediated phosphorylation of eIF2α inactivates (viral) protein synthesis, thereby affecting virus propagation. Stalled translation initiation complexes, together with nucleating factors like G3BP1, G3BP2, TIA-1 and many translation initiation factors like eIF3, form cytoplasmic aggregates, which are called stress granules (SGs). The role of these SGs remains controversial, but growing evidence points to a role of these SGs as a platform for antiviral signal transduction (3–5).

To ensure efficient virus replication, many viruses encode proteins with specialized functions to evade innate antiviral responses, although their mode of action and the point of interference may differ. Viruses usually interfere in several antiviral pathways and even disrupt pathways at multiple levels, to ensure efficient suppression of the host innate antiviral responses. A well-studied example is the Influenza A virus NS1 protein, which, among many other evasive functions, shields viral double-stranded RNA (dsRNA) from detection by both RLRs and PKR (6, 7), thus blocking IFN-α/β and antiviral stress response pathways, respectively.

Coronaviruses are large positive-stranded RNA viruses belonging to the order *Nidovirales*. The coronavirus genome is typically between 26 and 32 kb in size and encodes more than 20 proteins. The 5’ open reading frame (ORF)1ab encodes the non-structural proteins (nsps), which together form the replication-transcription machinery. The 3’ end of the coronavirus genome contains several additional

ORFs encoding the structural proteins and a varying number of accessory proteins. These accessory proteins often lack any detectable homology to other viral or host proteins and their function is unknown in many cases. A common feature, however, is that they are often not essential for virus replication *per se* but are important for virulence, suggesting that accessory proteins serve to modulate host antiviral responses (8–13).

Human coronaviruses generally cause mild respiratory symptoms. Exceptions are severe acute respiratory coronavirus (SARS-CoV), which emerged in China in 2002 through cross-species transmissions from bats and civet cats (14), and Middle East respiratory syndrome coronavirus (MERS-CoV), which emerged in the Arabian Peninsula in 2012. MERS-CoV causes acute and severe respiratory symptoms and continues to make a serious impact on the local as well as the global health system with over 1,694 laboratory confirmed cases and 605 deaths as of March 21st 2016 (15). This virus is believed to be transmitted to humans primarily via animal hosts, most likely dromedary camels (16, 17). As yet, little is known about how MERS-CoV modulates host antiviral responses. There is firm evidence that MERS-CoV inhibits IFN-α/β production (18–20) and several viral proteins have been implicated in this evasion mechanism – including accessory protein 4a (p4a), which is a dsRNA-binding protein (21–23) – but the inhibitory effect of these proteins on innate antiviral responses has thus far only been demonstrated in transfected cells expressing these viral proteins, not during virus infection. Whether MERS-CoV has also evolved mechanisms to modulate the stress response pathway is unknown thus far.

Here, we show for the first time that MERS-CoV actively suppresses the stress response pathway and we identify the accessory protein 4a as a potent inhibitor of the PKR-mediated stress response pathway. Furthermore, we provide evidence that the rescue of translation and inhibition of SG formation rely on p4a's dsRNA-binding function, suggesting that it exerts antagonistic activity by sequestering dsRNA from recognition by PKR. Moreover, evidence for the existence of at least one other MERS-CoV encoded stress response antagonist is provided.

Results

MERS-CoV blocks stress responses in infected cells. To investigate whether MERS-CoV infection activates the stress response pathway, Vero cells were infected with MERS-CoV (MOI=1) and analyzed for the occurrence of SG at regular time intervals by visualizing the subcellular localization of eIF3 and G3BP2, which are established markers for SGs. In parallel, the efficiency of virus infection was monitored by visualizing dsRNA using the J2 antibody. Despite efficient virus infection and replication, as indicated by the accumulation of considerable amounts of viral dsRNA in the cytosol, no SGs were observed at any of the indicated time points (Fig 1A). The lack of SGs was not due to an intrinsic defect in the stress response pathway of Vero cells as clear SGs were formed upon arsenic acid treatment and poly(I:C) transfection (Fig 1B). Together, these findings indicate that MERS-CoV either hides its viral RNA from detection by PKR, possibly through the formation of double membrane vesicles (24), and/or that it encodes one or more antagonists to suppress activation of the stress response pathway.

MERS-CoV p4a suppresses dsRNA- and PKR-dependent formation of SGs. To investigate whether MERS-CoV accessory proteins can suppress the stress response pathway, we expressed them individually as EGFP fusion proteins and monitored SG formation in transfected cells. This approach is based on the observation that transfection of plasmid DNA, and in particular the pEGFP plasmids, can activate PKR, most likely due to the production of dsRNA formed from positive and negative sense mRNA transcription from cryptic promoters in these plasmids (25). Indeed, we observed that transfection of pEGFP plasmid DNA in HeLa cells triggered SG formation in a PKR-dependent manner, as no SGs were observed in PKR knockout cells (HeLa-PKR^{KO}), which we generated using the CRISPR-Cas9 system (see Fig S1) (Fig 2A and B). Also, using the J2 anti-dsRNA antibody, we noticed a significant increase in dsRNA levels in cells transfected with pEGFP plasmid DNA and especially in cells that displayed SGs (Figs 2C and D). This phenomenon was not restricted to the pEGFP plasmid as all plasmids with eukaryotic promoters induced SG formation in our HeLa cells, albeit to different levels, while those with prokaryotic promoters did not (Fig S2). Together, these data support the idea that transfection of pEGFP plasmid DNA can trigger dsRNA-dependent and PKR-mediated SG formation, and provide the basis for a convenient and versatile method to test potential antagonistic activities of viral proteins by expressing them as EGFP fusion proteins.

Plasmids each encoding one of the four MERS-CoV accessory proteins fused to EGFP were transfected into HeLa cells. As a positive control, we took along an EGFP fusion of the influenza A virus (IAV) NS1 protein, which is an established PKR antagonist. As shown in Figure 2E, plasmid DNA transfection

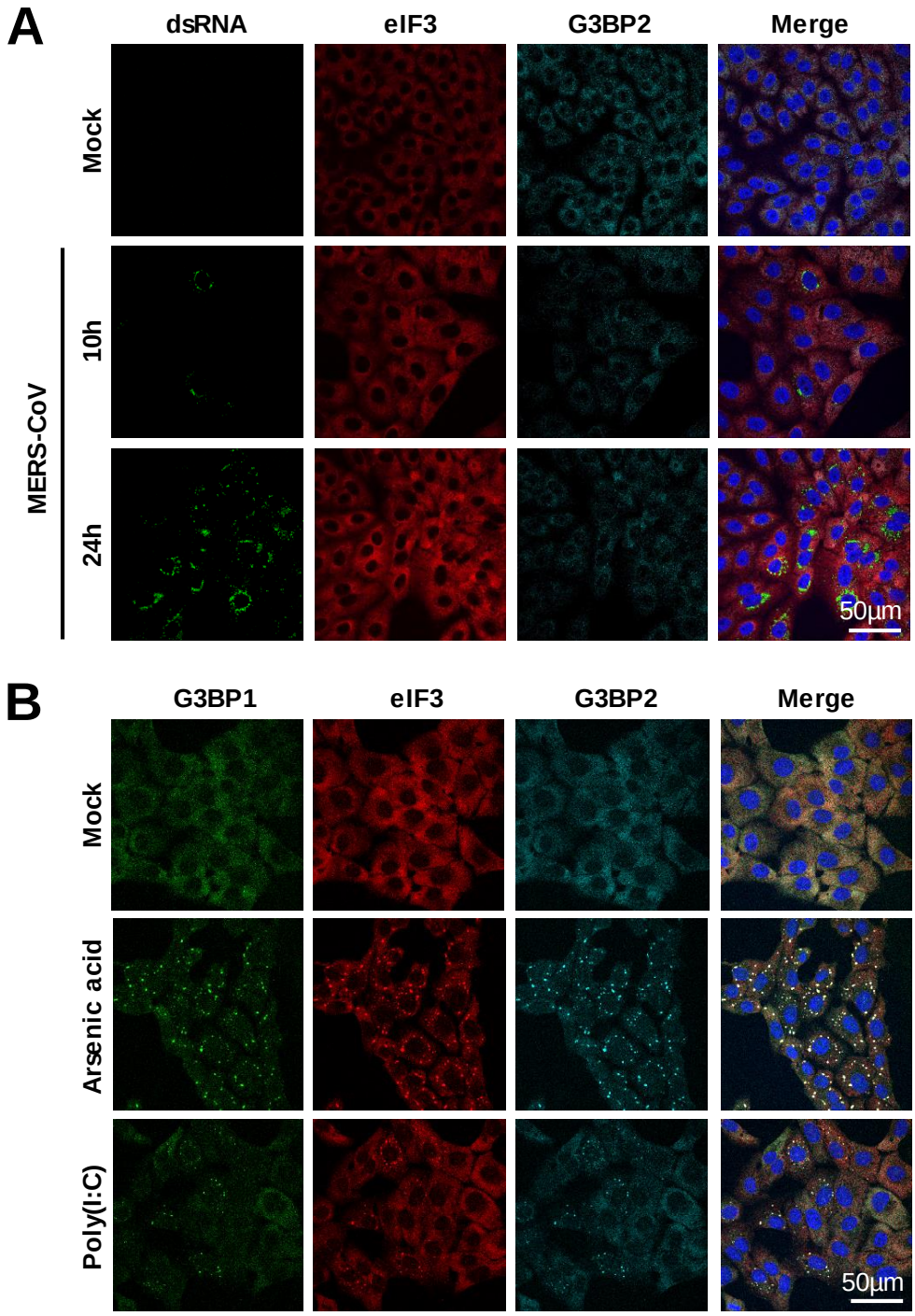

Figure 1. MERS-CoV infection fails to activate the stress response pathway. *(A) Immunofluorescence images of mock-treated an MERS-CoV infected Vero cells. Cells were infected with an MOI of 1 and fixed using 3% paraformaldehyde in PBS at 10 h or 24 h post infection. Cells were stained for dsRNA, and stress granule markers eIF3 and G3BP2. (B) Immune fluorescence images of cells treated with arsenic acid (0.5 mM for 60 min) or transfected with poly(I:C) and stained for eIF3, G3BP1 and G3BP2.*

induced SG formation except for the plasmids encoding the MERS-CoV p4a and IAV NS1 EGFP fusion proteins. The absence of SG formation (Fig 2E and 2F) coincided with a lack of PKR phosphorylation (Fig 2G). We also tested the ability of these MERS-CoV accessory proteins to suppress the stress response pathway induced by the more commonly applied method of poly(I:C) transfection. Again, we observed that p4a, but none of the other MERS-CoV accessory proteins, suppressed SG formation (Fig S3). The inhibitory effect of p4a, as well as that of NS1, was less pronounced in this assay, possibly because the relatively large amounts of poly(I:C) may exceed the maximum capacity of the PKR antagonists. Taken together, our data suggests that MERS-CoV p4a is a PKR antagonist and inhibits the stress response pathway at the level of, or upstream of, PKR phosphorylation.

MERS-CoV p4a suppresses PKR-mediated translation inhibition. We observed that the protein levels of p4a and NS1 were higher than those of the other MERS-CoV accessory proteins (Fig 2E). We reasoned that the inhibition of plasmid DNA-induced PKR activation may increase protein translation levels. Indeed, co-expression of p4a or NS1 together with *Renilla* luciferase (RLuc) caused a reproducible 5- to 10-fold increase in luciferase counts compared to the EGFP control plasmid (Fig. 3A). This effect was attributed to increased translation, since p4a expression had no effect on RLuc mRNA levels. In addition, RLuc counts were not increased in PKR^{KO} cells, indicating that p4a increases translation efficiency via inhibition of PKR (Fig S4). Other established viral PKR antagonists like the Vaccinia virus E3L (26) and Ebola virus VP35 (27) caused a similar increase in RLuc expression levels. Comparable results were obtained upon co-expression with an RFP expression plasmid (Fig 3B). These data are in line with the observation that MERS-CoV p4a antagonizes PKR activity, and provide another indication that viral PKR antagonists can rescue translation efficiency in cells in which the stress pathway is activated by (viral) dsRNA.

MERS-CoV p4a fails to inhibit PKR-independent stress pathway activation. Both MERS-CoV p4a and IAV NS1 are dsRNA binding proteins (6, 21), which suggests that p4a shields the viral dsRNA from detection by PKR. To test whether p4a can also inhibit stress pathway activation via PKR- and dsRNA-independent mechanisms, we used arsenic acid and heat shock to induce eIF2α-dependent stress pathway activation (28). Furthermore, we used pateamine A to induce SG formation via an eIF2α-independent mechanism (29). In agreement with earlier findings, IAV NS1 failed to inhibit PKR-independent SG formation (30). A small reduction in PKR-independent SG formation was observed in cells overexpressing p4a (Figs 4A and B). However, lack of SGs was only observed in cells expressing very high levels of p4a, whereas a moderate expression level of p4a was already sufficient to inhibit PKR-mediated SG formation (Figs 2E). To rule out any involvement of PKR expression in the small reduction of PKR-independent SG formation, we tested arsenic acid, heat shock and pateamine A-

induced stress pathway activation in HeLa-PKR^{KO} cells. Also under these conditions, expression of p4a affected SG formation only in a small fraction of the cells (Figs 4C and D). Thus, MERS-CoV p4a seems to predominantly suppress dsRNA-dependent PKR activation and does not efficiently target other parts of the stress response pathway.

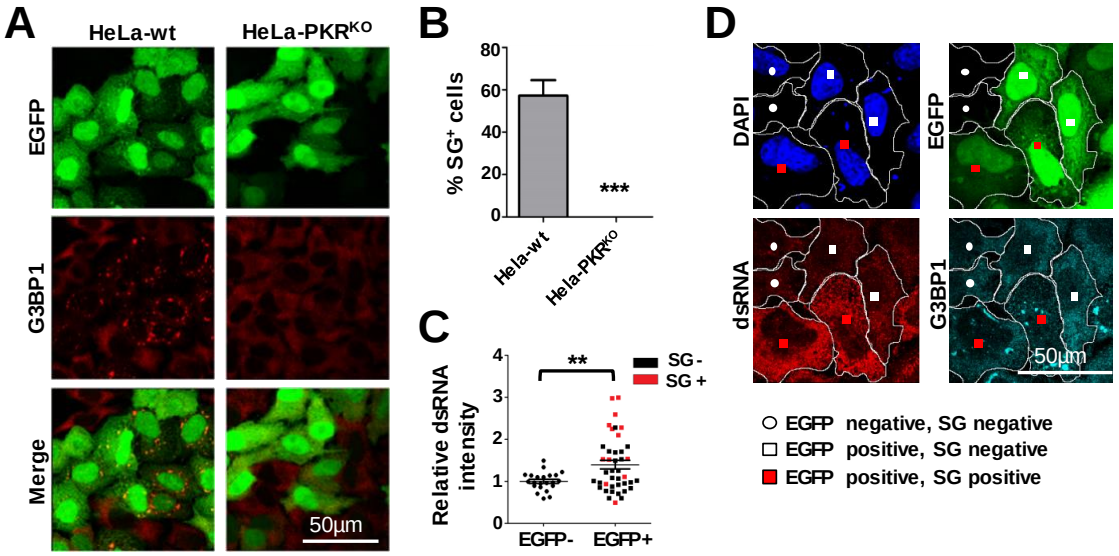

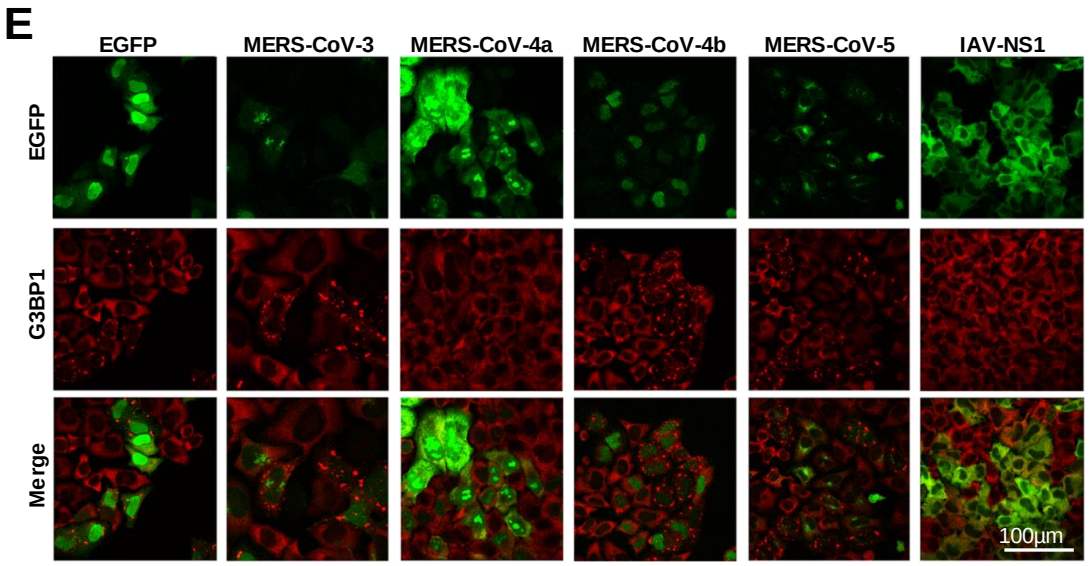

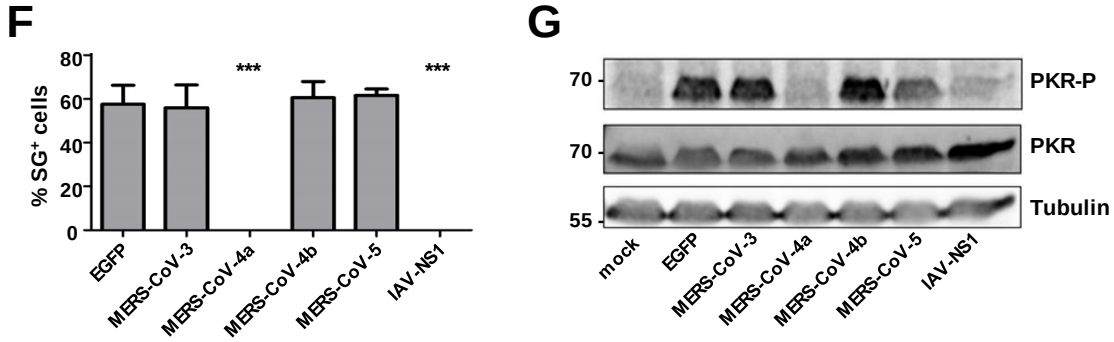

Figure 2. MERS-CoV p4a suppresses dsRNA-dependent and PKR-mediated stress in transfected cells. *(A) Immune fluorescence images of HeLa-wt or HeLa-PKR^{KO} cells transfected with pEGFP-N3 plasmid (500 ng/well). Cells were fixed at 24h post transfection using paraformaldehyde and stained for G3BP1 (shown in red). EGFP expression is shown in green. (B) Quantification of SG-positive cells. SG-positive cells were quantified from three randomly selected images. Shown are means with standard deviations, analyzed using an unpaired t-test (***, p<0.001). (C) Quantification of the average dsRNA staining intensity in individual cells using imageJ software. Intensity levels are plotted relative to that of the non-transfected cells from the same images. Cells were classified as non-transfected or transfected based on EGFP expression, and as SG-positive or SG-negative based on presence of G3BP1 aggregates. Differences in relative dsRNA intensity levels were analyzed using an unpaired t-test (**, p<0.01). (D) Typical example of the IFA images used for quantification in C. Borders of two cells of each phenotype (EGFP-; EGFP+SG-; EGFP+SG+) are indicated in white. (E) Immune fluorescence images of HeLa cells transfected with pEGFP expression plasmids. Cells were fixed at 24h post transfection and stained for G3BP1 (shown in red). EGFP expression is shown in green. (F) Quantification of SG-positive cells. Analysis was performed as described in panel B (***, p<0.001). (G) Western blot analysis of PKR and phospho-PKR in HeLa cell lysates at 24h post pEGFP plasmid transfection. Tubulin expression was detected as loading control.*

MERS-CoV p4a can functionally replace the PKR antagonist of a picornavirus. Studying immune evasion functions of viral proteins by transient overexpression from plasmid DNA may suffer from shortcomings. Transfection procedures fail to mimic the dynamic interplay between dsRNA and the antagonist, both of which gradually appear over time during the viral life cycle. Furthermore, transfection may yield non-physiologically high levels of viral proteins and/or dsRNA mimics which may blur results. Also, dsRNA-mimicking molecules, like poly(I:C), may be delivered to compartments where viral dsRNA does not naturally localize under infection conditions.

Therefore, we set out to investigate the function of p4a as an innate antiviral response antagonist under infection conditions. For this, we made use of a recombinant encephalomyocarditis virus (EMCV, strain mengovirus). EMCV is a member of the picornavirus family that, like coronaviruses, produces dsRNA replication intermediates during its life cycle. In the recombinant EMCV, the function of the leader (L) protein – which antagonizes the dsRNA-triggered IFN-α/β and stress response pathways – is disturbed by specific mutations in an essential zinc-finger motif (EMCV-L-Zn) (31, 32). By consequence, and in contrast to wt virus, EMCV-L-Zn causes strong activation of the IFN-α/β and stress response pathways (31, 32).

To study whether heterologous expression of p4a can prevent PKR activation, recombinant viruses were generated expressing Strep2-tagged MERS-CoV p4a or IAV NS1 (as a control) upstream of the inactivated L (Fig 5A). EMCV wt infection did not induce SG formation while EMCV-L-Zn induced SGs in

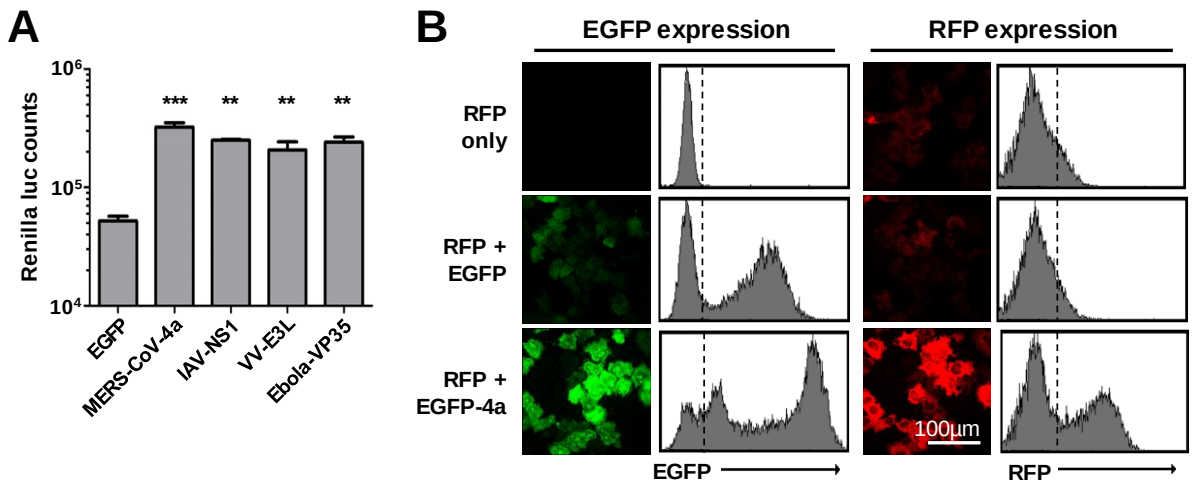

Figure 3. MERS-CoV p4a rescues protein translation upon plasmid DNA transfection-mediated stress. *(A) Bar-graph showing Renilla luciferase counts measured at 16h post co-transfection of pTK-RLuc and pEGFP expression plasmids. Means and standard deviations are shown of triplicate measurements. Data was analyzed using an unpaired t-test (***, p<0.001; **, p<0.01). (B) Flow cytometry analysis of HeLa cells expressing RFP, RFP and EGFP, or RFP and EGFP-p4a. The dashed lines in the histograms divide non-RFP/EGFP expressing cells from RFP/EGFP-expressing cells.*

~80% of the cells. Infection of cells with recombinant EMCV-L-Zn expressing p4a or NS1 protein resulted in SG formation in <20% of the cells (Figs 5B and C). This reduction was not due to differences in infection efficiency, since Strep2-tagged proteins were detected in the majority of cells (Fig 4B). In fact, SGs were only observed in cells displaying low expression levels of p4a or IAV NS1.

Western blot analysis was performed to assess the level of PKR phosphorylation. Total PKR levels were significantly reduced in EMCV-infected cells, a phenomenon that was described earlier by Dubois *et al*.(33), although the mechanism behind this remains unclear. Yet, even with these reduced PKR levels, EMCV-L-Zn infection induced strong PKR phosphorylation, which was reversed by the expression of p4a or NS1 (Fig 5D). Analysis of viral protein levels using an antibody directed against the viral capsid indicated that viral protein levels were higher in cells infected with p4a- and NS1-expressing viruses compared to EMCV-L-Zn infected cells, indicating that expression of these PKR antagonists increased virus replication efficiency. Taken together, these results indicate that MERS-CoV p4a can functionally replace the PKR antagonist of a picornavirus in infected cells.

The MERS-CoV p4a dsRNA-binding domain is crucial for its function. MERS-CoV p4a contains a dsRNA-binding motif similar to those found in some cellular proteins (Fig S5). Previously, a p4a mutant

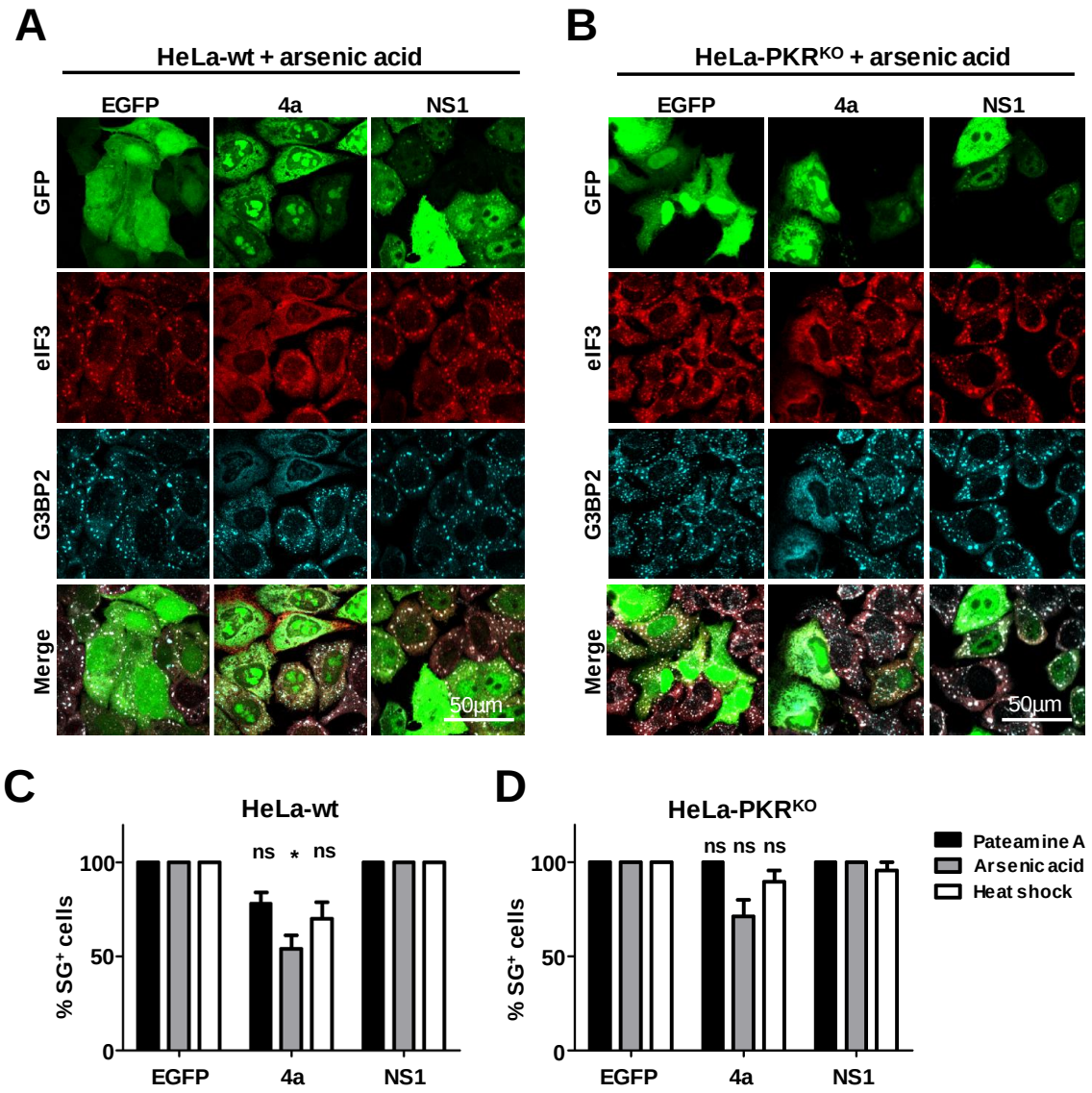

Figure 4. MERS-CoV p4a does not inhibit PKR-independent SG formation. *(A, B) Immune fluorescence images of HeLa-wt cells (A) and HeLa-PKR^{KO} cells (B) transfected with the indicated pEGFP-expression plasmids. Next day, SG formation was triggered using arsenic acid (0.5 mM for 30 min). Cells were fixed and stained for eIF3 (shown in red) or G3BP2 (shown in cyan). EGFP expression is shown in green. (C, D) Quantification of SG-positive HeLa-wt cells (C) and HeLa-PKR^{KO} cells (D) treated with Pateamine A (100 nM for 2h), arsenic acid (0.5 mM for 30 min), or heat shock (50 ℃ for 30 min). SG-positive cells were quantified from three randomly selected images. Shown are means with standard deviations, which were analyzed using an unpaired t-test. (*, p<0.05; ns, not significant).*

containing substitutions in its dsRNA-binding motif ($K^{63}A/K^{67}A$) was shown to be deficient in binding dsRNA (22). Based on the sequence similarity of this dsRNA-binding motif to those in Staufen, ADAR1, ADAR2 and PKR, and the published NMR structure of the ADAR2 dsRNA-binding domain in complex with its ligand (34), we designed a second mutant containing a single substitution ($Q^{9}P$) in another part

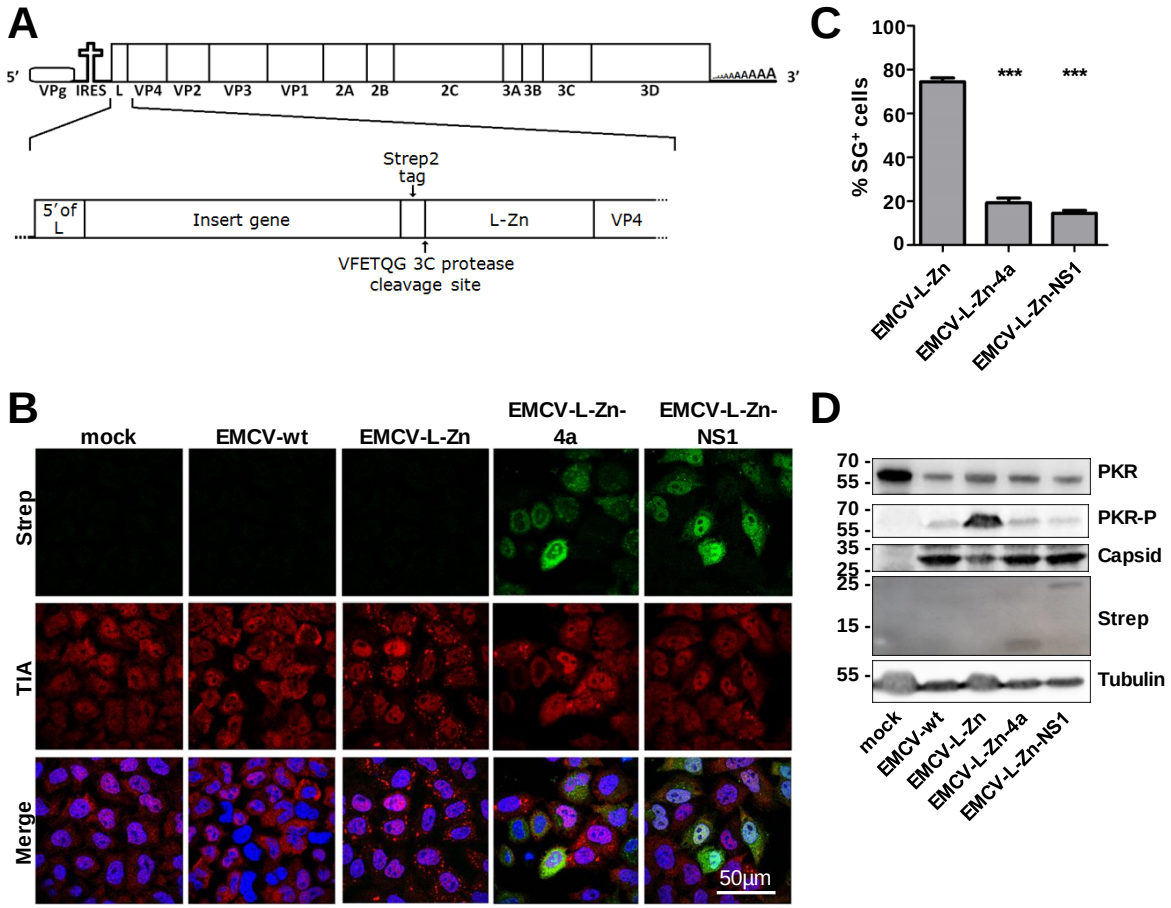

Figure 5. MERS-CoV p4a inhibits PKR activation during mengovirus infection. *(A) Schematic overview of the recombinant mengovirus system. The upper panel shows the wt mengovirus genome. The lower panel highlights the 5'-region showing the gene insertion upstream of the inactivated L. (B) Immune fluorescence images of HeLa-wt cells that were mock-infected or infected with wt mengovirus or the indicated recombinant mengoviruses (MOI=10). Cells were fixed at 6h post infection and stained for TIA1 (shown in red) and Strep-tagged p4a or NS1 (shown in green). Nuclei were stained using Hoechst-33258 (shown in blue). (C) SG-positive cells were quantified from three randomly selected images. Shown are means with standard deviations, which were analyzed using an unpaired t-test (***, p<0.001). (D) Western blot analysis of PKR and phospho-PKR in cells infected with indicated viruses. Capsid staining was used as a control for virus replication efficiency, tubulin staining was used as loading control and Strep-tag staining showed expression of the MERS-CoV p4a and IAV NS1.*

of the conserved dsRNA-binding motif (Fig S5). Infection of HeLa cells with recombinant EMCV-L-Zn viruses expressing either of these p4a mutants resulted in efficient SG formation, indicating a complete loss of the stress-antagonizing function (Figs 6A and B). In agreement herewith, analysis of the PKR phosphorylation status demonstrated that the p4a mutants failed to inhibit PKR phosphorylation (Fig 6C). Consistently, viruses expressing these mutants showed reduced capsid protein expression,

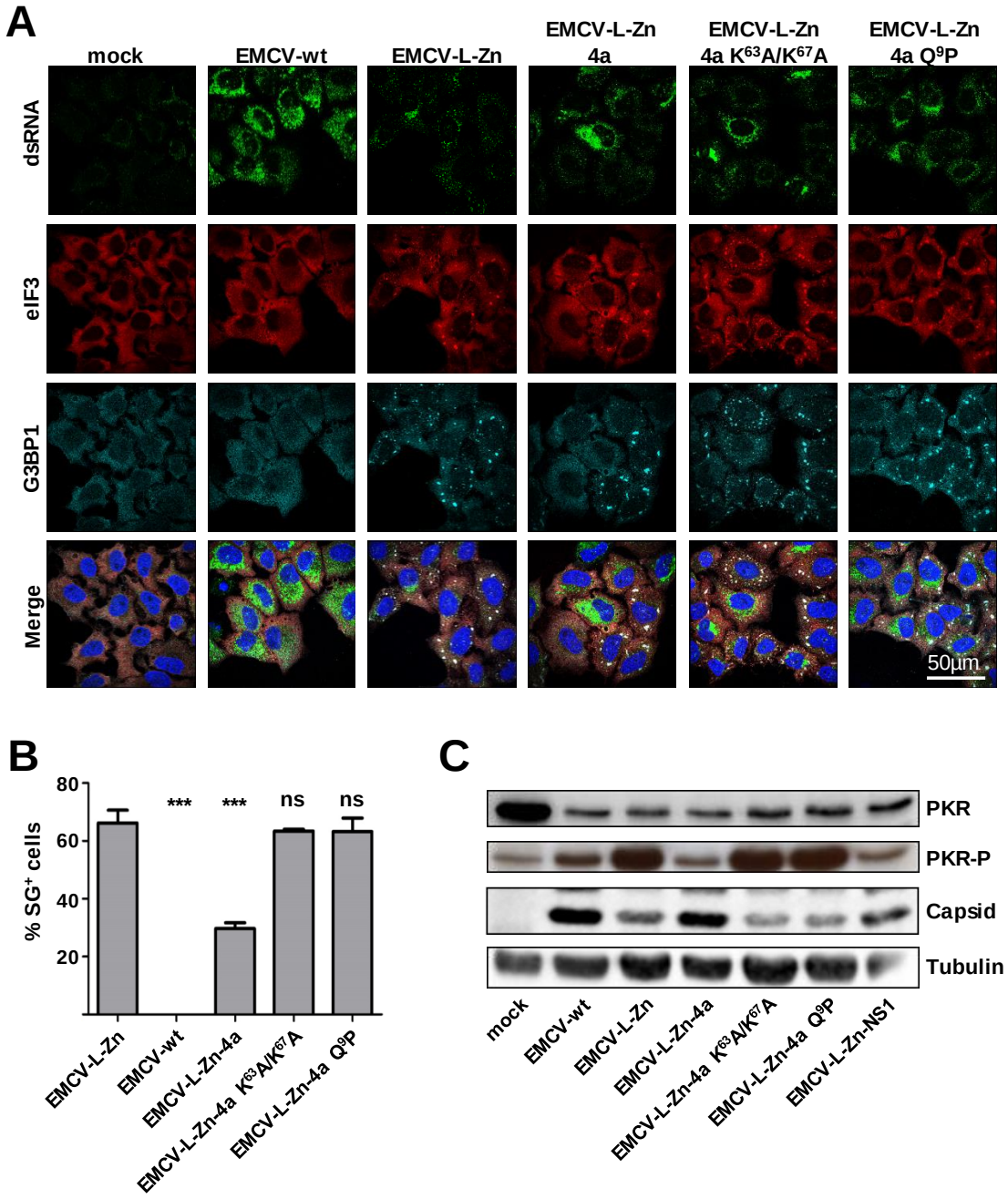

Figure 6. The dsRNA binding motif in MERS-CoV p4a is crucial for suppressing SG formation. *(A) Immune fluorescence images of HeLa-wt cells that were mock-treated or infected with wt mengovirus or the indicated recombinant mengoviruses (MOI=10). Cells were fixed at 6h post infection and stained for dsRNA (shown in green), eIF3 (shown in red), and G3BP1 (shown in cyan). Nuclei were stained using Hoechst-33258 (shown in blue). (B) SG-positive cells were quantified from three randomly selected images. Shown are means with standard deviations, analyzed using an unpaired t-test (***, p<0.001; ns, not significant). (C) Western blot analysis of PKR and phospho-PKR in cells infected with indicated viruses. Capsid staining was used as a control for virus replication efficiency and tubulin staining was used as loading control.*

possibly as a consequence of PKR-mediated translation inhibition. Thus, the dsRNA-binding motif in MERS-CoV p4a is essential for its function to antagonize PKR- mediated SG formation and translation shut-off.

Expression of MERS-CoV p4a also suppresses IFN-α/β pathway activation under infection conditions. Previous studies have shown that expression of p4a is able to reduce the level of IFN-α/β pathway activation in transiently transfected cells (21–23). Consistently, we observed that transient expression of p4a inhibited poly(I:C)-induced (Fig 7A) and dsRNA-induced (Fig 7B) *IFNβ* mRNA transcription. To assess whether p4a can also inhibit the IFN-α/β pathway in virus-infected cells, we compared *IFNβ* mRNA transcription levels in cells infected with recombinant EMCV-L-Zn viruses expressing either p4a or NS1. Both p4a and IAV NS1 significantly suppressed transcription of *IFNβ* mRNA (Fig 7C). This ability was lost in viruses expressing mutant p4a proteins that are unable to bind dsRNA (Fig 7). These data show that MERS-CoV p4a also inhibits the IFN-α/β response in EMCV-L-Zn-infected cells and that this function also requires its dsRNA-binding activity.

MERS-CoV p4a increases EMCV-L-Zn replication efficiency. Our data show that p4a is a multi-functional protein that antagonizes both the stress response and the IFN-α/β response pathways. To demonstrate the functional and beneficial role of p4a-mediated antagonism of the stress response pathway, we set out to compare the replication efficiency of recombinant viruses in HeLa-wt cells and cells that are defective in the PKR-induced stress response pathway (HeLa-PKR^{KO} cells). Infection of HeLa-PKR^{KO} cells with EMCV-L-Zn showed that these cells are unable to mount a stress response (Fig 8A), whereas IFN-α/β pathway activation was only slightly affected in these cells (Fig 8B), indicating that possible differences in virus fitness can be predominantly attributed to the defective stress response pathway. Replication of EMCV-L-Zn under low MOI infection conditions is severely impaired in HeLa-wt cells, whereas replication was fully rescued to the level of EMCV wt in HeLa-PKR^{KO} cells (Fig 8C). Comparison of the replication efficiency of recombinant viruses expressing p4a or the p4a mutant containing the K^{63}A/K^{67}A substitutions showed that the antagonistic activity of p4a provided a clear fitness advantage in HeLa-wt cells (Fig 8C). The observation that the p4a-expressing virus failed to replicate to similar titers as wt virus is unlikely due to inefficient PKR inhibition by p4a as comparable titers were obtained for the recombinant viruses expressing p4a or mutant p4a in HeLa-PKR^{KO} cells. Notwithstanding the lower virus titer, which may either be due to imperfect polyprotein processing due to introduction of p4a or to less efficient encapsidation of the larger viral genome, these results provide evidence that the PKR antagonistic function of MERS-CoV p4a can provide a virus fitness advantage in PKR-competent cells.

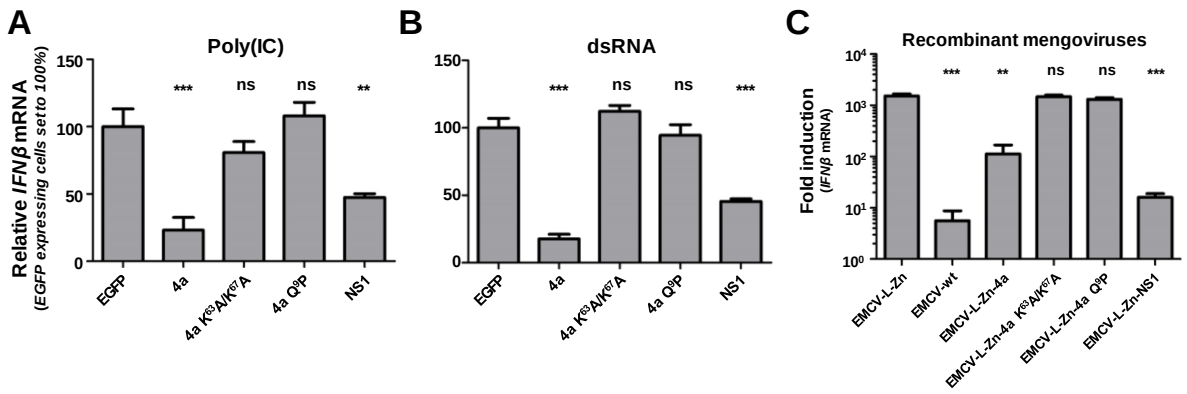

Figure 7. MERS-CoV p4a is a type I IFN antagonist. (A, B) Relative *IFNβ* mRNA levels induced by transfection of poly(I:C) (A) or 6.5 kb viral dsRNA (sequence derived from the Coxsackie virus B3 genome) (B) in HeLa-wt cells expressing EGFP or EGFP-p4a fusion proteins. To obtain a cell pool in which all cells express the protein of interest, plasmids encoding EGFP fusion proteins were co-transfected with a plasmid conferring puromycin resistance. Subsequent puromycin selection for two days eliminated non-transfected cells. RT-qPCR was used to quantify relative *IFNβ* mRNA levels 8h post RNA ligand transfection. Shown are means and standard deviations of the relative *IFNβ* mRNA levels compared to EGFP-expressing cells. Analysis was performed by unpaired t-test (***, p<0.001; **, p<0.01; ns, not significant). (C) Bar-graph showing *IFNβ* mRNA levels induced by recombinant mengovirus infection (MOI=10) of HeLa cells. RT-qPCR was used to quantify relative *IFNβ* mRNA levels at 8h post infection. Means and standard deviations of the relative *IFNβ* mRNA levels of triplicates are shown and analyzed using an unpaired t-test (***, p<0.001; **, p<0.01; ns, not significant).

Similar results were obtained in virus competition experiments (Fig 8D), which is a more sensitive method to compare virus fitness and can reveal smaller fitness differences. Upon low MOI infection, EMCV-L-Zn expressing p4a rapidly outgrew EMCV-L-Zn in HeLa-wt cells but not in HeLa-PKR^{KO} cells (Fig 8E). No fitness advantage was observed with virus expressing the mutant p4a (Fig 8F). We also co-infected cells with viruses expressing either p4a or mutant p4a. Since these viruses could not be distinguished based on their amplicon length, we used a HindIII restriction reaction to specifically cleave the wt 4a PCR fragment (the HindIII site is absent in the mutant 4a gene). Consistent with the results of the multi-cycle infection experiment shown in Fig 8C, the virus expressing p4a replicated better than the virus expressing mutant p4a in HeLa-wt cells whereas in PKR^{KO} cells only a minor advantage was observed (Fig 8G).

MERS-CoV encodes at least one other suppressor of the stress response pathway

Thus far, we used a recombinant picornavirus, EMCV, to analyze the function of p4a in virus-infected cells, in the absence of other MERS-CoV proteins. To assess the relevance of p4a for stress response antagonism in MERS-CoV infected cells, we used recombinant MERS-CoVΔORF4 that is deficient in p4a and p4b expression. Surprisingly, like wt MERS-CoV, MERS-CoVΔORF4 did not induce SG formation in Vero cells (Fig 9A), suggesting that MERS-CoV expresses at least one other protein that suppresses the stress response pathway. To gain more insight into the working mechanism of this

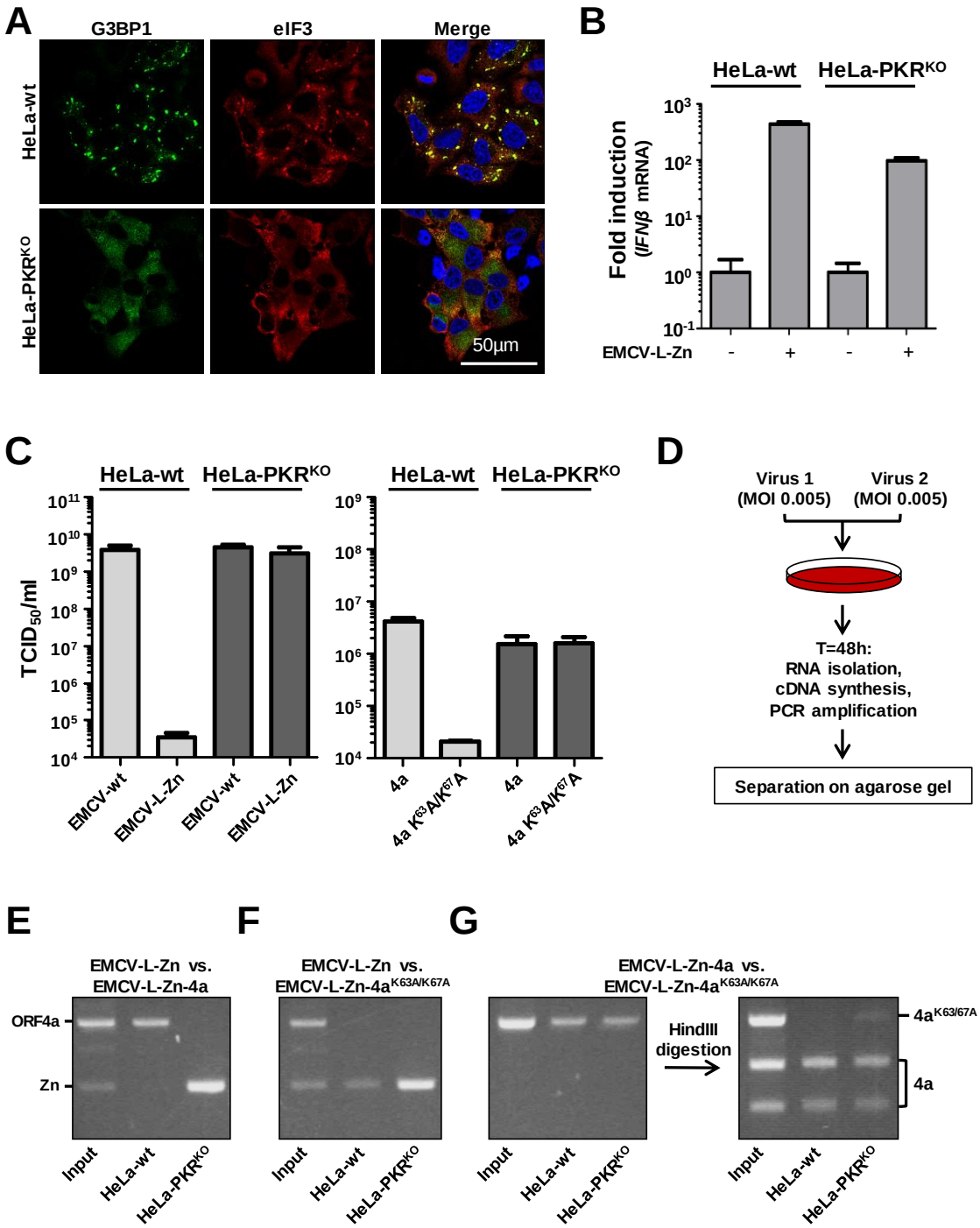

Figure 8. MERS-CoV p4a increases mengovirus fitness. (A) Immune fluorescence images of HeLa-wt and HeLa-PKR^{KO} cells infected with EMCV-L-Zn (MOI=10). Cells were fixed at 6h post infection and SG formation was visualized using antibodies directed against G3BP1 (shown in green) and eIF3 (shown in red). Nuclei were stained using Hoechst-33258 (shown in blue). (B) In parallel with *A*, RNA was isolated at 8h post infection and relative *IFNβ* mRNA levels were quantified by RT-PCR. Means and standard deviations of triplicate measurements are shown. (C) Virus production after wt and recombinant mengovirus infection (MOI=0.01) in HeLa and HeLa-PKR^{KO} cells. Supernatant was collected 24h post infection and virus progeny was titrated by end-point dilution with 3-fold dilution steps. (D) Schematic representation of the virus competition assay. Briefly, two viruses are mixed 1:1 and used to infection HeLa-wt or HeLa-PKR^{KO} cells. Progeny virus was collected 48h post infection and viral RNA was isolated. RT-PCR was used to amplify the MERS-CoV 4a insert, which was analyzed using agarose gel electrophoresis. (E, F, G) Agarose gel analysis of the 4a insert region from virus competition assays with the indicated viruses. To distinguish between wild-type and mutant 4a genes, 4a-wt specific HindIII digestion was used.

other stress response pathway antagonist, we treated MERS-CoV infected cells with arsenite. As demonstrated in Fig 9B, this treatment resulted in SG formation in all the uninfected cells, whereas no SGs were detected in cells infected with either MERS-CoV or MERS-CoVΔORF4 (Fig 9B). These findings strongly suggest that MERS-CoV encodes at least one other stress response antagonist with a mode of action that differs from that of p4a. We also tested the IFN-α/β pathway activation in cells infected with the mutant virus. In line with the reports that several MERS-CoV proteins can antagonize the IFN-α/β pathway (21, 23, 35–38), no increase in *IFNβ* mRNA levels was observed in Huh7 cells infected with MERS-CoV or MERS-CoVΔORF4 (Fig 9C). Taken together, these data provide evidence for substantial redundancy with respect to antagonism of innate antiviral responses in MERS-CoV infected cells.

Discussion

Most viruses have evolved mechanisms to antagonize innate antiviral responses. Coronaviruses encode a set of genus-specific, or in some cases even species-specific, proteins that are generally dispensable for replication *in vitro* but ensure efficient virus replication and/or spreading *in vivo* (10, 11, 39–41). Some of these so-called accessory proteins have been shown to antagonize specific innate antiviral responses, but the functions of most of them are still unknown (9, 10, 23, 42–44). Thus far, most studies concentrated on IFN-α/β pathway antagonists, whereas inhibition of the cellular stress response pathway by coronaviruses remains largely unexplored. In this study, we focussed on the recently identified MERS-CoV, and showed that infected cells fail to activate the stress response pathway. In our subsequent search for MERS-CoV-encoded stress response antagonists, each of its accessory proteins was tested individually for the ability to suppress this pathway. Transient expression of p4a specifically suppressed dsRNA-mediated and PKR-dependent translation inhibition and SG formation. Moreover, we showed that p4a can functionally substitute for the PKR antagonist of EMCV in infected cells. Introduction of specific mutations revealed that the ability of p4a to suppress activation of the stress response pathway depends on its dsRNA-binding function. Together, the data strongly suggest that p4a suppresses the PKR-mediated stress response pathway by sequestering viral dsRNA. Yet, infection of cells with a recombinant MERS-CoV deficient in p4a expression failed to trigger SG formation. This finding points to the expression of at least one other stress response antagonist by MERS-CoV. Importantly, this other suppressor(s) differs in its mode of action of p4a, since in contrast to p4a, it was able to suppress activation of the arsenite-induced stress pathway. Together, these data suggest that MERS-CoV has evolved redundant mechanisms to suppress the stress response pathway at multiple levels.

To our knowledge, MERS-CoV p4a is the first coronavirus protein identified as an antagonist of the dsRNA-dependent, PKR-mediated stress response. There are strong indications that other coronaviruses also encode stress response antagonists but their identity and mode of action remain to be determined. Infectious bronchitis virus (IBV, a γ-CoV) interferes with phosphorylation of both PKR and eIF2α through an unknown mechanism(s) (45). Transmissible gastroenteritis virus (TGEV) Transmissible gastroenteritis virus (TGEV) triggers SG formation, but causes a reduction in the amount of phosphorylated eIF2α over time, possibly by recruiting eIF2α phosphatase PP1 through accessory protein 7 (46, 47). Mouse hepatitis virus (MHV, a lineage A β-CoV) triggers eIF2α phosphorylation and SG formation relatively late in infection, suggesting that the virus actively delays the stress response pathway (48–50), but the mechanism is unknown. SARS-CoV (a lineage B β-CoV)

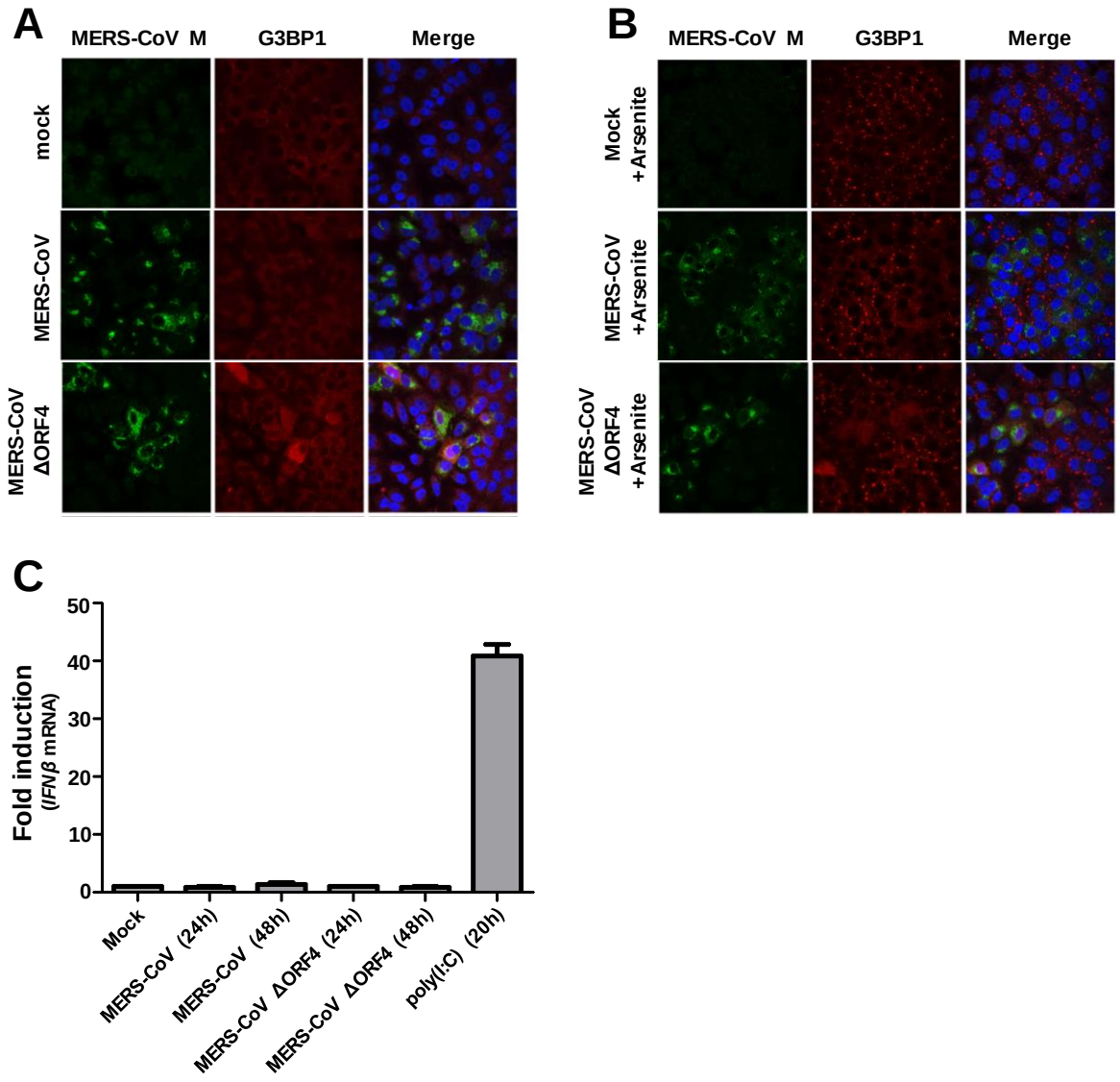

Figure 9. MERS-CoV encodes another suppressor of innate antiviral responses. (A, B) Vero cells were infected (MOI=1) with MERS-CoV wt or MERS-CoVΔORF4. At 16h p.i., cells were (A) mock treated, or (B) treated with 0.5 mM arsenic acid for 1h. Subsequently, MERS-CoV infection and SG formation were visualized by IFA using antibodies directed against MERS-CoV M, G3BP1, and eIF3, respectively. (C) Huh7 cells were transfected with poly(I:C), or infected (MOI=1) with the indicated viruses. RT-qPCR was used to quantify relative *IFNβ* mRNA levels at the indicated time points. Shown are means and standard deviations of the relative *IFNβ* mRNA levels compared to mock treated cells.

has been reported to trigger PKR activation but to be resistant to its antiviral activity (51), although in another study a strong antiviral effect of PKR was observed (52). Hence, the limited information that is available suggests that coronaviruses have acquired different strategies to antagonize the stress

response pathway. Importantly, none of these coronaviruses encode a protein with any homology to MERS-CoV p4a.

In this study, we assessed p4a's antagonistic activities not only upon transient overexpression, but also in the context of viral infection. For this, we introduced p4a in a recombinant EMCV (EMCV-L-Zn) in which the IFN-α/β and stress response pathway antagonist - the leader (L) protein - was inactivated. A p4a-expressing recombinant EMCV may provide several advantages over overexpression through transient transfection, as it likely better mimics the dynamic production of - as well as the interplay between - dsRNA and the viral antagonist. Using this approach, we showed that dsRNA sequestration by p4a efficiently suppresses the PKR-dependent stress response pathway as well as MDA5-mediated IFN-α/β responses under these infection conditions, and thereby provides a fitness advantage to this recombinant EMCV. Similar results were obtained with a recombinant virus expressing IAV NS1, which was included as a control. Together, these data suggests that p4a can be categorized in the group of previously identified viral dsRNA-binding antagonists of stress response and IFN-α/β pathways, which besides IAV NS1, also includes Ebola virus VP35 and Vaccinia virus E3L (26, 27).

Our results showed that besides p4a, MERS-CoV expresses at least one other stress response antagonist. This other antagonist(s) is likely one of the nsps or a structural protein, as we excluded stress-antagonizing roles of the other accessory proteins. At least one antagonist can also suppress the arsenite-induced stress response pathway, and is therefore unlikely to act directly at the level of PKR. Instead, it may act at the level of eIF2α phosphorylation or SG formation. Identification of the other stress response antagonist(s) and elucidation of its/their mode of action, awaits further investigation.

Functional redundancy in suppressing innate antiviral responses is a well-documented phenomenon for coronaviruses. The MERS-CoV accessory proteins (p4a, p4b, and p5) (21–23, 36) as well as the structural M protein and the ORF1ab-encoded nsp3 (37, 38), have all been implicated in antagonizing IFN-α/β pathway activation. This provides a likely explanation for our observation that recombinant MERS-CoV lacking p4a and p4b was still able to suppress *IFN-β* mRNA transcription. MERS-CoV p4a homologs have exclusively been identified in lineage C β-CoVs, which besides MERS-CoV comprises a MERS-like coronavirus found in European hedgehogs (53), and bat coronaviruses (BatCoV) HKU4 and HKU5 (54–56). The p4a-like accessory proteins of these other lineage C viruses all contain dsRNA-binding motifs and may therefore have similar functions as MERS-CoV p4a. Yet, a study by Siu *et al.* indicated that p4a of BatCoV-HKU4, in contrast to that of MERS-CoV and BatCoV-HKU5, does not bind poly(I:C) and does not inhibit IFN-α/β responses (22). If BatCoV-HKU4 p4a is indeed unable to

sequester dsRNA, then it is likely unable to suppress the dsRNA-triggered stress response pathway as well. Interestingly, sequence analysis of a MERS-CoV strain isolated from patients in Jordan identified a 16 amino acid deletion in p4a (57). This deletion does not affect the residues comprising the dsRNA binding site. However, as it removes the second β-strand in the classical αββββα-fold of the dsRNA binding domain, p4a's dsRNA binding properties and, in consequence, its function as antagonist, are most likely compromised. If so, stress antagonism by p4a may be dispensable for MERS-CoV replication and transmission among humans. Increasing evidence suggests that coronavirus accessory proteins often have niche-specific (e.g. organ- or tissue-specific) or host-tailored functions. For example, accessory protein 3c is required for replication of low-virulence feline enteric coronavirus (FECV), which primarily replicates in the enteric tract, but not for replication of FECV-derived, highly virulent feline infectious peritonitis virus (FIPV) isolates, which have acquired the ability to replicate in macrophages (58, 59). Also, accessory proteins contributing to viral fitness in one particular host species may sometimes prove less important in a novel host following a species-jump. For example, in SARS-CoV and CoV-229E some accessory genes were lost through gradual deletion following the introduction of these viruses into into humans (60, 61). Acquisition as well as loss of accessory proteins may reflect adaptations to different immunological environments in different niches or hosts. In this study, we showed that MERS-CoV p4a can potently antagonize innate antiviral responses in human cells. Yet, as suggested by the Jordan outbreak, p4a may not be critical for zoonotic transmission nor for limited human-to-human spread, possibly because of redundancy in viral anti-stress response strategies. Whether p4a will be lost or maintained in the hapless event MERS-CoV establishes sustained community transmission remains an open question.

Materials & Methods

Cell culture and viruses. HeLa-R19, Huh7 and BHK-21 cells were maintained in Dulbecco's Modified Eagle's Medium (DMEM) supplemented with 10% (V/V) fetal calf serum (FCS). Vero cells (ATCC CCL-81) were grown in Eagle's minimum essential medium with 8% FCS, 100 units/ml penicillin and streptomycin, 2 mM L-glutamine and non-essential amino acids.

MERS-CoV infections (62) were carried out as described previously (24, 63) inside biosafety cabinets in BSL III facilities at Leiden University Medical Center and Universidad Autonoma de Madrid. Recombinant MERS-CoVs that were used in Madrid have been described previously (63). Recombinant MERS-CoVs that were used in Leiden were derived from the previously described infectious MERS-CoV clone pBAC-MERS^{FL} (63), and adapted as follows using two step en-passant *in vivo* recombineering reactions in *E. coli* (64). The CMV promoter at the 5'end of the MERS-CoV cDNA sequence was replaced by a T7 RNA polymerase promoter and a unique NotI linearization site was inserted at the 3'end, so that the virus could be launched from transfecting *in vitro* synthesized RNA transcripts (produced using an mMESSAGE mMACHINE ® T7 transcription kit from ThermoFisher scientific). To construct MERS-CoVΔORF4 from this adapted clone, the coding sequence of MERS-CoV p4a/p4b was removed and replaced by a red fluorescent protein (RFP) gene, which however for unclear reasons did not result in red fluorescence during infection. All the genetic modifications to the original pBAC-MERS^{FL} were verified by sequencing. The MERS-CoVΔORF4 virus grew to similar titers as the recombinant wt MERS-CoV derived from the original clone.

Recombinant EMCV viruses were derived from the pM16.1 infectious clone (65). The pStrep2-VFETQG-Zn-M16.1 infectious clone was constructed using site-directed mutagenesis (SDM) using the pCVB3-3C^{pro}-QG-M16.1 as template DNA (32). The Zn-finger mutation in L was introduced by SDM using the following oligonucleotides: Fw; 5'-ATGACCTTTGAAGAAGCCCCAAAAGCCTCCGCCTTACAATAC-3' and Rv; 5'- GGAATGAGCACAAATCTCTTG-3'. The optimized 3C^{pro} recognition site (VFETQG) was introduced by SDM using the following oligonucleotides: Fw; 5'-GAAACTCAAGGCGCAACGACTATGGAGC-3' and Rv; 5'-AAAGACCGCGGCCGCTTGCTCATCATTG-3'. Finally, the Strep2-tag was introduced by SDM using the following oligonucleotides: Fw; 5'-GGCCGCCTGGTCACATCCTCAGTTTGAGAAGGGTGCCTGGTCTCATCCCCAATTCGAAAA-3' and Rv: 5'-GGCCTTTTCGAATTGGGGATGAGACCAGGCACCCTTCTCAAACTGAGGATGTGACCAGGC-3'. Genes of interest were inserted into the XhoI/NotI restriction sites of the pStrep2-VFETQG-Zn-M16.1 infectious clone. Viruses were recovered by transfection of run-off RNA transcripts into BHK-21 cells. Upon total CPE, cells were subjected to three freeze-thaw cycles and cell debris was pellet at 4,000x*g* for 15

minutes. Virus was concentrated by ultracentrifugation though a 30% sucrose cushion at 140,000x*g* for 16 hours in a SW32Ti rotor.

HeLa-PKR knockout cells. HeLa-R19 PKR^{KO} were generated using the CRISPR/Cas9 system as previously described (66). Briefly, gRNA encoding oligonucleotides cassettes to target human PKR (gRNA1: 5'-ACCGGACCTCCACATGATAGG-3' and 5'-AACCCTATCATGTGGAGGTCC-3', gRNA2: 5'-CCGTACTACTCCCTGCTTCTGAG-3' and 5'-AAACTCAGAAGCAGGGAGTAGTA-3') were cloned into the SapI restriction sites of the pCRISPR-hCas9-2xgRNA-Puro plasmid. HeLa-R19 cells were seeded in 6-well clusters (100,000 cells/well) and next day transfected with 2.5 μg plasmid DNA using Fugene6 (Promega) according to manufacturer's instructions. Next day successfully transfected cells were selected using puromycin and single-cell clones were generated using end-point dilutions. Knockout efficiency was determined by sequence analysis of the PKR locus in the genomic DNA and western blot analysis (Fig S1).

Chemicals and RNA ligands. Arsenic acid was purchased at Sigma-Aldrich and used at a final concentration of 0.5 mM in DMEM. Pateamine A was kindly provided by Prof. Jerry Pelletier (67) and used at a concentration of 100 nM in DMEM. Poly(I:C) was purchased from GE Healthcare and dsRNA ligand was prepared using the Replicator RNAi kit (Finnzymes) using the following oligonucleotides (Fw, possessing T7 promoter sequence) TAATACGACTCACTATAGGGGATACAGTGACAGGGCG and (Rv, possessing Phi6 promoter sequence) GGAAAAAAACCGCACCGAATGCGGAGAATTTAC and the pRib-CVB3/T7 Coxsackie virus B3 infectious clone as template (68).

Plasmids. Expression plasmids encoding enhanced green fluorescent protein (EGFP) tagged proteins were created by PCR amplification of the gene of interest with oligonucleotides flanked by XhoI (Fw) or BamHI (Rv) restriction sites (MERS-CoV ORF3: 5'-AAAAACTCGAGATGAGAGTTCAAAGACCACCC-3' and 5'-AAAAAGGATCCATTAACTGAGTAACCAACGTCAAAAAG-3', ORF4a: 5'-AAAAACTCGAGATG GATTACGTGTCTCTGCTTAATC-3' and 5'-AAAAAGGATCCGTGGGAGAATGGCTCCTC-3', ORF4b: 5'-AAAAACTCGAGATGGAGGAATCCCTGATGGATG-3' and 5'-AAAAAGGATCCAAA TCCTGGATGATGTAAAATGGGG-3', ORF5: 5'-AAAAACTCGAGATGGCTTTCTCGGCGTC-3' and 5'-AAAAAGGATCCAACGATAAGCGAGCTCGG-3', IAV NS1: 5'-AAAAACTCGAGATGGAT CCAAACACTGTGTC-3' and 5'-AAAAAGGATCCAACTTCTGACCTAATTGTTC-3', VV E3L: 5'-AAAAACTCGAGATGTCTAAGATCTATATTGACGAGCGTTCTG-3' and 5'-AAAAAGGATCCG AATCTAATGATGACGTAACCAAGAAGTTTATCTACTG-3', Ebola VP35: 5'-AAAAACTCGAGATGAC AACTAGAACAAAGGGCAGGG-3' and 5'-AAAAAGGATCCAATTTTGAGTCCAAGTGTTTTACC ATCTTGAAGC-3'. Digested PCR products were ligates into XhoI/BamHI digested pEGFP-N3 plasmid and gene integrity

was confirmed by sequencing analysis. pcDNA-RFP expression plasmid was constructed by PCR amplification of the RFP gene using oligonucleotides flanked by NheI (Fw) and NotI (Rv) restriction sites (Fw) GCTAGCGCCACAACCATGGCCTCCTCCGAGGAC and (Rv) GCGGCCGCCGGCGCCGGTGGAGTGGCGGCCCTC and subsequently cloning into the NheI/NotI digested pcDNA-EGFP plasmid (69). The pJET-puro (puromycin resistance vector) plasmid was developed by ligation of the EF1a-Puro fragment into the pJet1.2/blunt vector (Thermo Fisher). pRL-TK (Renilla luc expression vector) plasmid was purchased from Promega.

Renilla luciferase assay. HeLa-R19 cells were seeded in a 96-wells cluster (5,000 cells/well) and the next day they were transfected with the indicated plasmids (40 ng pEGFP, 10 ng pRL-TK) using Fugene6. 24 hours post transfection, cells were lysed in 20 µl passive lysis buffer (Promega) and analyzed on the Centro LB 960 Microplate Luminometer (Berthold technologies) using the Renilla luciferase reporter kit (Promega) according to manufacturer instructions.

Flow cytometry analysis. Cells were seeded in a 24-wells cluster (50,000 cells/well) and the next day they were transfected with the indicated plasmids (500 ng/well; 250 ng/plasmid) using Fugene6. Twenty-four hours post transfection, cells were released using trypsin, washed once in phosphate buffered saline (PBS) and fixed for 30 minutes with 2% paraformaldehyde (PFA) in PBS. Cells were analyzed on FACS Canto™ (BD) using BD FACS Diva software.

Immunofluorescence assay (IFA). Cells were seeded on glass slides in a 24 wells cluster (25,000 cells/well) and the next day they were infected (MOI=10) or transfected (500 ng total DNA) using Fugene6. At 6h post infection or 24h post transfection, cells were fixed using 4% PFA in PBS for 30 minutes at RT. Vero cells seeded on glass slides were transfected with 1 µg Poly(I:C) per 6-well using Lipofectamine 2000 (Thermo Fisher Scientific). Cells were permeabilized with PBS + 0.2% Triton X-100, washed trice with blocking buffer (PBS + 2% bovine serum albumin [BSA] + 50mM NH_4Cl), and incubated with blocking buffer for 1 h. Cell monolayers were incubated for 1 h with primary antibody mouse-α-G3BP1 (BD, 1:1,000), rabbit-α-TIA1 (Santa-Cruz, 1:50), mouse-α-dsRNA (J2, English&Scientific Consulting, 1:1,000), goat-α-eIF3 (Santa-Cruz, 1:100), rabbit-α-G3BP2 (Bethyl Laboratory, 1:200; or Assay Biotech, 1:500), or rabbit-α-MERS-CoV (1:500: raised against the MERS-CoV M carboxyl terminal peptide CRYKAGNYRSPPITADIELALLRA), and then for 30 min with secondary antibody donkey-α-mouse-Cy3 (Jackson ImmunoResearch, 1:1000), donkey-α-rabbit-Alexa488 (Jackson ImmunoResearch, 1:1000), bovine-α-goat-Alexa647 (Jackson ImmunoResearch, 1:1000), donkey-α-rabbit-Cy5 (Jackson ImmunoResearch, 1:200), donkey-α-mouse-Alexa 488 (Invitrogen,

1:200) or donkey-α-goat-Alexa 594 (Invitrogen, 1:200) and Hoechst-33258 (1:2,000) diluted in blocking buffer. Between and after the incubations, the cell monolayers were washed three times with blocking buffer. Finally, the cells were washed once with distilled water and coverslips were mounted on glass slides in FluorSafe (Calbiochem). Cells were examined by confocal microscopy (Leica SPE-II).

Western blot analysis. Cells were seeded in 10-cm dishes (2.5 x 10^6 cells/dish) and the next day cells were infected (MOI=10) or transfected (8 µg plasmid DNA) using Fugene6. At 6h post infection or 24h post transfection, cells were released using trypsin, washed once in wash buffer (100 mM Tris/HCl pH 8,0 + 1 mM EDTA + 50 mM NaCl) and lysed in 200 µl lysis buffer (100 mM Tris/HCl pH 8,0 + 1 mM EDTA + 50 mM NaCl + 1% NP40 + protease inhibitor mix [Roche] + phosphatase inhibitor cocktails #2 and #3 [Sigma-Aldrich]). Cell debris was pelleted at 15,000 x *g* for 15 min and 10 µl of cleared cell lysates were resolved using reducing sodium dodecyl sulfate-polyacrylamide gel electrophoresis (SDS-PAGE) and transferred to 0.2 µm nitrocellulose membranes by wet electrophoretic transfer. Membranes were washed once with washing buffer (PBS + 0.1% Tween 20) and incubated 1h in blocking buffer (PBS + 0.1% Tween 20 + 2% BSA). Membranes were successively incubated for 1 h with primary antibody mouse-α-PKR (BD, 1:1,000), rabbit-α-PKR-P[T446] (Abcam, 1:2.000), mouse-α-Tubulin (Sigma, 1:5.000), rabbit-α-mengovirus capsid (kindly provided by Prof. Ann Palmenberg ,1:1.000) or mouse-α-StrepMab classic (IBA, 1:1.000) and then for 30 min with goat-α-mouse-IRDye680 (Li-COR, 1:15,000) or goat-α-rabbit-IRDye800 (Li-COR, 1:15,000) diluted in blocking buffer. Between and after the incubations, the membranes were washed, thrice each time, with washing buffer. Finally, membranes were washed once with PBS and scanned using an Odyssey Imager (Li-COR).

RT-qPCR analysis. RNA isolation, cDNA synthesis, and RT-qPCR were performed as described elsewhere (63, 66).

Acknowledgments

We acknowledge Jerry Pelletier (McGill University; Canada) for supplying pateamine A, and Ann Palmenberg (University of Wisconsin-Madison; USA) for the rabbit anti-EMCV capsid polyclonal antibody. Eric Snijder, ,Diede Oudshoorn, Clara Posthuma and Jessika Zevenhoven (LUMC, The Netherlands) are kindly acknowledged for excellent technical assistance, useful discussions, and providing the MERS-CoV M antiserum, a MERS-CoV cDNA template and the T7 RNApol driven MERS-CoV infectious clone. Bart Haagmans and Ron Fouchier (Erasmus Medical Center, Rotterdam, The Netherlands) kindly provided EMC/2012 MERS-CoV.

References

1. K. Onomoto, *et al.*, Critical Role of an Antiviral Stress Granule Containing RIG-I and PKR in Viral Detection and Innate Immunity. *PLoS One* **7**, e43031 (2012)

2. J. P. White, R. E. Lloyd, Regulation of stress granules in virus systems. *Trends Microbiol.* **20**, 175–83 (2012).

3. F. Wippich, *et al.*, Dual specificity kinase DYRK3 couples stress granule condensation/ dissolution to mTORC1 signaling. *Cell* **152**, 791–805 (2013)

4. K. Arimoto, H. Fukuda, S. Imajoh-Ohmi, H. Saito, M. Takekawa, Formation of stress granules inhibits apoptosis by suppressing stress-responsive MAPK pathways. *Nat. Cell Biol.* **10**, 1324–1332 (2008)

5. W. J. Kim, S. H. Back, V. Kim, I. Ryu, S. K. Jang, Sequestration of TRAF2 into stress granules interrupts tumor necrosis factor signaling under stress conditions. *Mol. Cell. Biol.* **25**, 2450–2462 (2005)

6. Y. Lu, M. Wambach, M. G. Katze, R. M. Krug, Binding of the Influenza Virus NS1 Protein to Double-Stranded RNA Inhibits the Activation of the Protein Kinase That Phosphorylates the eIF-2 Translation Initiation Factor. *Virology* **214**, 222–228 (1995)

7. J. Talon, *et al.*, Activation of interferon regulatory factor 3 is inhibited by the influenza A virus NS1 protein. *J. Virol.* **74**, 7989–7996 (2000)

8. S. A. Kopecky-Bromberg, L. Martínez-Sobrido, M. Frieman, R. A. Baric, P. Palese, Severe acute respiratory syndrome coronavirus open reading frame (ORF) 3b, ORF 6, and nucleocapsid proteins function as interferon antagonists. *J. Virol.* **81**, 548–557 (2007)

9. L. Zhao, *et al.*, Antagonism of the interferon-induced OAS-RNase L pathway by murine coronavirus ns2 protein is required for virus replication and liver pathology. *Cell Host Microbe* **11**, 607–616 (2012)

10. A. Lorusso, *et al.*, Gain, preservation, and loss of a group 1a coronavirus accessory glycoprotein. *J. Virol.* **82**, 10312–7 (2008)

11. B. J. Haijema, H. Volders, P. J. M. Rottier, Live, attenuated coronavirus vaccines through the directed deletion of group-specific genes provide protection against feline infectious peritonitis. *J. Virol.* **78**, 3863–71 (2004).

12. D. X. Liu, T. S. Fung, K. K. L. Chong, A. Shukla, R. Hilgenfeld, Accessory proteins of SARS-CoV and other coronaviruses. *Antiviral Res.* **109**, 97–109 (2014)

13. A. A. P. M. Herrewegh, H. Vennema, M. C. Horzinek, P. J. M. Rottier, R. J. de Groot, The Molecular Genetics of Feline Coronaviruses: Comparitive Sequence Analysis of the ORF7a/7b Transcription Unit of Different Biotypes. *Virology* **212**, 622–631. (1995)

14. W. Li, *et al.*, Receptor and viral determinants of SARS-coronavirus adaptation to human ACE2. *EMBO J.* **24**, 1634–1643 (2005)

15. WHO | Middle East respiratory syndrome coronavirus (MERS-CoV) – Saudi Arabia. *WHO* (2016)

16. M. T. Azhar EI, El-Kafrawy SA, Farraj SA, Hassan AM, Al-Saeed MS, Hashem AM, Evidence for Camel-to-Human Transmission of MERS Coronavirus. *New Engl. J. Med.* **370**, 2499–2505 (2014)

17. T. Briese, *et al.*, Dromedary Camels in Saudi Arabia Include Homologues of Human Isolates Revealed through Whole-Genome analysis etc. *MBio* **5**, 1–5 (2014)

18. F. Zielecki, *et al.*, Human cell tropism and innate immune system interactions of human respiratory coronavirus EMC compared to those of severe acute respiratory syndrome coronavirus. *J. Virol.* **87**, 5300–4 (2013)

19. R. W. Y. Chan, *et al.*, Tropism of and innate immune responses to the novel human betacoronavirus lineage C virus in human ex vivo respiratory organ cultures. *J. Virol.* **87**, 6604–14 (2013)

20. E. Kindler, *et al.*, Efficient replication of the novel human betacoronavirus EMC on primary human epithelium highlights its zoonotic potential. *MBio* **4** (2013)

21. D. Niemeyer, *et al.*, Middle East respiratory syndrome coronavirus accessory protein 4a is a type I interferon antagonist. *J. Virol.* **87**, 12489–95 (2013)

22. K.-L. Siu, *et al.*, Middle east respiratory syndrome coronavirus 4a protein is a double-stranded RNA-binding protein that suppresses PACT-induced activation of RIG-I and MDA5 in the innate antiviral response. *J. Virol.* **88**, 4866–76 (2014)

23. Y. Yang, *et al.*, The structural and accessory proteins M, ORF 4a, ORF 4b, and ORF 5 of Middle East respiratory syndrome coronavirus (MERS-CoV) are potent interferon antagonists. *Protein Cell* **4**, 951–961 (2013)

24. A. H. de Wilde, *et al.*, MERS-coronavirus replication induces severe in vitro cytopathology and is strongly inhibited by cyclosporin A or interferon-α treatment. *J. Gen. Virol.* **94**, 1749–1760 (2013)

25. J. Nejepinska, R. Malik, M. Moravec, P. Svoboda, Deep sequencing reveals complex spurious transcription from transiently transfected plasmids. *PLoS One* **7** (2012)

26. H. W. Chang, J. C. Watson, B. L. Jacobs, The E3L gene of vaccinia virus encodes an inhibitor of the interferon-induced, double-stranded RNA-dependent protein kinase. *Proc. Natl. Acad. Sci. U. S. A.* **89**, 4825–4829 (1992)

27. Z. Feng, M. Cerveny, Z. Yan, B. He, The VP35 protein of Ebola virus inhibits the antiviral effect mediated by double-stranded RNA-dependent protein kinase PKR. *J. Virol.* **81**, 182–192 (2007)

28. E. McEwen, *et al.*, Heme-regulated inhibitor kinase-mediated phosphorylation of eukaryotic translation initiation factor 2 inhibits translation, induces stress granule formation, and mediates survival upon arsenite exposure. *J. Biol. Chem.* **280**, 16925–16933 (2005)

29. Y. Dang, *et al.*, Eukaryotic initiation factor 2α-independent pathway of stress granule induction by the natural product pateamine A. *J. Biol. Chem.* **281**, 32870–32878 (2006)

30. D. A. Khaperskyy, *et al.*, Influenza A Virus Host Shutoff Disables Antiviral Stress-Induced Translation Arrest. *PLoS Pathog.* **10** (2014)

31. S. V Hato, *et al.*, The mengovirus leader protein blocks interferon-alpha/beta gene transcription and inhibits activation of interferon regulatory factor 3. *Cell. Microbiol.* **9**, 2921–2930 (2007)

32. Q. Feng, *et al.*, Enterovirus 2Apro targets MDA5 and MAVS in infected cells. *J. Virol.* **88**, 3369–78 (2014)

33. M. F. Dubois, A. G. Hovanessian, Modified subcellular localization of interferon-induced p68 kinase during encephalomyocarditis virus infection. *Virology* **179**, 591–598 (1990)

34. R. Stefl, *et al.*, The solution structure of the ADAR2 dsRBM-RNA complex reveals a sequence-specific readout of the minor groove. *Cell* **143**, 225–37 (2010)

35. K.-L. Siu, *et al.*, Middle east respiratory syndrome coronavirus 4a protein is a double-stranded RNA-binding protein that suppresses PACT-induced activation of RIG-I and MDA5 in the innate antiviral response. *J. Virol.* **88**, 4866–76

(2014)

36. Y. Yang, *et al.*, Middle East respiratory syndrome coronavirus ORF4b protein inhibits type I interferon production through both cytoplasmic and nuclear targets. *Sci. Rep.* **5**, 17554 (2015)

37. P.-Y. Lui, *et al.*, Middle East respiratory syndrome coronavirus M protein suppresses type I interferon expression through the inhibition of TBK1-dependent phosphorylation of IRF3. *Emerg. Microbes Infect.* **5**, e39 (2016)

38. B. A. Bailey-Elkin, *et al.*, Crystal structure of the middle east respiratory syndrome coronavirus (MERS-CoV) papain-like protease bound to ubiquitin facilitates targeted disruption of deubiquitinating activity to demonstrate its role in innate immune suppression. *J. Biol. Chem.* **289**, 34667–34682 (2014)

39. C. A. M. de Haan, P. S. Masters, X. Shen, S. Weiss, P. J. M. Rottier, The group-specific murine coronavirus genes are not essential, but their deletion, by reverse genetics, is attenuating in the natural host. *Virology* **296**, 177–189 (2002)

40. A. Lissenberg, *et al.*, Luxury at a cost? Recombinant mouse hepatitis viruses expressing the accessory hemagglutinin esterase protein display reduced fitness in vitro. *J. Virol.* **79**, 15054–63 (2005)

41. A. A. P. M. Herrewegh, *et al.*, Detection of feline coronavirus RNA in feces, tissues, and body fluids of naturally infected cats by reverse transcriptase PCR. *J. Clin. Microbiol.* **33**, 684–689 (1995)

42. C. A. Koetzner, *et al.*, Accessory protein 5a is a major antagonist of the antiviral action of interferon against murine coronavirus. *J. Virol.* **84**, 8262–8274 (2010)

43. J. Kint, *et al.*, Infectious bronchitis coronavirus inhibits STAT1 signalling and requires accessory proteins for resistance to type I interferon. *J. Virol.* **89**, 12047-57 (2015)

44. R. J. De Groot, *et al.*, ICTV taxonomic assignation form Coronavirus 2008. *Taxon. Propos. to ICTV Exec. Comm.*, 1–37 (2008)

45. X. Wang, *et al.*, Inhibition of protein kinase R activation and upregulation of GADD34 expression play a synergistic role in facilitating coronavirus replication by maintaining de novo protein synthesis in virus-infected cells. *J. Virol.* **83**, 12462–12472 (2009)

46. J. L. G. Cruz, *et al.*, Coronavirus gene 7 counteracts host defenses and modulates virus virulence. *PLoS Pathog.* **7,** e1002090 (2011)

47. I. Sola, *et al.*, The polypyrimidine tract-binding protein affects coronavirus RNA accumulation levels and relocalizes viral RNAs to novel cytoplasmic domains different from replication-transcription sites. *J. Virol.* **85**, 5136–49 (2011)

48. M. Raaben, M. J. A. Groot Koerkamp, P. J. M. Rottier, C. A. M. de Haan, Mouse hepatitis coronavirus replication induces host translational shutoff and mRNA decay, with concomitant formation of stress granules and processing bodies. *Cell. Microbiol.* **9**, 2218–2229 (2007)

49. J. Bechill, Z. Chen, J. W. Brewer, S. C. Baker, Coronavirus infection modulates the unfolded protein response and mediates sustained translational repression. *J. Virol.* **82**, 4492–4501 (2008)

50. Y. Ye, K. Hauns, J. O. Langland, B. L. Jacobs, B. G. Hogue, Mouse hepatitis coronavirus A59 nucleocapsid protein is a type I interferon antagonist. *J. Virol.* **81**, 2554–2563 (2007)

51. V. Krähling, D. A. Stein, M. Spiegel, F. Weber, E. Mühlberger, Severe acute respiratory syndrome coronavirus triggers apoptosis via protein kinase R but is resistant to its antiviral activity. *J. Virol.* **83**, 2298–2309 (2009)

52. A. H. de Wilde, *et al.*, A kinome-wide siRNA screen identifies proviral and antiviral host factors in SARS-coronavirus replication, including PKR and early secretory pathway proteins. *J Virol* **89**, 8318-33 (2015)

53. V. M. Corman, *et al.*, Characterization of a novel betacoronavirus related to middle East respiratory syndrome coronavirus in European hedgehogs. *J. Virol.* **88**, 717–24 (2014)

54. P. C. Y. Woo, *et al.*, Molecular diversity of coronaviruses in bats. *Virology* **351**, 180–187 (2006)

55. P. C. Woo, S. K. Lau, K. S. Li, A. K. Tsang, K.-Y. Yuen, Genetic relatedness of the novel human group C betacoronavirus to Tylonycteris bat coronavirus HKU4 and Pipistrellus bat coronavirus HKU5. *Emerg. Microbes Infect.* **1**, e35 (2012)

56. P. C. Y. Woo, *et al.*, Comparative analysis of twelve genomes of three novel group 2c and group 2d coronaviruses reveals unique group and subgroup features. *J. Virol.* **81**, 1574–1585 (2007)

57. M. M. Lamers, *et al.*, Deletion Variants of Middle East Respiratory Syndrome Coronavirus from Humans, Jordan, 2015. *Emerg. Infect. Dis.* **22**, 716-9 (2016)

58. B. J. Haijema, P. J. Rottier, R. J. De Groot, *Feline coronaviruses: a tale of two-faced types*.

59. H. Vennema, A. Poland, J. Foley, N. C. Pedersen, Feline infectious peritonitis viruses arise by mutation from endemic feline enteric coronaviruses. *Virology* **243**, 150–157 (1998)

60. J. Min, *et al.*, Molecular evolution of the SARS coronavirus during the course of the SARS epidemic in China. *Science* **303**, 1666–1669 (2004)

61. V. M. Corman, *et al.*, Link of a ubiquitous human coronavirus to dromedary camels. *PNAS*. **113**, 9864-9 (2016)

62. F. R. Zaki AM1, van Boheemen S, Bestebroer TM, Osterhaus AD, Isolation of a Novel Coronavirus from a Man with Pneumonia in Saudi Arabia. *New Engl. J. Med.* **367**, 1814–20 (2012)

63. F. Almazan, *et al.*, Engineering a replication-competent, propagation-defective Middle East respiratory syndrome coronavirus as a vaccine candidate. *MBio* **4**, e00650-13 (2013)

64. B. K. Tischer, J. Von Einem, B. Kaufer, N. Osterrieder, Two-step Red-mediated recombination for versatile high-efficiency markerless DNA manipulation in Escherichia coli. *Biotechniques* **40**, 191–197 (2006)

65. G. M. Duke, A. C. Palmenberg, Cloning and synthesis of infectious cardiovirus RNAs containing short, discrete poly(C) tracts. *J. Virol.* **63**, 1822–1826 (1989)

66. M. A. Langereis, H. H. Rabouw, M. H. Holwerda, L. J. Visser, F. J. van Kuppeveld, Knockout of cGAS and STING Rescues Virus Infection of Plasmid DNA-transfected cells. *J. Virol.* **89**, 11169–11173 (2015)

67. M.-E. Bordeleau, *et al.*, Stimulation of mammalian translation initiation factor eIF4A activity by a small molecule inhibitor of eukaryotic translation. *Proc. Natl. Acad. Sci. U. S. A.* **102**, 10460–10465 (2005)

68. E. Wessels, *et al.*, A proline-rich region in the coxsackievirus 3A protein is required for the protein to inhibit endoplasmic reticulum-to-golgi transport. *J. Virol.* **79**, 5163–73 (2005)

69. M. A. Langereis, Q. Feng, F. J. van Kuppeveld, MDA5 localizes to stress granules, but this localization is not required for the induction of type I interferon. *J. Virol.* **87**, 6314–25 (2013)

Supplementary Figures

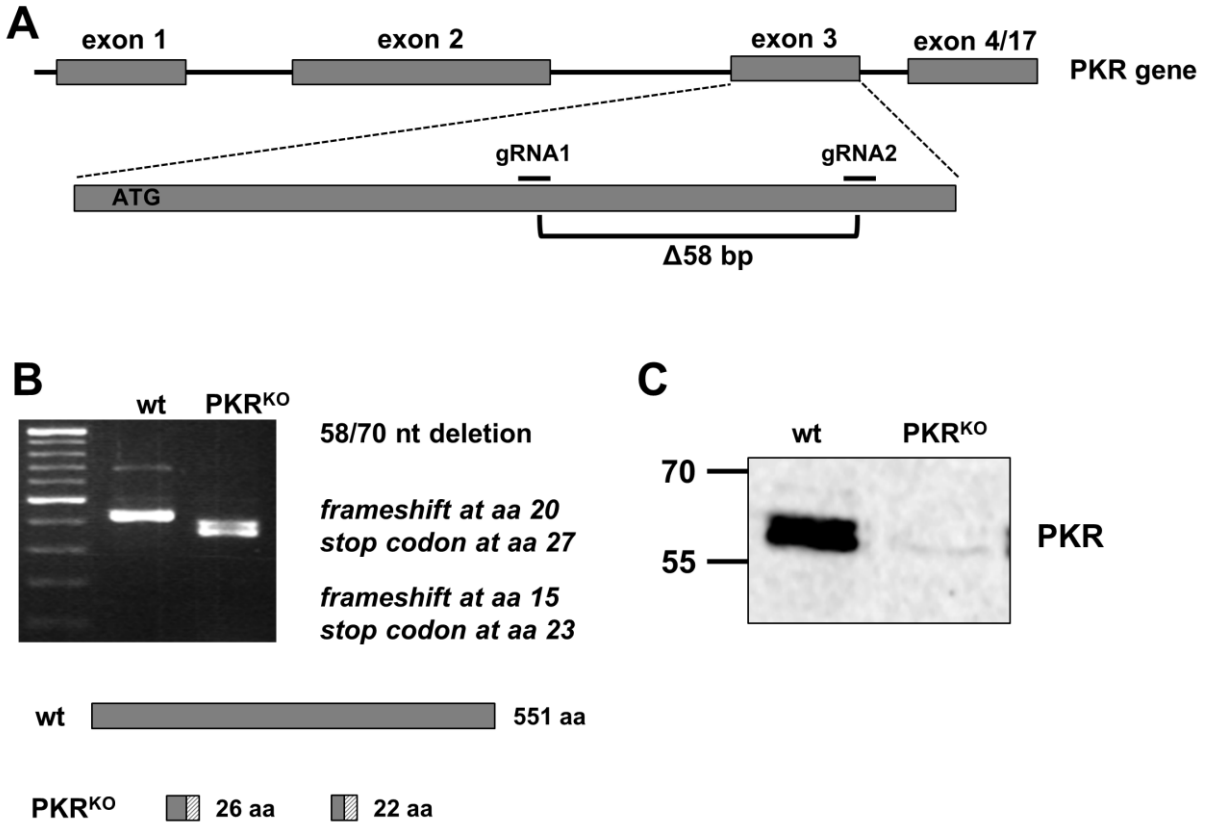

Figure S1. Construction of PKR knockout HeLa cells using the CRISPR-Cas9 system. *(A) Schematic representation of the PKR gene. Two guide RNAs were designed to target exon 3 of human PKR. (B) A single-cell clone was characterized by isolation of genomic DNA and integrity of human PKR gene was determined by sequence analysis. Both alleles contain a deletion resulting in a frame-shift event and a premature stop codon. (C) Western blot analysis of PKR protein levels in cell lysates from HeLa-wt or HeLa-PKR^{KO} cells.*

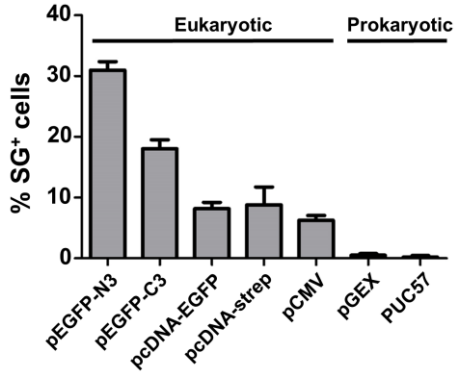

Figure S2. *Stress granule formation in HeLa cells transfected with different plasmids. HeLa cells were transfected with different plasmids (500 ng/well). At 24h post transfection, cells were fixed and IFA was used to quantify the level of cells that possess SGs. For each type of plasmid, SG-positive cells were quantified from three randomly selected images and depicted in a bar-graph.*

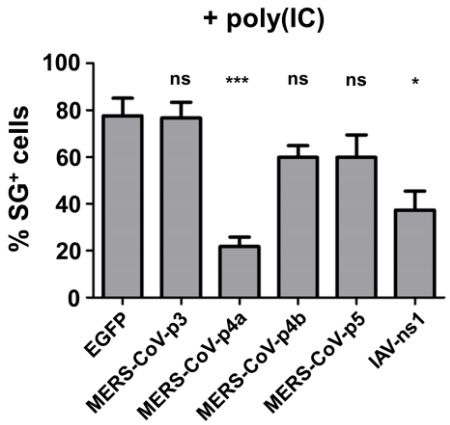

Figure S3. MERS-CoV p4a suppresses poly(I:C)-induced SG formation. *HeLa-wt cells were transfected with pEGFP-expression plasmids. Next day, SG formation was triggered by poly(I:C) transfection (100 ng/well). Cells were fixed using paraformaldehyde at 6h post RNA ligand transfection and SG formation was visualized using IFA . Quantification of SG-positive cells is shown as means and standard deviations of at least three randomly selected images per sample. Data was analyzed using an unpaired t-test (***, p<0.001; *, p<0.05; ns, not significant).*

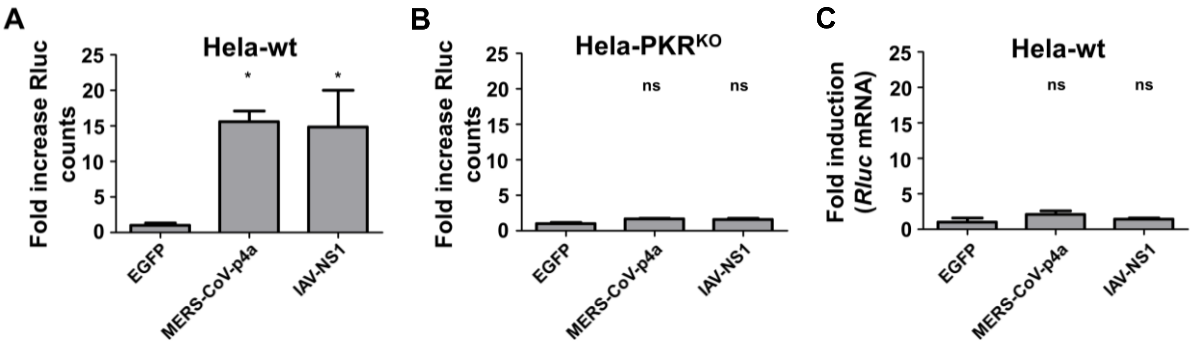

Figure S4. Increased transgene expression is caused by a rescue of translation efficiency. *(A, B) Relative luciferase mRNA (A) and protein (B) levels in HeLa-wt cells co-transfected with pTK-RLuc and pEGFP expression plasmids. (C, D) Relative luciferase counts measured at 16 h post co-transfection of pTK-RLuc and pEGFP expression plasmids in HeLa-wt (C) or Hela-PKR^{KO} (D) cells. Data was analyzed using an unpaired t-test (***, p<0.001; *, p<0.05; ns, not significant).*

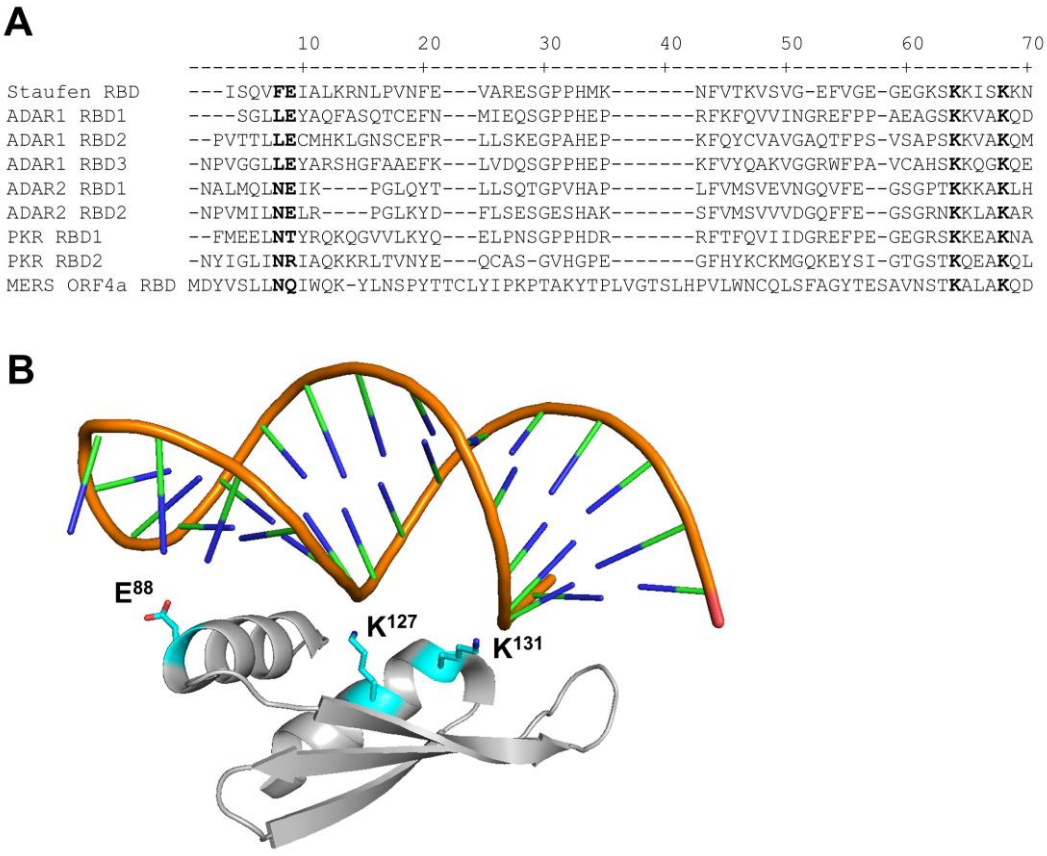

Figure S5. The MERS-CoV p4a dsRNA binding motif. *(A) Alignment of MERS-CoV p4a with other dsRNA binding motifs of several cellular proteins. In bold are the conserved residues crucial for dsRNA binding. (B) Structure of ADAR1 dsRNA binding motif in association with dsRNA. Highlighted are the corresponding ADAR1 residues that are mutated in MERS-CoV p4a in this study.*

Chapter 3

The small molecule ISRIB suppresses the integrated stress response within a defined window of activation

Huib H Rabouw[1,#], Martijn A Langereis[1,#], Aditya A Anand[2], Linda J Visser[1], Raoul J de Groot[1], Peter Walter[2,], Frank JM van Kuppeveld[1,*]*

[1]Virology Division, Department of Infectious Diseases and Immunology, Faculty of Veterinary Medicine, Utrecht University, 3584 CL Utrecht, The Netherlands

[2]Howard Hughes Medical Institute and Department of Biochemistry and Biophysics, University of California at San Francisco, San Francisco, CA 94143, USA

[*] These authors contributed equally

*PNAS **116**, 2097-2102 (2019)*

Significance

The integrated stress response (ISR) protects cells from a variety of harmful stressors by temporarily halting protein synthesis. However, chronic ISR activation has pathological consequences, and is linked to several neurological disorders. Pharmacological inhibition of chronic ISR activity emerges as a powerful strategy to treat ISR-mediated neurodegeneration but is typically linked to adverse effects due to the ISR's importance for normal cellular function. Paradoxically, the small-molecule ISR inhibitor ISRIB has promising therapeutic potential *in vivo* without overt side-effects. In this manuscript, we demonstrate that ISRIB inhibits low level ISR activity, but does not affect strong ISR signaling. We thereby provide a plausible mechanism how ISRIB counteracts toxic chronic ISR activity, without disturbing the cytoprotective effects of a strong acute ISR.

Abstract

Activation of the integrated stress response (ISR) by a variety of stresses triggers phosphorylation of the α-subunit of translation initiation factor eIF2. P-eIF2α inhibits eIF2B, the guanine nucleotide exchange factor (GEF) that recycles inactive eIF2•GDP to active eIF2•GTP. eIF2 phosphorylation thereby represses translation. Persistent activation of the ISR has been linked to the development of several neurological disorders, and modulation of the ISR promises new therapeutic strategies. Recently, a small-molecule ISR inhibitor (ISRIB) was identified that rescues translation in the presence of P-eIF2α by facilitating the assembly of more active eIF2B. ISRIB enhances cognitive memory processes and has therapeutic effects in brain-injured mice without displaying overt side-effects. While using ISRIB to investigate the ISR in picornavirus-infected cells, we observed that ISRIB rescued translation early in infection when P-eIF2α levels were low, but not late in infection when P-eIF2α levels were high. By treating cells with varying concentrations of poly(I:C) or arsenite to induce the ISR, we provide additional proof that ISRIB is unable to inhibit the ISR when intracellular P-eIF2α concentrations exceed a critical threshold level. Together, our data demonstrate that the effects of pharmacological activation of eIF2B are tuned by P-eIF2α concentration. Thus, ISRIB can mitigate undesirable outcomes of low-level ISR activation that may manifest neurological disease but leave the cytoprotective effects of acute ISR activation intact. The insensitivity of cells to ISRIB during acute ISR may explain why ISRIB does not cause overt toxic side-effects *in vivo*.

Introduction

Eukaryotic cells respond to intrinsic stress (e.g. ER stress or oncogene activation) as well as extrinsic stress (e.g. glucose or amino acid deprivation, hypoxia or virus infection) by activating the integrated stress response (ISR). The ISR comprises a complex, cytoprotective signaling pathway aimed at reducing global protein synthesis while allowing translation of a few select mRNAs to promote cell recovery and survival (1, 2).

A key factor in translation initiation is eIF2, a heterotrimeric complex composed of an α, β, and γ subunit. eIF2γ binds GTP and initiator Met-tRNA (Met-tRNAi) (3) to form a eIF2•GTP• Met-tRNAi ternary complex (TC). The TC, together with other translation initiation factors and the 40S ribosomal subunit, scans the mRNA for AUG start codons. Upon base pairing of Met-tRNAi to the start codon, eIF2-bound GTP is hydrolyzed and eIF2•GDP is released from the translation complex. To reactivate eIF2, GDP is displaced by eIF2B, a guanine nucleotide exchange factor (GEF). eIF2B is a large decamer composed of a homodimer of a heteropentamer protein complex (4). The interplay between eIF2 and eIF2B is targeted by the ISR to regulate translation efficiency. In response to stress, eIF2 kinases are activated and subsequently phosphorylate a single, conserved Ser-51 residue in eIF2α. Four eIF2α kinases have been identified: PKR (protein kinase R), which is activated by recognition of 'non-self' (e.g. viral) RNA (5, 6); PERK (PKR-like endoplasmic reticulum kinase), which responds to an accumulation of misfolded proteins in the ER (7); GCN2 (general control nonderepressible 2), which is activated by amino acid starvation and UV light (8, 9); and HRI (heme-regulated inhibitor), which is activated at low levels of heme and exposure to heavy metals (10). Phosphorylation of eIF2α inhibits eIF2B by stabilizing its association with eIF2•GDP (11). Since the levels of eIF2B levels are low compared to those of eIF2 (12), limited quantities of P-eIF2α can efficiently deplete available eIF2B pools and thus inhibit eIF2B-mediated nucleotide exchange (11). Impairing eIF2B leads to the general inhibition of protein synthesis and to the aggregation of inactive translation initiation complexes into stress granules (SGs). At the same time, it promotes translation of a selected group of genes, such as ATF4, a transcription factor that promotes cell recovery and survival. These particular mRNAs contain short, upstream open-reading frames (uORFs), whose inhibitory function is suppressed when TCs become limiting upon ISR induction.

Dephosphorylation of eIF2α signals to terminate the ISR and restore protein synthesis (13). However, upon severe or long-lasting cellular stress, the capacity of the ISR to resolve the stress can fail. In this case, the ISR initiates a cell death program through the increased production of proapoptotic components (14). ISR kinase-mediated phosphorylation and dephosphorylation of eIF2α are central to

normal cell functioning. They play roles in the regulation of translation during mitosis and thereby in cytokinesis and cell proliferation (15–17).

Dysregulation of the ISR has been linked to cancer, diabetes, and inflammation (18–20). Moreover, there is growing evidence of persistent, smoldering ISR activation in neurodegenerative diseases and conditions exhibiting memory consolidation defects, such as traumatic brain injury (18–21). Pharmacological modulation of the ISR has been proposed as a promising therapeutic strategy to treat these neurological conditions that are characterized by chronic eIF2α phosphorylation. Recently, a small molecule ISR inhibitor, ISRIB, was identified to rescue protein translation and prevent SG formation in the presence of P-eIF2α (19, 22). Structural, genetic and biochemical evidence revealed that ISRIB targets eIF2B. (23–26). ISRIB enhances eIF2B's GEF activity by promoting the assembly of the fully active heterodecameric eIF2B complex from smaller subcomplexes (24, 25). ISRIB's ability to restore the cellular translational capacity upon ISR activation implicated it as a promising tool to modulate ISR-regulated neurological processes and diseases. Indeed, ISRIB enhances cognitive memory processes (19), has beneficial effects in prion-diseased mice (27), and remedies cognitive defects resulting from brain injuries (21). Remarkably, ISRIB does so without causing the side-effects that were previously observed upon suppressing the ISR by approaches that directly targeted eIF2α kinases *in vivo* (27–29).

In this study, we initially set out to investigate the effect of ISRIB in cells infected with an ISR-inducing recombinant picornavirus lacking its PKR antagonist (30, 31). We observed that ISRIB suppressed the ISR early in infection, when the amount of viral dsRNA and the level of P-eIF2α were relatively low, but not late in infection, when dsRNA and P-eIF2α levels were relatively high. This prompted us to investigate more systematically ISRIB's ability to rescue translation at varying levels of P-eIF2α. To this end, we treated cells with different concentrations of poly(I:C) or arsenite, which trigger the ISR by activating PKR or HRI, respectively. The results show that ISRIB inhibits the ISR when P-eIF2α levels are below a critical threshold (i.e. 45%-70% of the maximum phosphorylation), but not when P-eIF2α levels exceed this threshold level. These findings are consistent with *in vitro* studies (24) and demonstrate that potentially negative effects of pharmacological eIF2B assembly may be side-stepped under conditions of enhanced phosphorylation of eIF2. The observation that ISRIB is only functional within a narrow range of P-eIF2α concentrations may explain the lack of toxic side-effects that ISRIB displays *in vivo*.

Results

ISRIB inhibits the ISR induced by a recombinant picornavirus only early in infection, when P-eIF2α levels are relatively low. Picornaviruses, like other RNA viruses, synthesize dsRNA in an indispensable intermediate step of their replication process. These dsRNAs are detected by PKR to activate the ISR and limit the production of viral proteins. As a counter measure, many viruses have evolved strategies to delay or suppress this antiviral response. We set out to test the ability of ISRIB to inhibit the ISR during infection with a recombinant encephalomyocarditis virus (EMCV) containing debilitating mutations in a zinc-finger domain of its Leader protein, the viral protein that serves as PKR antagonist (EMCV-L^{Zn}) (32, 33). To assess the effect of ISRIB on the ISR in virus-infected cells, we treated HeLa-R19 cells with ISRIB for 1 h from 5 h post-infection (p.i.) until 6 h p.i. and monitored active translation using a ribopuromycilation assay for 15 min at the 6 h time point p.i. (34). This time point is relatively late in the infection cycle, as a single round of replication of this virus only takes 6 to 8 h (Fig 1A). Viral dsRNA replication intermediates are readily detected at ~4 h p.i. and reach a maximum level at ~6 h p.i. (Fig 1B). As a positive control, we treated cells with 50 μM sodium arsenite, a commonly used method to trigger the ISR via HRI activation (35, 36). In both arsenite-treated and virus-infected cells, we observed eIF2α phosphorylation and concomitant translational repression. Remarkably, ISRIB treatment failed to restore translation efficiency in infected cells, while translation in arsenite-treated cells was largely rescued (Fig 1C). Similar results were obtained in U2OS cells, suggesting that this effect was not cell type specific (Supplementary Fig. S1). We noted that the level of eIF2α phosphorylation in virus-infected cells at 6 h p.i. was higher than in cells treated with 50 μM arsenite, suggesting a correlation between ISRIB's ability to inhibit the ISR and the extent of eIF2α phosphorylation.

We hypothesized that ISRIB is only functional when P-eIF2α levels are relatively low. To test this notion, we monitored the effects of ISRIB on SG formation in EMCV-L^{Zn} infected cells at earlier time points p.i., when smaller amounts of dsRNA were present. ISRIB suppressed SG formation at the earliest time point at which SGs were detected (4 h p.i.) but not later in infection (Fig 2A), suggesting that ISRIB's ability to antagonize the ISR indeed depends on the concentration of the stress trigger. We next quantified intracellular P-eIF2α levels by flow cytometry. Indeed, the level of P-eIF2α in virus-infected cells increased gradually from 3 to 6 h p.i. (Fig 2B), correlating with the timing of dsRNAs accumulation (Fig 1B) and the appearance of SGs (Fig 2A). Furthermore, our data indicated that a plateau level of P-eIF2α was reached late in infection (5 h – 6 h p.i.). To rule out that this observed maximum level of P-eIF2α was caused by a detection limit of our flow cytometry approach, we compared flow cytometry (Fig S2A) and Western blotting (Supplementary Fig. S2B) as readout methods for P-eIF2α levels in cells stressed with increasing arsenite concentrations. The arsenite concentration at which the plateau level

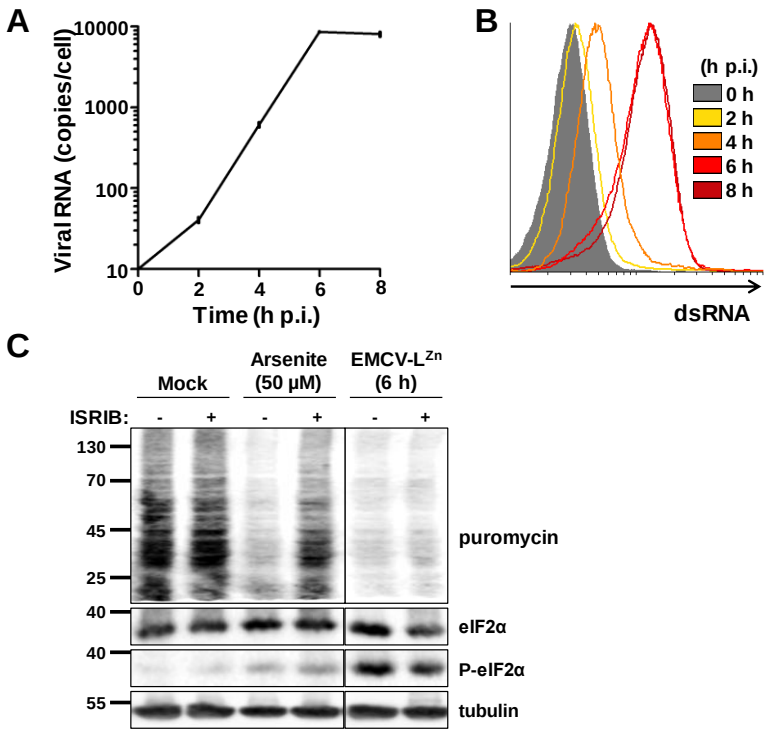

Figure 1. ISRIB does not inhibit virus-induced ISR activity late in infection. *(A/B) HeLa-R19 cells were infected at MOI 20 with EMCV-L^{Zn}. (A) At the indicated time-points, EMCV-L^{Zn} genome copies per cell was quantified by qPCR. A representative of two independent experiments is shown. Error bars indicate SEM of triplicate measurements. (B) At the same time-points, dsRNA content in EMCV-L^{Zn}-infected cells was analyzed by flow cytometry (n=3). (C) Cells were infected with EMCV-L^{Zn} for 6 h, or treated with 50 µM arsenite for 1 h. 1 h prior to harvesting, cells were treated with 200 nM ISRIB or left untreated. 15 min prior to harvesting, all samples were treated with 20 µg/ml puromycin. Arsenite and EMCV-L^{Zn} were kept the cells during these treatments. Subsequently, cells were harvested and analyzed by Western blot, using the indicated antibodies. A representative of two independent experiments is shown.*

of P-eIF2α level was reached (~250 µM) was similar between the two detection methods. By comparing Western blot band intensity ratios of P-eIF2α and (total) eIF2α in cell lysates to those of purified eIF2α samples containing known percentages of P-eIF2α (Fig S3), we furthermore showed that this upper limit of P-eIF2α levels (defined as 100% P-eIF2α) represents almost complete phosphorylation of the cellular eIF2α pool. Collectively, these data demonstrate that the maximum level of eIF2α phosphorylation observed under harsh stress conditions represents the upper limit of eIF2α phosphorylation that was reached.

Taken together, the data suggest that during EMCV-L^{Zn} infection, increasing concentrations of dsRNA cause the level of P-eIF2α to gradually increase until it reaches a plateau level from ~5 h p.i. onwards.

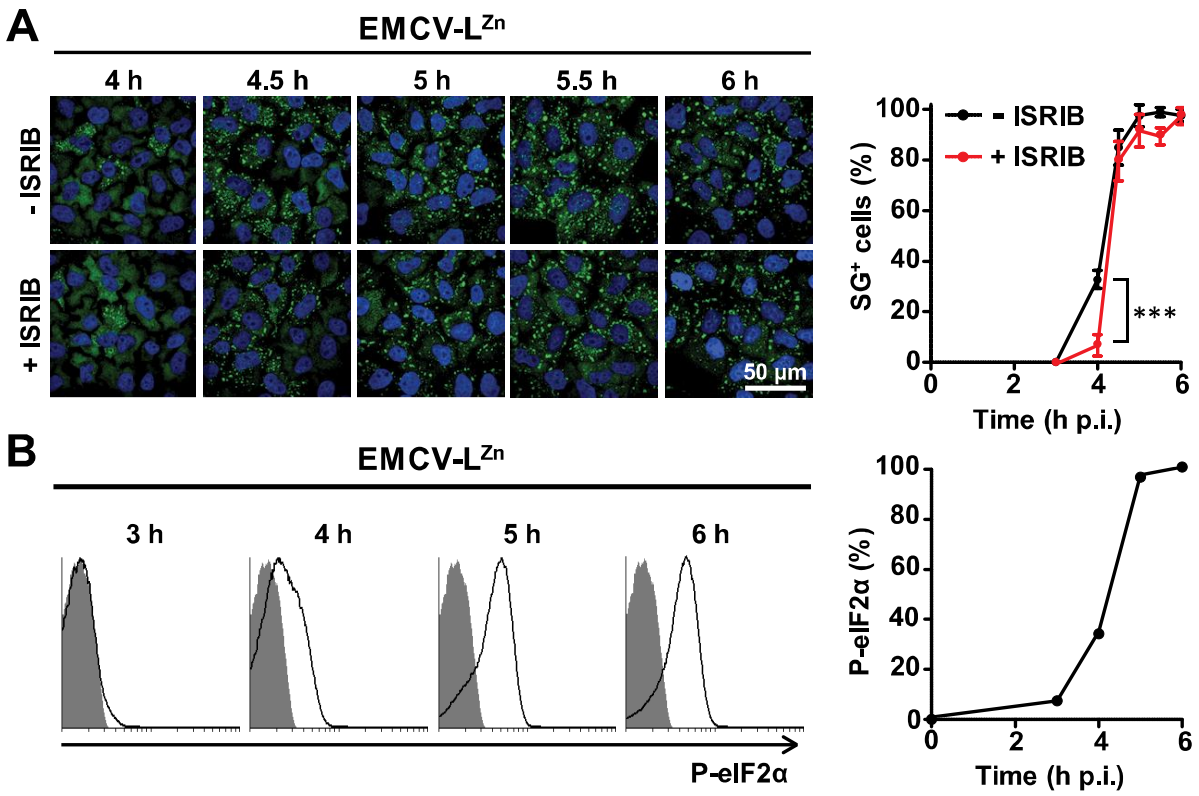

Figure 2. ISRIB only inhibits the virus-induced ISR early in infection, when P-eIF2α levels are relatively low. *HeLa-R19 cells were infected at MOI 20 with EMCV-L^{Zn}. (A) At the indicated time-points, cells were fixed in PFA and analyzed by IFA using antibodies specific to SG marker G3BP1. Percentages of SG positive cells were quantified from at least 4 images. Representative images are shown in the left panels, quantification is shown in the right panel. Error bars indicate SEM. Statistical significance was analyzed by a two-way ANOVA, with Bonferroni post-hoc test (***, p<0.001). (B) At the indicated time-points, cells were harvested and the level of P-eIF2α was analyzed by flow cytometry. Results are shown as histograms (left panels) and the percentage increase in MFI is shown in the right panel. Mock infected cells are set at 0% induction, maximum P-eIF2α level was set at 100% induction. Shown is a representative of two independent experiments.*

At these high P-eIF2α levels, ISRIB no longer antagonized the ISR. Upon further increasing the ISRIB concentration (up to 1600 nM), ISRIB still failed to suppress the ISR (Fig S4). By contrast, up to ~4 h p.i. when P-eIF2α levels were ~35% of the maximal level, ISRIB potently suppressed the ISR in infected cells.

ISRIB fails to antagonize the effects of high P-eIF2α levels induced by poly(I:C). Virus infections cause extensive changes in multiple processes in the host cell. Hence, we could not exclude that some virus-induced change(s) in one way or the other affected the ISRIB's ability to suppress the ISR in infected cells. To provide more direct support for the link between the level of P-eIF2α and the ability of ISRIB

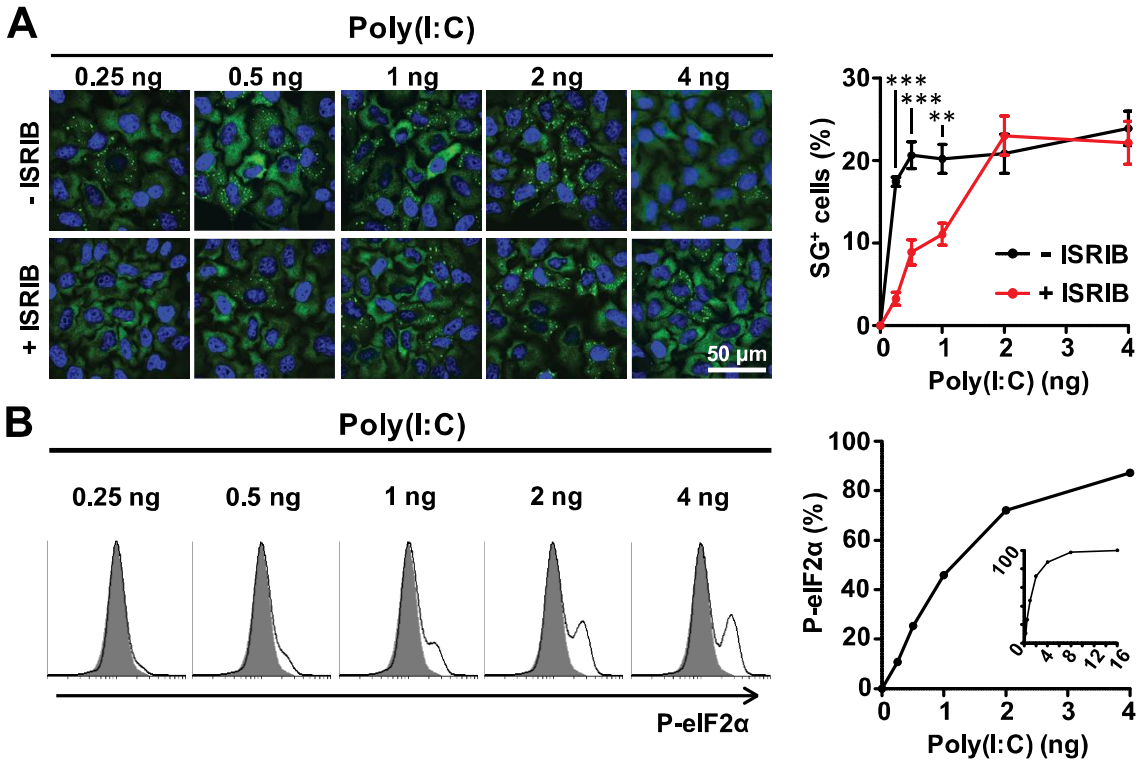

Figure 3. ISRIB fails to counteract high poly(I:C)-induced P-eIF2α levels. *HeLa-R19 cells were transfected with a total of 100 ng RNA, out of which the indicated amounts of poly(I:C), supplemented with total cellular RNA. (A) 6 h post transfection, cells were fixed in PFA and SG formation was analyzed by IFA. Shown are representative images (left panels) and quantifications of at least 4 images per sample (right panel). Error bars indicate SEM. Statistical significance was analyzed by a two-way ANOVA, with Bonferroni post-hoc test (**, p<0.01; ***, p<0.001). (B) 6 h post transfection, P-eIF2α levels in the transfected cell populations were analyzed by flow cytometry. Results are shown as histograms (left panels) and the percentage increase in P-eIF2α MFI is shown in the right panel. Mock infected cells are set at 0% induction, maximum P-eIF2α level was set at 100% induction. Shown is a representative of two independent experiments.*

to counteract the dsRNA-induced ISR, we next tested the efficacy of ISRIB in cells transfected with increasing concentrations of poly(I:C), a dsRNA mimic that – like EMCV-L^{Zn} infection – triggers the PKR branch of the ISR (Fig 3). In the absence of ISRIB, we observed SG formation in cells transfected with 0.25 ng of poly(I:C) or more. ISRIB only prevented SG formation in cells transfected with relatively low poly(I:C) concentrations (1 ng or less) but not when larger amounts of poly(I:C) were used (Fig 3A). At the highest concentration of poly(I:C) at which ISRIB could counteract the ISR (i.e., 1 ng), the P-eIF2α level was ~45% of the maximum (Fig 3B). Transfection of 2 ng of poly(I:C) induced >70% of the maximum P-eIF2α concentration and rendered ISRIB ineffective. Together, these data suggest that a threshold level of P-eIF2α exists in the range of 45%-70% of the maximum, above which ISRIB can no longer antagonize the ISR.

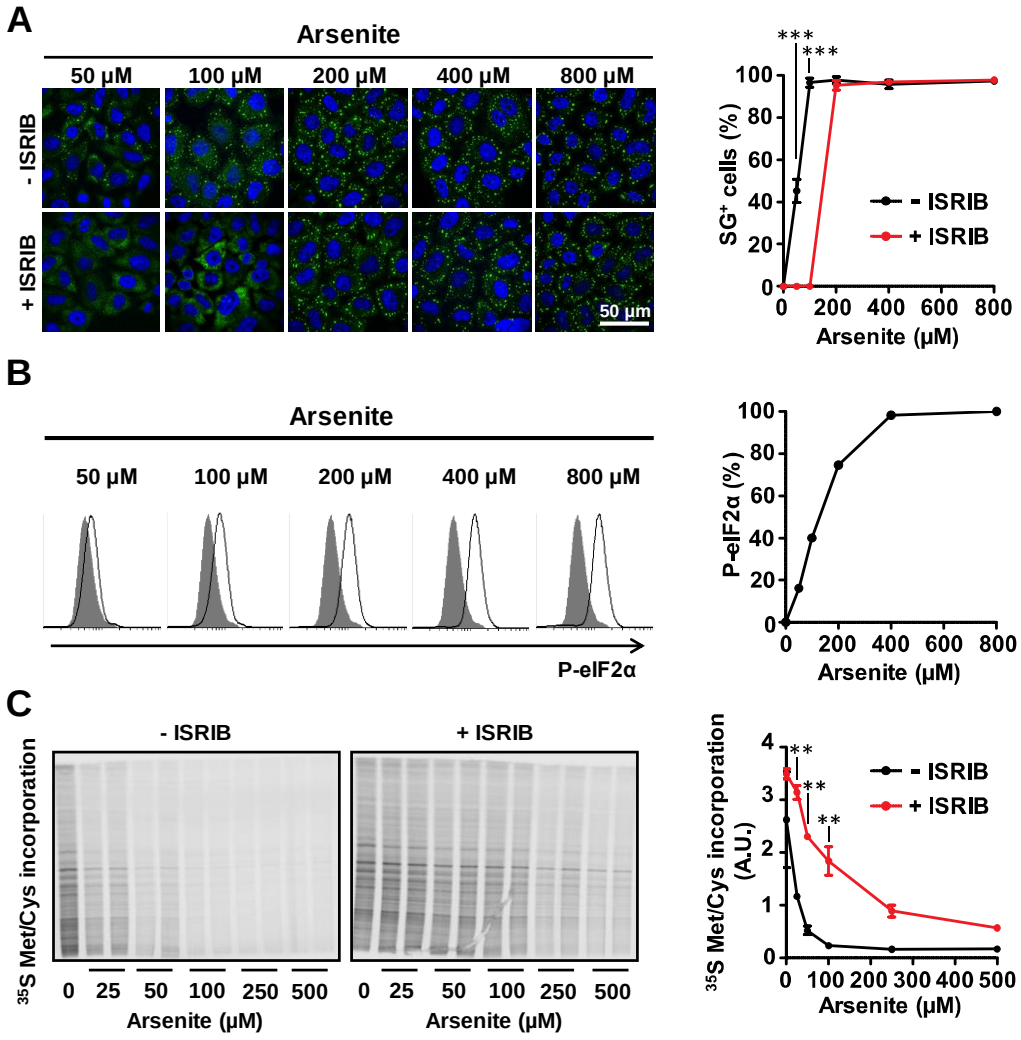

Figure 4. ISRIB does not rescue translation in the presence of high P-eIF2α levels irrespective of the eIF2α kinase involved. *HeLa-R19 cells were treated with the indicated arsenite concentrations for 1 h. (A) Cells were fixed in PFA and SG formation was analyzed by IFA, using antibodies specific to G3BP1. Shown are representative images (left panels) and quantifications of at least 4 images per sample (right panel). Error bars indicate SEM. Statistical significance was analyzed by a two-way ANOVA, with Bonferroni post-hoc test (***, p<0.001). (B) P-eIF2α levels were analyzed by flow cytometry. Results are shown as histograms (left panels) and the percentage increase in P-eIF2α MFI is shown in the right panel. Mock infected cells are set at 0% induction, maximum P-eIF2α level was set at 100% induction. Shown is a representative of three independent experiments. (C) Cells were treated for 30 min with the indicated arsenite concentrations, and subsequently translation was pulse labeled using ^{35}S Met/Cys for another 90 min in medium containing the same arsenite concentrations. ^{35}S incorporation into newly synthesized proteins was analyzed using a phosphor imager (left panel), and quantified using ImageJ software (right panel). Error bars indicate SEM of duplicate measurements. A representative of two independent experiments is shown. Statistical significance was analyzed by a two-way ANOVA, with Bonferroni post-hoc test (**, p<0.01).*

ISRIB also fails to antagonize high P-eIF2α levels induced by arsenite treatment. Thus far, we tested ISRIB in cells exposed to EMCV-L^{Zn} infection or poly(I:C) transfection, both of which induce the ISR via activation of the dsRNA sensor PKR. Since ISRIB acts downstream of P-eIF2α, we expected similar results irrespective of which stress sensor was activated. To provide further support for this notion, we used multiple arsenite concentrations to induce HRI-mediated ISR activation. Again, we correlated the ability of ISRIB to counteract SG formation (Fig 4A) to P-eIF2α levels (Fig 4B). In the absence of ISRIB, SG formation was observed in cells treated with 50 µM arsenite or more. The presence of ISRIB increased the arsenite concentration required to induce SG formation to 200 µM or more (Fig 4A). The highest arsenite concentration at which ISRIB blocked SG formation (100 µM) resulted in ~40% of the maximum P-eIF2α level. At 200 µM arsenite, which induced ~75% P-eIF2α, ISRIB showed no effect. Importantly, the P-eIF2α threshold level above which ISRIB no longer antagonized the ISR (between 40% and 70%) was similar to that observed in poly(I:C) transfected cells (i.e. between 45 and 70%).

To directly determine ISRIB's influence on translation rates, we performed [^{35}S]methionine pulse labelling to monitor active translation in cells exposed to different arsenite concentrations in the presence or absence of ISRIB (Fig 4C). In the absence of ISRIB, arsenite concentrations of 25 µM and higher were sufficient to inhibit translation. ISRIB largely rescued translation in cells treated with low arsenite concentrations (between 25 µM and 100 µM). However, upon treatment with higher arsenite concentrations (>250 µM), translation was severely impaired even in the presence of ISRIB. These data

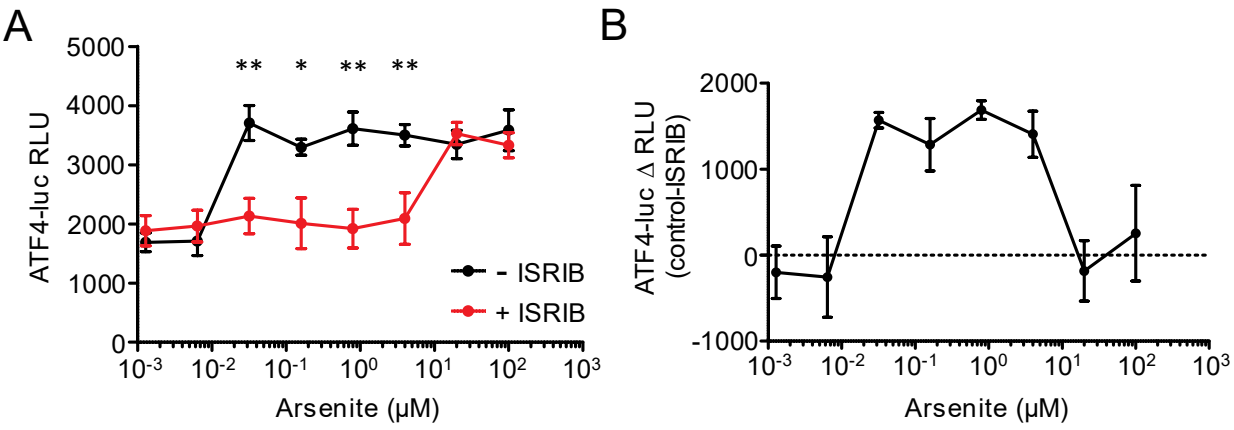

Figure 5. ISRIB interfere with ATF4 expression only within a defined window of P-eIF2α concentrations. *HEK293T cells stably expressing the ATF4-luc reporter were treated with the indicated amounts of arsenite for 2 h in the presence or absence of ISRIB. Shown are the RLU values (A), plotted once more as the difference in RLU values between cells treated with ISRIB and without ISRIB (B). Error bars indicate SEM of triplicate measurements. A representative of two independent experiments is shown. Statistical significance was analyzed by a two-way ANOVA, with Bonferroni post-hoc test (*, p<0.05; **, p<0.01).*

are in line with our immunofluorescence data (Fig 4A) showing the formation of SGs in ISRIB treated cells exp osed to arsenite c oncentrations of 200 µM and higher. Besides the inhibitory effect on general translation, the ISR mediates enhanced translation of a subset of mRNAs that contain uORFs, such as ATF4 mRNA. To test the effects of ISRIB on the expression of these stress-induced proteins, we used a HEK293T reporter cell line that expresses firefly luciferase under the control of the ATF4 uORFs (19). To activate the ISR, we treated cells with the indicated arsenite concentrations for two hours. In the absence of ISRIB, we observed increased ATF4 reporter expression upon treatment with arsenite concentrations of 32 nM and higher (Fig 5A). This is in line with a previous report which shows that less p-eIF2α is required for the induction of ATF4 than for translational inhibition (37). At low arsenite concentrations (32 nM – 4 µM), ISRIB prevented the enhanced expression of the ATF4 reporter (Fig 5B). In contrast, we found that upon treatment with higher concentrations of arsenite (≥20 µM), ATF4 reporter expression was induced even in the presence of ISRIB.

Discussion

In this study, we provide evidence that ISRIB antagonizes the ISR only when P-eIF2α levels are below a critical threshold. By analyzing translation efficiency and stress granule formation in HeLa or U2OS cells infected with a recombinant picornavirus lacking its PKR antagonist, we showed that ISRIB inhibited the ISR early in infection, when levels of viral dsRNA and P-eIF2α were relatively low, but not at later time points when levels of dsRNA and P-eIF2α were high. To extend this observation, we performed a detailed analysis of the P-eIF2α levels and the ability of ISRIB to inhibit the ISR upon treatment of HeLa cells with varying concentrations of poly(I:C) or arsenite. We found that the level of P-eIF2α correlated with the concentration of stress trigger used but reached a plateau under severe stress conditions. Thus, the extent of eIF2α phosphorylation is graduated, quantitatively reflecting the severity of the stress situation. Importantly, the P-eIF2α concentration continued to increase even beyond the concentration necessary to suppress protein synthesis. Irrespective of the stress inducer used, ISRIB antagonized the ISR only when P-eIF2α levels were below a critical threshold. This threshold was determined to be somewhere between 45% and 70% of the maximum P-eIF2α level that could be observed in HeLa cells and was similar in cells infected with virus, transfected with poly(I:C), or treated with arsenite. Using an ATF4 reporter cell line, we also showed that ISRIB failed to block the expression of stress-induced proteins in the presence of high intracellular P-eIF2α levels. Taken together, our data show that ISRIB is only effective under conditions of limited stress.

Early studies of translation repression by P-eIF2α have shown that partial eIF2α phosphorylation could efficiently block translation. In reticulocyte lysates, translation initiation was suppressed when the fraction of phosphorylated eIF2α was increased from ~10% under basal conditions to 20%-40% (38). In line with these data, our results show that only ~20% of the maximum level of P-eIF2α is sufficient to block translation and induce the formation of SGs in living cells. In the presence of ISRIB, this threshold level of P-eIF2α was increased to 45%-70% of the maximum. Importantly, this threshold level of P-eIF2α appeared independent of the stress trigger, and hence of the eIF2α kinase involved. These data are in line with published *in vitro* data showing that ISRIB increased the GEF activity of eIF2B in the presence of P-eIF2, but failed to do so when the P-eIF2:eIF2 ratio was increased further (24). Taken together, the data from these *in vitro* GEF assays and our data from assays in live cells suggest that ISRIB desensitizes cells to P-eIF2α, unless the P-eIF2α concentration exceeds a critical threshold level.

Formation of decameric eIF2B requires dimerization of eIF2B(βγδε) subcomplexes. The resulting octamers contain an interface for association of an eIF2Bα dimer (25). Since eIF2Bα is essential for P-eIF2's ability to inhibit eIF2B (39), P-eIF2 likely only binds the full eIF2B decamer, not its subcomplexes. Thereby, P-eIF2 likely promotes eIF2B decamer formation and mediates sequestration of eIF2B

subcomplexes into inactive P-eIF2•eIF2B complexes. Consequently, high P-eIF2 concentrations may deplete the cytoplasmic pools of eIF2B building blocks. This provides a plausible explanation for ISRIB's lack of effect in the presence of high P-eIF2 levels, since the absence of eIF2B subcomplexes prevents ISRIB from assembling active eIF2B decamers.

In most studies that investigate the ISR, eIF2α phosphorylation is induced by exposing cells to sodium arsenite, thapsigargin, tunicamycin, DTT, MG132, poly(I:C), or heat shock. It is unclear to what extent these treatments reflect physiologically relevant stress situations. In this study, we used a virus lacking its PKR antagonist to assess the ability of ISRIB to antagonize the ISR induced by a viral stress trigger (i.e. viral dsRNA) with natural intracellular localization and in physiological quantities. We showed that ISRIB inhibits the ISR early in infection, when little viral dsRNA has been produced and P-eIF2α levels are relatively low, but not late in infection, when viral dsRNA and P-eIF2α levels are high. Thus, levels of P-eIF2α that can no longer be antagonized by ISRIB can be reached in living cells under natural conditions.

While the ISR protects cells from stressful situations, dysregulated ISR signaling may have pathological consequences *in vivo*, and may be involved in the presentation of cognitive defects neurological disorders like Parkinson's disease, Alzheimers disease, Huntington's disease, amylotropic lateral sclerosis (ALS), and prion diseases (40–44). ISRIB provided significant beneficial effects in a mouse model of prion disease, and it also reversed neurological damage caused by traumatic brain injury (21), all without exhibiting overt toxic side-effects (27,45). By contrast, pharmacological inhibition of PERK caused pancreatic toxicity in mice, and knockdown of PKR had aberrant effect on cytokinesis (15, 28). Paradoxically, ISRIB did not display such adverse side effects *in vivo* (27). Our observation that ISRIB is functional only within a narrow range of P-eIF2α levels resolves this paradox. According to this notion ISRIB does not negatively affect high(er) P-eIF2α levels that may be relevant for certain stages during cell growth or proliferation. The fact that ISRIB has beneficial effects *in vivo* against several neurological disorders and other stress-induced pathologies suggests that P-eIF2α levels would be relatively modest under these conditions. These considerations stress the importance to obtain quantitative data on how much eIF2α phosphorylation occurs in neurological disorders. More insight into levels of eIF2B, eIF2, and P-eIF2α and the assembly state of these multiprotein complexes in different cell / tissue types exposed to different stress and disease conditions will be invaluable to predict and/or to evaluate effects of ISRIB treatment.

Materials & Methods

Chemical inhibitors and RNA ligands. ISRIB (SML0843) and puromycin (P9620) were purchased at Sigma-Aldrich and used at 200 nM and 20 μg/ml, respectively, unless indicated otherwise. Poly(I:C) was purchased at GE Healthcare. Sodium arsenite was purchased at Riedel-de-Haën.

Cells and viruses. HEK293T, HeLa-R19, U2OS and BHK-21 cells were maintained in Dulbecco's modified Eagle's medium (Lonza) supplemented with 10% fetal calf serum (FCS) and penicillin-streptomycin (100 U/ml and 100 μg/ml). Recombinant EMCV with Zn-finger domain mutation in the Leader protein (EMCV-L^{Zn}, (31)) was propagated in BHK-21 cells.

Poly(I:C) transfection. Semi-confluent monolayers of HeLa-R19 cells grown in 24-well clusters were transfected with poly(I:C) using Lipofectamine2000 (ThermoFisher) according to manufacturer's instructions. For each transfection, the indicated amounts of poly(I:C) were combined with total cellular RNA from resting HeLa-R19 to a constant 100 ng per well.

ATF4 reporter assay. HEK293T cells carrying an ATF4 luciferase reporter (19) were plated on poly-lysine coated 96 well plates (Greiner Bio-One, Monroe, NC) at 25,000 cells per well. Cells were simultaneously treated with or without 200 nM ISRIB, and with sodium arsenite at increasing concentrations. Luminescence was measured using One Glo (Promega, Madison, WI) as specified by the manufacturer.

Ribopuromycilation assay. Cells in 10-cm dishes were either mock treated, treated with 50 μM arsenite, or infected with EMCV-L^{Zn} (MOI=20) in the presence or absence of 200 nM ISRIB. After the indicated incubation time puromycin (20 μg/ml) was added to the medium and incubated for another 15 min. Cells were collected and used for Western blot analysis.

^{35}S pulse labelling of active translation. Semi-confluent cell monolayers were first starved in medium lacking methionine and cysteine for 30 min, and then treated with the indicated arsenite concentrations for 30 min with or without ISRIB. Subsequently, newly synthesized proteins were labelled with 50 μCi/ml ^{35}S Met/Cys (Perkin Elmer) for another 90 min. Cells were then lysed, and proteins were separated using SDS-PAGE. Subsequently, gels were dried on whatman paper and analyzed using a phosphor imager.

Immunofluorescence assay. Immunofluorescence assays were performed as described previously (46), using primary antibody mouse-α-G3BP1 (BD Biosciences, #611126, 1:1,000), and secondary antibody donkey-α-mouse-Alexa488 (ThermoFisher, #A-21202, 1:200).

Western blot analysis. Western blot assays were performed as described previously (46), using primary antibodies rabbit-α-puromycin (Merck Millipore, MABE343, 1:1,000), rabbit-α-eIF2α (Cell Signaling, #9722 1:2,000), rabbit-α-eIF2α-P (Abcam, ab32157 1:1,000) or mouse-α-Tubulin (Sigma-Aldrich, T9026, 1:5,000), and secondary antibodies goat-α-mouse-IRDye680 (LI-COR, 1:15,000) or goat-α-rabbit-IRDye800 (LI-COR, 1:15,000).

Flow cytometry analysis of eIF2α phosphorylation. Cells were released using trypsin and fixed with paraformaldehyde (2% in PBS) for 20 min. Cells were washed once with FACS buffer (PBS + 1% BSA) and incubated in ice-cold methanol for 10 min. Cells were washed once with FACS buffer and incubated for 45 min with primary rabbit-α-eIF2α-P (Abcam, ab32157 1:100) and then for 45 min with donkey-α-rabbit-Alexa647 (ThermoFisher, #A-31573, 1:200) diluted in FACS buffer at room temperature. In between and after the incubations the cells were washed, twice each time, with FACS buffer. Finally, the cells were suspended in PBS + 1% paraformaldehyde and analyzed on the FACSCanto II (BD Biosciences).

Purification of eIF2α and phosphorylated eIF2α. Human eIF2, codon-optimized for *E. coli*, was cloned into a pET28a expression vector. This plasmid was co-transformed with the chaperone plasmid pG-Tf2 (Takara Bio) and, for phosphorylated eIF2, an additional plasmid expressing PERK kinase domain. eIF2α was purified by sequential nickel-affinity, cation-exchange, and size exclusion chromatography. Details are included in the supplement.

Acknowledgments

The work is supported by the Netherlands Organization for Scientific Research through a Vici grant (NWO-918.12.628) to Frank van Kuppeveld and a Veni grant (NWO-863.13.008) to Martijn Langereis. Peter Walter is an Investigator of the Howard Hughes Medical Institute. We thank Carolin Klose for assistance with (p-)eIF2α expressions.

References

1. Arimoto K, Fukuda H, Imajoh-Ohmi S, Saito H, Takekawa M, Formation of stress granules inhibits apoptosis by suppressing stress-responsive MAPK pathways. *Nat Cell Biol* **10**, 1324–1332 (2008)

2. Takahara T, Maeda T, Transient Sequestration of TORC1 into Stress Granules during Heat Stress. *Mol Cell* **47**, 242–252. (2012)

3. Pain VM, Initiation of Protein Synthesis in Eukaryotic Cells. *Eur J Biochem* **236**, 747–771 (1996)

4. Hinnebusch AG, Lorsch JR, The mechanism of eukaryotic translation initiation: new insights and challenges. *Cold Spring Harb Perspect Biol* **4**, a011544- (2012)

5. Levin D, London IM, Regulation of protein synthesis: activation by double-stranded RNA of a protein kinase that phosphorylates eukaryotic initiation factor 2. *PNAS.* **75**, 1121–5. (1978)

6. Samuel C, The eIF-2 alpha protein kinases, regulators of translation in eukaryotes from yeasts to humans. *J Biol Chem* **268**, 7603–7606. (1993)

7. Harding HP, Zhang Y, Ron D, Protein translation and folding are coupled by an endoplasmic-reticulum-resident kinase. *Nature* 397, 271–274 (1999)

8. Dever TE, et al., Phosphorylation of initiation factor 2 alpha by protein kinase GCN2 mediates gene-specific translational control of GCN4 in yeast. *Cell* **68**, 585–596 (1992)

9. Marbach I, Licht R, Frohnmeyer H, Engelberg D, Gcn2 mediates Gcn4 activation in response to glucose stimulation or UV radiation not via GCN4 translation. *J Biol Chem* **276**, 16944–51 (2001)

10. Ranu RS, et al., Regulation of protein synthesis in rabbit reticulocyte lysates by the heme-regulated protein kinase: inhibition of interaction of Met-tRNAfMet binding factor with another initiation factor in formation of Met-tRNAfMet.40S ribosomal subunit complexes. *PNAS.* **75**, 745–9 (1978)

11. Matts RL, Levin DH, London IM, Effect of phosphorylation of the alpha-subunit of eukaryotic initiation factor 2 on the function of reversing factor in the initiation of protein synthesis. *PNAS* **80**, 2559–63 (1983)

12. Kulak NA, Pichler G, Paron I, Nagaraj N, Mann M, Minimal, encapsulated proteomic-sample processing applied to copy-number estimation in eukaryotic cells. *Nat Methods*. **11**, 319-24 (2014)

13. Ma Y, Hendershot LM (2003) Delineation of a negative feedback regulatory loop that controls protein translation during endoplasmic reticulum stress. *J Biol Chem* 278(37):34864–34873.

14. Matsumoto H, et al., Selection of autophagy or apoptosis in cells exposed to ER-stress depends on ATF4 expression pattern with or without CHOP expression. *Biol Open* **2**, 1084–1090 (2013)

15. Kim Y, et al., PKR is activated by cellular dsRNAs during mitosis and acts as a mitotic regulator. *Genes Dev* **28**, 1310–1322 (2014)

16. Datta B, Datta R, Mukherjee S, Zhang Z, Increased phosphorylation of eukaryotic initiation factor 2α at the G2/M boundary in human osteosarcoma cells correlates with deglycosylation of p67 and a decreased rate of protein

synthesis. *Exp Cell Res* **250**, 223–230 (1999)

17. Tinton S a, Schepens B, Bruynooghe Y, Beyaert R, Cornelis S, Regulation of the cell-cycle-dependent internal ribosome entry site of the PITSLRE protein kinase: roles of Unr (upstream of N-ras) protein and phosphorylated translation initiation factor eIF-2alpha. *Biochem J.* **385**, 155–163 (2005)

18. Halliday M, Mallucci GR, Review: Modulating the unfolded protein response to prevent neurodegeneration and enhance memory. *Neuropathol Appl Neurobiol* **41**, 414–427 (2015)

19. Sidrauski C, et al., Pharmacological brake-release of mRNA translation enhances cognitive memory. *Elife* **2**, e00498 (2013)

20. Moreno JA, et al., (2012) Sustained translational repression by eIF2α-P mediates prion neurodegeneration. *Nature* **485**, 507–511 (2012)

21. Chou A, et al., Inhibition of the integrated stress response reverses cognitive deficits after traumatic brain injury. *PNAS.* **114**, E6420-E6426 (2017)

22. Sidrauski C, McGeachy AM, Ingolia NT, Walter P, The small molecule ISRIB reverses the effects of eIF2α phosphorylation on translation and stress granule assembly. *Elife* **4** (2015)

23. Sekine Y, et al. Mutations in a translation initiation factor identify the target of a memory-enhancing compound. *Science* **348**, 1027-30 (2015)

24. Sidrauski C, et al., Pharmacological dimerization and activation of the exchange factor eIF2B antagonizes theintegrated stress response. *Elife* **4** (2015)

25. Tsai JC, et al., Structure of the nucleotide exchange factor eIF2B reveals mechanism of memory-enhancing molecule. *Science* **359**, pii: eaaq0939 (2018)

26. Zyryanova AF, et al., Binding of ISRIB reveals a regulatory site in the nucleotide exchange factor eIF2B. *Science* **359**, 1533-1536 (2018)

27. Halliday M, et al., Partial restoration of protein synthesis rates by the small molecule ISRIB prevents neurodegeneration without pancreatic toxicity. *Cell Death Dis* **6**, e1672 (2015)

28. Moreno JA, et al., Oral treatment targeting the unfolded protein response prevents neurodegeneration and clinical disease in prion-infected mice. *Sci Transl Med* **5**, 206ra138 (2013)

29. Harding HP, et al., Diabetes mellitus and exocrine pancreatic dysfunction in Perk-/- mice reveals a role for translational control in secretory cell survival. *Mol Cell* **7**, 1153–1163 (2001)

30. Feng Q, et al., Enterovirus 2Apro targets MDA5 and MAVS in infected cells. *J Virol* **88**, 3369–78 (2014)

31. Hato S V, et al., The mengovirus leader protein blocks interferon-alpha/beta gene transcription and inhibits activation of interferon regulatory factor 3. *Cell Microbiol* **9**, 2921–2930 (2007)

32. Langereis MA, Feng Q, van Kuppeveld FJ, MDA5 localizes to stress granules, but this localization is not required for the induction of type I interferon. *J Virol* **87**, 6314–25 (2013)

33. Borghese F, Michiels T, The Leader Protein of Cardioviruses Inhibits Stress Granule Assembly. *J Virol* **85**, 9614–9622 (2011)

34. Schmidt EK, Clavarino G, Ceppi M, Pierre P, SUnSET, a nonradioactive method to monitor protein synthesis. *Nat Methods* **6**, 275–277 (2009)

35. Rozelle DK, Filone CM, Kedersha N, Connor JH, Activation of Stress Response Pathways Promotes Formation of Antiviral Granules and Restricts Virus Replication. *Mol Cell Biol*. **34**, 2003-16 (2014)

36. Humoud MN, et al., Feline Calicivirus Infection Disrupts Assembly of Cytoplasmic Stress Granules and Induces G3BP1 Cleavage. *J Virol*. **90**, 6489-6501 (2016)

37. Lu PD, Harding HP, Ron D, Translation reinitiation at alternative open reading frames regulates gene expression in an integrated stress response. *J Cell Biol*. **167**, 27-33 (2004)

38. Leroux A, London I, Regulation of protein synthesis by phosphorylation of eukaryotic initiation factor 2 alpha in intact reticulocytes and reticulocyte lysates. *PNAS.* **79**, 2147–2151 (1982)

39. Pavitt GD, Ramaiah KVA, Kimball SR, Hinnebusch AG, eIF2 independently binds two distinct eIF2b subcomplexes that catalyze and regulate guanine-nucleotide exchange. *Genes Dev* **12**, 514–526 (1998)

40. Chang RC-C, et al., Involvement of double-stranded RNA-dependent protein kinase and phosphorylation of eukaryotic initiation factor-2alpha in neuronal degeneration. *J Neurochem* **83**, 1215–1225 (2002)

41. Hoozemans JJM, et al., Activation of the unfolded protein response in Parkinson's disease. *Biochem Biophys Res Commun* **354**, 707–711 (2007)

42. Atkin JD, et al., Endoplasmic reticulum stress and induction of the unfolded protein response in human sporadic amyotrophic lateral sclerosis. *Neurobiol Dis* **30**, 400–407 (2008)

43. Hetz C, Russelakis-Carneiro M, Maundrell K, Castilla J, Soto C, Caspase-12 and endoplasmic reticulum stress mediate neurotoxicity of pathological prion protein. *EMBO J* **22**, 5435–5445 (2003)

44. Hoozemans JJM, et al., The Unfolded Protein Response Is Activated in Pretangle Neurons in Alzheimer's Disease Hippocampus. *Am J Pathol* **174**, 1241–1251 (2009)

45. Wong YL, et al., eIF2B activator prevents neurological defects caused by a chronic Integrated Stress Response. *bioRxiv*. (2018)

46. Rabouw HH, et al. Middle East Respiratory Coronavirus Accessory Protein 4a Inhibits PKR-Mediated Antiviral Stress Responses. *PLoS Pathog* **12**, e1005982 (2016)

Supplementary Figures

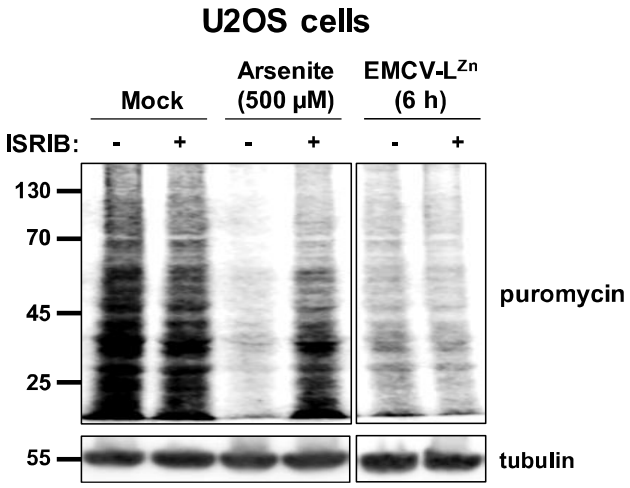

Figure S1. ISRIB does not inhibit EMCV-L^{Zn}-induced ISR activity late in infection in U2OS cells. *U2OS were infected with EMCV-L^{Zn} for 6 h, or treated with 500 µM arsenite for 1 h. 1 h prior to harvesting, cells were treated with 200 nM ISRIB or left untreated. 15 min prior to harvesting, all samples were treated with 20 µg/ml puromycin. Arsenite and EMCV-L^{Zn} containing supernatants were kept on the cells during these treatments. Subsequently, cells were harvested and analyzed by Western blot, using the indicated antibodies.*

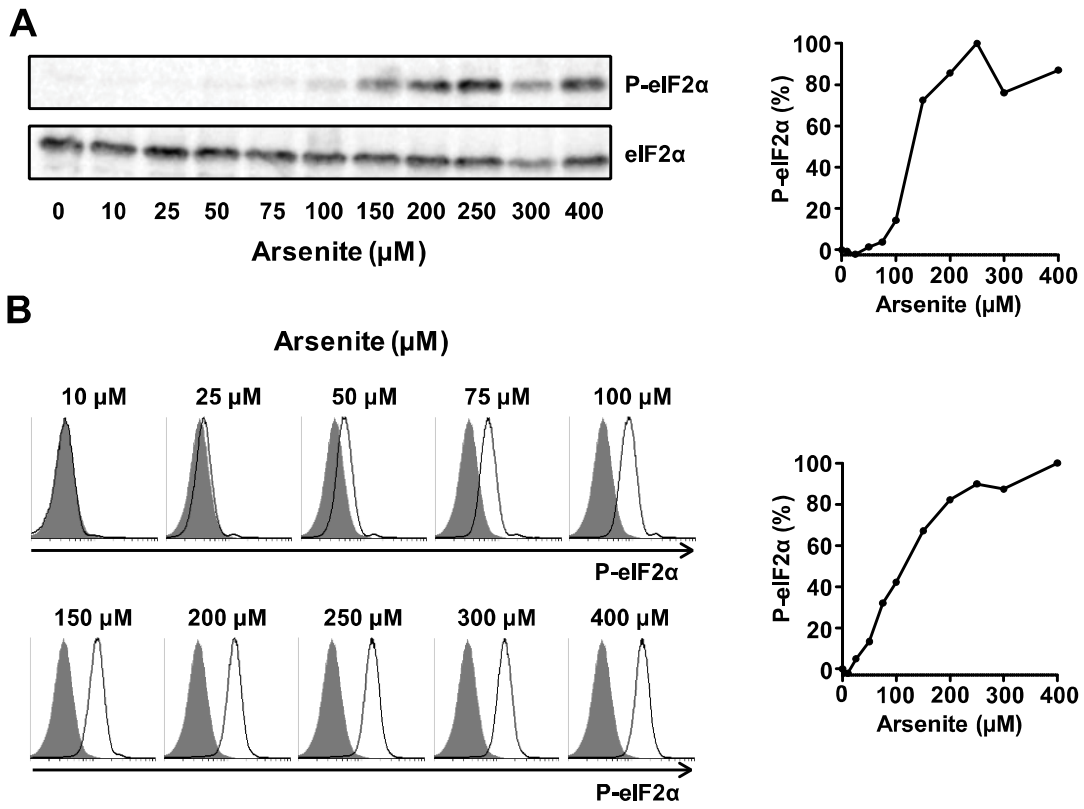

Figure S2. Comparison of Western blot and flow cytometry as read-out method for intracellular P-eIF2α levels. *HeLa-R19 cells were treated with the indicated arsenite concentrations for 1 h. Each sample was split in two, and analyzed by both Western blot and flow cytometry. (A) Western blot analysis of P-eIF2α and eIF2α levels in cells treated with different arsenite concentrations (left panel). Quantification of P-eIF2α band intensities, corrected for eIF2α band intensity, is shown in the right panel. Mock infected cells are set at 0% induction, maximum P-eIF2α level was set at 100% induction. (B) Flow cytometry analysis of P-eIF2α levels in cells treated with different arsenite concentrations. Results are shown as histograms (left panels) and the percentage increase in P-eIF2α MFI is shown in the right panel. Mock infected cells are set at 0% induction, maximum P-eIF2α level was set at 100% induction. A representative of two independent experiments is shown.*

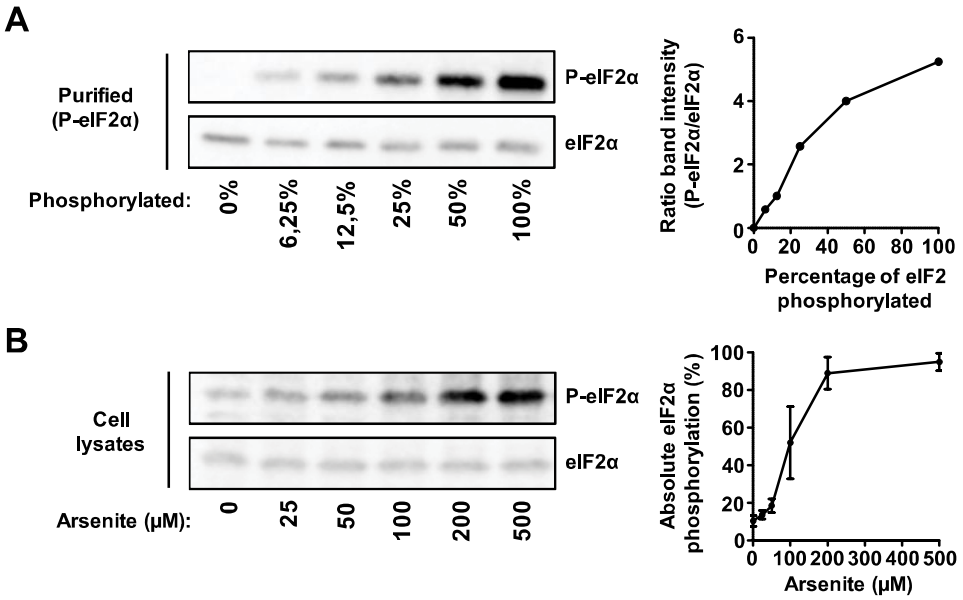

Figure S3. The P-eIF2α plateau level corresponds to almost complete phosphorylation of the eIF2α pool. *(A) purified eIF2α and P-eIF2α samples, as well as mixtures containing the indicated percentages of phosphorylated eIF2α were analyzed by Western blotting. The ratios in band intensities of P-eIF2α and total eIF2α were quantified in ImageJ software, and used to create the standard curve shown in the right panel. (B) Cell lysates from Hela-R19 cells treated with the indicated arsenite concentrations for 1 h were analyzed by Western blotting, and ratios between P-eIF2α and total eIF2α signals were quantified in ImageJ software. Using the standard curve from (A) as reference, we calculated approximate values for the percentages of eIF2α molecules that are phosphorylated in arsenite treated cells (right panel). Averages and standard deviations of two independent experiments are shown.*

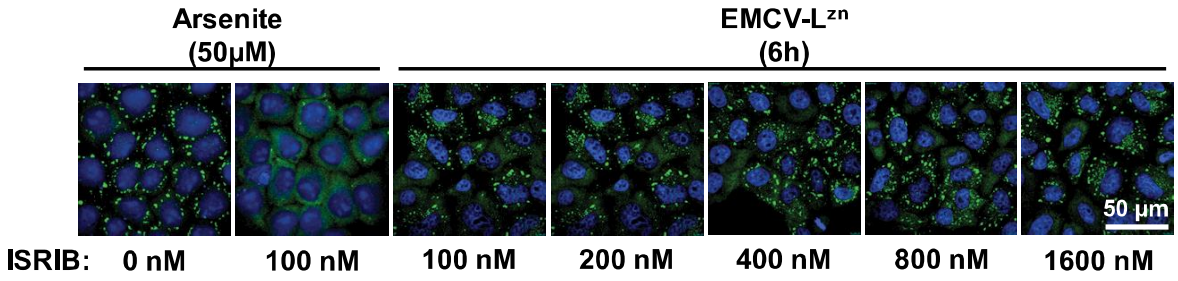

Figure S4. EMCV-L^{Zn} induced ISR activity late in infection is not inhibited by increased ISRIB concentrations. *HeLa-R19 cells were infected with EMCV-L^{Zn} (MOI=10) for 6 h, or treated with 50 μM arsenite for 1 h. 1 h prior to harvesting, cells were treated with the indicated concentrations of ISRIB. Cells were fixed in PFA and SG formation was analyzed by IFA, using antibodies specific to G3BP1.*

Chapter 4

Inhibition of the integrated-stress-response by a viral protein that blocks p-eIF2•eIF2B association

Huib H Rabouw[1], Linda J Visser[1], Tim C Passchier[1], Martijn A Langereis[1], Fan Liu[2], Piero Giansanti[2], Aditya A Anand[3], Mikael E Trellet[4], Alexandre MJJ Bonvin[4], Peter Walter[3], Albert JR Heck[2], Raoul J de Groot[1,#], Frank JM van Kuppeveld[1,#]

[1]Virology Division, Department of Infectious Diseases and Immunology, Faculty of Veterinary Medicine, Utrecht University, Utrecht, The Netherlands

[2]Biomolecular Mass Spectrometry and Proteomics, Utrecht Institute for Pharmaceutical Sciences and Bijvoet Centre for Biomolecular Research, Utrecht University, Utrecht, The Netherlands

[3]Howard Hughes Medical Institute and Department of Biochemistry and Biophysics, University of California at San Francisco, San Francisco, CA 94143, USA

[4]Bijvoet Center for Biomolecular Research, Faculty of Science, Utrecht University, Utrecht, the Netherlands.

[#]These authors share senior authorship.

Submitted, Nature Microbiology (2019)

Abstract

Eukaryotic cells, when exposed to environmental or internal stress, activate the integrated stress response (ISR) to restore homeostasis and promote cell survival. Specific stress stimuli prompt dedicated stress kinases to phosphorylate translation initiation factor 2 (eIF2). Phospho-eIF2 (p-eIF2) in turn sequesters the eIF2-specific guanidine exchange factor (GEF) eIF2B to block eIF2 recycling, thereby halting translation initiation and reducing global protein synthesis. To circumvent stress-induced translational shut-down, viruses encode ISR antagonists. Those identified so far prevent or reverse eIF2 phosphorylation. We now describe a viral protein that counteracts the ISR at its very core by acting as a competitive inhibitor of p-eIF2•eIF2B interaction. This allows continued formation of the eIF2-GTP-Met-tRNAi ternary complex and unabated global translation at high p-eIF2 levels that would otherwise cause translational arrest. We conclude that eIF2 and p-eIF2 differ in their interaction with eIF2B to such effect that p-eIF2•eIF2B association can be selectively inhibited.

Introduction

Translation is a fundamental, energy-intensive biosynthetic process. When exposed to a variety of environmental and internal stress conditions, eukaryotic cells switch on a regulatory pathway, the integrated stress response (ISR), that acts at the level of translation initiation (reviewed in (1)). Global protein production is suppressed and the synthesis of a select number of proteins is stimulated to aid cellular recovery. While primarily aimed at energy conservation, restoration of homeostasis, and cell survival, the ISR will signal towards cell death under conditions of severe and unmitigated stress.

In mammalian cells, ISR signaling is initiated by any of four distinct serine/threonine kinases, called PKR, PERK, HRI, and GCN2, each of which is dedicated to sense different types of stress stimuli. For example, PKR - the ISR sensor protein most relevant during viral infection - is triggered by cytoplasmic dsRNA (2). Upon detection of their respective stimulus, the eIF2-kinases self-activate through homodimerization and autophosphorylation, and subsequently converge on phosphorylating a common target, the α-subunit of eukaryotic translation initiation factor 2 (eIF2). Native, non-phosphorylated eIF2 is a heterotrimeric protein complex that associates with GTP and Met-tRNAi to form the ternary complex (TC) as a key step in translation initiation. The initiation process causes hydrolysis of the GTP to GDP, and ongoing translation requires continuous eIF2 recycling by the eIF2-specific guanine exchange factor (GEF) eIF2B (3). Phosphorylated eIF2 (p-eIF2) interferes with this process by engaging in a high affinity, stable interaction with eIF2B, thereby prohibiting eIF2•GDP/GTP exchange (4). As cellular concentrations of eIF2 greatly exceed those of eIF2B (5, 6), even modest levels of p-eIF2 suffice to effectively inhibit eIF2B function (7), causing TC levels to drop and translation to halt.

ISR-induced downregulation of virus protein synthesis acts as an effective antiviral defense mechanism. Many viruses encode antagonistic proteins that allow them to evade or divert the detrimental consequences of the ISR. These viral ISR antagonists fall into different groups. Class 1 antagonists avert eIF2 kinase activation, for example by sequestering or degrading the stressor. To illustrate, influenza A virus NS1 (8) and MERS CoV 4a (9) bind to dsRNA and thereby prevent activation of PKR. By contrast, Class 2 antagonists prevent induction of the ISR by direct interference with the sensor, exemplified by vaccinia virus K3L (10, 11), an eIF2α homologue that binds and inhibits PKR. Finally, Class 3 antagonists, comprising amongst others ICP34.5 of herpes simplex virus and p7 of alphacoronavirus-1, induces dephosphorylation of eIF2α by recruiting the cellular phosphatase PP1 (12, 13). In a search for novel types of ISR antagonists, we focused on coronaviruses (CoVs), a group of positive-strand RNA viruses of exceptional genetic complexity. In addition to a strictly conserved set of structural and non-structural proteins, coronaviruses code for a wide variety of accessory proteins that

are genus-, clade- or sometimes even species-specific. One of these, the ORF10-encoded accessory protein of beluga whale coronavirus SW1 (BwCoV AcP10), attracted our attention because of its sequence similarity to cellular uridine cytidine kinases (UCKs) (14). Here we show that AcP10, while retaining UCK activity, also has a UCK-independent function as an ISR antagonist. We demonstrate that AcP10 differs in its mode of action from all other viral ISR antagonists described so far and counteracts the ISR at its core by acting as a competitive inhibitor of the p-eIF2•eIF2B interaction. AcP10 thereby allows TC formation and translation to proceed unimpaired even at very high levels of p-eIF2 that would otherwise cause translational arrest.

Results

AcP10 is a uridine kinase and an ISR antagonist. AcP10 is encoded by one of eight accessory genes found in beluga whale coronavirus SW1 and related viruses in bottlenose dolphins (for a schematic representation of the 31.7-kb viral genome, see Fig 1A). In accordance with its sequence similarity to cellular UCKs (Figs 1B and 1C), recombinant AcP10 catalyzed the ATP-dependent conversion of uridine into UMP *in vitro* (Fig 1D). This enzymatic activity was lost upon substitution of residues in the predicted catalytic and ATP-binding sites (Asp^{41} to Ala or Lys^{16} to Asn, respectively), that are strictly conserved among cellular UCKs and critical for their function. Thus, AcP10 was unambiguously identified as a uridine kinase. Remarkably, however, AcP10 has an addition al function as ISR anta gonist as we discovered in transient expression experiments. We and others previously reported that transfection of HeLa cells with pEGFP plasmids triggers the ISR via dsRNA-dependent activation of PKR resulting in the formation of stress granules (SGs) (9, 15, 16). Activation can be blocked by expression of dsRNA-binding ISR antagonists, such as influenza virus NS1 and MERS CoV p4a(9). Surprisingly, cells expressing AcP10-EGFP were consistently devoid of SGs (Fig 1F, left panels) providing a first indication that AcP10 counteracts the ISR.

To test whether AcP10, like NS1, acts in a PKR-specific manner, transfected cells were treated with arsenite, to induce the ISR also via activation of HRI. Under these conditions, AcP10 –but not NS1– prevented SG formation (Fig 1F, middle panels). However, AcP10 did not block SG production in cells treated with pateamine A, a drug that inhibits translation initiation by sequestering DEAD box helicase eIF4A (Fig 1F, right panels). The data thus suggest that AcP10 specifically targets the ISR, acting at a level downstream of the eIF2α kinases. This function is UCK-independent, because UCK-deficient AcP10 mutants still suppressed SG formation (Fig. 1G). To identify AcP10 residues that are critical to ISR inhibition, we performed alanine screening on a selection of histidines, and potentially phosphorylated serines and threonines (sixteen in total), all surface exposed in the UCK-fold (for a predicted 3D structure, see Fig S1). Of the mutants tested, AcP10-H^{193}A, AcP10-H^{200}A, and double mutant AcP10-$H^{193/200}$A [henceforth called AcP10(SA-)] no longer suppressed the formation of SGs (Fig 1G). However, they still exhibited uridine kinase activity (Fig 1E), demonstrating that the ISR inhibitor and UCK functions of AcP10 are separable and hence independent.

Consistent with a role as UCK and ISR antagonist, AcP10-EGFP localized to the cytosol. We did note, however, that the protein largely accumulated in perinuclear deposits, apparently in aggregated form (Fig. 1F and 1G). Indeed, upon fractionation of Triton X100-lysates of transfected cells, most AcP10 was insoluble and resided in the pellet with only about 20% remaining in the supernatant (Fig S2). Importantly, SG formation was blocked also in cells that expressed AcP10-EGFP at very low levels, and that lacked AcP10 deposits (see also Fig S3B). The aggregation of AcP10-EGFP at high intracellular

concentrations thus appears irrelevant to ISR inhibition. In addition, the inactive mutant AcP10(SA-) also accumulated in aggregates, indicating that the presence of perinuclear deposits *per se* does not interfere with SG formation.

AcP10 rescues global translation in the presence of p-eIF2. As AcP10's ability to inhibit the ISR is not specific for a particular eIF2-kinase nor type of stressor, its mode of action would seem to differ from that of viral ISR antagonists that sequester dsRNA to prevent PKR activation or that bind to activated

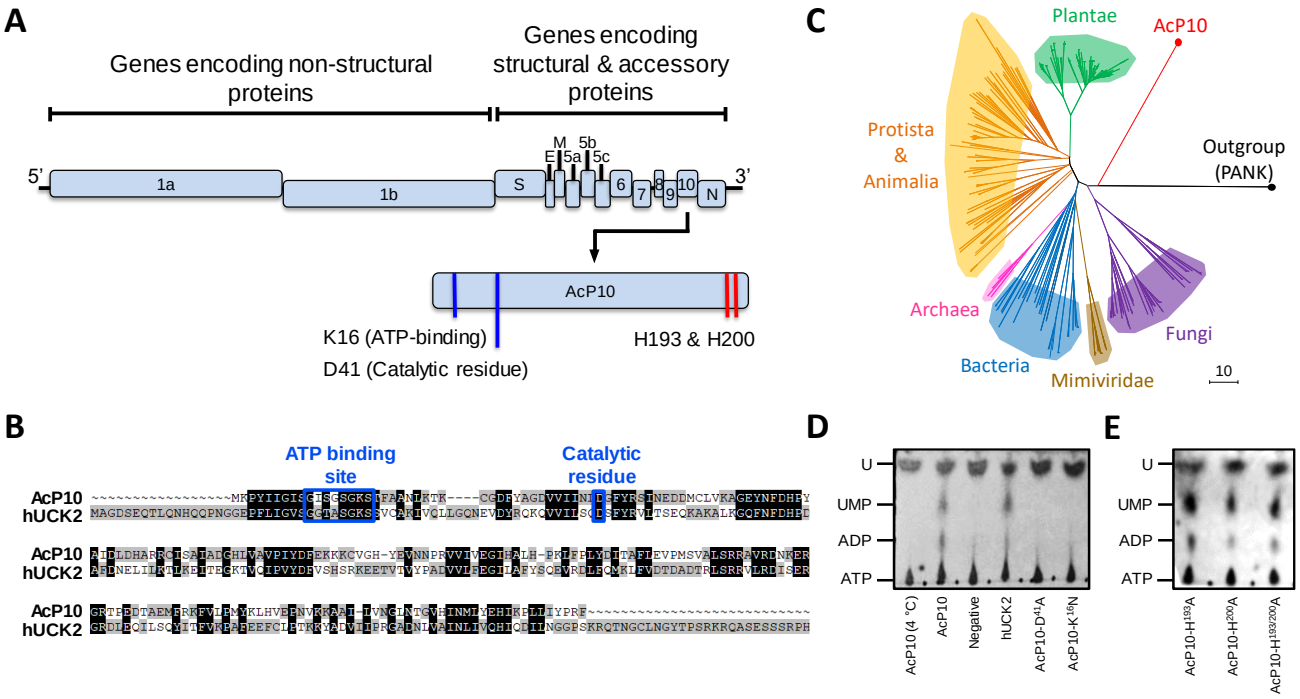

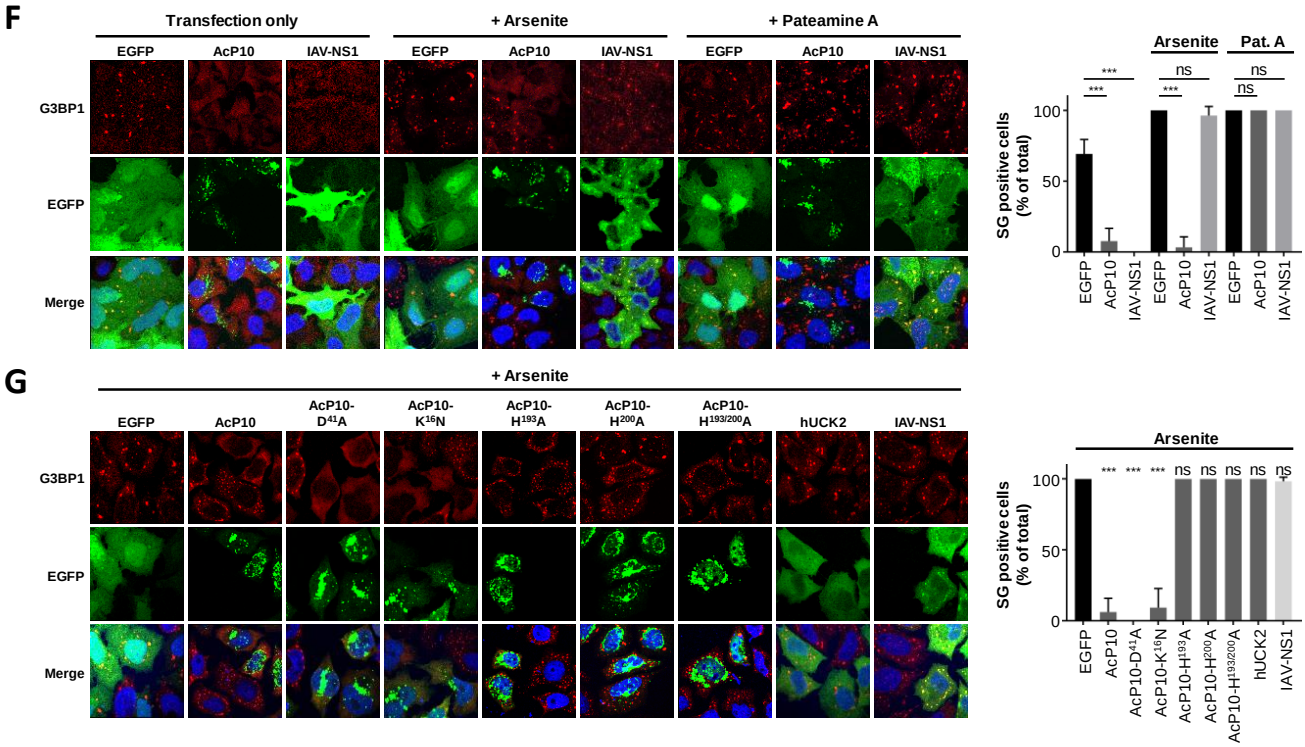

Figure 1. AcP10 is a uridine kinase and an ISR antagonist. *(A) Schematic representation of the Bw-CoV genome and the ORF10-encoded protein AcP10. (B) Alignment of AcP10 with human uridine cytidine kinase 2 (UCK2). The ATP binding domain (consensus sequence, GXXXGKS) and the (putative) catalytic aspartic acid are indicated in blue boxes. (C) Phylogenetic tree of uridine kinases originating from various branches of the tree of life, including a structurally related distant relative of uridine kinases (panthothenate kinase; PANK) as outgroup[57]. The scale bar indicates the number of amino differences between sequences. A full list of the protein sequences used for this analysis is given in Supplementary Data 1. (D) Thin-layer chromatography analysis of an in vitro uridine kinase assay using the indicated proteins. Highlighted are the positions of the substrates (ATP and U) and end products (ADP and UMP) of the uridine kinase reaction. (E) Thin-layer chromatography analysis of an in vitro uridine kinase assay using AcP10 mutants that lack the ability to antagonize the ISR. Highlighted are the positions of the substrates (ATP and U) and end products (ADP and UMP) of the uridine kinase reaction. (F) Immunofluorescence analysis of stress granule (SG) formation in HeLa cells transiently overexpressing the indicated EGFP fusion-proteins, without additional treatment (PKR-dependent plasmid DNA-induced stress), after treatment with 500 µM arsenite for 45 min (HRI-dependent stress), or after treatment with 100 nM pateamine A for 2 h (eIF2α-independent stress). EGFP expression is shown in green, and SG marker G3BP1 is shown in red. Quantifications of the percentage of SG positive cells are given in the bar graph in the right panel. (G) Immunofluorescence analysis of SG formation in arsenite-treated HeLa cells transiently overexpressing the indicated EGFP fusion-proteins. K16N (ATP-binding pocket) and D41A (catalytic residue) mutations in AcP10 abolish its uridine kinase activity, the H193A and H200A mutations abolish AcP10's ability to block the ISR. Quantifications of the percentage of SG positive cells are given in the bar graph in the right panel.*

PKR to directly prevent eIF2 phosphorylation. To study whether AcP10 is a Class 3 antagonist and induces eIF2 dephosphorylation, we determined the effect of AcP10 expression on p-eIF2α levels in stressed cells. Cells, dually stressed by DNA transfection and arsenite treatment, had high levels of p-eIF2α in comparison to non-stressed cells, and global translation was markedly reduced as measured by Western blot detection of puromycin incorporation (Fig 2A). AcP10 did not affect eIF2 phosphorylation, as p-eIF2α levels in AcP10-expressing cell populations were identical to those in the controls. Nevertheless, AcP10 –and also UCK-deficient AcP10-$D^{41}A$– rescued global protein synthesis. In contrast, translation was not restored to any detectable degree in cells expressing AcP10(SA-) nor in cells expressing EGFP or NS1. Of note, the analyses were performed on total cell populations in which only 30-50% of the cells produced AcP10. To quantitatively assess to what extent AcP10 rescues translation during stress, global protein synthesis was measured in individual cells by flow cytometry. In cells stressed by DNA transfection exclusively (Fig. 2B) or by a combination of transfection and arsenite treatment (Fig S3A), AcP10 allowed protein synthesis to proceed unhindered at rates indistinguishable from those in non-stressed cells. Notably, minute amounts of AcP10, barely

detectable by fluorescence microscopy or flow cytometry, sufficed to block SG formation (Fig S3B), and to fully rescue translation (Fig S3C).

The experiments described so far entailed transient overexpression of AcP10. Unfortunately, we were unable to study the role of AcP10 in cells infected with BwCoV SW1, as this virus has not yet been isolated in cultured cells and, hence, no reverse genetics system has been established. To investigate

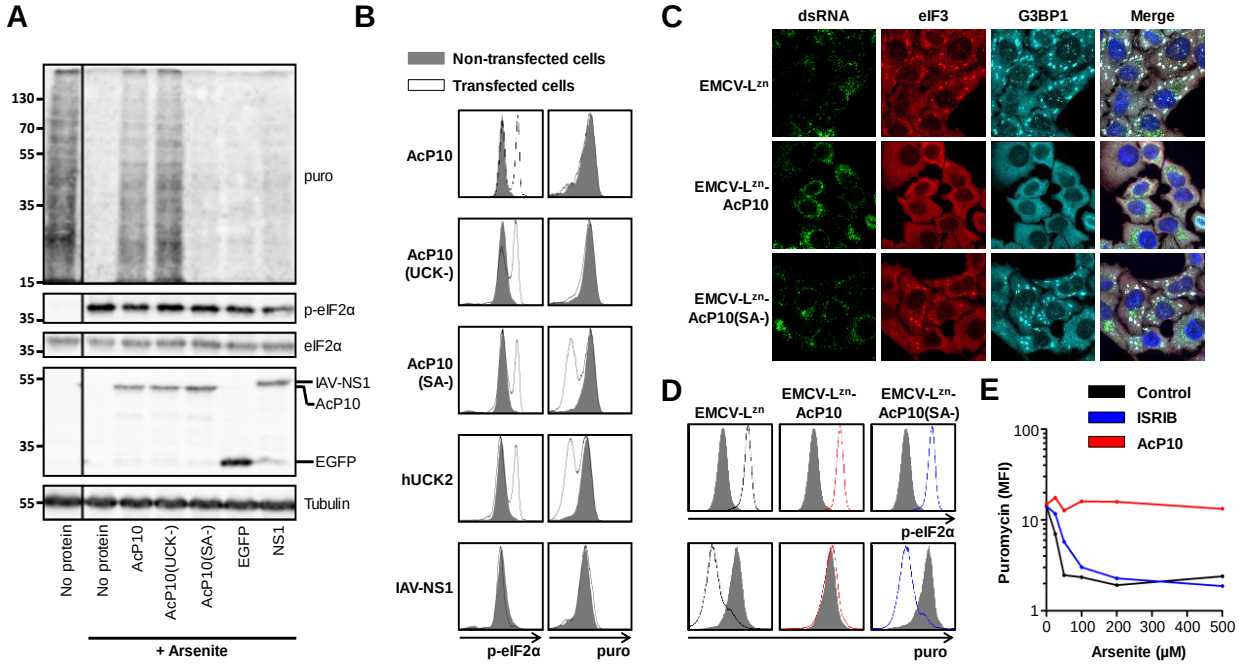

Figure 2. AcP10 rescues global translation in the presence of p-eIF2. *(A) Western blot analysis of p-eIF2 levels and translation rates as labeled by puromycin treatment for 15 min[58], in cells expressing the indicated EGFP fusion-proteins and treated with 500 µM arsenite for 45 min. AcP10 mutants lacking the stress antagonist function (AcP10-H$^{193/200}$A) or UCK function (AcP-D^{41}A) are indicated as AcP10(SA-) and ACP(UCK-), respectively. (B) Flow cytometry analysis of p-eIF2 levels (left panels) and active translation (right panels) in cells transiently transfected with plasmids encoding the indicated proteins. Transfected cells were identified based on EGFP signal, and non-transfected cells (indicated in grey) from the same wells served as internal controls. (C) The AcP10- or AcP10(SA-)-gene were inserted into the genome of a picornavirus that efficiently induces ISR activation (EMCV-L^{zn}). Cells were infected (MOI=2) with the indicated recombinant viruses and SG formation was monitored at 5 h pi. by immunofluorescence. dsRNA synthesis was used as marker for virus replication, and SG markers eIF3 and G3BP1 were visualized to assess SG formation. (D) Flow cytometry analysis of p-eIF2α levels (top panels) and active translation (bottom panels) in cells infected (MOI=5) with the indicated viruses at 5 h pi. (E) Direct comparison of the ISR inhibition by the eIF2B binders AcP10 and ISRIB. Shown are the translation rates, as determined by a flow cytometry analysis, in mock treated cells, cells treated with 200 nM ISRIB, or cells overexpressing AcP10, in the presence of different concentrations of arsenite.*

whether AcP10 also inhibits the ISR in virus-infected cells, we resorted to a model based on recombinant encephalomyocarditis virus mutant EMCV-L^{zn}, in which the autologous ISR antagonist, the leader protein (L), is inactivated. Consequently, the mutant virus can no longer counteract the ISR (17) and thus can be used as a convenient platform to identify and characterize ISR antagonists of other viruses (9, 18). Infection with EMCV-L^{zn}, EMCV-L^{zn}-AcP10 or EMCV-L^{zn}-AcP10(SA-) (Fig S4) induced eIF2α phosphorylation to similar extents. However, only cells infected with EMCV-L^{zn}-AcP10 were devoid of SGs (Fig 2C) and displayed translation rates similar as those in non-infected cells (Fig 2D). These observations provide formal evidence that AcP10 also counters the ISR in virus-infected cells.

Recently, a small molecule inhibitor of the ISR (ISRIB) was described to render cells less sensitive to p-eIF2. ISRIB promotes the assembly of the fully active decameric eIF2B complex, and thereby increases eIF2B GEF activity (19–22). However, ISRIB does not prevent p-eIF2 from binding eIF2Band thus cannot counteract the ISR at high intracellular p-eIF2 concentrations which sequester virtually all eIF2B. For this reason, ISRIB fails to rescue translation in HeLa cells treated with arsenite concentrations >100 µM (23), even at high ISRIB concentrations (200 nM, which is 40 times ISRIB's reported EC50). In contrast to ISRIB, AcP10 remained fully active even in cells exposed to arsenite concentrations of up to 500 µM (Fig 2E). The combined data suggest that AcP10 blocks the ISR downstream of eIF2α phosphorylation, not by any mechanism previously described for other viral ISR antagonists or ISRIB, but by allowing global translation to proceed seemingly unimpaired even at high intracellular concentrations of p-eIF2α.

AcP10 prevents uORF-mediated translation upregulation in stressed cells. In stressed cells, increasing levels of p-eIF2 result in decreasing TC levels, and while global translation diminishes, the production of a subset of proteins is promoted. Among these proteins is ATF4, a key effector of the ISR. Its synthesis is under the control of a cis-acting mRNA element, which is located upstream of the ATF4 ORF and comprises two upstream ORFs (uORF1 and uORF2). The regulatory mechanism is based on cap-dependent translation of uORF1 with resumed scanning of 40S ribosomes and re-initiation at downstream start codons dependent on the rate of TC formation and TC recruitment. At physiological TC concentrations, re-initiation preferentially occurs at uORF2, preventing ATF4 expression. When TC concentrations drop, however, the ribosomes will bypass the uORF2-AUG and ATF4 expression is switched on. Predictably, when TC concentrations fall even further, also the ATF4-

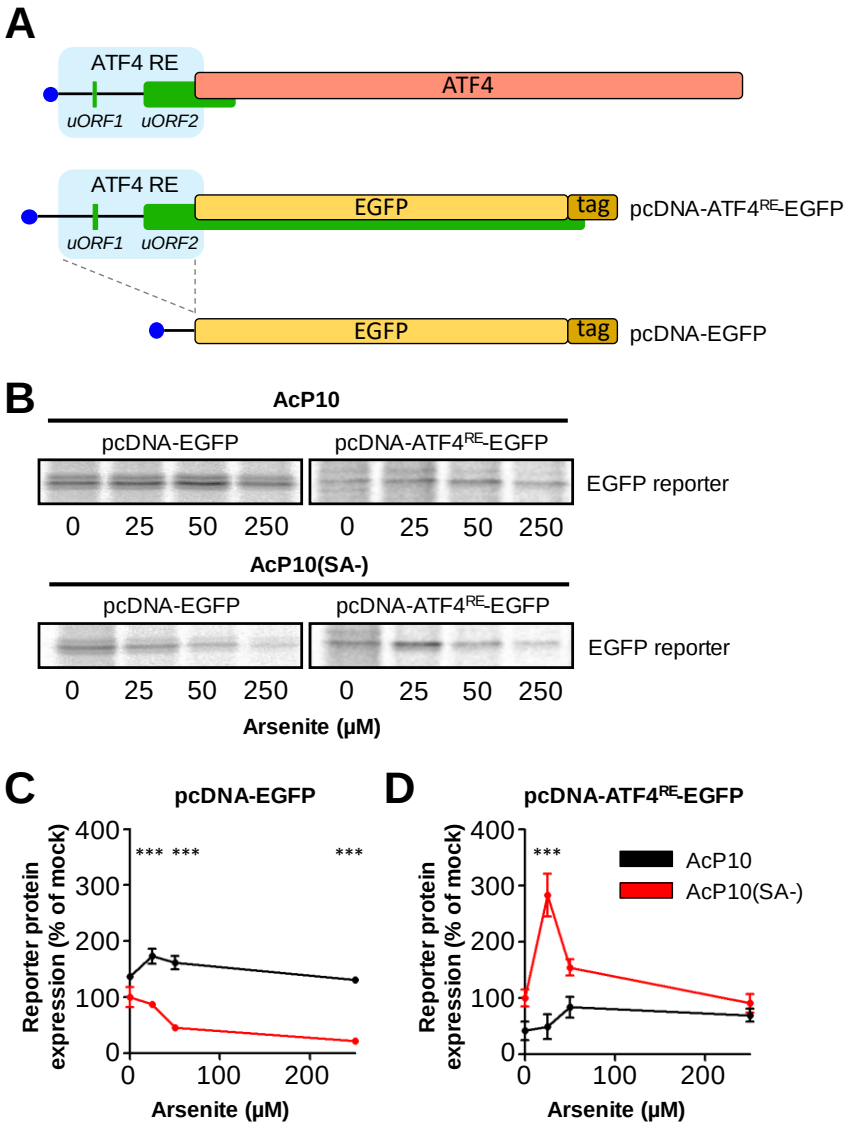

Figure 3. AcP10 prevents uORF-mediated translation upregulation in stressed cells. *(A) Schematic representation of the cellular ATF4 mRNA (top panel), and the mRNAs encoded by the ATF4 reporter construct (middle panel) or the control reporter construct lacking the ATF4 regulatory element (RE) (bottom panel). The cap structure is indicated in blue and the ATF4 uORFs are indicated in green. The ATF4 gene and EGFP reporter gene are indicated in orange and yellow, respectively. (B) HeLa-PKR^{KO} cells were cotransfected with plasmids encoding AcP10 or AcP10(SA-), and the plasmids encoding strep-tagged EGFP reporter protein shown in (A). Cells were treated with the indicated arsenite concentrations for 30 min, and reporter protein was pulse labelled by ^{35}S Met/Cys incorporation for an additional 90 min. Strep-tagged EGFP was purified from cell lysates and separated with SDS-PAGE. Presence of radioactive label was determined using a phosphorimager. (C) Quantification of reporter protein expression from (B). Reporter protein expression levels are shown relative to those in untreated cells expressing AcP10(SA-). Indicated are mean values +/- SEM of duplicate independent measurements. Statistical significance was determined by One-way ANOVA and Bonferroni post-hoc test (***, p<0.001).*

AUG is bypassed causing ATF4 expression to be switched off again (24–26). To study whether AcP10 affects uORF-mediated translation regulation under conditions of stress, an expression vector was constructed in which EGFP was placed under the control of the ATF4 regulatory element. A plasmid lacking uORF1 and uORF2 sequences was used to monitor conventional cap-dependent translation initiation at 5'-proximal start codons (Fig 3A). EGFP expression was measured in cells under conditions of increasing stress and the effect of AcP10 co-expression was assessed with inactive mutant AcP10(SA-) serving as negative control. In accordance with our observations for global protein synthesis, translation initiation at 5'-proximal start codons was salvaged by wildtype AcP10 even under conditions of extreme stress: EGFP expression levels remained identical to those in non-stressed controls even in cells exposed to 250 µM arsenite. For comparison, in cells co-expressing EGFP and AcP10(SA-), EGFP expression plummeted to ~20% (Fig 3B and 3C). Conversely, EGFP expression under control of the ATF4 regulatory element was upregulated in AcP10(SA-)-producing cells albeit only when exposed to moderate stress (25 µM arsenite) (Fig 3D). Importantly, under identical conditions this upregulation did not occur in AcP10-expressing cells, suggesting that AcP10 promoted translation reinitiation at uORF2. The combined data suggest that AcP10 allows formation of TCs to proceed, not only in moderately stressed cells, but also in severely stressed cells with exceedingly high p-eIF2 levels.

eIF2B is a cellular interaction partner of AcP10. To determine how AcP10 renders cells resistant to p-eIF2α and maintains TC concentrations at sufficient levels to allow unperturbed translation, its cellular interaction partners were identified by tandem affinity purification (TAP) mass spectrometry. To this end, we purified TAP-tagged AcP10 and associated cellular proteins from transfected HEK293T cell lysates. For comparison, the same procedure was performed with AcP10(SA-), hUCK2, and an unrelated picornavirus protein (FMDV L^{pro}). Figure 4A shows a STRING analysis of all proteins that were 2- to 5-fold, 5- to 10-fold, and >10-fold enriched in peptide spectral matches (# PSMs) in the AcP10 sample as compared to each of the controls, using a threshold of at least 25 PSMs detected. SAINT probability scores (27) and fold-enrichment in spectral counts as calculated relative to the L^{pro} negative control are shown in Fig 4B. Importantly, among the hits with highest PSM enrichment factors were all three subunits of eIF2 (eIF2α, eIF2β, eIF2γ) and all five of eIF2B (eIF2Bα, eIF2Bβ, eIF2Bγ, eIF2Bδ, eIF2Bε) (See also: Supplementary Table 1 and Supplementary Data 2). Since the eIF2B subunits of humans and beluga whales are 92-96% identical, AcP10 likely has the same interaction, and consequently function, in its natural host.

The interaction of AcP10 with eIF2 and eIF2B was confirmed by Western blot analysis using antibodies directed against eIF2Bε (representing the eIF2B complex) and eIF2α (representing the eIF2

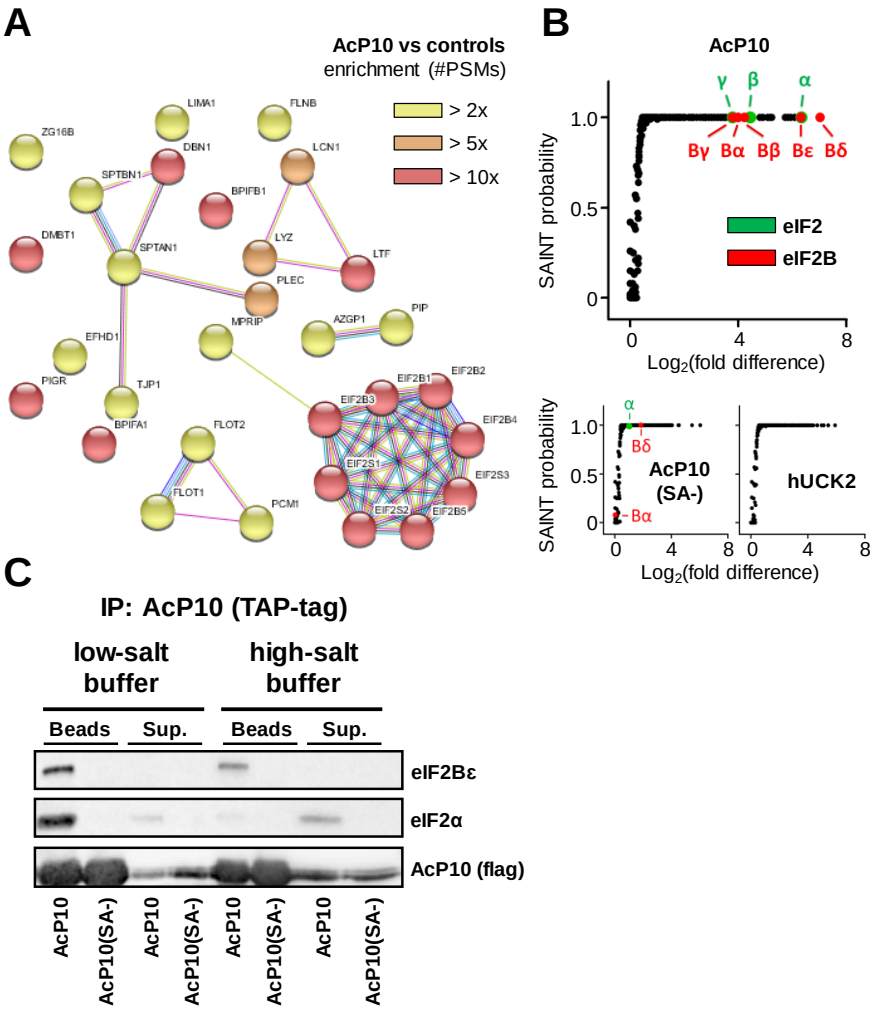

Figure 4. eIF2B is a cellular interaction partner of AcP10. *(A) TAP-tagged AcP10 was transiently overexpressed in and purified from HEK293T cells. Copurified cellular interaction partners were analyzed by mass spectrometry. Shown is a STRING interactome analysis of the proteins that were found to be co-enriched with AcP10 relative to each of the controls by 2-5 fold (yellow), 5-10 fold (orange), or >10 fold (red), with a threshold of at least 25 PSMs detected per protein (See also Supplementary table 1 and Supplementary dataset 2). (B) Graphs showing SAINT probability scores*(27) *and fold difference in spectral counts compared to the* L^{pro} *negative control sample. Indicated are the subunits of eIF2 in green and eIF2B in red. These subunits all show a very confident SAINT score (>0.98) and fold change in the AcP10 pull-down (top panel) and not in the controls (bottom two panels). Preys with a* log_2*(fold difference) < 0 are considered background and were therefore discarded from the analysis. (C) TAP-tagged AcP10 or AcP10(SA-) was purified from HEK293T cells. Subsequently, the beads were incubated for 5 min in standard wash buffer, or in high salt buffer (500 mM KCl) to dissociate eIF2 from eIF2B*(28)*. Supernatant fractions and bead fractions were analyzed by Western blot for presence of eIF2 (represented by eIF2α) and eIF2B (represented by eIF2Bε).*

complex) (Fig 4C). Notably, yeast eIF2 was shown to stably interact with eIF2B under the conditions used in these pull-down experiments, but to dissociate from eIF2B under high-salt conditions (28). To determine whether AcP10 binds eIF2, eIF2B, or the eIF2•eIF2B macrocomplex, the pulldown samples were subjected to high-salt elution to disrupt eIF2•eIF2B interaction (28). While most eIF2α ended up in the supernatant fraction (Fig. 4C, lanes marked "Sup."), eIF2Bε remained AcP10-associated (Fig. 4C, lanes marked "Beads"). To corroborate the observations and to gain further insight into how AcP10 associates with eIF2B, the AcP10 affinity pulldown samples, purified from HEK293T cell lysates, were treated by chemical cross-linking and subsequently analyzed by mass spectrometry using procedures described previously (29). Of the 86 cross-linked di-peptides that could be identified, most were intra-links within AcP10 or eIF2B, but six of them involved a linkage of AcP10 lysine residues with lysine residues of eIF2Bε (n=2) or eIF2Bδ (n=4). One additional dipeptide arose from a cross-link between the N-terminal S-tag of AcP10 and eIF2Bε (Fig S5; Supplementary Data 3). Collectively, the data suggest that AcP10 binds directly to eIF2B, and that eIF2 is co-purified in AcP10•eIF2B complexes owing to its association with eIF2B.

eIF2B preferentially binds eIF2 over p-eIF2 in the presence of AcP10. In stressed cells, AcP10 renders eIF2B insensitive to the inhibitory effect of eIF2 phosphorylation but does not noticeably affect translation in non-stressed cells. The data therefore suggest that AcP10 affects the interaction of eIF2B with p-eIF2, but not with eIF2. The fact that eIF2, through its association with eIF2B copurifies with the AcP10•eIF2B complex (Fig. 4C) provided an experimental approach to study this in more detail. HEK293T cells, transfected to transiently express TAP-tagged AcP10, were stressed to different extent by exposure to arsenite with concentrations of up to 500 µM, and AcP10•eIF2B complexes, isolated from cell lysates by TAP-tag purification, were analysed for eIF2 and p-eIF2 content by Western blot analysis. The antisera detect either total eIF2α –the phosphorylated as well as non-phosphorylated forms– or p-eIF2 exclusively. Strikingly, even under conditions of severe stress (Fig. 5A, "Total lysate", 500 µM arsenite), AcP10•eIF2B complexes were devoid of detectable p-eIF2 (Fig. 5A, "TAP-tag pulldown"). The data thus suggest that AcP10•eIF2B-associated eIF2 is in the non-phosphorylated form and that AcP10 precludes the p-eIF2•eIF2B interaction in stressed cells.

For independent confirmation of these observations, we performed the reciprocal experiment entailing a pull-down analysis targeting eIF2B instead of AcP10. HeLa cells stably expressing flag-tagged eIF2Bβ (30) were transfected to transiently express EGFP-tagged AcP10 or AcP10(SA-) and either left untreated or exposed to severe stress (500 µM arsenite). Then, eIF2Bβ and associated

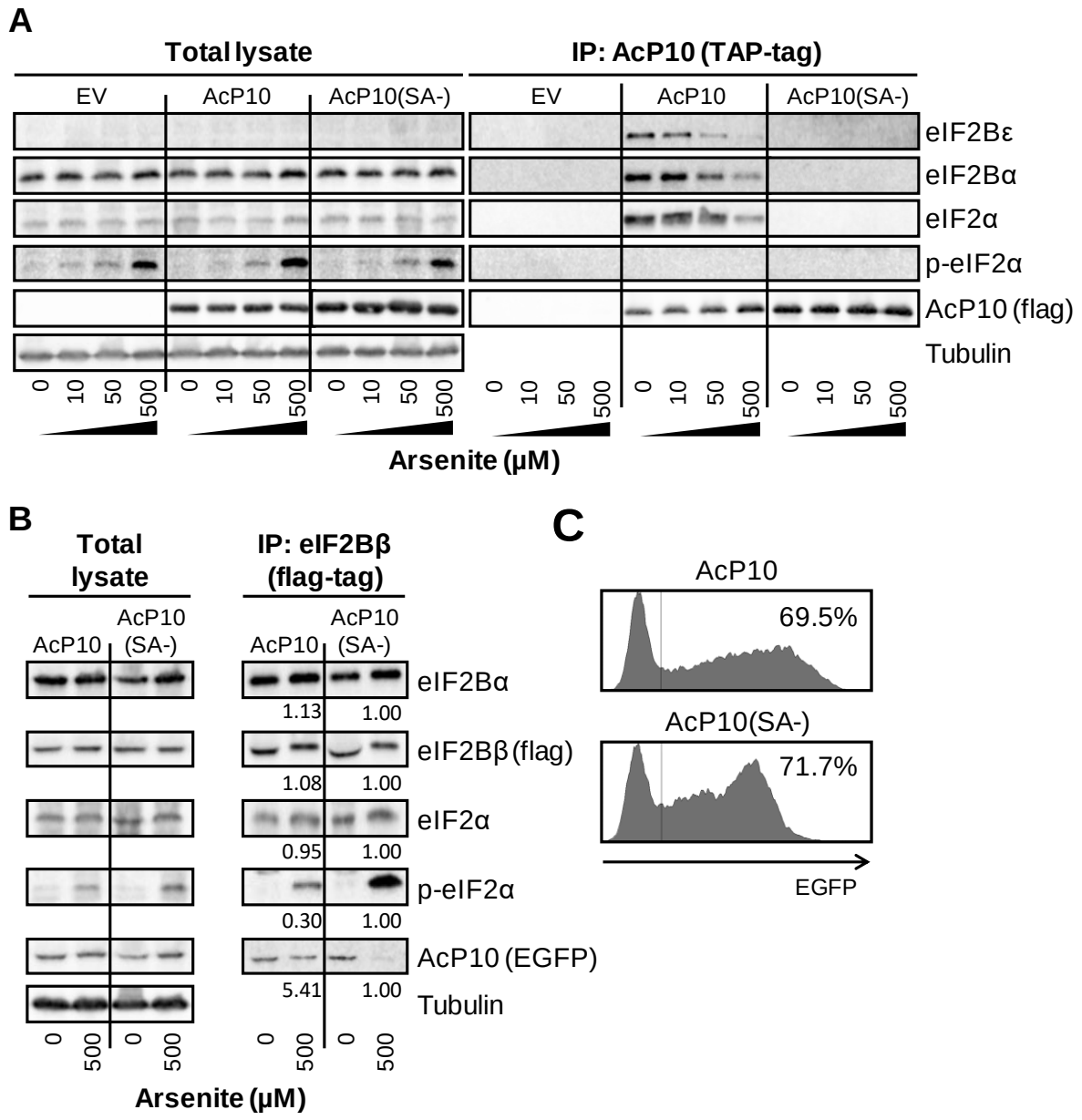

Figure 5. eIF2B preferentially binds eIF2 over p-eIF2 in the presence of AcP10. *(A) The indicated TAP-tagged proteins were transiently overexpressed in HEK293T, and after treatment with the indicated arsenite concentrations for 1 h, purified from cell lysates. Association of eIF2B, eIF2, and/or p-eIF2 to AcP10 was analyzed by Western blot using antibodies directed against eIF2Bα, eIF2Bε, eIF2α, and p-eIF2α, respectively. (B) HeLa cells stably expressing endogenous levels of 3Xflag-tagged eIF2Bβ* (30) *were transfected with plasmids encoding EGFP-tagged AcP10 or AcP10(SA-). After treatment with the indicated arsenite concentrations for 1 h, eIF2B was purified from cell lysates and association of AcP10, eIF2, and p-eIF2 was analyzed using antibodies directed against EGFP, eIF2α, and p-eIF2α, respectively. (C) Flow cytometry histograms indicating the transfection efficiencies in the experiment shown in (B).*

proteins were purified by flag-tag chromatography, and amounts of co-purified eIF2α, p-eIF2α, and AcP10 were assessed (Fig 5B). Co-purification of eIF2Bα was taken as evidence that this procedure allowed isolation of complete eIF2B complexes. In stressed cell cultures expressing AcP10(SA-), eIF2B macrocomplexes contained large quantities of p-eIF2. The amount of p-eIF2 associated with eIF2B from cultures expressing wildtype AcP10 was reduced by 70%. Since this reduction was achieved within a cell population in which 70% of the cells expressed AcP10 (Fig 5C), this finding suggests that very little, if any, p-eIF2 binds to eIF2B in AcP10 expressing cells. The results strongly support the notion that AcP10, through its association with eIF2B, selectively hampers p-eIF2•eIF2B interaction and thereby promotes continued eIF2B-mediated eIF2•GDP/GTP exchange, TC formation and translation. The data also provide an indication of the AcP10 mechanism. In TAP-tagged purified AcP10•eIF2B complexes, the amounts of associated eIF2B (Fig. 5A, right panel) consistently declined with increasing intracellular levels of p-eIF2 (Fig. 5A, left panel). This finding strongly supports a mechanism of competitive binding. Additional support comes from experiments that revealed an association also between AcP10(SA-) and eIF2B in non-stressed cells, but not in stressed cells (Fig 5B). Apparently, the mutations in AcP10(SA-) reduce its binding affinity for eIF2B rather than prevent binding altogether, explaining why eIF2B was lost during protracted (20 h), multistep TAP-tag purification (Fig. 5A) but not during the relatively rapid (3 h), one-step flag-tag isolation procedure. Importantly, eIF2B purified from stressed cells was associated with large quantities of p-eIF2 but no AcP10(SA-). The data suggest that, as a consequence of its reduced affinity, AcP10(SA-) is displaced from eIF2B by p-eIF2 more readily than wildtype AcP10, again consistent with competitive binding. From the combined results, we conclude that AcP10 salvages global translation in stressed cells in the face of ISR-activation by acting as a competitive inhibitor of p-eIF2•eIF2B association. This competition may be achieved by overlapping binding sites of AcP10 and p-eIF2 on eIF2B. Alternatively, the AcP10•eIF2B interaction may lock eIF2B in a conformation that does not allow p-eIF2 binding and *vice versa*.

Discussion

ISR-mediated inhibition of (viral) protein synthesis presents a potent antiviral defense mechanism. Consequently, numerous viruses have evolved strategies to either prevent activation of ISR sensor proteins or to reverse eIF2 phosphorylation. Here, we describe what we think is the first example of a viral ISR antagonist that does not impact the level of p-eIF2, but instead targets the ISR at its core: the interplay between p-eIF2 and eIF2B. The coronaviral protein AcP10 engages into a highly stable interaction with eIF2B and acts as a competitive inhibitor of p-eIF2 binding, without affecting the association of eIF2B's substrate eIF2. In consequence, eIF2B GEF activity cannot be inhibited by p-eIF2, ensuring ongoing translation even under stress conditions in which the majority of the cellular eIF2 pool is phosphorylated. In line with the classification of viral ISR inhibition as presented in the introduction, we refer to this mode as "Class 4 inhibition".

AcP10: mode of action and implications. The results from reciprocal affinity purification assays, and (cross-linking) MS provide unambiguous evidence that AcP10 associates with eIF2B. It remains to be determined whether AcP10 prevents p-eIF2 from binding by directly blocking the p-eIF2 binding site, or indirectly by inducing an eIF2B conformation incompatible with the p-eIF2•eIF2B interaction. Interestingly, recent cryo-EM structures for mammalian eIF2•eIF2B and p-eIF2•eIF2B complexes (31, 32) combined with the results from our cross-linking/MS analysis of AcP10•eIF2B suggest that AcP10 roughly localizes to an area of eIF2B, close to the eIF2Bα/eIF2Bδ interface, which is occupied by p-eIF2α, but not eIF2α. Whether AcP10 binds eIF2B as a monomer or homomultimer and whether AcP10 does so in its UCK fold or in an alternative conformation remain open questions. Elucidation of the details of the molecular mechanism by which AcP10 inhibit the ISR awaits structural analysis of their complexes with eIF2B. This notwithstanding, our findings challenge the view in the field that eIF2 and p-eIF2 bind to eIF2B in essentially identical fashion (33, 34); if this were the case, we would expect any antagonist disrupting p-eIF2 binding to affect also the binding of eIF2. As AcP10 distinguishes between eIF2•eIF2B and p-eIF2•eIF2B, blocking formation of the latter complex exclusively, eIF2 and p-eIF2 must differ in their binding characteristics. These findings not only further our molecular insight into the eIF2•eIF2B interaction but may also be of future clinical relevance. Chronic activation of the ISR has been implicated in a variety of conditions, including developmental defects, prion disease, traumatic brain injury and cancer (20, 35–37). There is proof of principle that adverse effects of the ISR can be alleviated through pharmacological modulation, as was demonstrated with the small molecule inhibitor ISRIB (20, 37–41). This compound boosts eIF2B's basal GEF activity by promoting eIF2B dimerization (19). Our observations suggest that the p-eIF2•eIF2B association may present another

druggable vulnerability of the ISR. Future comparative structural analyses of eIF2B macrocomplexes containing AcP10, eIF2, and/or p-eIF2 may reveal target binding sites on eIF2B amenable to structure-based drug design and thereby facilitate the development of novel, possibly more potent, ISR inhibitors of therapeutic relevance.

AcP10 origin and evolution: from UCK to ISR antagonist. Coronaviruses are exceptional among RNA viruses with respect to genetic complexity and genome plasticity, likely owing to their propensity for frequent heterologous RNA recombination. During coronavirus radiation and diversification, a basic set of genes for the replication machinery and structural proteins was complemented by a specific set of accessory genes, which are unique to specific virus (sub)groups and reflect their different evolutionary trajectories. These accessory genes, encoding proteins that increase viral fitness in a variety of ways, often are of unknown origin without cellular or viral counterpart, and in many cases may well have evolved *de novo*. AcP10 is one of the few CoV accessory proteins for which an origin may be inferred. AcP10 shares ~30% sequence identity with cellular UCKs, an ancient protein family widely distributed in *Bacteria* and *Eukarya* (42), and hence its gene is clearly of cellular origin, either acquired directly from a host or through an as yet unknown viral intermediate. The donor of the gene is not immediately evident as AcP10 is distinct from all cellular UCKs described so far as well as from those found in giant viruses, and the phylogenetic signal has been blurred likely due to extensive genetic drift. Importantly, however, AcP10's function as UCK is conserved, indicating that the UCK function has been advantageous to the virus over the course of evolution. The acquisition of a novel gene would have presented the virus with an opportunity to explore sequence space, possibly leading to the acquisition of additional functions. We propose a scenario in which a fortuitous interaction of an AcP10 progenitor protein with eIF2B interfered with p-eIF2•eIF2B complex formation to some extent, and that this interaction – which provided the virus some gain in fitness – was optimized during subsequent rounds of mutation and selection. This ultimately yielded a second, UCK-independent function for AcP10 as an extraordinarily potent antagonist of the ISR with a novel mode of action.

Materials & Methods

Cell lines. HeLa-R19, BHK-21, and HEK293T cells were cultured in Dulbecco's Modified Eagle's Medium (DMEM) supplemented with 10% (V/V) fetal calf serum (FCS) at 37 °C. HeLa-R19 cells were obtained from G. Belov (University of Maryland and Virginia-Maryland Regional College of Veterinary Medicine, US) (43, 44). HeLa-R19-eIF2Bβ-3xflag cells were kindly provided by the lab of David Ron, and were previously created by inserting a triple flag sequence at the N-terminus of the eIF2Bβ gene by CRISPR-Cas9 gene editing(30). HeLa-R19 PKR^{KO} were created by inactivating the PKR gene using CRISPR-Cas9. Knockout was confirmed using Western blotting and PCR amplification of the genomic region of interest(9).

Plasmids. Recombinant proteins for uridine kinase assays were expressed in E. Coli using pCAGGS plasmids that encode the indicated strep-tagged proteins under the control of a chicken β-actin promoter. For mammalian overexpression of EGFP fusions proteins in IFA and flow cytometry experiments, we used pEGFP-N constructs.

The ATF4 reporter construct (pcDNA-$ATF4^{RE}$-EGFP) induces expression of an mRNA that contains the ATF4 upstream ORFs, and an ORF encoding a strep-tagged EGFP protein. The mRNA encoded by the ATF4 reporter construct, as well as the mRNA encoded by the negative control (pcDNA-EGFP) reporter construct, are schematically shown in figure 3A.

For overexpression of tandem affinity purification (TAP) tagged proteins in co-IP experiments, we used pcDNA3 constructs encoding the indicated proteins with an N-terminal multi-component tag (S-tag, 3Cpro cleavage site, Strep2-tag, Flag-tag). The EMCV infectious clone pM16.1 (17) was described previously. A full list of the plasmids used in this study is given in supplementary table 2.

Viruses. EMCV-L^{zn} was described previously (17). The gene encoding AcP10 or AcP10(SA-) with a C-terminal VFETQ|G cleavage site were inserted at the 5' end of the viral polyprotein coding sequence in the pM16.1 infectious clone (17). To create infectious virus, the pM16.1 plasmid were linearized by BamHI restriction and infectious RNA was synthesized by *in vitro* transcription from a T7 promoter using the RiboMAX *in vitro* transcription system (Promega). The RNA was purified (Macherey-Nagel) and a total of 1 µg RNA was subsequently transfected in a sub confluent T225 flask of BHK-21 cells using Lipofectamine 2000 (Invitrogen) transfection reagent. After 2-4 days, when complete CPE was observed, virus stocks were freeze-thawed three times and cell debris spun down. Virus in the supernatants was purified and concentrated by ultracentrifugation (100,000 g) for 16 h on a 30% sucrose cushion, and virus pellets were resuspended in PBS. The integrity of the ORF10 gene in EMCV-L^{zn}-AcP10 and EMCV-L^{zn}-AcP10(SA-) was confirmed by isolation of the viral RNA (Macherey-Nagel),

cDNA synthesis (Invitrogen), and PCR amplification of the region of interest followed by Sanger sequencing.

Uridine kinase assay. Purified protein samples were prepared by transient transfection of pCAGGS-Strep constructs encoding the relevant proteins in HEK293T cells. After overnight expression, cells were lysed in lysis buffer (40 mM Tris-HCl pH7.4, 50 mM NaCl, 10 mM EDTA, 1% NP-40, protease inhibitors [Roche]) and cell debris was removed by centrifugation. Subsequently, soluble strep-tagged proteins were bound to Strep-Tactin beads (IBA) for 2 h at 4 °C. Samples were washed three times in wash buffer (40 mM Tris-HCl pH7.4, 50 mM NaCl, 1 mM EDTA) and the protein was eluted in wash buffer containing 10 mM of desthiobiotin. Protein concentrations were measured on the NanoDrop 1000 spectrophotometer (Thermo Scientific). Reaction mixtures were set up using 100 ng of the indicated purified strep-tagged protein, 2 µg Uridine, 4 µg ATP, 1 mM DTT, and 0.1 µg BSA in 1X NEBuffer2 (New England Biolabs) in a total volume of 10 µl. After 1 h incubation at 37 °C, a total of 1.5 µl was applied stepwise (6 x 0.25 µl) on a PEI Cellulose F plate (Merck Millipore). The plate was dried after each application. The base of the plate was then put in the mobile phase solution (dH_2O + 500 mM NaCl + 1 mM LiCl) until the liquid front almost reached the top of the plate. Presence of U, UMP, ATP, and ADP was visualized under a short wavelength (254 nm) UV lamp.

Immunofluorescence assay. HeLa cells were seeded on glass cover slips in a 24-wells cluster at sub confluent densities. The cells were transfected overnight with 500 ng of the indicated plasmids using FUGENE 6 reagent (Roche) according to manufacturer's protocol. Next day, cells were left untreated, treated with 500 µM arsenite (Riedel-de Haën), or treated with 100 nM pateamine A for 30 minutes and subsequently fixed in PBS + 4% paraformaldehyde (PFA). Alternatively, cells were infected with the indicated recombinant EMCV (MOI=2) for 5 h and fixed in PBS + 4% PFA. Samples were permeabilized by incubation in PBS + 0.1% Triton X100 for 5 min and blocked in block buffer (PBS + 2% BSA + 50 mM NH_4Cl) for 1 h. The cells were incubated in block buffer containing mouse anti-hG3BP1 (1:200; BD Biosciences), rabbit anti-hG3BP1 (1:200; Aviva), goat anti-eIF3η (1:200; SantaCruz), rabbit anti-G3BP2 (1:200; Bethyl) and/or mouse anti-dsRNA (1:1000; English&Scientific consulting) for 45 minutes. After three wash steps in block buffer, cells were incubated with secondary antibody donkey anti-Mouse cy5 (Jackson Lab), donkey anti-Rabbit Alexa647 (Life Technologies), donkey anti-Goat Alexa568 (Life Technologies), and/or donkey anti-Mouse Alexa488 (Life Technologies) at a concentration of 1:200 in block buffer. Cells were washed once in block buffer and once in dH_2O. Cover glasses were then mounted on slides in FluorSave Reagent (Calbiochem) and visualized by confocal microscopy using a Leica SPE-II (Leica Microsystems).

Flow cytometry assay. HeLa cells were seeded on glass cover slips in a 24-wells cluster at sub confluent densities. Next day, cell layers were transfected with 500 ng of the indicated plasmids using FUGENE 6 reagent (Roche) according to manufacturer's protocol. After overnight incubation, cells were treated with 500 µM arsenite or left untreated. Alternatively, cells were infected with the indicated recombinant EMCV (MOI=5) for 5 h. Puromycin labeling of active translation was done by exposing cells to 20 µg/ml puromycin during the final 15 min of the assay. Cells were then released by trypsin treatment and fixed in 4% PFA in PBS for 30 min, and subsequently permeabilized in ice-cold MeOH for 10 min. The samples were washed twice in FACS buffer (PBS + 1% BSA) and subsequently incubated with primary antibodies mouse anti-Puromycin (Merck Millipore) and rabbit anti-p-eIF2α (Abcam) at 1:100 dilution in FACS buffer for 45 min. Samples were washed twice in FACS buffer and subsequently incubated in secondary antibodies donkey anti-Mouse Cy5 (Jackson lab) and goat anti-Rabbit Alexa594 (Invitrogen) at 1:200 dilution in FACS buffer for 45 min. Samples were washed once in FACS buffer and kept in FACS buffer + 2% PFA at 4 °C until analysis at the FACS Canto II (BD Biosciences). The gating strategy used in the flow cytometry analyses is briefly explained in Fig S6.

Western blot analysis. Cells were lysed in ice-cold lysis buffer (40 mM Tris-HCl pH7.4, 150 mM NaCl, 10 mM EDTA, 1% NP-40, phosphatase inhibitors [Sigma-Aldrich], and protease inhibitors [Roche]) for 30 min. Cell debris was pelleted and protein concentration in the supernatant was determined using the Pierce BCA assay (Thermo Scientific) according to manufacturer's protocol. For each sample, 35 µg protein in 1x Laemmli Sample Buffer (LSB) was separated on 12.5% SDS-PAGE gels and transferred to nitrocellulose membranes by wet transfer. Membranes were probed with the indicated primary antibodies, mouse anti-Puromycin (Merck Millipore), rabbit anti-p-eIF2α (Abcam), rabbit anti-eIF2α (Cell Signaling), rabbit anti-EGFP, mouse anti-Tubulin (Sigma-Aldrich), mouse anti-Flag (Sigma-Aldrich), rabbit anti-eIF2Bε (Abcam), or rabbit anti-eIF2Bα (Protein Tech), all used at 1:1000 dilution. After three wash steps, membranes were incubated in secondary antibodies goat anti-Mouse IRDye680 (LI-COR, 1:15,000) or goat anti-Rabbit IRDye800 (LI-COR, 1:15,000). Fluorescence images were captured using the Odyssey Imager (LI-COR). Unless indicated otherwise, all Western blots shown within the same figure panels were performed in parallel and analyzed using the same settings.

^{35}S Radiolabeling assay. HeLa-PKR^{KO} cells were seeded in 6-wells clusters to sub confluent densities. Next day, cells were co-transfected with 1.5 µg pEGFP-N1 plasmid encoding AcP10-EGFP or AcP10(SA-)-EGFP together with 0.5 µg of the indicated pcDNA3 reporter construct using FUGENE 6 transfection reagent. After overnight incubation, medium was replaced with medium without methionine and cysteine for 30 min. Subsequently, arsenite was added to the medium at the indicated final concentrations for another 30 min. Then, ^{35}S Met/Cys (Perkin Elmer) was added to the medium at a final concentration of 10 µCi/ml for 90 minutes. Supernatant was removed, and cells were washed

three times in PBS and then lysed in lysis buffer (20 mM Tris-HCl pH7.4, 100 mM NaCl, 1 mM EDTA, 1% Triton X100, protease inhibitors [Roche]). Cell debris was spun down, and supernatants were transferred to new tubes. 10 µl of Strep-Tactin beads (IBA) was added to each sample and incubated rotating overnight at 4 °C. Next day, beads were washed three times in RIPA buffer (10 mM Tris-HCl pH7.4, 150 mM NaCl, 0.1% SDS, 1% sodium deoxycholate (NaDOC), 1% NP-40) and resuspended in 1x LSB. Subsequently, samples were separated by SDS-PAGE, and gels were vacuum-dried on whatman paper at 80 °C. Gels were subsequently analyzed on a phosphorimager (FUJI). Background subtraction and signal intensity analysis was done in ImageJ software.

Immunoprecipitation of TAP-tagged AcP10. HEK293T cells were transiently transfected with pcDNA3 plasmids encoding the indicated TAP-tagged (S-tag, 3C cleavage site, strepII-tag, and flag-tag, fused to the protein N-terminus) proteins under the control of a CMV promoter using PEI transfection. For each sample, $2*10^7$ cells were lysed in lysis buffer (40 mM Tris-HCl pH7.4, 50 mM NaCl, 10 mM EDTA, 1% NP-40, protease inhibitors [Roche], phosphatase inhibitors [Sigma-Aldrich]) for 15 min on ice. After spinning down cell debris, supernatants were incubated with 20 µl of S-beads (Novagen) for 2 hrs at 4 °C. S-beads were washed three times in wash buffer (40 mM Tris-HCl pH7.4, 50 mM NaCl, 1 mM EDTA), and once in $3C^{pro}$ cleavage buffer (Thermo Scientific), and subsequently resuspended in 200 µl 3C cleavage buffer. Protein was released from beads by adding $3C^{pro}$ overnight at 4 °C, according to the HRV 3C Protease Solution Kit manufacturer's protocol (Thermo Scientific). Next day, beads were spun down and supernatant transferred to a new tube. 10 µl of Strep-Tactin beads (IBA) was added to each sample and incubated for 1 h at 4 °C. Beads were washed three times in wash buffer and then resuspended in 1x LSB. Samples were run on SDS-PAGE gels and used for Western blotting or mass spectrometry analysis.

Immunoprecipitation of flag-tagged eIF2Bβ. HeLa cells stably expressing flag-tagged eIF2Bβ(30) were seeded at $2.5*10^6$ cells/dish (surface area = 180 cm^2), with four dishes per sample. Next day, cells were transfected with 15 µg of the indicated plasmids using Lipofectamine 2000 (Invitrogen) reagent according to the manufacturer's instructions. After 2 days, ~4*10^7 cells per sample were harvested and lysed in 500 µl lysis buffer (50 mM Tris-HCl pH7.4, 150 mM NaCl, 1 mM EDTA, 1 mM DTT, 10% glycerol, 1% Triton X100, protease inhibitors [Roche], phosphatase inhibitors [Sigma-Aldrich]). After spinning down cell debris, supernatants were incubated for 2 h with 20 µl anti-flag beads (Sigma-Aldrich), rotating at 4 °C. Beads were washed four times with wash buffer (50 mM Tris-HCl pH7.4, 150 mM NaCl, 1 mM EDTA, 1 mM DTT, 10% glycerol, 1% Triton X100), and resuspended in 1x LSB. Samples were run on SDS-PAGE gels and subsequently used for Western blotting.

AP-MS. Protein samples prepared as described above were separated by SDS-PAGE and stained with Coomassie colloidal blue (Bio-Rad). Four bands were sliced out from each gel lane which were then reduced, alkylated, and digested as previously described (45). Digests were subjected to nLC–MS/MS analysis using an Agilent 1290 Infinity UHPLC system (Agilent) coupled to an Orbitrap Q Exactive Plus mass spectrometer (Thermo Scientific). Dried peptides were reconstituted in 10% formic acid (FA) and delivered to a trap column (Dr Maisch Reprosil C18, 3 µm, 2 cm × 100 µm) at 5 µl/min with solvent A (0.1% FA in water). Next, peptides were chromatographically separated onto an analytical column (Agilent Poroshell EC-C18, 2.7 µm, 50 cm × 75 µm) at 300 nL/min, as previously described(46). The gradient was as follows: 13-40% solvent B (0.1% FA in 80% Acetonitrile) in 65 min, to 100% solvent B in 3 min, 1 min of 100% solvent B, and finally equilibration of the chromatographic columns with 100% solvent A for the following 10 min before injection of the next sample. Total analysis time was 90 min. The eluent was sprayed via distal coated emitter tips butt-connected to the analytical column. The mass spectrometer was operated in data-dependent mode, automatically switching between MS and MS/MS. Full-scan MS spectra (from m/z 375 to 1600) were acquired in the Orbitrap with a resolution of 35,000 at m/z 400. The 10 most intense ions within the survey scan were selected for HCD fragmentation with normalized collision energy set to 25%. The MS/MS AGC target value was set to 5e4 with a maximum ion injection time of 120 ms. Dynamic exclusion was set to 12 s. Each raw data file recorded by the mass spectrometer was processed and quantified with Proteome Discoverer (version 2.1, Thermo Scientific), and searched against a Swissprot human database (version 2016 03, 20,199 sequences) supplemented with the Beluga whale coronavirus SW1 AcP10 sequence (Uniprot id B2BW43) using Mascot software (version 2.5.1, Matrix Science). Trypsin/P was chosen as the protease, cysteine carbamidomethylation was selected as fixed modification, and oxidation of methionine as variable modifications. Precursor and fragments mass tolerance were set to 20 ppm and 0.05 Da, respectively. All peptide-spectrum matches (PSM) were validated with 1% false discovery rate using Percolator(47). Only PSMs with a minimum length of 6 amino acids were kept. Proteins were further filtered for contaminants and highly abundant proteins (such as keratins, tubulins, and ribosomal proteins), number of unique peptides (> 0), and number of peptides (> 1). Subsequently, the list of identified proteins was subjected to CRAPome analysis(48), using default settings. To discriminate bona fide protein interactors of AcP10 from the background, we set a SAINT score threshold of 0.9, and a FC-B scores threshold (spectral count fold change between bait and Lpro control) of 2.

The mass spectrometry proteomics data have been deposited in the ProteomeXchange Consortium via the PRIDE partner repository(49) with the dataset identifier PXD011879.

Cross-linking LC/MS and data analysis. A total of $5*10^8$ HEK293T cells in 40 dishes were transiently transfected with pcDNA3 plasmids encoding TAP-tagged AcP10 using PEI transfection. Briefly, for each

dish, 15 µg DNA was mixed with 1.5 ml OptiMEM. Subsequently, 100 µl of a 1 mg/ml PEI solution was added, mixed thoroughly, and incubated for 30 min at RT before adding to the cells. Next day, cells were lysed in lysis buffer (40 mM Tris-HCl pH7.4, 50 mM NaCl, 10 mM EDTA, 1% NP-40, protease inhibitors [Roche]) for 15 min on ice. After spinning down cell debris, supernatants were incubated with 50 µl Strep-Tactin beads (IBA) for 2 h at 4 °C. Beads were washed four times in wash buffer (40 mM Tris-HCl pH7.4, 50 mM NaCl, 1 mM EDTA) and once in PBS. The isolated proteins were then cross-linked on-beads using 1 mM disuccinimidyl sulfoxide (DSSO) cross-linker in cross-linking buffer (20 mM HEPES, pH 7.8 and 150 mM NaCl) for 30 min. The cross-linking reaction was quenched with 20 mM Tris-HCl (pH 7.8) for 30 min at room temperature. For on-beads digestion, cross-linked proteins were denatured with 2 mM urea, reduced with 4 mM DTT at 56 °C for 30 min and alkylated with 8 mM iodoacetamide at room temperature for 30 min in the dark. Proteins were digested using trypsin at an enzyme-to-protein ratio of 1:20 (w/w) at 37 °C for 2 hr. The supernatant was removed from the beads and further digested at 37 °C overnight. Protein digests were desalted using Sep-Pak C18 cartridges (Waters) and dried under vacuum concentrator. The digests were fractionated by strong cation exchange (SCX) chromatography and five late SCX fractions were collected for further LC/MS analysis. Protein digests including cross-linked peptides were analyzed using an ultra HPLC Agilent 1200 system (Agilent Technologies) coupled on-line to an Orbitrap Fusion mass spectrometer (Thermo Fisher Scientific). LC/MS/MS analysis was performed as previously described using the CID-MS2-MS3-ETD-MS2 acquisition strategy (29). Cross-link identification was performed using standalone XlinkX software (29). Results were filtered by 1% false discovery rate and all reported cross-links were manually validated.

Homology modelling of AcP10 from hUCK1. Models of AcP10 were obtained via homology modelling using, as a template, a crystal structure of a homologue, hUCK1 (human uridine cytidine kinase 1 - PDBid 2UVQ). They share about 30% identity and 50% similarity. We performed the modelling with Modeller 9.12 (50) and its standard loop modelling protocol (51). The sequence alignment used comes from NEEDLE (52) used with its default parameters. 25 models were generated from which the best model after ranking by DOPE score (53) was kept.

Phylogenetic analysis of Uridine kinases. A list of uridine kinases was obtained with the ncbi BLAST tool using the AcP10 sequence as query, and subsequent selection of sequences with at least 95% coverage. To obtain a list of representative sequences from all relevant phylogenetic groups, the resulting sequence list was manually supplemented with sequences from Animalia, Archaea, Bacteria and Mimiviridae. The total sequence list was aligned using the MUltiple Sequence Comparison by Log-Expectation (MUSCLE) method. Subsequently, a phylogenetic tree was created in MEGAX software (54)

by the Neighbor-Joining Method, using the Number of Differences substitutions model, and a site coverage cut-off of 99%. The final dataset included 173 positions from 300 amino acid sequences.

Statistics. All uridine kinase, immunofluorescence, flow cytometry, and Western blot data shown in the figures originate from representative experiments of at least three independent replicates. Quantifications of immunofluorescence images was done using at least three images containing >10 cells each. The ^{35}S radiolabeling data was based on duplo independent experiments. The TAP-MS and Cross-linking LC/MS were single experiments. All statistical analyses were done using a one-way ANOVA with Bonferroni post-hoc test, unless indicated otherwise.

Acknowledgments

We thank dr. Adri Thomas and dr. Jolanda de Groot-Mijnes for critical reading of the manuscript and helpful suggestions. We thank Prof. David Ron for kindly providing HeLa cells stably expressing 3Xflag-tagged eIF2Bβ, dr. Alex Greninger for the pAV aichivirus cDNA clone, dr. George Belov for HeLa-R19 cells, and prof. Jerry Pelletier for translation inhibitor Pateamine A. The work was supported by the Netherlands Organization for Scientific Research through a Vici grant (NWO-918.12.628) to FJMvK and a Veni grant (NWO-863.13.008) to MAL. PG, FL and AJRH acknowledge support from the Netherlands Organization for Scientific Research (NWO) funding the large-scale proteomics facility Proteins@Work (project 184.032.201) embedded in the Netherlands Proteomics Centre. Work in the labs of FJMvK and AJRH is supported by the ULS Molecular Immunology Hub. PW is an Investigator of the Howard Hughes Medical Institute.

Author Contributions

Conceptualization, HHR, MAL, RJG, and FJMvK; Investigation, HHR, LJV, TCP, FL, PG, JGD, SGvdG, JGS, AAA, MET, and AMJJB; Resources, AAA and PW; Writing – Original Draft, HHR, RJG, and FJMvK; Writing – Review & Editing, all authors; Visualization, HHR, RJG, and FJMvK; Supervision, MAL, AMJJB, PW, AJRH, RJG, and FJMvK; Funding Acquisition, MAL, PW, AJRH, and FJMvK;

Declaration of interests

The authors declare no competing interests.

Data Availability

There are no restrictions on data availability. All relevant data are shown in the figures, or available in the supplementary datasets 1-3. The AcP10 tandem affinity purification mass spectrometry data have been deposited in the ProteomeXchange Consortium via the PRIDE partner repository with the dataset identifier PXD011879.

References

1. K. Pakos-Zebrucka, *et al.*, The integrated stress response. *EMBO Rep.* **17**, 1374-1395 (2016)

2. D. Levin, I. M. London, Regulation of protein synthesis: activation by double-stranded RNA of a protein kinase that phosphorylates eukaryotic initiation factor 2. *PNAS.* **75**, 1121–5 (1978)

3. R. Panniers, E. C. Henshaw, A GDP/GTP exchange factor essential for eukaryotic initiation factor 2 cycling in Ehrlich ascites tumor cells and its regulation by eukaryotic initiation factor 2 phosphorylation. *J. Biol. Chem.* **258**, 7928-34 (1983)

4. a G. Rowlands, R. Panniers, E. C. Henshaw, The catalytic mechanism of guanine nucleotide exchange factor action and competitive inhibition by phosphorylated eukaryotic initiation factor 2. *J. Biol. Chem.* **263**, 5526-33 (1988)

5. N. A. Kulak, G. Pichler, I. Paron, N. Nagaraj, M. Mann, Minimal, encapsulated proteomic-sample processing applied to copy-number estimation in eukaryotic cells. *Nat. Methods* **11**, 319-24 (2014)

6. C. R. Singh, *et al.*, Change in Nutritional Status Modulates the Abundance of Critical Pre-initiation Intermediate Complexes During Translation Initiation in Vivo. *J Mol Biol*. **370**, 315–330 (2007)

7. A. Leroux, I. London, Regulation of protein synthesis by phosphorylation of eukaryotic initiation factor 2 alpha in intact reticulocytes and reticulocyte lysates. *PNAS.* **79**, 2147–2151 (1982)

8. Y. Lu, M. Wambach, M. G. Katze, R. M. Krug, Binding of the Influenza Virus NS1 Protein to Double-Stranded RNA Inhibits the Activation of the Protein Kinase That Phosphorylates the eIF-2 Translation Initiation Factor. *Virology* **214**, 222–228 (1995)

9. H. H. Rabouw, *et al.*, Middle East Respiratory Coronavirus Accessory Protein 4a Inhibits PKR-Mediated Antiviral Stress Responses. *PLoS Pathog.* **12**, e1005982 (2016)

10. A. C. Dar, F. Sicheri, X-ray crystal structure and functional analysis of vaccinia virus K3L reveals molecular determinants for PKR subversion and substrate recognition. *Mol. Cell* **10**, 295-305 (2002)

11. M. Kawagishi-Kobayashi, J. B. Silverman, T. L. Ung, T. E. Dever, Regulation of the protein kinase PKR by the vaccinia virus pseudosubstrate inhibitor K3L is dependent on residues conserved between the K3L protein and the PKR substrate eIF2alpha. *Mol. Cell. Biol.* **17**, 4146-58 (1997)

12. J. L. G. Cruz, *et al.*, Coronavirus gene 7 counteracts host defenses and modulates virus virulence. *PLoS Pathog.* **7,** e1002090 (2011)

13. Y. Li, *et al.*, ICP34.5 protein of herpes simplex virus facilitates the initiation of protein translation by bridging eukaryotic initiation factor 2alpha (eIF2alpha) and protein phosphatase 1. *J. Biol. Chem.* **286**, 24785-92 (2011)

14. K. A. Mihindukulasuriya, G. Wu, J. St. Leger, R. W. Nordhausen, D. Wang, Identification of a Novel Coronavirus from a Beluga Whale by Using a Panviral Microarray. *J. Virol.* **82**, 5084-8 (2008)

15. J. Nejepinska, R. Malik, S. Wagner, P. Svoboda, Reporters transiently transfected into mammalian cells are highly sensitive to translational repression induced by dsRNA expression. *PLoS One* **9**, e87517 (2014)

16. J. Nejepinska, R. Malik, M. Moravec, P. Svoboda, Deep sequencing reveals complex spurious transcription from transiently transfected plasmids. *PLoS One* **7**, e43283 (2012)

17. S. V Hato, *et al.*, The mengovirus leader protein blocks interferon-alpha/beta gene transcription and inhibits activation of interferon regulatory factor 3. *Cell. Microbiol.* **9**, 2921–2930 (2007)

18. L. J. Visser, *et al.*, FMDV leader protease cleaves G3BP1 and G3BP2 and inhibits stress granule formation. *J. Virol.* **93**, pii: e00922-18 (2018)

19. C. Sidrauski, *et al.*, Pharmacological dimerization and activation of the exchange factor eIF2B antagonizes the integrated stress response. *Elife* **4**, e07314 (2015).

20. C. Sidrauski, *et al.*, Pharmacological brake-release of mRNA translation enhances cognitive memory. *Elife* **2**, e00498 (2013).

21. A. F. Zyryanova, *et al.*, Binding of ISRIB reveals a regulatory site in the nucleotide exchange factor eIF2B. *Science.* **359**, 1533-1536 (2018)

22. J. C. Tsai, *et al.*, Structure of the nucleotide exchange factor eIF2B reveals mechanism of memory-enhancing molecule. *Science.* **359**, pii: eaaq0939 (2018)

23. H. H. Rabouw, *et al.*, The small molecule ISRIB suppresses the integrated stress response within a defined window of activation. *PNAS*, **116**, 2097-2102 (2019)

24. H. P. Harding, *et al.*, Regulated translation initiation controls stress-induced gene expression in mammalian cells. *Mol. Cell* **6**, 1099-108 (2000)

25. P. D. Lu, H. P. Harding, D. Ron, Translation reinitiation at alternative open reading frames regulates gene expression in an integrated stress response. *J. Cell Biol.* **167**, 27-33 (2004)

26. K. M. Vattem, R. C. Wek, Reinitiation involving upstream ORFs regulates ATF4 mRNA translation in mammalian cells. *PNAS.* **101**, 11269-74 (2004)

27. H. Choi, *et al.*, Analyzing protein-protein interactions from affinity purification-mass spectrometry data with SAINT. *Curr. Protoc. Bioinforma.* Chapter 8, Unit 8.15 (2012)

28. S. S. Mohammad-Qureshi, *et al.*, Purification of FLAG-Tagged Eukaryotic Initiation Factor 2B Complexes, Subcomplexes, and Fragments from Saccharomyces cerevisiae. *Methods Enzymol.* **431**, 1-13 (2007)

29. F. Liu, P. Lössl, R. Scheltema, R. Viner, A. J. R. Heck, Optimized fragmentation schemes and data analysis strategies for proteome-wide cross-link identification. *Nat. Commun.* **8**, 15473 (2017)

30. Y. Sekine, *et al.*, Mutations in a translation initiation factor identify the target of a memory-enhancing compound. *Science.* **348**, 1027-30 (2015)

31. K. Kashiwagi, *et al.*, Structural basis for eIF2B inhibition in integrated stress response. *Science.* **364**, 495-499 (2019)

32. L. R. Kenner, *et al.*, eIF2B-catalyzed nucleotide exchange and phosphoregulation by the integrated stress response. *Science.* **364**, 491-495 (2019)

33. A. M. Bogorad, K. Y. Lin, A. Marintchev, Novel mechanisms of eIF2B action and regulation by eIF2α phosphorylation. *Nucleic Acids Res.* **45**, 11962-11979 (2017)

34. K. Kashiwagi, *et al.*, Crystal structure of eukaryotic translation initiation factor 2B. *Nature* **531**, 122–5 (2016)

35. M. Halliday, G. R. Mallucci, Review: Modulating the unfolded protein response to prevent neurodegeneration and enhance memory. *Neuropathol. Appl. Neurobiol.* **41**, 414–427 (2015)

36. J. A. Moreno, *et al.*, Sustained translational repression by eIF2α-P mediates prion neurodegeneration. *Nature* **485**, 507–511 (2012)

37. C. Wang, *et al.*, Inhibiting the integrated stress response pathway prevents aberrant chondrocyte differentiation thereby alleviating chondrodysplasia. *Elife* **7**, pii: e37673 (2018)

38. M. Halliday, *et al.*, Partial restoration of protein synthesis rates by the small molecule ISRIB prevents neurodegeneration without pancreatic toxicity. *Cell Death Dis.* **6**, e1672 (2015)

39. Y. L. Wong, *et al.*, The small molecule ISRIB rescues the stability and activity of vanishing white matter disease eIF2B mutant complexes. *Elife* **7**, pii: e32733 (2018)

40. H. G. Nguyen, *et al.*, Development of a stress response therapy targeting aggressive prostate cancer. *Sci. Transl. Med.* **10**, pii: eaar2036 (2018)

41. A. Chou, *et al.*, Inhibition of the integrated stress response reverses cognitive deficits after traumatic brain injury. *PNAS.* **114**, E6420-E6426 (2017)

42. D. Armenta-Medina, L. Segovia, E. Perez-Rueda, Comparative genomics of nucleotide metabolism: A tour to the past of the three cellular domains of life. *BMC Genomics* **15**, 800 (2014)

43. G. a Belov, M. H. Fogg, E. Ehrenfeld, Poliovirus Proteins Induce Membrane Association of GTPase ADP-Ribosylation Factor Poliovirus Proteins Induce Membrane Association of GTPase ADP-Ribosylation Factor. *J Virol* **79**, 7207–7216 (2005)

44. C. M. Dorobantu, *et al.*, Recruitment of PI4KIII to Coxsackievirus B3 Replication Organelles Is Independent of ACBD3, GBF1, and Arf1. *J. Virol.* **88**, 2725-36 (2014)

45. A. Shevchenko, M. Wilm, O. Vorm, M. Mann, Mass spectrometric sequencing of proteins from silver-stained polyacrylamide gels. *Anal. Chem.* **68**, 850-8 (1996)

46. A. Cristobal, *et al.*, In-house construction of a UHPLC system enabling the identification of over 4000 protein groups in a single analysis. *Analyst* **137**, 3541-8 (2012)

47. L. Käll, J. D. Canterbury, J. Weston, W. S. Noble, M. J. MacCoss, Semi-supervised learning for peptide identification from shotgun proteomics datasets. *Nat. Methods* **4**, 923-5 (2007)

48. D. Mellacheruvu, *et al.*, The CRAPome: A contaminant repository for affinity purification-mass spectrometry data. *Nat. Methods* **10**, 730-6 (2013)

49. J. A. Vizcaíno, *et al.*, The Proteomics Identifications (PRIDE) database and associated tools: Status in 2013. *Nucleic*

Acids Res. **41**, (Database issue) D1063-9 (2013)

50. A. Šali, T. L. Blundell, Comparative protein modelling by satisfaction of spatial restraints. *J. Mol. Biol.* **234**, 779–815 (1993)

51. A. Fiser, R. K. G. Do, A. Šali, Modeling of loops in protein structures. *Protein Sci.* **9**, 1753-73 (2000)

52. H. McWilliam, *et al.*, Analysis Tool Web Services from the EMBL-EBI. *Nucleic Acids Res.* **41**, (Web Server issue) W597-600 (2013)

53. M. Shen, A. Sali, Statistical potential for assessment and prediction of protein structures. *Protein Sci.* **15**, 2507-24 (2006)

54. S. Kumar, G. Stecher, M. Li, C. Knyaz, K. Tamura, MEGA X: Molecular evolutionary genetics analysis across computing platforms. *Mol. Biol. Evol.* **35**, 1547-1549 (2018)

55. N. N. Suzuki, K. Koizumi, M. Fukushima, A. Matsuda, F. Inagaki, Structural basis for the specificity, catalysis, and regulation of human uridine-cytidine kinase. *Structure* **12**, 751-64 (2004)

56. E. K. Schmidt, G. Clavarino, M. Ceppi, P. Pierre, SUnSET, a nonradioactive method to monitor protein synthesis. *Nat. Methods* **6**, 275–277 (2009)

Supplementary Information

Supplementary Data 1. List of uridine kinase protein sequences used for phylogenetic analysis of AcP10.

Supplementary Data 2. Tandem affinity purification MS analysis of cellular AcP10 interaction partners.

Supplementary Data 3. Cross-linking LC/MS analysis of eIF2•eIF2B•TAP-AcP10 complexes purified from HEK293T cell lysates.

Supplementary Table 1. Co-purified subunits of the eIF2 and eIF2B complexes in the affinity pull-down experiments using TAP-AcP10, with as controls TAP-Lpro, TAP-hUCK2 and TAP-AcP10(SA-). The number of peptide-to-spectrum matches (PSM) is given for each detected subunit. The number of detected unique peptides and sequence coverage relate to the TAP-AcP10 data.

Supplementary Table 2. Plasmids used in this study

Supplementary Figures

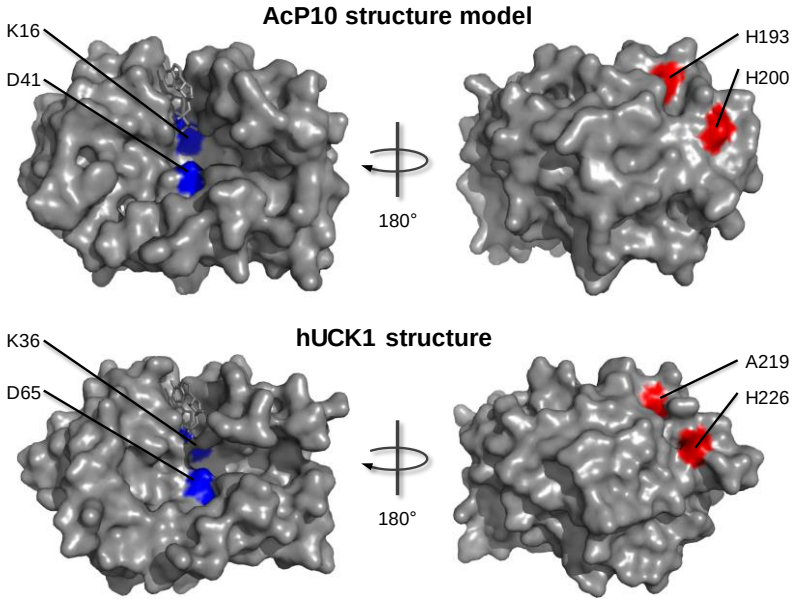

Figure S1. Structural modelling of AcP10. *The AcP10 structure was modelled based on its homology to human uridine cytidine kinase 1 (hUCK1, accession number; pdb file 2UVQ). Indicated are the residues important for uridine kinase function (In blue; ATP binding site K16 and catalytic site D41), and those important for AcP10's ability to antagonize the ISR (In red; H193 and H200).*

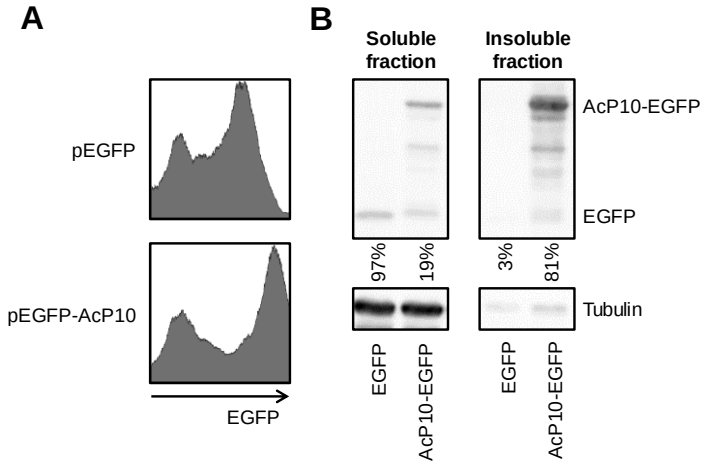

Figure S2. AcP10 is highly insoluble. *(A) Flow cytometry analysis of EGFP expression levels in cells expressing EGFP (top panel) or the AcP10-EGFP fusion protein (bottom panel). (B) Cells overexpressing AcP10-EGFP or EGFP were lysed in buffer containing 1% triton X100. The soluble fraction obtained after centrifugation, and the insoluble fraction obtained after resuspension of the cell debris in 8 M urea, were analyzed by Western blot for presence of the overexpressed protein, using an antibody directed against EGFP.*

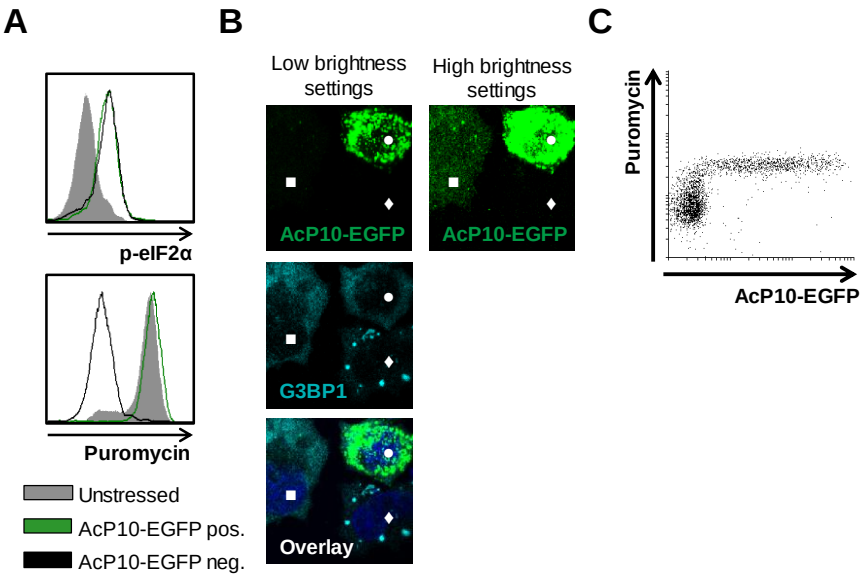

Figure S3. Low levels of AcP10 are sufficient to fully rescue translation. *(A) Flow cytometry analysis of p-eIF2 levels and ongoing translation in pEGFP-AcP10 transfected cells treated with arsenite for 30 min. A mock treated sample is shown in grey fill. AcP10-positive cells are indicated in green, and AcP10-negative cells from the same well are shown in black. (B) Immune fluorescence analysis of SG formation in pEGFP-AcP10 transfected cells treated with arsenite for 30 min. Shown are three cells, one of which expresses AcP10 at relatively high levels (●), one expresses AcP10 at low levels (■), and one does not express AcP10 (◆). SG marker G3BP1 were visualized to assess SG formation. (C) Flow cytometry analysis of EGFP expression and ongoing translation in a pEGFP-AcP10 transfected cell population treated with arsenite for 30 min.*

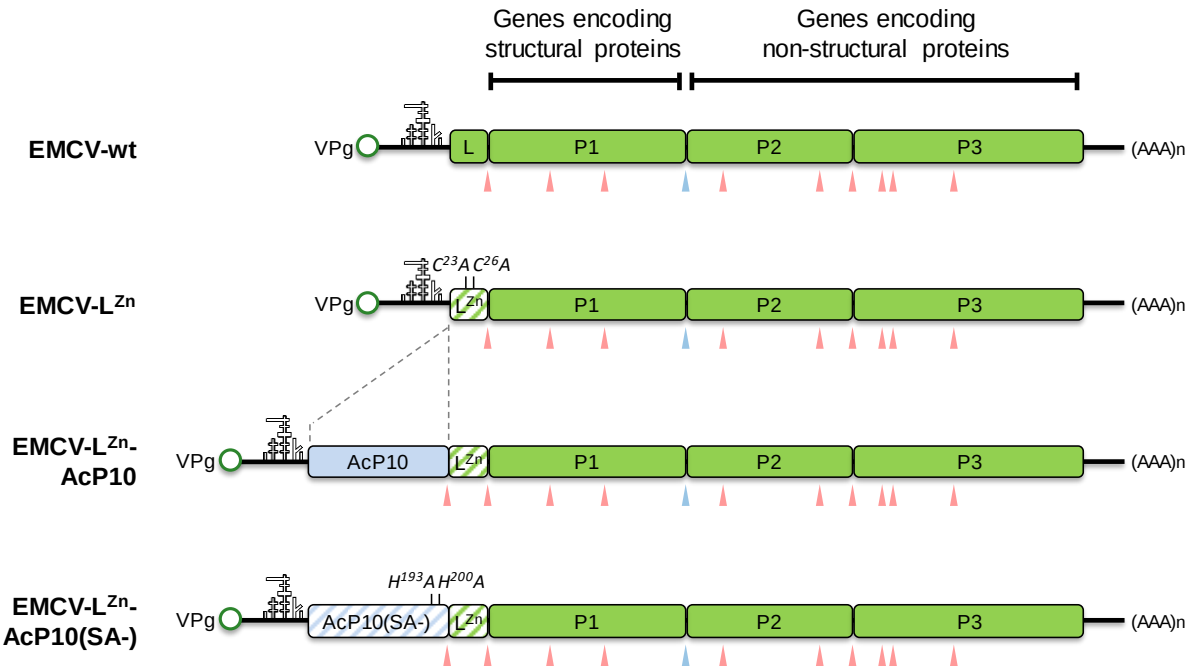

Figure S4. Genome compositions of recombinant EMCVs used in this study. *The EMCV genome contains of a 5' VPg viral protein, a 5' UTR which includes the EMCV IRES, a single ORF encoding the EMCV polyprotein, and a 3' UTR which includes a poly-A tail (top panel). In the EMCV-L^{zn} virus, the endogenous ISR antagonist (L) is inactivated by a double point mutation (second panel). The genes encoding AcP10 or AcP10(SA-) were inserted into the EMCV-L^{zn} genome to obtain EMCV-L^{zn}-AcP10 and EMCV-L^{zn}-AcP10(SA-), respectively. (bottom two panels). The viral proteins are separated from the polyprotein by a 2A skip site (indicated by the blue arrowhead), or through catalytic activity of the 3C viral protease (cleavage sites indicated by red arrowheads).*

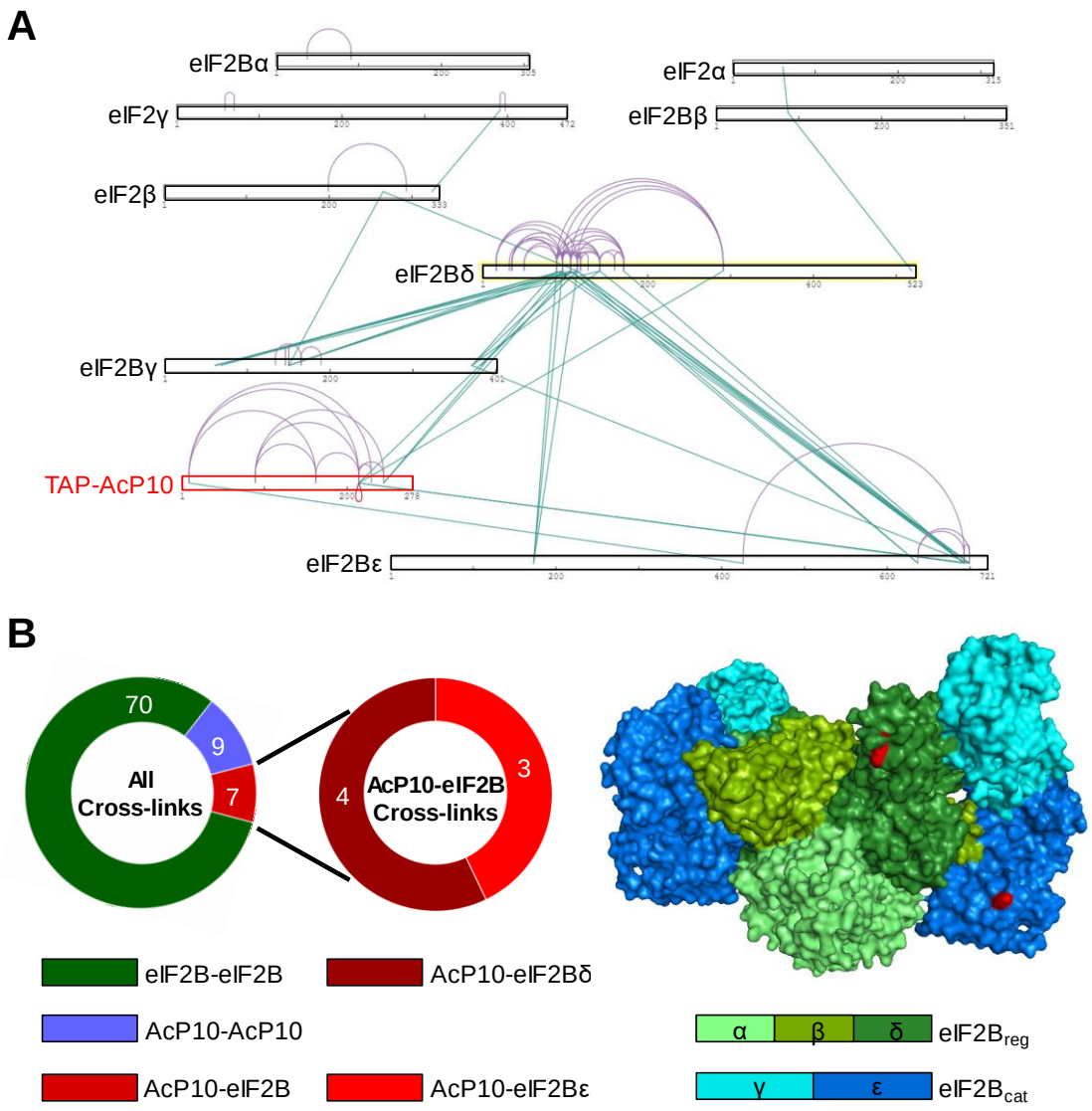

Figure S5. Cross-linking mass-spectrometry analysis of AcP10-eIF2B-eIF2 complexes. *(A) Schematic overview of the cross-links identified in AcP10-eIF2B-eIF2 complexes that were affinity purified using TAP-AcP10. Indicated in teal are inter-protein cross-links and indicated in purple are intra-protein cross-links. A single cross-link was formed between two of the same peptides from AcP10 (indicated in red), which may have occurred due to AcP10's tendency to aggregate. (B) Schematic overview of the total number of cross-links found within AcP10 (blue), within the eIF2B complex (green), and between AcP10 and eIF2B subunits (red). If present in resolved parts of eIF2B, the eIF2B residues that cross-linked with AcP10 are indicated in red in the right panel. The subunits of the eIF2B regulatory subcomplex (eIF2B$_{reg}$) and eIF2B catalytic subcomplex (eIF2B$_{cat}$) are shown in shades of green or blue, respectively, as indicated.*

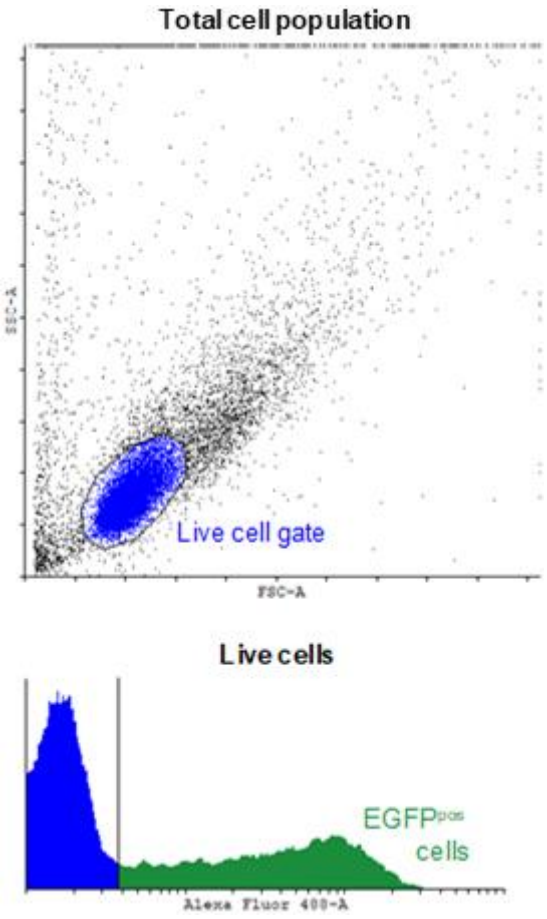

Figure S6. Gating strategy used for flow cytometry analyses. *For all flow cytometry samples, live cells were identified based on FSC/SSC profile (top panel). When indicated, transfected cells within the live cell population were selected based on EGFP expression (bottom panel).*

Chapter 5

The Aichivirus leader protein inhibits the integrated stress response by preventing p-eIF2-mediated inhibition of eIF2B function

Huib H Rabouw[1,#], Linda J Visser[1,#], José G Dekker[1], Piero Giansanti[2,‡], Jesús G. Saucedo[1], Susanne G van der Grein[1], Martijn A Langereis[1], Albert JR Heck[2], Raoul J de Groot[1], Frank JM van Kuppeveld[1,]*

[1]Virology Division, Department of Infectious Diseases and Immunology, Faculty of Veterinary Medicine, Utrecht University, 3584 CL, Utrecht, The Netherlands

[2]Molecular Virology Laboratory, Department of Medical Microbiology, Leiden University Medical Center, 2333 ZA, Leiden, The Netherlands

[3]Department of Molecular and Cell Biology, National Center of Biotechnology (CNB-CSIC), Campus Universidad Autonoma de Madrid, Madrid, Spain

[#]*These authors contributed equally*

This chapter was partly integrated in the final submission of chapter 4

Abstract

Under conditions of stress, eukaryotic cells activate the integrated stress response (ISR) to temporarily block translation initiation, and restore cellular homeostasis. The ISR can be activated by four stress kinases, which, upon sensing specific stress stimuli, converge on phosphorylation of translation initiation factor eIF2. p-eIF2 sequesters the eIF2-specific guanidine exchange factor (GEF) eIF2B, which prevents eIF2•GDP/GTP exchange, an essential step in translation initiation. Many viruses avoid the detrimental effects of the ISR on viral protein synthesis by encoding specific ISR antagonists. We describe the mechanism through which aichivirus (AiV; family picornavirus, genus *kobuvirus* KoV), interferes with the ISR. Whereas almost all ISR antagonist prevent or reverse eIF2 phosphorylation, AiV allows ongoing translation in the presence of high concentrations of p-eIF2, through the function of its leader protein (AiVL). AiVL binds eIF2B and blocks subsequent association of p-eIF2, thus preventing p-eIF2 from interfering with eIF2B GEF function. Besides AiVL, also the closely related mouse KoV leader, but not other KoV leaders, inhibits the ISR, suggestive of a relatively recent gain-of-function event. A mode of action similar to that of AiVL was recently described for a phylogenetically unrelated coronavirus accessory protein (AcP10), which shares no similarity with AiVL. Thus, the ability to bind eIF2B and render it insensitive to p-eIF2 was acquired by at least two unrelated virus species through convergent evolution.

Introduction

To ensure efficient virus propagation, viruses evade several antiviral pathways within the infected host cell. One of these pathways, the integrated stress response (ISR), can be activated in response to a variety of intracellular danger signals including viral infection. The ISR mediates a temporal stop in translation, conserving energy and redirecting cellular resources towards resolving the stress situation (1). In mammalian cells, four ISR-sensor proteins have been described. Protein kinase R (PKR) detects cytoplasmic dsRNA, and is considered the most important ISR sensor protein during virus infections (2). PKR-like ER-resident kinase (PERK) responds to ER-stress that causes misfolded proteins to accumulate in the ER lumen (3, 4). General control non-derepressible (GCN2) is best known for its ability to detect nutrient deprivation and subsequent accumulation of uncharged tRNA molecules (5). Finally, Heme-responsive inhibitor (HRI) is activated by heme deficiency or the presence of toxic heavy metals (6, 7). Upon sensing their respective activating trigger, these proteins homodimerize and autophosphorylate, and subsequently phosphorylate translation initiation factor eIF2. Phosphorylated eIF2 (p-eIF2) tightly binds the eIF2-specific guanidine exchange factor (GEF) eIF2B, thereby inhibiting eIF2 recycling and preventing translation initiation. The stalled translation initiation complexes then condense to form cytoplasmic foci called stress granules (SGs).

In virus infected cells, ISR-mediated inhibition of translation severely represses production of viral proteins, and consequently the generation of progeny virus. Therefore, viruses have evolved multiple ways to circumvent the ISR, either by preventing eIF2α kinase activation (Class 1 antagonist), by preventing eIF2α phosphorylation (Class 2 antagonist), or by actively inducing dephosphorylation of p-eIF2 (Class 3 antagonist) (8). Recently, a novel mode of action was described for a coronavirus accessory protein, AcP10, that rescues cellular and viral translation without affecting eIF2α phosphorylation by preventing the formation of p-eIF2•eIF2B complexes (Class 4 antagonist, (8)).

The picornavirus family encompasses a large group of non-enveloped positive-strand RNA viruses. This family includes many well-known pathogens of relevance to the health of humans and animals, such as enteroviruses (e.g. poliovirus), hepatoviruses (e.g. hepatitis A virus), and apthoviruses (e.g. foot-and-mouth disease virus), and cardioviruses (e.g. encephalomyocarditis virus). Picornaviral genomes are 7,5-8 kb in length, and contain a single open reading frame that encodes a large polyprotein. This polyprotein is processed by viral proteases to yield the structural capsid proteins (VP1-4) and various proteins involved in replication (2A-2C and 3A-3D). Besides this conserved set of proteins, several picornaviruses also encode a leader (L) protein upstream of the capsid coding region. L proteins are highly diverse in sequence, structure, and function, and are considered to be accessory proteins involved in optimizing virus replication, e.g. through suppression of the host cell's antiviral responses

(9). The best known are the L protease of FMDV, which cleaves eIF4G to mediate host shut-off (10), and the L proteins of cardioviruses, which block IFN induction and stress responses (11, 12).

In 1991, a novel species of picornavirus, called aichivirus (AiV), was described as the causative agent of outbreaks of gastroenteritis in humans (13). Aichivirus was classified within a novel genus of picornaviruses, *kobuvirus* (KoV). Since then, related KoVs have been found in various other mammalian species. KoVs are further subdivided into the lineages Aichi A (e.g. Aichivirus) , Aichi B (e.g. Bovine KoV), and Aichi C (e.g. Porcine KoV) viruses, based on sequence analyses of their 3CD-polymerase genes. In this study, we sought to determine whether and how KoVs evade inhibition by the ISR. We show that AiV actively blocks the ISR, both when activated in a PKR-dependent or HRI-dependent manner. Overexpression experiments demonstrate that the AiV-encoded L protein (AiVL) is a highly potent ISR antagonist in the absence of other viral proteins. Consistently, a recombinant AiV lacking a functional AiVL protein induces full-blown ISR activity, indicating that AiVL is the main, and possibly the sole ISR antagonist encoded by AiV. AiVL does not counteract the upstream signaling events of the ISR pathway, but rescues global translation in the presence of (high levels of) p-eIF2. This effect is mediated by its association to eIF2B, which prevents subsequent binding of p-eIF2, and thus renders eIF2B insensitive to inhibition by p-eIF2. We show that the closely related mouse kobuvirus L protein (M-KoVL) has a similar function, but that other tested KoVLs do not, suggesting that the ISR antagonist function was obtained through a gain-of-function event relatively late in the KoVL evolutionary trajectory. AiVL's mode of action strongly resembles that of Beluga-whale coronavirus AcP10, and defines it as a Class 4 ISR antagonist (8). Thus, the ability to bind eIF2B and prevent inhibition by p-eIF2 independently developed within at least two unrelated viruses, in non-homologous proteins, through convergent evolution.

Results

Aichivirus prevents ISR activity in infected cells. To test whether AiV suppresses the ISR in infected cells, we assessed SG formation in AiV-infected cells. For this, we first established replication kinetics in infected Vero cells. A single-step growth curve, in which we quantified the production of progeny infectious virus at the indicated time points pi. (Fig 1A), indicated that most virus is produced between 6 and 10 h pi. In line with these data, an immunofluorescence assay (IFA) shows large quantities of dsRNA, indicative of active virus replication, at the same time points (Fig 1B). Interestingly, despite the appearance of dsRNA, which could activate the ISR sensor protein PKR, infected cells were consistently devoid of SGs throughout the infection cycle, up to and including the moment they started displaying cytopathic effects at 10 h pi. These data provided first indication that AiV counteracts the ISR. This was further corroborated by the observation that AiV-infected cells failed to assemble SGs in response to arsenite treatment, which activates the eIF2α kinase HRI (Fig 1C).

The Aichivirus-encoded L protein rescues cellular translation in the presence of p-eIF2. Multiple picornavirus L proteins have been shown to repress cellular antiviral responses, including the ISR (11, 12, 14, 15). To test whether the AiV Leader protein (AiVL) is responsible for inhibiting the ISR in AiV-infected cells, we transiently overexpressed EGFP-tagged AiVL in absence of other viral proteins, and assessed SG formation in response to (i) the pEGFP plasmid DNA transfection itself, which induces PKR- and p-eIF2-dependent stress in some of the transfected cells (Fig 2A,(16, 17)), (ii) treatment with sodium arsenite, which induces HRI- and p-eIF2-dependent stress in all treated cells (Fig 2B), or (iii) treatment with pateamine A, which blocks translation independently of p-eIF2 (Fig 2C). Expression of AiVL prevented p- eIF2-mediated SG formation (Fig 2A and 2B), but not p-eIF2-independent SG formation induced by pateamine A (Fig 2C), indicating that AiVL is indeed a functional ISR antagonist. Furthermore, these data suggest that AiVL targets a downstream step in the ISR pathway that is shared by transfection-induced and arsenite-induced ISR activity. To determine which step of the ISR is targeted by AiVL, we performed flow cytometry analyses to quantify p-eIF2α levels and active translation rates in cells overexpressing AiVL. pEGFP plasmid DNA transfection induces elevated levels of p-eIF2 in a portion of the transfected cells, while the remainder of the cells are unstressed (16, 17), resulting in a mixed population of transfected cells with either high (shown in red) or low (shown in green) levels of p-eIF2α (Fig. 2D). The level of p-eIF2α was similar between AiVL expressing cells and cells expressing negative control EGFP, suggesting that AiVL neither impacts eIF2α phosphorylation, nor induces eIF2α dephosphorylation. As expected, EGFP expressing cells with high p-eIF2α levels displayed impaired translation rates (as measured by puromycin labeling) (Fig 2D, lower panels). In

contrast, in AiVL expressing cells p-eIF2α had no detectable effect on translation, suggesting that AiVL renders cellular translation insensitive to eIF2α phosphorylation.

A putative Zn-finger domain is essential for ISR antagonism by AiVL. To obtain a non-functional AiVL mutant, we performed alanine screening, and substituted specific tryptophans, histidines, cysteines, or potential phosphorylation sites by alanines (Fig 3A, residues indicated in red). The mutant proteins were overexpressed as EGFP fusion proteins and tested for their ability to inhibit arsenite-induced SG formation using IFA. Out of the twenty mutations tested, five (H20A, H24A, H40A, C53A, and C56A)

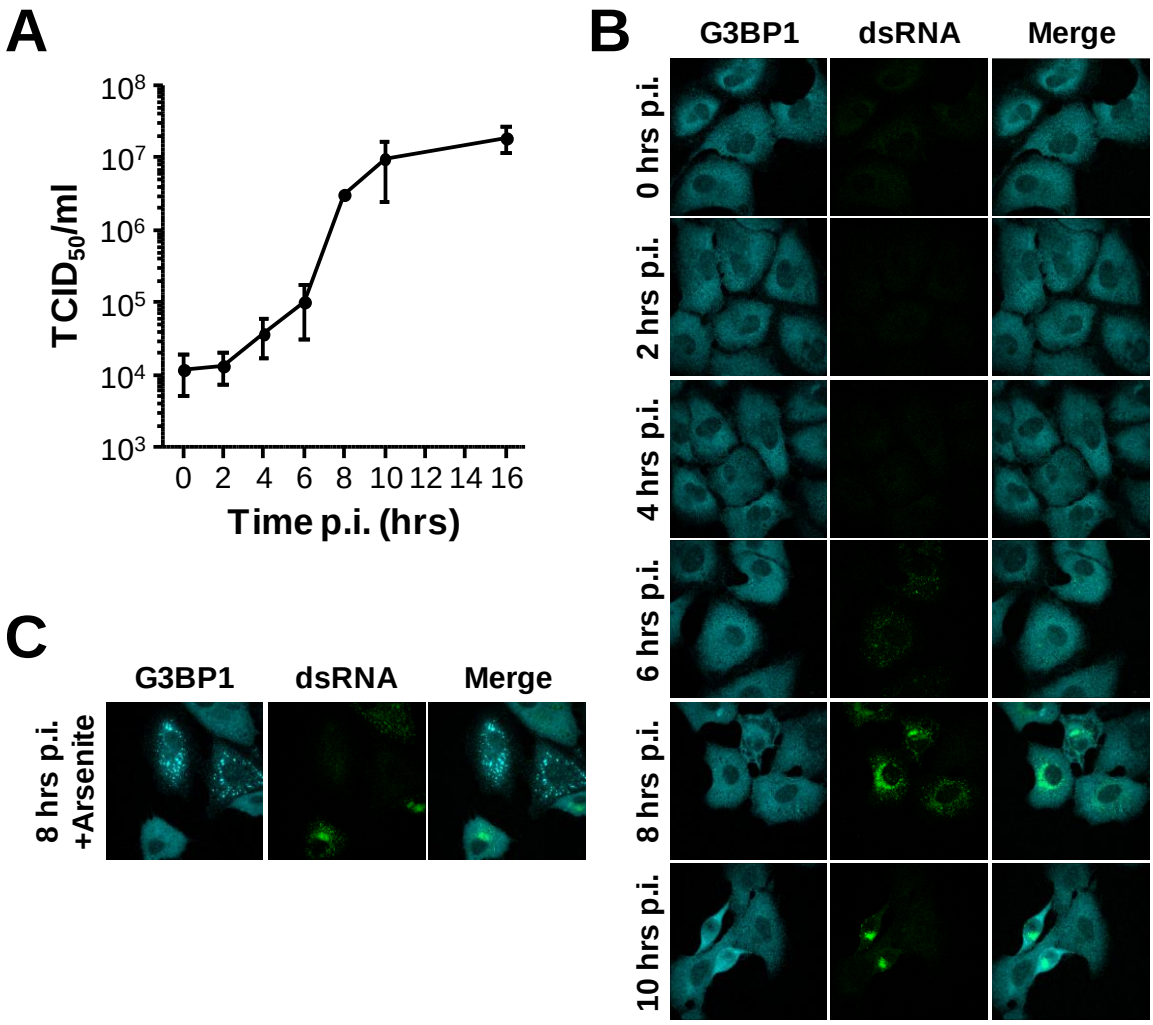

Figure 1. Aichivirus counteracts the ISR. *Vero cells were infected with aichivirus at a multiplicity of infection (MOI) of 2. (A) At the indicated time points, progeny infectious virus particles were harvested and quantified by end-point titrations (B) At the indicated time-points, cells were fixed and stress granule (SG) formation was analyzed by immunofluorescence using an antibody directed against SG marker G3BP1. dsRNA staining was used to identify cells that were actively replicating AiV. (C) Aichivirus-infected cells were treated with 1 mM arsenite from 7 hrs pi. until 8 hrs pi., and SG formation was analyzed as in (B).*

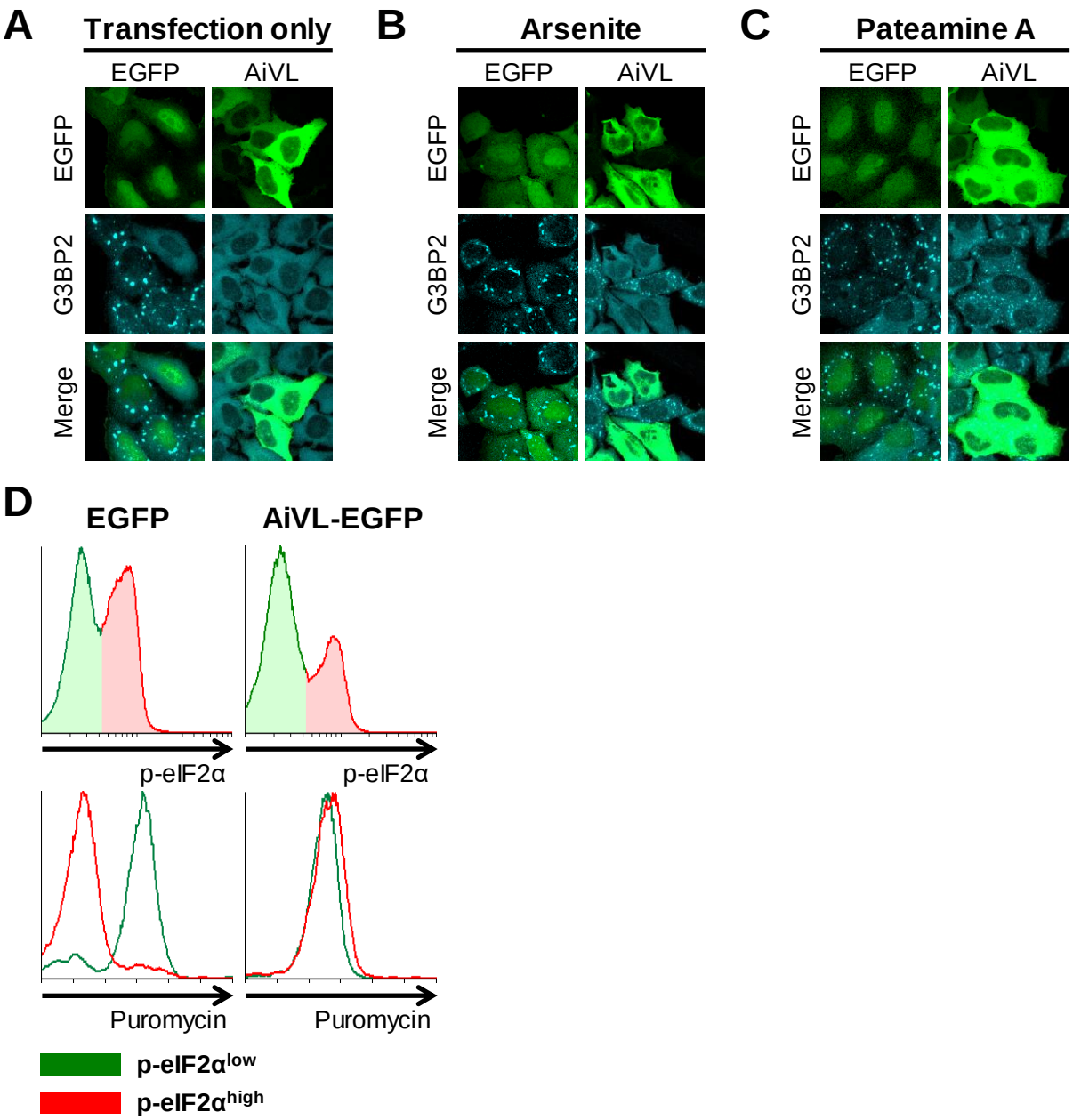

Figure 2. AiVL rescues translation in the presence of p-eIF2. *Hela cells were transfected with plasmids encoding EGFP or AiVL-EGFP. Subsequently, SG formation was monitored by immunofluorescence in cells without additional treatment (A), cells treated with 250 µM arsenite for 1 hour (B), or cells treated with 100 nM pateamine A for 1 hour (C). (D) Cells were transfected with pEGFP or pEGFP-AiVL. Next day, active translation was labeled using 20 µg/ml puromycin for 15 min. Subsequently, cells were fixed and analyzed by flow cytometry for p-eIF2α content and the level of puromycin incorporation. Shown are cells positive for EGFP, with either low p-eIF2α levels (indicated in green) or high p-eIF2α levels (indicated in red).*

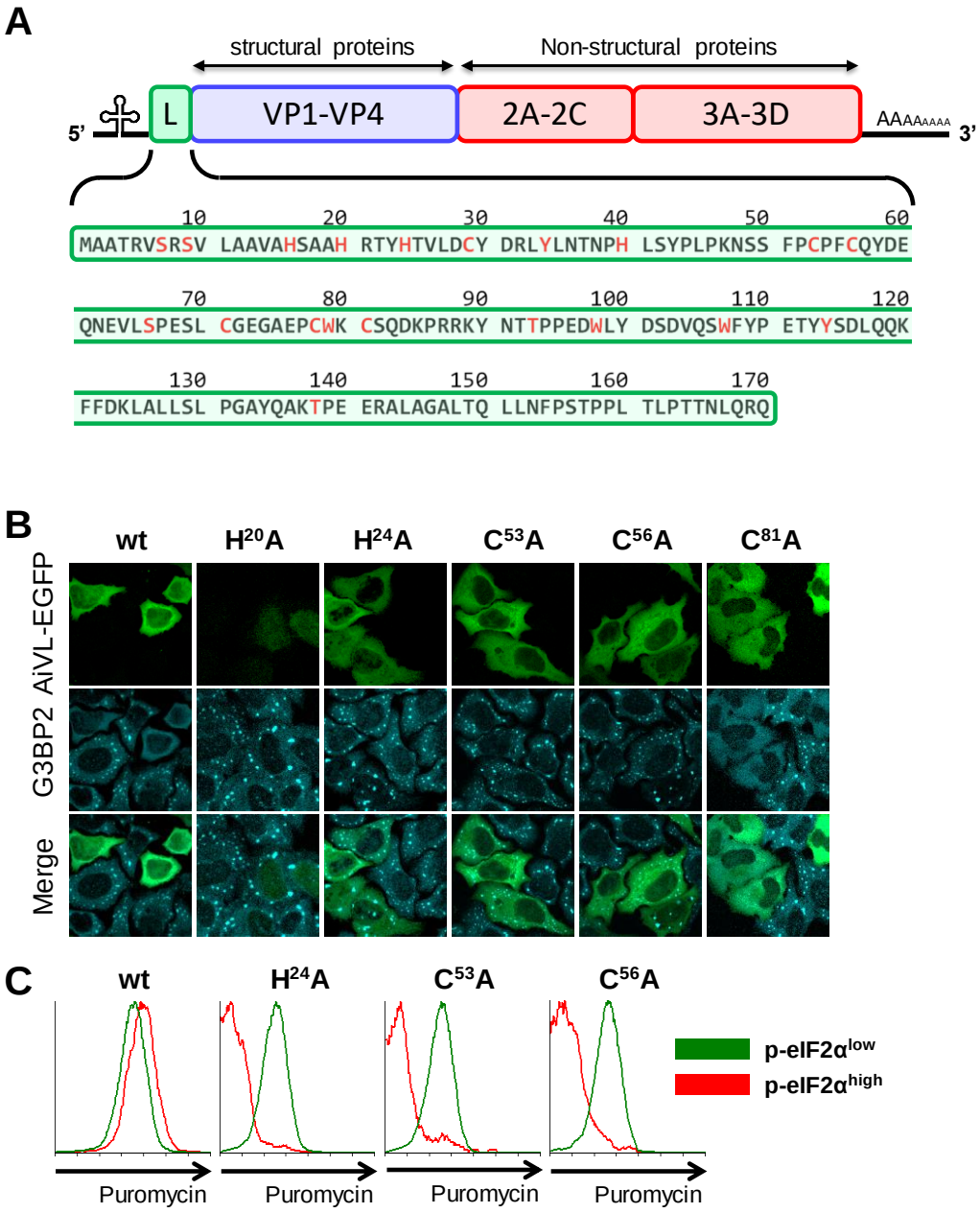

Figure 3. A putative Zn-finger domain is essential for ISR antagonism by AiVL. *(A) Schematic representation of the AiV genome. The position of the gene encoding AiVL is indicated in green. The amino acid sequence of AiVL is shown in the bottom panel, and each residue that was mutated in the alanine screening approach is indicated in red. (B) The AiVL mutants were overexpressed in cells, and their ability to prevent SG formation upon arsenite treatment was analyzed by immunofluorescence using antibodies directed against G3BP1. A small selection out of the total panel of mutants is shown. See Fig S1 for a complete overview. (C) wt AiVL, as well as AiVL mutants H24A, C53A, and C56A, were transiently overexpressed, and after overnight incubation, active translation was labeled using 20 µg/ml puromycin for 15 min. Cells were subsequently analyzed by flow cytometry for active translation rates as described in Fig 2D.*

rendered the AiVL non-functional, three of which (H24A, C53A, C56A) did so without significantly impacting AiVL-expression level or its intracellular localization (Fig 3B). A full overview of the mutants tested is given in supplementary figure S1. Flow cytometry analysis confirmed that the mutant AiVL proteins failed to rescue translation in the presence of elevated p-eIF2α levels (Fig 3C). Interestingly, two of the inactivating mutations affected residues that make up an *in silico* predicted Zn-finger ribbon (C53 and C56). Most Zn-fingers consist of two C/H – X_{2-4} – C/H motifs, which mediate a quadruple interaction with a divalent cation such as Zn^{2+}. In the case of AiVL, the second C/H – X_{2-4} – C/H motif was not predicted *in silico*, but may consist of H20 and H24, since both these residues were also found to be essential for AiVL's function as ISR antagonist (Fig 3B and S1).

AiVL is the main antagonist encoded by Aichivirus. To corroborate our findings that AiVL functions as ISR antagonist rescuing translation in the presence of p-eIF2α, and to show that it functions in the context of AiV infection, we created a recombinant AiV in which the L protein was inactivated by two point mutations (C53A & C56A). Vero cells were infected with wt AiV or AiV-L-C53A/C56A, and analyzed by flow cytometry for p-eIF2α levels and active translation rates (Fig 4A), or by IFA for dsRNA content and SG formation (Fig 4B), at 8 hrs pi. Cells infected with AiV or AiV-L-C53A/C56A contained comparable quantities of dsRNA and similar levels of p-eIF2α, indicating efficient virus replication and ISR activation. However, cells infected with AiV-L-C53A/C56A –but not with wt virus– displayed impaired translation rates and contained SGs. These data unambiguously show that AiVL is an ISR antagonist that rescues translation in the presence of elevated p-eIF2α levels in AiV-infected cells.

AiVL interacts with translation initiation factor eIF2B. To determine how AiVL rescues translation, we identified its cellular interaction partners by mass spectrometry analysis. HEK293T cells were transiently transfected with plasmids encoding tandem affinity purification (TAP) tagged AiVL. AiVL and its cellular interaction partners, were purified as described previously (8) and analyzed by LC-MS/MS. Two out of five eIF2B subunits (eIF2Bγ and eIF2Bδ) were modestly but significantly enriched in AiVL pull-down samples relative to empty vector control samples (Fig 5A). To confirm the interaction with eIF2B, AiVL purification samples were analyzed by Western blot using an antibody directed against eIF2Bα. Indeed, eIF2Bα co-purified with AiVL, albeit to a much lesser extent than when using AcP10, which was included as positive control (Fig 5B). Importantly, no interaction was found between the phenotypically inactive mutant AiVL C56A and eIF2B.

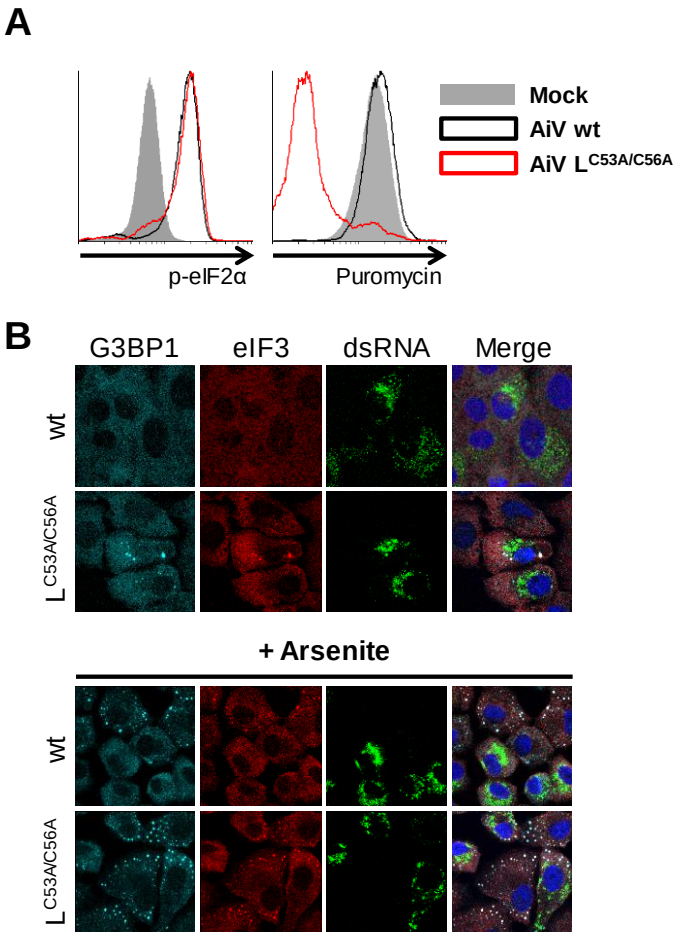

Figure 4. AiVL is the main antagonist encoded by aichivirus. *(A) Vero cells were infected with the indicated recombinant aichiviruses at an MOI of 10 for 8 hrs. Translation was labeled with 20 µg/ml puromycin during the final 15 min of the experiment. Puromycin incorporation, and p-eIF2α content were measured by flow cytometry. (B) Vero cells were infected with the indicated recombinant aichiviruses at an MOI of 1 for 8 hrs. Cells were either left untreated (top panels), or treated with 1.5 mM arsenite during the final hour of the experiment. dsRNA content and the presence of SGs were assessed by IFA using antibodies directed against dsRNA and G3BP1, respectively.*

As reported, purification of AcP10 also indirectly co-purifies eIF2α, since the eIF2•eIF2B macrocomplex remains intact during this purification procedure (8, 18). No eIF2α band was observed in the AiVL pulldown sample, but given the low co-IP efficiency when using AiVL as bait, it is to be expected that the eIF2α signal may fall below the detection limit even if eIF2α is in fact present (Fig 5B). To address the possibility that AiVL may interact with eIF2 rather than eIF2B, we disrupted the eIF2•eIF2B interaction using a high-salt wash (500 µM KCl) (Fig 5B, right panels), and found that eIF2B still associates with AiVL under these conditions. This demonstrates that AiVL directly binds eIF2B, independent of the presence of eIF2.

As a complimentary approach, we pulled down eIF2B from HeLa cells stably expressing flag-tagged eIF2Bβ (HeLa-eIF2Bβ-3Xflag,(19)), and analyzed co-purified eIF2α and AiVL by Western blot (Fig 5C). AiVL, like AcP10, could be detected in eIF2Bβ pulldown samples, again suggesting that AiVL interacts with eIF2B. A high-salt wash step that disturbs the eIF2•eIF2B interaction, released most of the eIF2 into the supernatant fraction, but had only a minor impact on the association of AiVL (Fig 5C, compare lanes 1 and 2 with lanes 7 and 8). Taken together, the data suggest that AiVL rescues translation in presence of p-eIF2 through its binding to eIF2B. The amount of eIF2Bα co-purified with AiVL is consistently low (Fig 5B), while the reverse IP using eIF2B as bait efficiently yields AiVL (Fig 5C). This is likely caused by a vast excess of AiVL protein over eIF2B complexes upon transient overexpression, which causes most AiVL to be free of eIF2B. Additionally, and unlike the AcP10•eIF2B interaction, the AiVL•eIF2B association may be unstable, and less likely to survive the lengthy TAP-AIVL pulldown procedure (~20 hrs) than the shorter eIF2B-flag pulldown procedure (~3 hrs). A relatively unstable AiVL•eIF2B interaction can also be deduced from the observation that incubation of AiVL•eIF2B complexes in wash buffer for 15 min released approximately half of the AiVL protein from eIF2B into the supernatant fraction (Fig 5C, lanes 1 and 2).

AiVL counteracts the association of p-eIF2 to eIF2B. AcP10 binding to eIF2B prohibits the inhibition of eIF2B GEF function through competitive displacement of p-eIF2 (8). To test the effects of AIVL on the formation of p-eIF2•eIF2B complexes, we transfected HeLa-eIF2Bβ-3Xflag cells with plasmids encoding AiVL or control proteins, and treated them with arsenite to induce eIF2 phosphorylation. We subsequently pulled down eIF2B from cell lysates and analyzed the amount of co-immunoprecipitated p-eIF2α by Western blotting. AcP10 expression interfered with p-eIF2•eIF2B complex formation, resulting in a significant reduction in the amount of p-eIF2α bound to eIF2B ((8), Fig 6A). AiVL expression has a similar effect, suggesting that AiVL –like AcP10– keeps eIF2B active despite eIF2 phosphorylation by counteracting p-eIF2•eIF2B complex formation. The remaining p-eIF2α signal (approximately 27% of the control sample) corresponds to the background level that is expected at the transfection efficiencies of ~70% obtained in this experiment (Fig 6B). Our data thus suggest that the AiVL•eIF2B interaction prevents p-eIF2 binding to eIF2B. This effect is p-eIF2-specific, since the total amount of eIF2 bound to eIF2B was unaffected by the presence of AiVL.

Next, we overexpressed TAP-tagged AiVL or control proteins in HEK293T cells, which were subsequently treated with several arsenite concentrations to induce increasing levels of p-eIF2. We then tandem affinity purified the overexpressed proteins and assessed co-purified eIF2B and (p-)eIF2, using antibodies directed against eIF2Bα, eIF2α and p-eIF2α (Fig 6C). In line with previously published data, the efficiency of eIF2B co-purification with AcP10 is lower when cells were treated with arsenite to induce eIF2 phosphorylation, indicative of a competition between AcP10 and p-eIF2 for eIF2B

binding. In contrast, AiVL•eIF2B complexes, while present in relatively low quantities, were not affected by p-eIF2 concentrations. Importantly, neither AcP10•eIF2B, nor AiVL•eIF2B complexes contained detectable amounts of p-eIF2, again indicating that AiVL counteracts the p-eIF2•eIF2B interaction. Collectively, our data indicate that AiVL has a similar effect as AcP10, rendering eIF2B

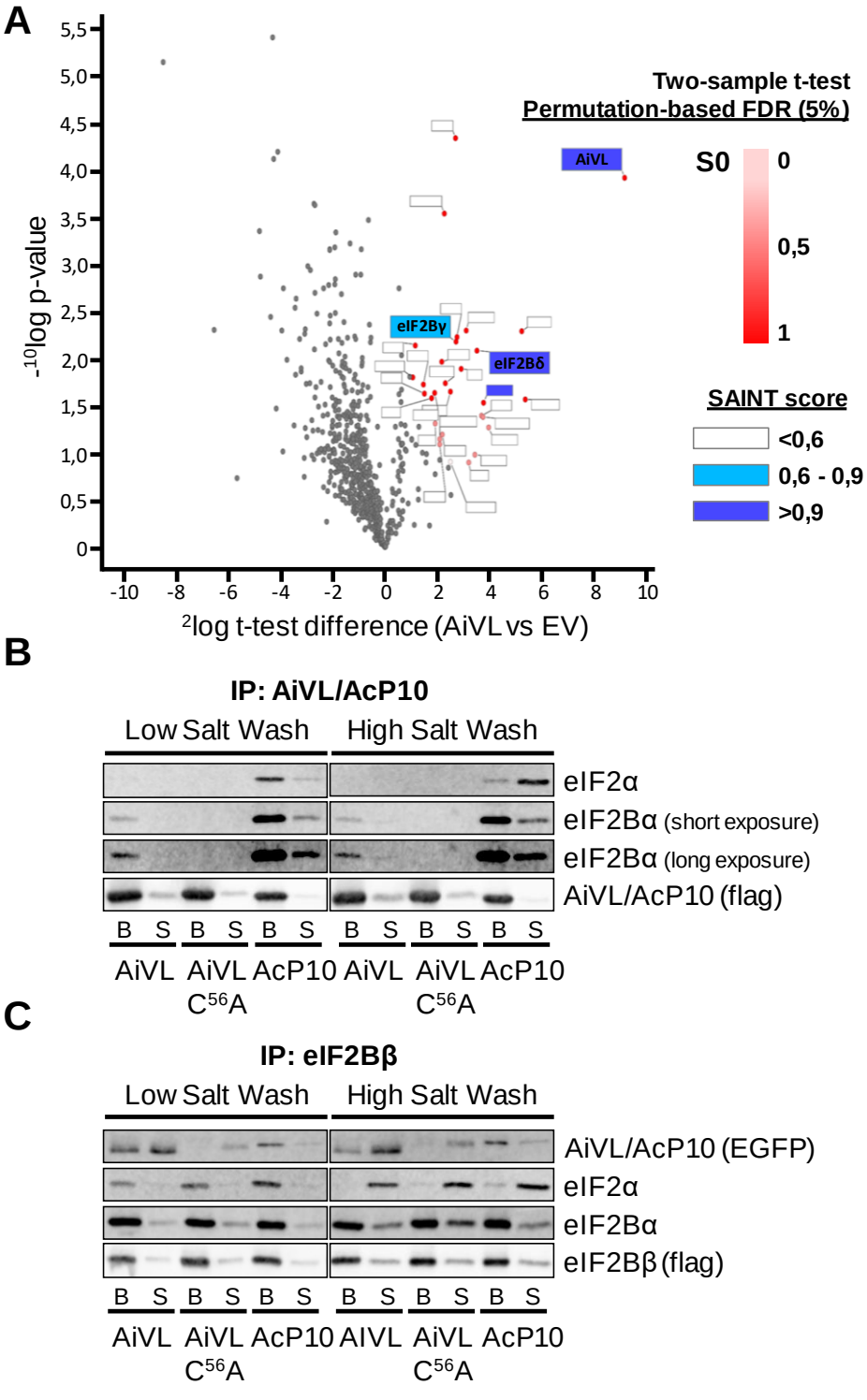

Fig 5. AiVL interacts with translation initiation factor eIF2B. *(A) Vulcano plot showing the proteins differentially co-immunoprecipitated with TAP-AiVL pulldown compared to empty vector control. Significantly enriched proteins as determined by a t-test (5% permutation-based FDR) are indicated in shades of red that indicate the values set for s0. SAINT scores for each of the enriched proteins are indicated by the blue colored labels. (B) The indicated TAP-tagged proteins were transiently overexpressed in HEK293T cells. These proteins were subsequently purified as described previously (8). The final wash step was performed either in low-salt buffer to keep the eIF2•eIF2B interaction intact (left panels), or in high salt buffer (500 mM KCl) to disrupt eIF2•eIF2B interactions (right panels). For each sample, the bead-associated protein fraction (indicated as "B"), and the supernatant fraction (indicated as "S") is shown. The presence of co-purified eIF2 and eIF2B was analyzed by Western blotting, using antibodies directed against their respective α-subunits. (C) The indicated EGFP-tagged proteins were transiently overexpressed in HeLa-R19-eIF2Bδ-3Xflag cells. Subsequently, eIF2B complexes were purified from cell lysates as described previously (8). The washes were performed the same way as in (B), and again the bead-associated protein fraction (indicated as "B"), and the supernatant fraction (indicated as "S") are shown for each sample. The presence of co-purified eIF2 (represented by its α-subunit) and AcP10/AiVL (assessed using an antibody directed against EGFP) was analyzed by Western blotting.*

GEF function insensitive to inhibition by p-eIF2, but some aspects of AiVL's interaction with eIF2B are remarkably different from those of AcP10. First, the amount of eIF2B co-purified with AiVL is consistently and significantly lower than with AcP10 (Fig 5B and 7). Second, AiVL's interaction with eIF2B seems relatively unstable (Fig 5C, lanes 1 and 2). Third, the AiVL•eIF2B interaction is insensitive to high levels of p-eIF2 (Fig 6). Fourth, AiVL is a highly soluble protein, in stark contrast to AcP10, which was shown to largely aggregate in insoluble perinuclear deposits upon overexpression (8).

Mouse KoVL, but not the KoVLs from more distantly related species, can also antagonize the ISR. Besides AiVL, the kobuvirus family consists of viruses that infect mammalian species such as mice (Mouse KoV), dogs (Canine KoV), pigs, (Porcine KoV), and cattle (Bovine KoV). Each of these viruses contains an L protein homologous to AiVL (Fig 7A), with amino acid identities ranging from ~55% to ~80%. To test whether the ISR inhibiting function of AiVL is conserved for KoVL proteins throughout the *kobuvirus* genus, we separately overexpressed the L proteins of AiV, Mouse KoV (M-KoVL), Canine KoV (C-KoVL), Roller KoV (R-KoVL), Bovine KoV (B-KoVL), Ferret KoV (F-KoVL), and Porcine KoV (P-KoVL) in HeLa cells and tested their ability to counteract arsenite-induced SG formation.

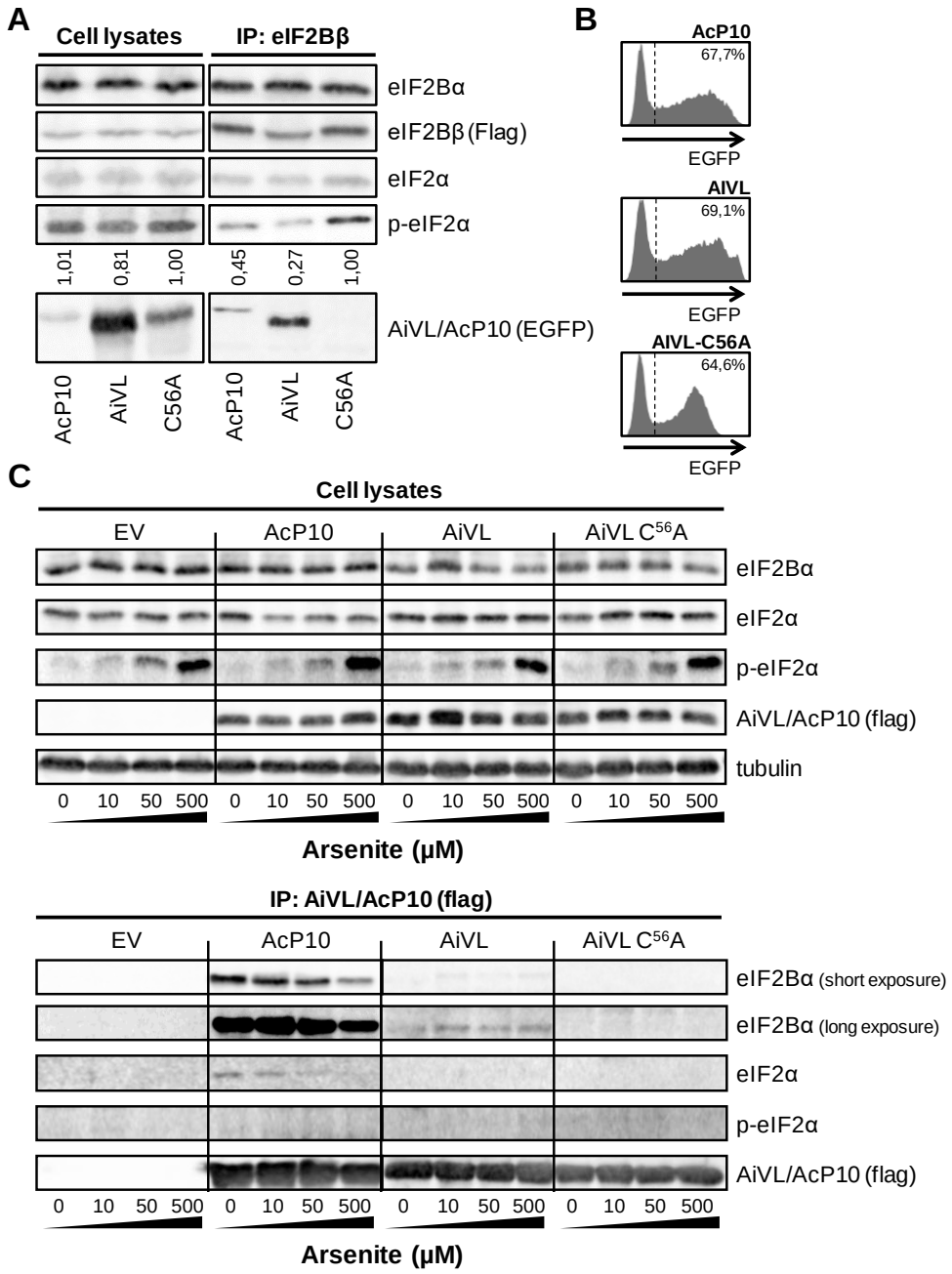

Fig 6. AiVL counteracts the association of p-eIF2 to eIF2B. *The indicated EGFP-tagged proteins were transiently overexpressed in HeLa-R19-eIF2Bδ-3Xflag cells. Cells were treated with 250 μM arsenite for 1 hr to induce phosphorylation of eIF2α. (A) eIF2B complexes were purified from cell lysates as described previously (8). The presence of co-purified eIF2, p-eIF2, and AcP10/AiVL was assessed by Western blotting using antibodies directed against eIF2α, p-eIF2α, and EGFP, respectively. (B) Flow cytometry analysis of the transfection efficiencies obtained in the experiment shown in (A). (C) HEK293T cells were transiently transfected with plasmids encoding the indicated TAP-tagged proteins. Cells were subsequently treated with the indicated arsenite concentrations for 1 hr, and the overexpressed proteins were purified from cell lysates. The presence of co-purified eIF2, p-eIF2, and eIF2B was assessed by Western blotting using antibodies directed against eIF2α, p-eIF2α, and eIF2Bα, respectively.*

Surprisingly, only Mouse KoV-L –which is phylogenetically most related to AiVL– was able to prevent SG formation (Fig 7B). These data were corroborated by FACS experiments showing that AiVL or M-KoVL expressing cells display unimpaired translation rates irrespective of the phosphorylation status of eIF2, either upon DNA transfection alone (Fig 7C), or after arsenite treatment (Fig 7D). Furthermore, in a KoVL co-IP experiment we show that only AiVL and M-KoVL detectably interact with eIF2B (Fig 7E). Consistently, the four residues that may form the Zn-finger structure (H20, H24, C53, and C56) and are essential for AiVL's ISR antagonist function (Figs 3 and S1), are strictly conserved in AiVL and M-KoVL, whereas the other KoVLs lack residues homologous to H20 and H24 in AiVL. Despite high conservation of the eIF2B subunits between mammalian species, we could not exclude the possibility that the KoVL proteins interact specifically with eIF2B from their respective host species. Therefore, we tested ISR antagonism by a selection of KoVL proteins (AiVL, M-KoVL, C-KoVL, and P-KoVL) in cell lines of mouse (LR7) and pig (PD-5) origin, using transient overexpression and subsequent analysis of arsenite-induced SG formation. In both LR7 cells (Fig 7F) and PD-5 cells (Fig 7G), only AiVL and M-KoVL are functional ISR antagonists, demonstrating that host species specificities do not underlie the differences in ISR antagonism between KoVL proteins. Rather, these data suggest that besides AiVL and M-KoVL none of the KoVLs function as ISR antagonist. Thus, the acquisition of AiVL's ISR antagonist function was likely a relatively recent evolutionary event that occurred within the Aichi A lineage.

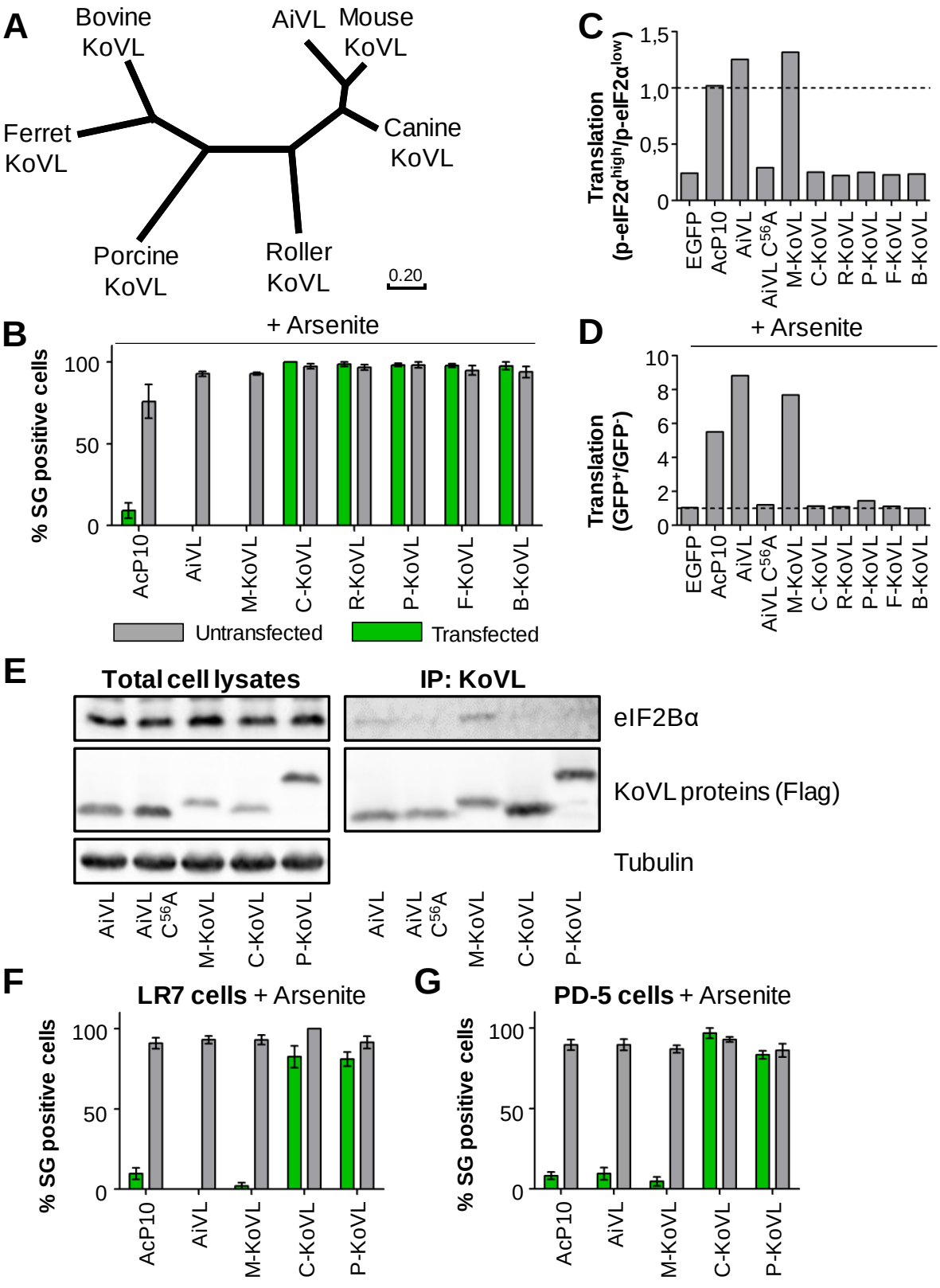
A
Bovine KoVL
AiVL
Mouse KoVL
Ferret KoVL
Canine KoVL
Porcine KoVL
Roller KoVL
0.20
C
Translation (p-eIF2α^high/p-eIF2α^low)
1,5
1,0
0,5
0
EGFP
AcP10
AiVL
AiVL C56A
M-KoVL
C-KoVL
R-KoVL
P-KoVL
F-KoVL
B-KoVL
B
+ Arsenite
% SG positive cells
100
50
0
AcP10
AiVL
M-KoVL
C-KoVL
R-KoVL
P-KoVL
F-KoVL
B-KoVL
Untransfected
Transfected
D
+ Arsenite
Translation (GFP+/GFP-)
10
8
6
4
2
0
EGFP
AcP10
AiVL
AiVL C56A
M-KoVL
C-KoVL
R-KoVL
P-KoVL
F-KoVL
B-KoVL
E
Total cell lysates
IP: KoVL
eIF2Bα
KoVL proteins (Flag)
Tubulin
AiVL
AiVL C56A
M-KoVL
C-KoVL
P-KoVL
AiVL
AiVL C56A
M-KoVL
C-KoVL
P-KoVL
F
LR7 cells + Arsenite
% SG positive cells
100
50
0
AcP10
AiVL
M-KoVL
C-KoVL
P-KoVL
G
PD-5 cells + Arsenite
% SG positive cells
100
50
0
AcP10
AiVL
M-KoVL
C-KoVL
P-KoVL

Fig 7. Mouse KoVL, but not the KoVLs from other species, also acts as ISR antagonist. *(A) phylogenetic tree of kobuvirus L proteins. The scale bar represents the number of substitutions per site. (B) Analysis of the ISR antagonist function of the indicated kobuvirus L proteins in HeLa cells by IFA. Shown is the percentage of cells that contain SGs after treatment with 250 µM arsenite for 1 hr, within the population of transfected cells (EGFP positive, shown in green), as well as untransfected cells from the same wells (EGFP negative, shown in grey). (C) HeLa cells were transiently transfected with plasmids encoding the indicated EGFP tagged proteins and subsequently analyzed by flow cytometry as in Fig 2D and 3C. Plotted is the ratio in mean fluorescence intensity (MFI) values of the puromycin staining, between the p-eIF2α^{high} (stressed) and p-eIF2α^{low} (unstressed) cell populations. A ratio of 1 (indicated by the dotted line) indicates that the presence of p-eIF2α has no impact on translation, and thus that the overexpressed protein renders translation insensitive to p-eIF2. (D) HeLa cells transiently overexpressing the indicated EGFP tagged proteins were treated with 250 µM arsenite for 1 hr, and translation was labeled using puromycin during the final 15 min of the experiment. Puromycin incorporation was analyzed by flow cytometry. Plotted is the ratio in mean fluorescence intensity (MFI) values between the EGFP^{high} (transfected) and EGFP^{low} (untransfected) cell populations. A ratio of 1 (indicated by the dotted line) indicates that the overexpressed protein has no impact on translation in stressed cells. Values higher than 1 indicate that the overexpressed protein rescues translation in arsenite-treated cells. (E) The indicated TAP-tagged proteins were overexpressed in HEK293T cells and purified as described above. The presence of co-purified eIF2B was analyzed by Western blotting using antibodies directed against eIF2Bα. (F) LR7 cells or (G) PD-5 cells were transfected with plasmids encoding the indicated EGFP-tagged proteins. SG formation in response to treatment with 500 µM arsenite for 1 hr was assessed by IFA and plotted as in (B).*

Discussion

We set out to investigate how kobuviruses, and AiV in particular, counteract antiviral ISR activity. We determine that AiV encodes a highly potent ISR antagonist (AiVL) that prevents cellular translational arrest in the presence of p-eIF2. AiVL binds translation initiation factor eIF2B, and thereby specifically prevents subsequent association of p-eIF2. Consequently, in the presence of AiVL, eIF2B preferentially binds its substrate (non-phosphorylated eIF2) over its inhibitor (phosphorylated eIF2), and thus remains active even under conditions of stress. This mode of action is similar to that of the recently described coronavirus protein AcP10, and differs from that of all other known ISR antagonists. AcP10 and AiVL are prototypes of a new Class of ISR antagonist, that targets the ISR downstream of eIF2 phosphorylation, at the level of eIF2B GEF function inhibition. ISR inhibition by precluding the p-eIF2•eIF2B interaction thus appeared at least twice, in phylogenetically distinct virus families, through convergent evolution.

AiVL and AcP10 both bind eIF2B, and correspondingly, they localize to the cytoplasm. However, AiVL has a diffuse localization, whereas AcP10 is largely aggregated in insoluble perinuclear deposits. Consequently, only low AcP10 concentrations remain soluble and can participate in competition with p-eIF2 for eIF2B binding (8), while soluble AiVL levels may vastly exceed those of p-eIF2 or eIF2B (Fig S2). Furthermore, in contrast to AcP10, AiVL has a low stability interaction with eIF2B, purification of AiVL yields little co-purified eIF2B, and AiVL was not detectably displaced from eIF2B by high p-eIF2 levels. These differences between AiVL and AcP10 may be related to their difference in solubility. First, since soluble AiVL is present in vast excess over eIF2B, most AiVL will not be bound to eIF2B and thus eIF2B co-IP should be inefficient when using AiVL as bait (Figs 5 and 6). AcP10 on the other hand is largely insoluble and thus the levels of soluble AcP10 available for eIF2B binding remain relatively low. Second, increasing p-eIF2 concentrations might be unable to outcompete AiVL due to a large excess of soluble AiVL over p-eIF2, even under severe stress conditions (Fig 6). Third, given such high levels of AiVL, a relatively low stability eIF2B interaction would suffice to prevent inhibition of eIF2B activity (Fig 5).

ISR antagonists can be classified in several categories based on which signal transduction event in the ISR pathway they counteract. Most ISR antagonists are specific to a particular eIF2α kinase, preventing either its activation (class 1 antagonist) or its kinase activity on eIF2α (class 2 antagonist). However, virus infection often causes extensive changes in the intracellular environment and may activate more than one eIF2 kinase. Thus, these antagonists may fail to prevent ISR activity entirely. Alternatively, an antagonist may induce dephosphorylation of p-eIF2 (class 3 antagonist), which counters the ISR irrespective of the kinase involved. However, this approach only mediates a reduction in p-eIF2 levels

to some extent based on the cell's capacity for eIF2 dephosphorylation, and thus the ISR may still signal under conditions of severe stress (20, 21). AiVL does not belong to any of these classes, and instead renders eIF2B immune to eIF2 phosphorylation. Thereby, it blocks the ISR regardless of the nature or severity of the stress trigger, or the eIF2 kinase(s) involved. Thus, AiVL's mode of action is arguably the most effective way to block the ISR described so far.

RNA viruses typically obtain their genes via recombination events, and thus the chance of acquiring antagonists with a certain mode-of action-depends on the availability of other (cellular) RNAs that encode proteins with such functions. For example, dsRNA binding domains are relatively common, so recombination events that lead to the acquisition of dsRNA binding proteins should occur often. In line with this, many viruses encode specific PKR inhibitors that act by sequestering dsRNA (17, 22–25). In contrast, no host cell proteins have been described that bind eIF2B and interfere with p-eIF2 binding, and thus a protein with this mode of action is unlikely to be obtained by viruses. In line with this notion, both proteins that prevent p-eIF2 from inhibiting eIF2B, AcP10 and AiVL, seem to have obtained their ISR antagonist function not via recombinations with RNAs encoding eIF2B-binding proteins, but via gain-of-function substitutions in pre-existing viral proteins. Our data indicate that most L proteins encoded by related viruses in the KoV family do not function as ISR antagonists. Thus, it is highly likely that the ancestral KoVL protein was not an ISR inhibitor, and that this function was obtained relatively recently within the AiV A lineage. Remarkably, since we also demonstrate that Aichivirus has no ISR antagonists besides AiVL, the other KoVs must either lack ISR antagonists altogether, or encode an antagonist(s) that is absent in AiV.

The ISR plays a role in a variety of different cell biological processes, both during normal cell function and under conditions of stress (26–29). Its activity is typically balanced and proportional to the situation at hand, and deviations from this balance, both towards a hypoactive or hyperactive ISR, may have pathological consequences (30–32). Most notoriously, a variety of neurodegenerative diseases have been linked to an overactive ISR, including but not limited to Parkinson's disease, Alzheimer's disease, Vanishing White Matter, and prion disease (33–37). A causal connection was even established between neuropathology and an overactive ISR by showing that ISR inhibitors may alleviate neurotoxicity (28, 33, 36, 38–40). Viruses, through their rapid rates of evolution over extensive periods of time, and under strong selective pressure to countermeasure the ISR, could teach us the most effective ways to interfere with ISR signaling. The identification of novel types of ISR antagonists like AiVL and AcP10 and elucidation of the details of their mode of action, may therefore provide the basis for novel strategies to modulate the ISR for therapeutic purposes.

Acknowledgments

The work was supported by the Netherlands Organization for Scientific Research through a Vici grant (NWO-918.12.628) to FJMvK and a Veni grant (NWO-863.13.008) to MAL. We thank Prof. David Ron for kindly providing HeLa cells stably expressing 3Xflag-tagged eIF2Bβ, dr. Alex Greninger for the pAV aichivirus cDNA clone, dr. George Belov for HeLa-R19 cells, and prof. Jerry Pelletier for translation inhibitor Pateamine A.

Materials & Methods

Chemical compounds. ISRIB (SML0843) and puromycin (P9620) were obtained from Sigma-Aldrich and used at a final concentration of 200 nM and 20 µg/mL, respectively. Sodium arsenite was purchased at Riedel-de-Haën (UN1686).

Cells and Viruses. HEK293T, HeLa-R19, and Vero cells were maintained in DMEM (Lonza) supplemented with 10% FCS and penicillin–streptomycin (100 units/mL and 100 µg/mL). To create recombinant AiV-$C^{53}A/C^{56}A$, the double mutation was introduced in the AiV infectious clone pAV (41) by site-directed mutagenesis. The infectious clones were linearized by HindIII digestion and infectious RNA was synthesized by a T7 *in vitro* transcription reaction (Promega). Infectious RNA was transfected in Vero cells using Lipofectamine 2000 reagents (Invitrogen), and AiV stocks (encoding either wt AiVL or AiVL $C^{53}A/C^{56}A$) were harvested three days post transfection. Integrity of the AiVL gene was confirmed by sanger sequencing, and virus titers were determined using end-point dilution assays on Vero cells.

Immunofluorescence Assay. Immunofluorescence assays were performed as described previously (17), using primary antibodies rabbit-α-G3BP2 (A302-040A, 1:200; Bethyl Laboratories) mouse-α-dsRNA J2 (1:1000; English Scientific & Consulting), rabbit-α-G3BP1 (ARP37713-T100, 1:200; Aviva), goat-α-eIF3η (sc-16377, 1:200; SantaCruz) and secondary antibodies donkey-α-mouse-Alexa488 (A-21202, 1:200; Thermo Fisher Scientific), donkey-α-goat-Alexa568 (A-11058, 1:200; Thermo Fisher Scientific), donkey-α-rabbit-Alexa647 (A-31573, 1:200; Thermo Fisher Scientific).

Western Blot Analysis. Western blot assays were performed as described previously (17), using primary antibodies rabbit-α-eIF2α (9722, 1:1000; Cell Signaling), rabbit-α-p-eIF2α (ab32157, 1:1000; Abcam), mouse-α-tubulin (T9026, 1:2000; Sigma-Aldrich), rabbit-α-eIF2Bα (18010-1-AP, 1:1000; Protein Tech), mouse-α-Flag (F3165, 1:1000; Sigma-Aldrich), or rabbit-α-EGFP (42), and secondary antibodies goat-α-mouse-IRDye680 (926-68070, 1:15,000; LI-COR) or goat-α-rabbit-IRDye800 (926-32211, 1:15,000; LI-COR).

Flow Cytometry Analysis of eIF2α Phosphorylation. Cells were released using trypsin and fixed with paraformaldehyde (4% in PBS) for 20 min. Cells were washed with FACS buffer (PBS + 1% BSA) and subsequently incubated for 10 min in ice-cold methanol. Cells were washed once with FACS buffer and incubated with primary antibodies rabbit-α-p-eIF2α (ab32157, 1:100; Abcam) and mouse-α-puromycin (MABE343, 1:100; Merck Millipore) for 45 min. After 3 wash steps in FACS buffer, cells were incubated in secondary antibodies donkey-α-mouse-cy5 (715-175-150, 1:200; Jackson ImmunoResearch) and goat-α-rabbit-Alexa594 (A-11012, 1:200; Invitrogen) for 45 min at room temperature in FACS buffer. Cells were washed twice, resuspended in PBS + 1% paraformaldehyde and analyzed on the FACSCanto II (BD Biosciences).

AP-MS. Protein samples were separated by SDS-PAGE, and stained with Coomassie colloidal blue (Bio-Rad). After a short run, the entire sample between running fronts was sliced out and reduced, alkylated, and digested as previously described (43). Digests were subjected to nLC–MS/MS analysis using an Agilent 1290 Infinity UHPLC system (Agilent) coupled to an Orbitrap Q Exactive Plus mass spectrometer (Thermo Scientific). Dried peptides were reconstituted in 10% formic acid (FA) and delivered to a trap column (Dr Maisch Reprosil C18, 3 µm, 2 cm × 100 µm) at 5 µl/min with solvent A (0.1% FA in water). Next, peptides were chromatographically separated onto an analytical column (Agilent Poroshell EC-C18, 2.7 µm, 50 cm × 75 µm) at 300 nL/min, as previously described (44). The gradient was as follows: 13-40% solvent B (0.1% FA in 80% Acetonitrile) in 65 min, to 100% solvent B in 3 min, 1 min of 100% solvent B, and finally equilibration of the chromatographic columns with 100% solvent A for the following 10 min before injection of the next sample. Total analysis time was 90 min. The eluent was sprayed via distal coated emitter tips butt-connected to the analytical column. The mass spectrometer was operated in data-dependent mode, automatically switching between MS and MS/MS. Full-scan MS spectra (from m/z 375 to 1600) were acquired in the Orbitrap with a resolution of 35,000 at m/z 400. The 10 most intense ions within the survey scan were selected for HCD fragmentation with normalized collision energy set to 25%. The MS/MS AGC target value was set to 5e4 with a maximum ion injection time of 120 ms. Dynamic exclusion was set to 12 s. Each raw data file recorded by the mass spectrometer was processed and quantified with Proteome Discoverer

(version 2.1, Thermo Scientific), and searched against a Swissprot human database (version 2016 03, 20,199 sequences) supplemented with the Aichivirus polyprotein sequence (Uniprot id A0A2S1JL36) using Mascot software (version 2.5.1, Matrix Science). Trypsin/P was chosen as the protease, cysteine carbamidomethylation was selected as fixed modification, and oxidation of methionine as variable modifications. Precursor and fragments mass tolerance were set to 20 ppm and 0.05 Da, respectively. Proteins were further filtered for contaminants and highly abundant proteins (such as keratins, tubulins, and ribosomal proteins), number of unique peptides (> 0), and number of peptides (> 1). All peptide-spectrum matches (PSM) were validated with 5% false discovery rate using Percolator (45). Only PSMs with a minimum length of 6 amino acids were kept. To discriminate bona fide protein interactors of AiVL from the background, we further analyzed the hits by SAINT scoring (46).

Immunoprecipitation of flag-tagged eIF2Bβ. HeLa-R19-eIF2Bβ-3Xflag were transfected with plasmids encoding the indicated EGFP-tagged proteins using Lipofectamine 2000 transfection reagent according to the manufacturer's protocol. Transfection medium was replaced by fresh medium 24 hrs post transfection, and cells were allowed to express the protein of interest for a total of 48 hours. For each sample, $3.0*10^7$ cells were lysed in 500 µl lysis buffer (50 mM Tris-HCl pH7.4, 150 mM NaCl, 1 mM EDTA, 1 mM DTT, 10% glycerol, 1% Triton X100, protease inhibitors [Roche], phosphatase inhibitors [Sigma-Aldrich]) for 15 min on ice. After spinning down to remove cell debris, 10 µl magnetic anti-Flag Beads (Sigma-Aldrich) was added to the supernatants and incubated rotating for 2 hours at 4˚C. Beads were then washed four times in wash buffer (50 mM Tris-HCl pH7.4, 150 mM NaCl, 1 mM EDTA, 1 mM DTT, 10% glycerol, 1% Triton X100), and resuspended in 1X LSB. If indicated (See Fig 5), the third wash step was done for 15 min in standard wash buffer, or high salt wash buffer (50 mM Tris-HCl pH7.4, 150 mM NaCl, 500 mM KCl, 1 mM EDTA, 1 mM DTT, 10% glycerol, 1% Triton X100) to dissociate eIF2 from eIF2B. Samples were then separated by SDS-PAGE and analyzed by Western blotting using the indicated antibodies.

Immunoprecipitation of TAP-tagged AiVL. $1.5*10^7$ HEK cells were transfected with plasmid encoding the indicated TAP-tagged protein using PEI transfection reagents as described previously (47). 24 hrs post transfection, cells were harvested and lysed in 500 µl lysis buffer (50 mM Tris-HCl pH7.4, 150 mM NaCl, 1 mM EDTA, 1 mM DTT, 10% glycerol, 1% Triton X100, protease inhibitors [Roche]). 20 µl S-beads was added to each sample, and incubated rotating for 2 hours at 4˚C. Beads were washed twice in wash buffer (50 mM Tris-HCl pH7.4, 150 mM NaCl, 1 mM EDTA, 1 mM DTT, 10% glycerol, 1% Triton X100), once in $3C^{pro}$ cleavage buffer (HRV 3C Protease Solution Kit; Thermo Scientific), and resuspended in 250 µl $3C^{pro}$ cleavage buffer. $3C^{pro}$ was then added to proteolytically release proteins from the S-beads rotating overnight at 4˚C. Supernatants were collected and transferred to new tubes. 10 µl Strep-Tactin beads (IBA) was added to each sample and incubated rotating for 1 hour at 4˚C. Beads

were washed three times in wash buffer and subsequently resuspended in 1X LSB. Samples were then separated by SDS-PAGE and analyzed by Western blotting using the indicated antibodies.

Single-step growth curve. Vero cells were infected with AiV at an MOI of 10. After 1 hr, the cells were washed three times in PBS to remove excess virus. At 0, 2, 4, 6, 8, 10, or 16 hrs pi., samples were freeze-thawed three times to release intracellular virus. The total amount of infectious virus in each sample was quantified by end-point dilution assays.

Phylogenetic analysis of KoVL proteins. KoVL protein sequences (AiVL, NP_047200.1; M-KoVL, YP_004782207.1; C-KoVL, AHK60486.1; R-KoVL, AIK67137.1; P-KoVL, YP_002473934.1; F-KoVL, AGU62946.1; B-KoVL, NP_859018.1) were aligned in MEGAX software (48) using the MUltiple Sequence Comparison by Log-Expectation (MUSCLE) method. A phylogenetic tree was created by the Maximum Likelyhood Method, using a JTT model (49), and a site coverage cut-off of 99%. The final dataset included 155 positions.

References

1. K. Pakos-Zebrucka, *et al.*, The integrated stress response. *EMBO Rep.* **17**, 1374–1395 (2016)

2. D. Levin, I. M. London, Regulation of protein synthesis: activation by double-stranded RNA of a protein kinase that phosphorylates eukaryotic initiation factor 2. *PNAS.* **75**, 1121–5 (1978)

3. H. P. Harding, Y. Zhang, D. Ron, Protein translation and folding are coupled by an endoplasmic- reticulum-resident kinase. *Nature* **397**, 271-4 (1999)

4. H. P. Harding, Y. Zhang, A. Bertolotti, H. Zeng, D. Ron, Perk is essential for translational regulation and cell survival during the unfolded protein response. *Mol. Cell* **5**, 897-904 (2000)

5. J. Dong, H. Qiu, M. Garcia-Barrio, J. Anderson, A. G. Hinnebusch, Uncharged tRNA activates GCN2 by displacing the protein kinase moiety from a bipartite tRNA-binding domain. *Mol. Cell* **6**, 269-79 (2000)

6. J. J. Chen, I. M. London, Regulation of protein synthesis by heme-regulated eIF-2α kinase. *Trends Biochem. Sci.* **20**, 105-8 (1995)

7. R. L. Matts, J. R. Schatz, R. Hurst, R. Kagen, Toxic heavy metal ions activate the heme-regulated eukaryotic initiation factor-2α kinase by inhibiting the capacity of hemin-supplemented reticulocyte lysates to reduce disulfide bonds. *J. Biol. Chem.* **266**, 12695-702 (1991)

8. H. H. Rabouw, *et al.*, Inhibition of the integrated-stress-response by viral proteins that block p-eIF2•eIF2B association. *This Thesis*, Chapter 3 (2019)

9. V. I. Agol, A. P. Gmyl, Viral security proteins: Counteracting host defences. *Nat. Rev. Microbiol.* **8**, 867-78 (2010)

10. M. a Devaney, V. N. Vakharia, R. E. Lloyd, E. Ehrenfeld, M. J. Grubman, Leader protein of Foot-and-mouth disease virus is required for cleavage of the p220 component of the cap-binding protein complex. *J. Virol.* **62**, 4407-9 (1988)

11. J. Zoll, W. J. G. Melchers, J. M. D. Galama, F. J. M. van Kuppeveld, The Mengovirus Leader Protein Suppresses Alpha/Beta Interferon Production by Inhibition of the Iron/Ferritin-Mediated Activation of NF- B. *J. Virol.* **76**, 9664-72 (2002)

12. F. Borghese, T. Michiels, The Leader Protein of Cardioviruses Inhibits Stress Granule Assembly. *J. Virol.* **85**, 9614–9622 (2011)

13. T. Yamashita, *et al.*, Isolation of cytopathic small round viruses with BS-C-1 cells from patients with gastroenteritis. *J. Infect. Dis.* **164**, 954-7 (1991)

14. L. J. Visser, *et al.*, FMDV leader protease cleaves G3BP1 and G3BP2 and inhibits stress granule formation. *J. Virol.* **93** pii: e00922-18 (2018)

15. V. van Pesch, O. van Eyll, T. Michiels, The Leader Protein of Theiler's Virus Inhibits Immediate-Early Alpha/Beta Interferon Production. *J. Virol.* **75**, 7811-7 (2002)

16. J. Nejepinska, R. Malik, M. Moravec, P. Svoboda, Deep sequencing reveals complex spurious transcription from

transiently transfected plasmids. *PLoS One* **7**, e43283 (2012)

17. H. H. Rabouw, *et al.*, Middle East Respiratory Coronavirus Accessory Protein 4a Inhibits PKR-Mediated Antiviral Stress Responses. *PLoS Pathog.* **12**, e1005982 (2016)

18. S. S. Mohammad-Qureshi, *et al.*, Purification of FLAG-Tagged Eukaryotic Initiation Factor 2B Complexes, Subcomplexes, and Fragments from Saccharomyces cerevisiae. *Methods Enzymol.* **431**, 1-13 (2007)

19. Y. Sekine, *et al.*, Mutations in a translation initiation factor identify the target of a memory-enhancing compound. *Science.* **348**, 1027-30 (2015)

20. J. L. G. Cruz, *et al.*, Coronavirus gene 7 counteracts host defenses and modulates virus virulence. *PLoS Pathog.* **7** e1002090 (2011).

21. S. Kazemi, *et al.*, Control of Subunit of Eukaryotic Translation Initiation Factor 2 (eIF2) Phosphorylation by the Human Papillomavirus Type 18 E6 Oncoprotein: Implications for eIF2 -Dependent Gene Expression and Cell Death. *Mol. Cell. Biol.* **24**, 3415-29 (2004)

22. M. Bergmann, *et al.*, Influenza virus NS1 protein counteracts PKR-mediated inhibition of replication. *J. Virol.* **74**, 6203–6206 (2000)

23. Z. Feng, M. Cerveny, Z. Yan, B. He, The VP35 protein of Ebola virus inhibits the antiviral effect mediated by double-stranded RNA-dependent protein kinase PKR. *J. Virol.* **81**, 182–192 (2007)

24. H. W. Chang, J. C. Watson, B. L. Jacobs, The E3L gene of vaccinia virus encodes an inhibitor of the interferon-induced, double-stranded RNA-dependent protein kinase. *PNAS.* **89**, 4825–4829 (1992)

25. Y. Lu, M. Wambach, M. G. Katze, R. M. Krug, Binding of the Influenza Virus NS1 Protein to Double-Stranded RNA Inhibits the Activation of the Protein Kinase That Phosphorylates the eIF-2 Translation Initiation Factor. *Virology* **214**, 222–228 (1995)

26. Y. Kim, *et al.*, PKR is activated by cellular dsRNAs during mitosis and acts as a mitotic regulator. *Genes Dev.* **28**, 1310–1322 (2014)

27. V. Zismanov, *et al.*, Phosphorylation of eIF2α is a Translational Control Mechanism Regulating Muscle Stem Cell Quiescence and Self-Renewal. *Cell Stem Cell* **18**, 79-90 (2016)

28. C. Wang, *et al.*, Inhibiting the integrated stress response pathway prevents aberrant chondrocyte differentiation thereby alleviating chondrodysplasia. *Elife* **7**, pii: e37673 (2018)

29. S. S. Cao, *et al.*, Phosphorylation of eif2α is dispensable for differentiation but required at a posttranscriptional level for paneth cell function and intestinal homeostasis in mice. *Inflamm. Bowel Dis.* **20**, 712–722 (2014)

30. H. Chen, *et al.*, OLA1 regulates protein synthesis and integrated stress response by inhibiting eIF2 ternary complex formation. *Sci. Rep.* **5**, 13241 (2015)

31. W. Lin, *et al.*, The integrated stress response prevents demyelination by protecting oligodendrocytes against immune-mediated damage. *J. Clin. Invest.* **117**, 448-56 (2007)

32. L. Wang, B. Popko, R. P. Roos, An enhanced integrated stress response ameliorates mutant SOD1-induced ALS. *Hum. Mol. Genet.* **23**, 2629-38 (2014)

33. M. Halliday, *et al.*, Partial restoration of protein synthesis rates by the small molecule ISRIB prevents neurodegeneration without pancreatic toxicity. *Cell Death Dis.* **6**, e1672 (2015)

34. J. A. Moreno, *et al.*, Sustained translational repression by eIF2α-P mediates prion neurodegeneration. *Nature* **485**, 507–511 (2012)

35. M. V. Lourenco, S. T. Ferreira, F. G. De Felice, Neuronal stress signaling and eIF2α phosphorylation as molecular links between Alzheimer's disease and diabetes. *Prog. Neurobiol.* **129**, 37–57 (2015)

36. Y. L. Wong, *et al.*, The small molecule ISRIB rescues the stability and activity of vanishing white matter disease eIF2B mutant complexes. *Elife* **7**, pii: e32733 (2018)

37. J. J. M. Hoozemans, *et al.*, Activation of the unfolded protein response in Parkinson's disease. *Biochem. Biophys. Res. Commun.* **354**, 707–711 (2007)

38. A. Chou, *et al.*, Inhibition of the integrated stress response reverses cognitive deficits after traumatic brain injury. *PNAS.* **114**, E6420-E6426 (2017)

39. H. G. Nguyen, *et al.*, Development of a stress response therapy targeting aggressive prostate cancer. *Sci. Transl. Med.* **10**, pii: eaar2036 (2018)

40. C. Sidrauski, *et al.*, Pharmacological brake-release of mRNA translation enhances cognitive memory. *Elife* **2**, e00498 (2013).

41. N. Takeda, *et al.*, Construction of an Infectious cDNA Clone of Aichi Virus (a New Member of the Family Picornaviridae) and Mutational Analysis of a Stem-Loop Structure at the 5' End of the Genome. *J. Virol.* **75**, 8021-30 (2002)

42. A. S. De Jong, *et al.*, Determinants for membrane association and permeabilization of the coxsackievirus 2B protein and the identification of the Golgi complex as the target organelle. *J. Biol. Chem.* **278**, 1012-21 (2003)

43. A. Shevchenko, M. Wilm, O. Vorm, M. Mann, Mass spectrometric sequencing of proteins from silver-stained polyacrylamide gels. *Anal. Chem.* **68**, 850-8 (1996)

44. A. Cristobal, *et al.*, In-house construction of a UHPLC system enabling the identification of over 4000 protein groups in a single analysis. *Analyst* **137**, 3541-8 (2012)

45. L. Käll, J. D. Canterbury, J. Weston, W. S. Noble, M. J. MacCoss, Semi-supervised learning for peptide identification from shotgun proteomics datasets. *Nat. Methods* **4**, 923-5 (2007)

46. H. Choi, *et al.*, Analyzing protein-protein interactions from affinity purification-mass spectrometry data with SAINT. *Curr. Protoc. Bioinforma.* Chapter 8: Unit 8.15 (2012)

47. R. P. de Vries, *et al.*, The influenza A virus hemagglutinin glycosylation state affects receptor-binding specificity. *Virology* **403**, 17-25 (2010)

48. S. Kumar, G. Stecher, M. Li, C. Knyaz, K. Tamura, MEGA X: Molecular evolutionary genetics analysis across computing platforms. *Mol. Biol. Evol.* **35**, 1547-1549 (2018)

49. D. T. Jones, W. R. Taylor, J. M. Thornton, The rapid generation of mutation data matrices from protein sequences. *Bioinformatics* **8**, 275-82 (1992)

Supplementary Figures

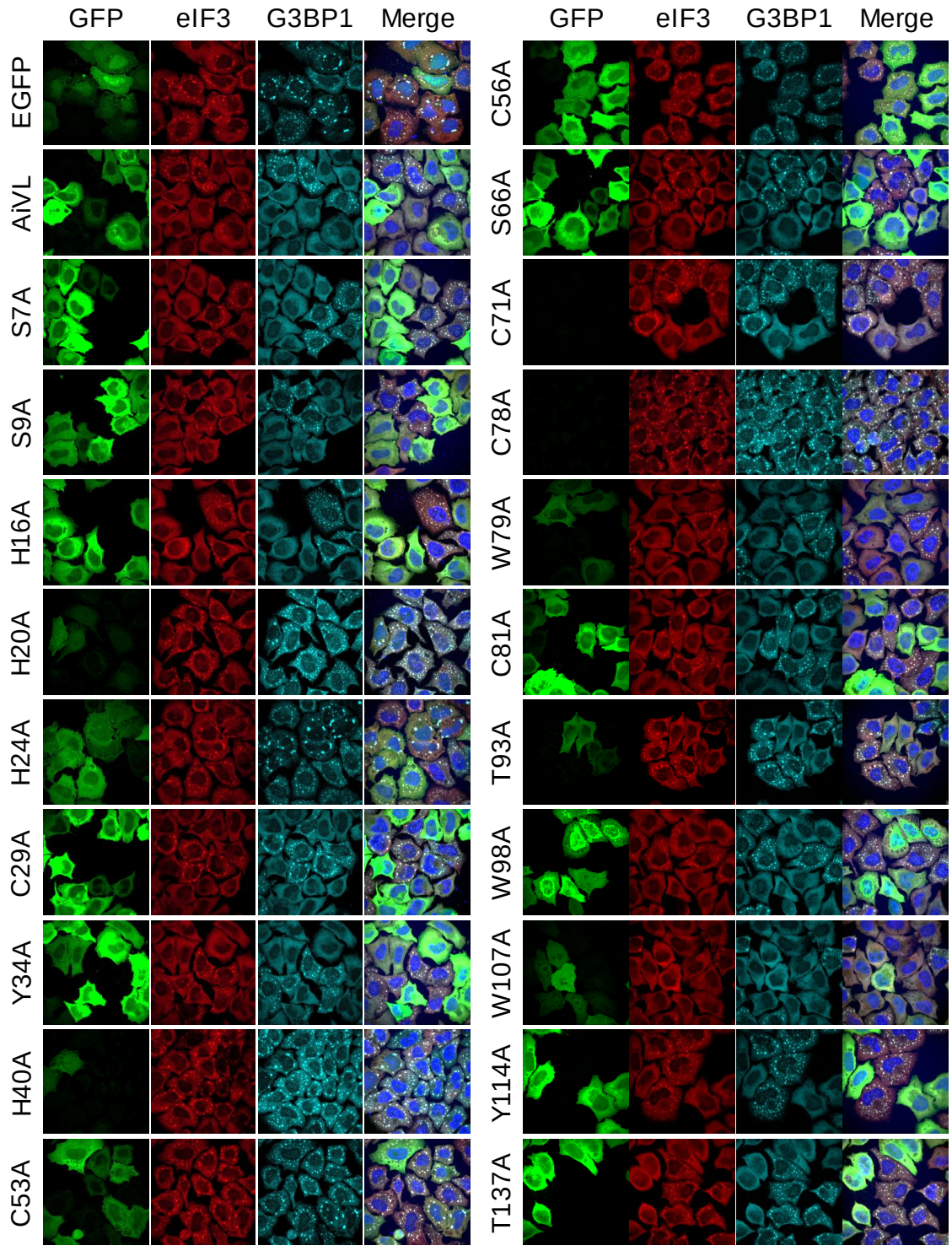

Fig *S1. IFA analysis of SG inhibition by the full panel of AiVL point mutants.* *The indicated EGFP-tagged AiVL mutant proteins were transiently overexpressed in HeLa cells. Next day, cells were treated with 250 µM arsenite for 1 hr, and SG formation was analyzed by IFA using antibodies directed against SG markers G3BP1 and eIF3.*

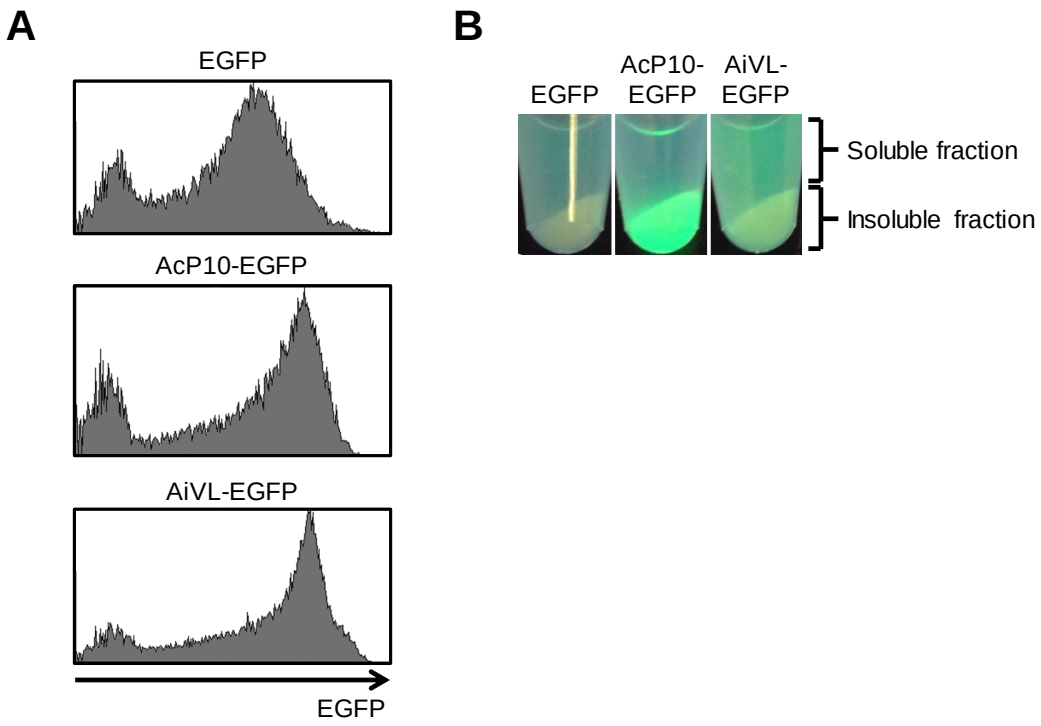

Fig S2. Transient AiVL overexpression yields high concentrations of soluble protein. *(A) Flow cytometry analysis of HeLa cells transiently overexpressing the indicated proteins. (B) In parallel, cells were lyzed In lysis buffer, and cell debris was spun down. In the resulting samples, containing an insoluble pellet and a soluble supernatant fraction, EGFP content was visualized under UV-light.*

Chapter 6

Summary and General Discussion

Summary and General Discussion

Proteins are the molecular machines that are essential for virtually every biological process. The production of proteins is therefore one of the most fundamental processes in life. A cell's genetic material, DNA, contains the blueprints required for the synthesis of proteins. First, DNA is used to create messenger RNA (mRNA) molecules in a process called transcription. The information stored on mRNAs is subsequently used to create proteins in a process called translation. To respond to changes in the environment, cells often alter the numbers or types of proteins that are being synthesized. This regulation includes changes in transcription to affect how many mRNA molecules are made as well as translation to determine how efficiently mRNAs are translated into proteins. In this thesis, we studied one particular regulatory pathway, the integrated stress response (ISR), which regulates translation under conditions of stress such as a virus infection. When activated, the ISR halts almost all translation, with the aim of conserving a cell's energy and allowing it time to resolve the stress situation.

The ISR pathway comprises four different sensor proteins, PKR, PERK, HRI, and GCN2, each of which detects specific disruptions from normal cellular homeostasis (collectively referred to as cellular "stress"). In response to their respective stressors, these proteins signal by phosphorylating a conserved serine 51 residue in the α-subunit of translation initiation factor eIF2. In non-stressed cells, eIF2 in complex with a GTP molecule and an initiator $tRNA^{Met}$ forms the Ternary Complex (TC). The TC mediates start codon recognition during mRNA scanning by ribosomes. Upon start codon recognition, the eIF2-bound GTP is hydrolyzed, which lowers eIF2's affinity for the initiator $tRNA^{Met}$ by several orders of magnitude. Consequently, eIF2•GDP is released from the ribosome while the tRNA remains, and translation elongation starts. New rounds of translation initiation require reloading of eIF2 with a new initiator $tRNA^{Met}$ and thus recycling of eIF2•GDP to eIF2•GTP, which is mediated by the eIF2-specific guanine exchange factor (GEF) eIF2B. In times of stress, when the ISR is active and the eIF2 α-subunit is being phosphorylated, eIF2B GEF function is inhibited by a stable and non-productive interaction with phospho-eIF2 (p-eIF2). As a consequence, translation is blocked at its initiation step.

One of the conditions that may activate the ISR is an infection with a virus. Since viruses depend on cellular translation machinery to synthesize viral protein, ISR-mediated inhibition of translation may prevent the generation of new infectious virus particles. Consequently, evolutionary pressure has caused many different viruses to develop means to counteract the ISR. Elucidation of the mechanisms by which viruses achieve ISR inhibition will not only further our understanding of the ongoing battle between viruses and antiviral responses, but may also teach us the most effective ways to prevent (hyperactive) ISR signaling. Ultimately, this may help in the development of new therapeutic strategies that target the ISR.

In this thesis, we focused on the identification of viral ISR antagonists and determination of their modes of action. In this discussion chapter we will briefly summarize the findings of each chapter and place them in the broader context of existing literature.

Summary of main findings

In **chapter 2**, we described the function of an accessory protein (p4a) encoded by Middle-East Respiratory Syndrome coronavirus (MERS-CoV) as inhibitor of PKR-mediated ISR activation (1). MERS-CoV was first identified in 2012 and is highly pathogenic to humans (2). This virus occasionally jumps from dromedary camels to humans, but thus far has not established itself as an endemic human virus. One of the barriers a virus needs to overcome to establish itself in a new host species, is the host cell's antiviral response, including the ISR. PKR is the most important ISR-sensor during most virus infections. It detects cytoplasmic dsRNAs that are formed during replication of both RNA and DNA viruses (3). PKR-mediated ISR activation occurs only when dsRNA is sufficiently accessible for PKR molecules to bind and to subsequently homodimerize. One of the ISR inhibition strategies employed by viruses is to express dsRNA-binding proteins that cover dsRNA molecules to make them less accessible to PKR (4–6). We identified MERS-CoV p4a as such dsRNA binding PKR-specific ISR antagonist. p4a also prevents the activation of another antiviral pathway, the type I IFN induction pathway, that is activated by cytoplasmic dsRNA. p4a is the first coronavirus protein identified as a PKR-specific ISR antagonist.

In **chapter 3**, we assessed the function of a small-molecule inhibitor of the ISR (ISRIB). ISRIB suppresses the ISR downstream of p-eIF2 via a physical interaction with eIF2B. ISRIB acts by promoting the assembly of full (decameric) eIF2B complexes from pre-existing eIF2B building blocks (8–12). eIF2B assembly is a step-wise process, in which first four eIF2B subunits (β,γ,δ,ε) assemble into eIF2B tetramers. These tetramers subsequently form eIF2B octamers (2β,2γ,2δ,2ε), thereby forming a binding pocket that facilitates association of an eIF2Bα homodimer, yielding the full eIF2B complex (2α,2β,2γ,2δ,2ε). ISRIB associates with eIF2B at the interface of two eIF2Bδ and two eIF2Bβ molecules, thus interacting with two eIF2B tetramers and stabilizing them into octamers. Since eIF2B has higher GEF activity when fully assembled, ISRIB-mediated eIF2B assembly boosts the total basal eIF2B GEF activity within a cell and thereby counters the inhibitory effect of the ISR. ISRIB's ability to enhance eIF2B assembly does not interfere with the p-eIF2•eIF2B interaction and therefore does not prevent ISR-mediated inhibition of eIF2B GEF activity. We showed that ISRIB, while functional under conditions of mild stress, fails to antagonize the ISR when high levels of p-eIF2 are present. Importantly, ISRIB has yielded highly promising effects in animal model systems for prion disease (13), vanishing white matter

disease (14, 15), and traumatic brain injury (16), providing proof-of-principle that ISR-targeting therapies can be used to treat disorders related to a hyperactive ISR. Our findings are important to predict and/or evaluate the result of experiments with ISRIB, both in vitro and in vivo. The fact that ISRIB selectively prevents mild ISR activation without affecting the function of the ISR under severe stress conditions may be the basis for the apparent lack of side-effects of ISRIB treatments in vivo.

In **chapter 4**, we described an accessory protein encoded by Beluga whale coronavirus (AcP10). AcP10 does not affect activation of PKR or any of the other eIF2 kinases nor their ability to phosphorylate eIF2. Instead, AcP10 interacts directly with eIF2B, likely at a position that overlaps the interaction site for p-eIF2, but not for native eIF2. As a result, AcP10 competes with p-eIF2 for eIF2B binding, thus preventing a stable and inhibitory p-eIF2•eIF2B interaction to favor binding of non-phosphorylated eIF2 to eIF2B. This mode of action is fundamentally different from that of ISRIB, and allows AcP10 to rescue eIF2B GEF activity in the presence of high levels of p-eIF2. With its unprecedented mode of action, AcP10 is a prototype of a novel class of ISR antagonists.

In **chapter 5**, we described the ISR inhibiting function of the Leader protein encoded by the picornavirus Aichivirus (AiVL). Aichivirus was first described in 1991 as the causative agent of a gastroenteritis outbreak in the Japanese village Aichi (7), and is classified in the kobuvirus genus together with several related viruses in animals. We show that AiV infection induces efficient eIF2 phosphorylation, without impacting cellular translation or causing stress granule formation. This effect depends on the expression of AiVL. We determined that AiVL, like AcP10, binds eIF2B to prevent subsequent association of p-eIF2. Thereby, AiVL rescues translation in the presence of p-eIF2 by favoring the eIF2•eIF2B over p-eIF2•eIF2B. Despite the similarities with AcP10, AiVL has no homology to AcP10 and seemingly evolved independently. AcP10 evolved from an ancestral cellular protein with uridine kinase activity, while AiVL likely originates from a pre-existing kobuvirus leader protein that lacked the ability to counteract the ISR. Thus, we identify two ISR antagonists with a novel mode of action, which arose through convergent evolution of two phylogenetically distinct viruses.

Viruses and antiviral responses

Eukaryotic cells are equipped with several antiviral pathways which are activated in response to virus-induced changes. These include for example the type I IFN system, the RNase L response, and the ISR. Type I IFN (IFN-α and IFN-β) expression leads to the expression of several hundred proteins collectively termed interferon stimulated genes (ISGs). These proteins have a broad range of functions which are often unknown but are together involved in combating infections. RNase L and the ISR induce the degradation of viral RNAs and prevent the synthesis of viral proteins, respectively. To efficiently replicate, viruses are required to evade or inhibit antiviral pathways within the infected host cell. In many cases, this is achieved by viral proteins that interfere at some point in these pathways. These so-called antagonists are not essential to virus replication *per sé* but assist in creating optimal circumstances for virus replication. Recombinant viruses lacking their respective antagonists often replicate less efficiently, especially *in vivo*. Such weakened viruses could be used as live attenuated vaccine strains.

The classification of ISR antagonists

In the preceding chapters, we proposed a classification of the ISR antagonists based on what signal transduction event in the ISR they counter. Class 1 antagonists prevent ISR sensor activation, Class 2 antagonists prevent eIF2α phosphorylation, and Class 3 antagonists induce dephosphorylation of p-eIF2. In chapters 3 and 4, we extend these three existing categories with Class 4 antagonists. These are not aimed at limiting p-eIF2 levels, but instead they interfere with p-eIF2's ability to inhibit eIF2B GEF function (Fig 1). The two Class 4 antagonists described so far both act by binding eIF2B in such a way that subsequent association of p-eIF2 is prevented, likely by steric hindrance (17, 18). Possibly, as more class 4 antagonists are discovered, other modes of action will be described that prevent p-eIF2 from affecting eIF2B. Theoretically, the list of ISR antagonist classes might be extended in the future by one other class of antagonists. As a logical extension to the abovementioned Classes 1 to 4, a Class 5 antagonist should act in the ISR pathway one step further downstream than Class 4 antagonists do. That is, they should allow an ISR-mediated decline in TC availability but change the translation initiation process in such a way that TCs are no longer required. Such a hypothetical ISR antagonist could for example bind Met-tRNAi and conduct a function in translation initiation similar to that of eIF2•GTP, with the exception that it should not depend on eIF2B GEF activity for its recycling. Thus far, such a mode of action is only a theoretical possibility, since nothing resembling a Class 5 antagonist has ever been discovered.

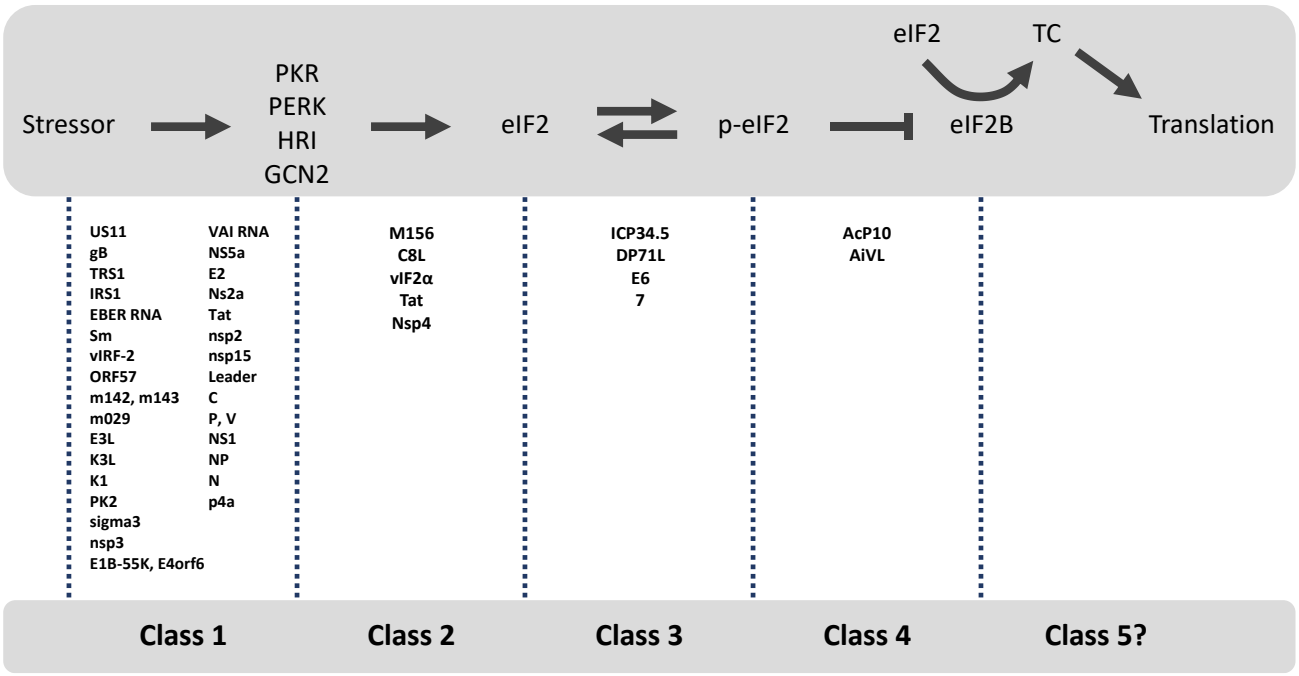

Figure 1. Schematic overview of the ISR, viral ISR antagonists, and their classification. *ISR antagonists can be classified based on which step of the ISR pathway they interfere with. Most viral ISR antagonists belong to Class 1 and affect the activation of the ISR-sensor. A small number of viral ISR antagonists have been described that prevent eIF2 phosphorylation (Class 2), that reverse eIF2 phosphorylation (Class 3), or that rescue eIF2B GEF activity in the presence of p-eIF2 (Class 4). Possibly, one final additional Class of ISR antagonist may exist, that renders translation insensitive to depletion of TCs. However, since no Class 5 ISR antagonist has thus far been identified, such antagonists are hypothetical.*

ISR antagonists differ not only in their mode of action, but also in their specificity, i.e. the ISR sensors they counteract. Class 1 antagonists are often specific for a single ISR sensor or stressor. For example, the best studied Class 1 antagonist, the dsRNA binding protein Influenza A virus NS1, efficiently prevents PKR activation but entirely fails to counteract the ISR when activated in a PKR-independent manner (1, 19). Exceptions are the Class 1 antagonists that target PKR's kinase domain, since the kinase domains are conserved between the ISR sensor proteins (20, 21). For example, the cytomegalovirus TRS1 protein was shown to inhibit activation of PKR as well as HRI (22–24). Since no evidence has thus far been found that HRI is activated in virus-infected cells, it is likely that TRS1-mediated inhibition of HRI is a side-effect of its PKR inhibition. Still, a broadly active Class 1 ISR antagonist may have its advantages over PKR-specific ones, particularly for viruses that activate more than one ISR sensor protein. Unfortunately, in many cases antagonists are only tested for their ability to counteract a single ISR sensor, so their effects on other ISR sensors are unknown. To the best of my knowledge, all Class 2 antagonists identified so far have only been tested against a single ISR sensor. However, it is plausible that some Class 2 antagonists, particularly those that are structural mimics of eIF2α, have a broader

activity. Class 3 and 4 antagonists target the ISR at a step downstream of eIF2α phosphorylation, and thus the function of these antagonists is not limited to a specific ISR sensor(s). This implies that Class 3 and 4 antagonists would be particularly useful to viruses that activate the ISR via more than one route.

Several virus genomes contain internal ribosomal entry sites (IRES) that regulates ribosome recruitment and thus viral translation. These viruses include members of the picornaviridea, dicystroviridae, flaviviridae, and retroviridae. IRESes have been classified into four types based on their function and structural characteristics. A selection of these IRESes provide the virus with natural resistance against the effects of ISR activity, since they function in the absence of ternary complexes. In those cases, even when the ISR prevents host cell translation, IRES-driven viral translation remains intact. The most well-known example of such IRES is the IRES in the cricket paralysis virus (CrPV) genome. This IRES resembles a tRNA/mRNA structure in its pre-translocation state and may drive translation elongation directly in the absence of initiation factors such as eIF2 (25). The third type of IRESes, also referred to as HCV-like IRESes, are found in flaviviridae and some picornaviridae and require fewer translation initiation factors but still depend on some (26, 27). Type I and type II IRESes are found primarily in picornaviridae (e.g. poliovirus and human rhinovirus contain type I IRESes, encephalomyocarditis virus and foot-and-mouth-disease virus contain type II IRESes). These IRESes require all translation initiation factors, with the exception of some cap binding factors (28, 29). The only IRESes that provide full protection from the ISR are the type IV IRESes in dicystroviridae. Still, even IRESes that require TCs for translation may give partial resistance against the ISR, such as the poliovirus IRES which sustains translation under stress conditions in the presence of the viral protein 2A (30, 31). While IRESes are not ISR antagonists, since they do not interfere in ISR signalling in any way, they may (partially) prevent the ISR from affecting viral translation specifically.

ISR antagonism by MERS coronavirus

MERS-CoV is one of the most studied coronaviruses. Its pathogenicity to humans is thus far unequalled by other coronaviruses, with a mortality rate of approximately 35% (2). However, MERS-CoV transmission to humans is inefficient. Most human MERS-CoV cases are associated with direct contact with dromedary camels, which are an animal reservoir for MERS-CoV. The determinants for MERS-CoV's transmissibility or pathogenesis remain poorly understood. Antiviral responses such as the ISR are a hurdle that needs to be overcome by the virus in order to efficiently replicate in a new host. Coronaviruses, like many other viruses, encode proteins that prevent antiviral responses from

inhibiting virus replication (32–35). We identified the MERS-CoV-encoded accessory protein p4a as a PKR-specific Class 1 ISR antagonist. Its ability to prevent PKR activation and thus ISR signaling depends entirely on its dsRNA-binding domain, which suggests that it functions via sequestration of dsRNA. While such mode of action was described before for other viruses (4), p4a is the first coronaviral protein with this function. All lineage C β-coronaviruses identified so far encode a p4a-like protein with a dsRNA binding motif. A phylogenetic analysis of the ORF4a gene shows that human and dromedary camel ORF4a sequences cluster together, suggesting the absence of a species-specific function (36). While dsRNA sequestration by p4a should prevent PKR activation in any cell type or host species, its impact on MERS-CoV replication may widely vary. In chapter 2, we describe that deletion of p4a does not lead to SG formation in MERS-CoV infected cells. Consistently, a later publication reported that MERS-CoV-Δp4a replicated to similar titers in Vero cells as wt MERS-CoV and did not cause ISR-mediated translational arrest or SG formation (34). However, MERS-CoV-Δp4a was sensitive to ISR activity in Hela cells, suggesting that p4a is important to MERS-CoV replication under specific situations (34). To rationalize the insensitivity of MERS-CoV-Δp4a to the ISR in Vero cells, we and others proposed the existence of a second MERS-CoV-encoded ISR antagonist (1, 37). Recently, the non-structural protein (nsp) 15 of β-coronavirus MHV-A59 and α-coronavirus HCoV-229E has been shown to act as ISR antagonist (38). This protein is part of the polyprotein encoded by ORF1ab and has endonuclease activity. Its proposed mechanism of action is degradation of superfluous dsRNA to prevent activation of dsRNA sensors like PKR. Nsp15 is conserved throughout the coronavirus family and it is thus plausible that the MERS-CoV-encoded nsp15 also inhibits PKR. Whether nsp15, or perhaps one of the other MERS-CoV proteins acts as ISR antagonist alongside p4a will have to be determined in the future. Interestingly, a recent MERS-CoV outbreak in hospitals in Jordan which encompassed 16 individuals was characterized by deletions in p4a, and in some cases also accessory proteins 3, 4b, or 5 (39). All of the reported deletions in p4a spanned (parts of) its dsRNA-binding domain and should render it unable to conduct its function as ISR antagonist. Despite this, these MERS-CoV strains retained their transmissibility and virulence. Whether this was related to the specific conditions of this particular hospital outbreak, or instead suggests that p4a is not important for MERS-CoV infections in humans in general remains to be determined.

eIF2B's function and regulation

In comparison to most GEF proteins, eIF2B is of extraordinary complexity, consisting of two copies of each of five different subunits (eIF2Bα-eIF2Bε). The eIF2B γ- and ε-subunit are partially homologous to each other and together form the catalytic subcomplex $eIF2B_{cat}$. eIF2Bα, β, and δ together form the

regulatory subcomplex (eIF2B$_{reg}$). In 2016, the first structure of (*S. Pombe*) decameric eIF2B was published (40). This structure showed that the regulatory core (2α, 2β, and 2δ) is flanked by two eIF2B$_{cat}$ subcomplexes. The catalytic domain of eIF2B resides in the C-terminus of eIF2Bε, the HEAT domain, which was not resolved in the crystal structure since it is connected to the rest of the complex via a ~100 amino acid flexible linker. Later, two independent groups published cryo-EM structures of human eIF2B, of which the overall fold corresponded well to the *S. Pombe* eIF2B structure, and in which the catalytic subunit of eIF2B was again not resolved (10, 12). Recently, several groups have reported eIF2•eIF2B co-structures, either with non-phosphorylated eIF2(α) or phosphorylated eIF2(α) (41–44). eIF2 consists of three subunits, the central guanidine nucleotide binding γ-subunit, flanked by the α- and β-subunits. eIF2γ interacts with eIF2B$_{cat}$, which is required for eIF2B-mediated GDP/GTP exchange, and (p-)eIF2α interacts with eIF2B$_{reg}$ to regulate eIF2B activity. Remarkably, most of the p-eIF2•eIF2B co-structures suggest that eIF2 and p-eIF2 have different and non-overlapping binding sites on eIF2B (41, 42). The N-terminal domains of both p-eIF2α and eIF2α approach the same cavity between eIF2Bα, β, and δ in eIF2B$_{reg}$, but are coming in from different angles. p-eIF2 extends towards one of the two flanking eIF2B$_{cat}$ complexes, while non-phosphorylated eIF2 extends towards the other (Fig 2). The catalytic eIF2Bε C-terminal HEAT domain was resolved to relatively high resolution in one of the cryo-EM structures (41), likely due to the stabilizing effects of eIF2. The eIF2B catalytic activity was attributed to the dual interaction of eIF2γ with the eIF2Bε-NTD on one side, and the eIF2Bε HEAT domain on the other side, which pulls open the nucleotide binding pocket to mediate GDP release. Unfortunately, despite several independent groups reporting p-eIF2(α)•eIF2B co-structures, the inhibitory effect of p-eIF2 on this process is still poorly understood. Since eIF2 and p-eIF2 have a non-overlapping binding sites, p-eIF2 should not prevent eIF2 from binding. Neither does p-eIF2 have a significant impact on the overall eIF2B structure, so an indirect effect via conformational changes is also unlikely. It was suggested that the inhibition of GEF function is mediated not by the α-subunit of p-eIF2, but rather by its β- and/or γ-subunits (42). Due to eIF2B's two-fold symmetry, the β- and/or γ-subunit of p-eIF2 may clash with the HEAT domain of the opposing eIF2B pentamer, preventing it from engaging in a productive interaction with eIF2γ•GDP (Fig 2, bottom panels). Collectively, the available data suggest that p-eIF2 stably binds eIF2B through its α-subunit, but that the inhibitory effect on GEF function is mediated by its β- or γ-subunit affecting eIF2Bε-HEAT. Interestingly, the flexible linker of eIF2Bε-HEAT is heavily modified by phosphorylation, and at least one of these phosphorylations was shown to be important for eIF2B GEF activity, supporting the notion that affecting the positioning eIF2Bε-HEAT could regulate eIF2B function (45).

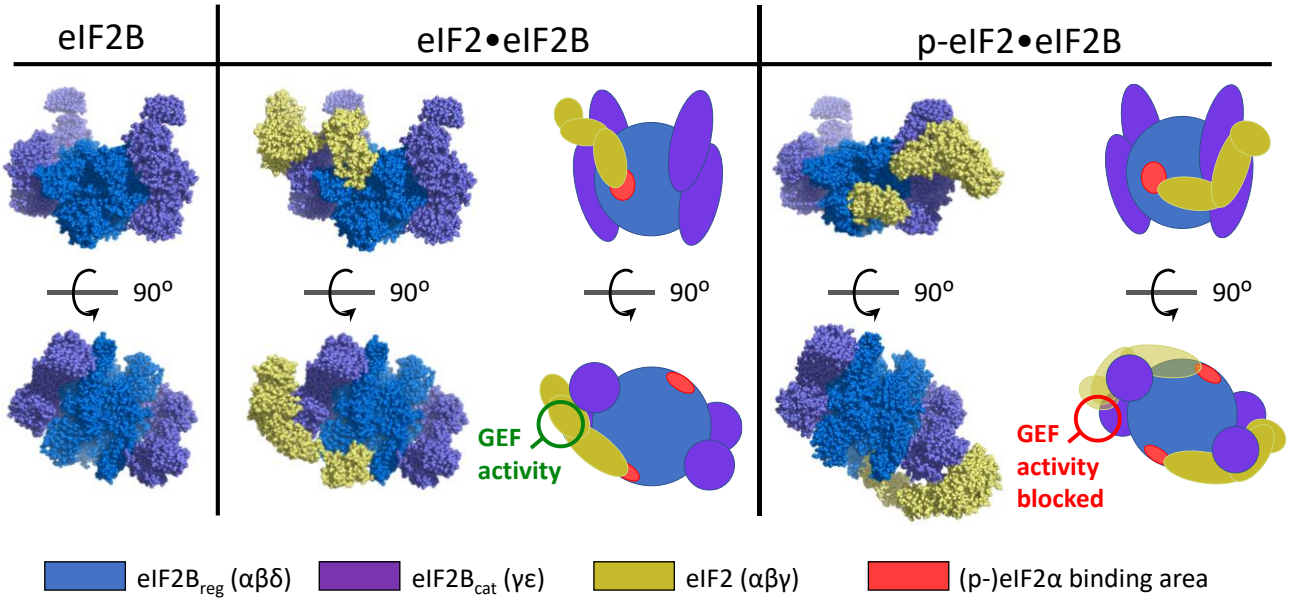

Figure 2. Structures of eIF2B bound to eIF2 or p-eIF2. *eIF2B is color-coded in blue (eIF2B regulatory subcomplex, eIF2B$_{reg}$) and purple (eIF2B catalytic subcomplex, eIF2B$_{cat}$). eIF2 or p-eIF2 are shown in yellow. The area on eIF2B$_{reg}$ that binds (p-)eIF2α is colored red in the schematic representations. eIF2 and p-eIF2 bind seemingly non-overlapping sites on eIF2B. Likely, p-eIF2 inhibits eIF2B GEF function by interfering with eIF2B$_{cat}$ using its eIF2β and/or eIF2γ subunits, as indicated in the bottom right panel. Structures shown in this figure were obtained from (42). NB: the eIF2Bε-HEAT domain is not shown in these images.*

Some discrepancies were reported about the binding sites of eIF2(α) and p-eIF2(α) to eIF2B. One paper showed that eIF2 and p-eIF2 bind in virtually identical fashion, at the position where other groups reported the p-eIF2 binding site to be (44). Another paper mentioned that while the full eIF2 and p-eIF2 complexes bind different sites on eIF2B, the α-subunits of eIF2 and p-eIF2 both bind to the p-eIF2α binding site in the absence of eIF2β and eIF2γ (42)itoito. Therefore, the authors hypothesize that eIF2 and p-eIF2 may both interact with eIF2B in a non-productive way, but that only eIF2•eIF2B can subsequently mature into a productive complex. These data correspond well to earlier (p-)eIF2•eIF2B cross-linking experiments that yielded highly similar cross-links for eIF2α and p-eIF2α, except for two cross-links specific to non-phosphorylated eIF2 close to the 'productive' interaction site on eIF2B (40). Collectively these data suggest that non-phosphorylated eIF2α has affinity for the p-eIF2α binding pocket in eIF2B, but the physiological relevance of this interaction is unclear. The cross-linking MS data of AcP10•eIF2B complexes shown in chapter 3 strongly suggest that AcP10 binds at the area on eIF2B that is occupied by p-eIF2α (17). Thereby, binding of AcP10 would prevent p-eIF2 from binding the p-eIF2α binding site on eIF2B$_{reg}$ and simultaneously inhibiting eIF2B GEF function with its β/γ subunits. Although the AcP10•eIF2B interaction site awaits structural validation, it explains the competition observed between p-eIF2 and AcP10 for eIF2B binding. The identification of viral proteins that displace

p-eIF2 from eIF2B without affecting the eIF2•eIF2B interaction indicates that the p-eIF2 binding area on eIF2B is irrelevant to the eIF2B interaction of non-phosphorylated eIF2. Furthermore, since we show that neither AcP10 nor AiVL has a negative impact on translation, we conclude that the eIF2 association to eIF2B's p-eIF2 binding site (42, 44), *if* it occurs in cells, is of no importance to translation initiation. Taken together, our data support different eIF2B interaction sites of eIF2 and p-eIF2, and are at odds with the notion that an interaction of eIF2α with the p-eIF2α binding site on eIF2B would be relevant for translation in any way.

The evolutionary background of Class 4 ISR antagonists

RNA viruses may obtain additional genetic material through recombination events. These extra sequences may come from related or unrelated viruses, from the host cell, or they may result from duplication events within the viral genome itself. As is the case for most random evolutionary changes, most incorporations of exogenous genetic material will not increase virus fitness and will not be selected for at the population level. In rare cases, however, these recombination events will cause the gain of genetic material that assists virus replication. After such an acquisition event, the gene is likely to undergo rapid changes as it is further optimized to support virus replication. As a result of these changes, the evolutionary origin of such a gene often cannot be retraced.

In contrast, the Bw-CoV accessory gene ORF10 encodes a protein (AcP10) which has sequence motifs similar to those of uridine-cytidine kinases (UCKs) expressed in most living cells (46), thereby revealing important indications about its evolutionary origin. We showed that AcP10 indeed functions as a UCK, which makes Bw-CoV the first RNA virus for which it was demonstrated that it encodes a *bona fide* uridine kinase. UCKs catalyze the conversion of pyrimidines (uridine and cytidine) into pyrimidine monophosphates. Boosting this rate-limiting step in the pyrimidine salvage pathway increases the availability of mono-, di-, and tri-phosphate pyrimidines. Possibly, by increasing the concentration of uridine and cytidine nucleotides, a virus may boost the cellular capacity to synthesize (viral) RNAs, and thereby enhance virus reproduction. Irrespective of how a UCK benefits the virus, the conservation of the UCK function over time -despite extensive evolutionary change- demonstrates that this function provides a fitness gain for the virus. Residues that are not absolutely required for this primary function were free to change over time as the virus evolved, enabling the ancestral AcP10 protein to acquire an additional function(s). This may have led to the development of an additional function as ISR antagonist.

We show that Aichivirus Leader (AiVL) has a similar ISR antagonist function as AcP10, preventing the association of p-eIF2 to eIF2B. In contrast to AcP10, AiVL has no homology to any other protein of known function and thus its evolutionary origin is as yet unknown, as is the case for most accessory proteins. Both AiVL and the closely related Mouse Kobuvirus Leader (M-KoVL) function as ISR antagonists. Several other KoVs, however, encode Leader proteins that are highly similar to AiVL but lack the ability to counteract the ISR. Their conservation throughout the KoV genus demonstrates that they must have a function through which they enhance virus replication. One publication reported that AiVL plays a dual role during infection, in replication as well as encapsidation (47). Possibly, the primary function of KoVL proteins is to assist in the encapsidation process through an unknown mechanism, while our description of AiVL as ISR antagonist explains its impact on Aichivirus replication. Aichivirus and Mouse KoV are closely related members in the Aichi A lineage of the Kobuvirus genus and therefore the ISR antagonist function of the AiVL is likely a late acquisition within the Aichi A lineage. AiVL and M-KoVL do not contain additional –or substantially distinct– domains in comparison to the other KoV L proteins, which suggests that the ISR antagonist of AiVL function arose through gain-of-function point mutations. Interestingly, using a recombinant AiV that lacks a functional L protein, we show that AiVL is the only ISR antagonists encoded by AiV. This suggests that before AiVL acquired its ISR antagonist function, the ancestral KoV encoded no ISR antagonists. Hence, KoVs that encode a Leader protein without ISR antagonist function may lack protection against the ISR. Whether this is indeed the case remains to be determined. In summary, two proteins (AcP10 and AiVL) encoded by viruses from distinct virus families seem to have acquired the ability to counteract the ISR with a similar mode of action providing an interesting example of convergent evolution.

The ISR in neuropathology

ISR signaling prevents apoptosis caused by stressful conditions. At the same time, the ISR causes upregulation of pro-apoptotic factors, that mediate cell death if the ISR is chronically activated. This latter effect may be important in clinical setting, since chronically elevated levels of p-eIF2 are associated with several neurological disorders such as Alzheimer's disease (48), Parkinson's disease (49), and prion disease (50). The common feature between these disorders is the progressive loss of neuronal cells, presumably through the induction of (ISR-induced) apoptosis in otherwise long-lived cells. What factors cause the chronic activation of the ISR, and why the ISR's negative feedback loop fails to inactivate the ISR in a timely manner, remains unknown in many cases. It was suggested however, that protein aggregates, such as amyloid plaques or prion oligomers may activate ISR sensor proteins, including PKR and PERK (50, 51). This implies that ISR activation is not the primary cause of these diseases, but that it is an important link between disease onset and neuronal loss. In contrast, Vanishing White Matter Disease (VWMD) is causally linked to lower eIF2B GEF activity, since it is often linked to mutations in eIF2B which impair its function. VWMD mutations thus mimic the effects of a chronically active ISR (15, 52, 53). Interference with ISR signaling may be an effective therapeutic strategy for several of these ISR-related disorders. Consistently, multiple different ways of ISR inhibition were shown to counteract neuropathology in a variety of mouse model systems (13, 15, 16, 54, 55). However, due to the importance of the ISR for normal cell function, such ISR-inhibiting therapeutic strategies usually cause adverse side-effects, primarily toxicity in secretory cells of the pancreas (13, 56).

The recently described small-molecule ISR inhibitor (ISRIB) increases basal eIF2B GEF activity and thereby counteracts the inhibitory effect of p-eIF2. The eIF2B decamer is assembled in a stepwise manner, first into tetramers of eIF2Bβ/γ/δ/ε and these subcomplexes subsequently dimerize into octamers. In the final step, an eIF2Bα homodimer binds to form the full eIF2B complex, in which state it has highest GEF activity. The binding site of ISRIB on eIF2B has been identified by the elucidation of cryo-EM co-structures of eIF2B and ISRIB (10, 12). ISRIB binds eIF2B at the interface of two eIF2Bβ and two eIF2Bδ subunits. Thereby, ISRIB bridges two eIF2Bβ/γ/δ/ε tetramers, boosting the assembly of full eIF2B complexes (8, 10). However, all data available thus far indicates that ISRIB does not affect p-eIF2 binding to eIF2B nor its impact on eIF2B function. Thus, ISRIB and p-eIF2 may simultaneously act on eIF2B GEF function, to opposing effects. As we show in chapter 5, under harsh stress conditions, when p-eIF2 concentrations exceed a critical threshold value, p-eIF2 will overrule ISRIB's function and prevent eIF2B GEF function. In short, ISRIB counters the ISR only within a narrow window of intracellular p-eIF2 concentrations. ISRIB – or the next-generation ISRIB-like molecule 2BAct – were

shown to be highly potent in countering neuropathology in mouse model systems for traumatic brain injury (16), prion disease (13), and VWMD (15). Crucially, ISRIB, in contrast to previous ISR-targeting strategies, does not lead to side-effects *in vivo*. Apparently, ISRIB prevents 'toxic' ISR activity without affecting 'healthy' ISR activity. These data suggest that ISR-induced neurotoxicity is mediated by chronic, slightly elevated p-eIF2 levels that can be counteracted by ISRIB, while healthy ISR activity encompasses short-lived high p-eIF2 levels. Unfortunately, no quantitative data is available on the exact levels of p-eIF2 present *in vivo*, in any of the relevant cell types or tissues, neither under healthy nor disease conditions. Whether the results of ISRIB treatments in mouse studies – both the alleviation of neuropathology and the apparent lack of side-effects – can be extrapolated to humans remains to be determined.

In the search for novel (types of) ISR inhibitors, the study of viral antagonists may provide valuable insights. Specifically, the identification of Class 4 antagonists may provide the basis of novel therapeutic strategies. We demonstrate that a protein (AcP10) can target the p-eIF2α binding site on eIF2B, thereby preventing p-eIF2 binding, without interfering with eIF2B GEF activity. Thus, this site on eIF2B is a druggable vulnerability that could be exploited by structure-based drug design to develop new small molecule ISR antagonists. Furthermore, we show that a sufficiently strong interaction with eIF2B at this site may fully block the ISR, irrespective of p-eIF2 concentrations. Thus, such approach could be significantly more potent than an ISRIB treatment. Considering the possibility of side-effects, it is unknown whether such high-potency ISR inhibition would be desirable *in vivo*, but this will have to be assessed. Consistent with an essential role of the ISR during normal cellular processes, we have been unable to generate stable cell lines expressing AcP10 or AiVL. While neither AcP10 nor AiVL seems toxic to cells *per sé*, cells expressing AcP10 or AiVL quickly stop dividing, suggesting an essential role of the ISR in mitosis (unpublished data). This is consistent with previous observations that the ISR is activated during the G2 and M phases in mitotic cells (57). It may be possible to create small molecules that act like Class 4 antagonists but with lower affinities for eIF2B, resulting in milder ISR inhibition to such effect that the optimal balance can be achieved between allowing healthy ISR signaling and preventing toxic ISR signaling.

Concluding remarks

The ISR is ubiquitously present in all cells and conserved throughout eukaryotes and is an important regulatory mechanism for cellular translation. The ISR is involved in basal cellular processes, as well as cellular responses to stressful conditions. Hyperactivation of the ISR has been linked to a variety of

disorders and thus the ability to modify ISR signaling is of high importance. Viruses, to ensure efficient synthesis of viral proteins, often encode antagonists that hinder ISR signal transduction. In this thesis we aimed to learn more about ISR inhibition by viruses, and thereby we hoped to learn more about the ISR pathway itself and about the most efficient ways to counteract it. We identified three new viral ISR antagonists (MERS-CoV p4a, Bw-CoV AcP10, and Aichivirus Leader), of which p4a inhibits PKR by binding to dsRNA, and AcP10 and AiVL prevent the translational control of p-eIF2 by binding to eIF2B. We also looked into the function of a small-molecule inhibitor of the ISR (ISRIB), and found that it counteracts the ISR only as long as p-eIF2 levels remain low. ISRIB is currently being tested for its applicability in the treatment of ISR-related disorders, and our findings could help in the prediction and/or evaluation of the outcomes of such studies. Whether the novel mode of ISR inhibition as identified for AcP10 and AiVL can be used as the basis for new generation of ISR inhibitors will have to be determined.

References

1. H. H. Rabouw, *et al.*, Middle East Respiratory Coronavirus Accessory Protein 4a Inhibits PKR-Mediated Antiviral Stress Responses. *PLoS Pathog.* **12**, e1005982 (2016)

2. , WHO | Middle East respiratory syndrome coronavirus (MERS-CoV) – Saudi Arabia. *WHO*, https://www.who.int/emergencies/mers-cov/en/ (2019)

3. K.-N. Son, Z. Liang, H. L. Lipton, Double-Stranded RNA Is Detected by Immunofluorescence Analysis in RNA and DNA Virus Infections, Including Those by Negative-Stranded RNA Viruses. *J. Virol.* **89**, 9383-92 (2015)

4. M. Bergmann, *et al.*, Influenza virus NS1 protein counteracts PKR-mediated inhibition of replication. *J. Virol.* **74**, 6203–6206 (2000)

5. Z. Feng, M. Cerveny, Z. Yan, B. He, The VP35 protein of Ebola virus inhibits the antiviral effect mediated by double-stranded RNA-dependent protein kinase PKR. *J. Virol.* **81**, 182–192 (2007)

6. H. W. Chang, J. C. Watson, B. L. Jacobs, The E3L gene of vaccinia virus encodes an inhibitor of the interferon-induced, double-stranded RNA-dependent protein kinase. *Proc. Natl. Acad. Sci. U. S. A.* **89**, 4825–4829 (1992)

7. T. Yamashita, *et al.*, Isolation of cytopathic small round viruses with BS-C-1 cells from patients with gastroenteritis. *J. Infect. Dis.* **164**, 954-7 (1991)

8. C. Sidrauski, *et al.*, Pharmacological dimerization and activation of the exchange factor eIF2B antagonizes theintegrated stress response. *Elife* **4**, e07314 (2015)

9. C. Sidrauski, *et al.*, Pharmacological brake-release of mRNA translation enhances cognitive memory. *Elife* **2**, e00498 (2013)

10. J. C. Tsai, *et al.*, Structure of the nucleotide exchange factor eIF2B reveals mechanism of memory-enhancing molecule. *Science.* **359**, pii: eaaq0939 (2018)

11. Y. Sekine, *et al.*, Mutations in a translation initiation factor identify the target of a memory-enhancing compound. *Science.* **348**, 1027-30 (2015)

12. A. F. Zyryanova, *et al.*, Binding of ISRIB reveals a regulatory site in the nucleotide exchange factor eIF2B. *Science.* **359**, 1533-1536 (2018)

13. M. Halliday, *et al.*, Partial restoration of protein synthesis rates by the small molecule ISRIB prevents neurodegeneration without pancreatic toxicity. *Cell Death Dis.* **6**, e1672 (2015)

14. Y. L. Wong, *et al.*, The small molecule ISRIB rescues the stability and activity of vanishing white matter disease eIF2B mutant complexes. *Elife* **7**, pii: e32733 (2018)

15. Y. L. Wong, *et al.*, eIF2B activator prevents neurological defects caused by a chronic integrated stress response. *Elife* **8**, pii: e42940 (2019)

16. A. Chou, *et al.*, Inhibition of the integrated stress response reverses cognitive deficits after traumatic brain injury.

PNAS. **114**, E6420-E6426 (2017)

17. H. H. Rabouw, *et al.*, Inhibition of the integrated-stress-response by viral proteins that block p-eIF2•eIF2B association. *This Thesis*, Chapter 3 (2019)

18. L. J. Visser, *et al.*, The aichivirus leader protein inhibits the integrated stress response by preventing p-eIF2-mediated inhibition of eIF2B function. *This Thesis*, Chapter 4 (2019)

19. D. A. Khaperskyy, *et al.*, Influenza A Virus Host Shutoff Disables Antiviral Stress-Induced Translation Arrest. *PLoS Pathog.* **10,** e1004217 (2014)

20. N. Pavio, P. R. Romano, T. M. Graczyk, S. M. Feinstone, D. R. Taylor, Protein synthesis and endoplasmic reticulum stress can be modulated by the hepatitis C virus envelope protein E2 through the eukaryotic initiation factor 2 alpha kinase PERK. *J. Virol.* **77**, 3578-85 (2003)

21. D. R. Taylor, S. T. Shi, P. R. Romano, G. N. Barber, M. M. C. Lai, Inhibition of the interferon-inducible protein kinase PKR by HCV E2 protein. *Science.* **285**, 107-10 (1999)

22. H. A. Vincent, B. Ziehr, N. J. Moorman, Mechanism of Protein Kinase R Inhibition by Human Cytomegalovirus pTRS1. *J. Virol.* **91**, 1–16 (2017)

23. K. A. Cassady, Human Cytomegalovirus TRS1 and IRS1 Gene Products Block the Double-Stranded-RNA-Activated Host Protein Shutoff Response Induced by Herpes Simplex Virus Type 1 Infection. *J. Virol.* **79**, 8707-15 (2005)

24. B. Ziehr, H. A. Vincent, N. J. Moorman, Human Cytomegalovirus pTRS1 and pIRS1 Antagonize Protein Kinase R To Facilitate Virus Replication. *J. Virol.* **90**, 3839-3848 (2016)

25. I. S. Fernández, X. C. Bai, G. Murshudov, S. H. W. Scheres, V. Ramakrishnan, Initiation of translation by cricket paralysis virus IRES requires its translocation in the ribosome. *Cell* 157, 823-31 (2014)

26. Z. A. Jaafar, A. Oguro, Y. Nakamura, J. S. Kieft, Translation initiation by the hepatitis C virus IRES requires eIF1A and ribosomal complex remodeling. *Elife* **5**, pii: e21198 (2016)

27. E. González-Almela, H. Williams, M. A. Sanz, L. Carrasco, The initiation factors eIF2, eIF2A, eIF2D, eIF4A, and eIF4G are not involved in translation driven by hepatitis C virus IRES in human cells. *Front. Microbiol.* **9**, 207 (2018)

28. Y. V. Svitkin, *et al.*, Eukaryotic Translation Initiation Factor 4E Availability Controls the Switch between Cap-Dependent and Internal Ribosomal Entry Site-Mediated Translation. *Mol. Cell. Biol.* **25**, 10556-65 (2005)

29. D. Etchison, S. C. Milburn, I. Edery, N. Sonenberg, J. W. Hershey, Inhibition of HeLa cell protein synthesis following poliovirus infection correlates with the proteolysis of a 220,000-dalton polypeptide associated with eucaryotc initiation factor 3 and a cap binding protein complex. *J. Biol. Chem.* **257**, 14806-10 (1982)

30. N. Redondo, M. A. Sanz, E. Welnowska, L. Carrasco, Translation without eIF2 promoted by poliovirus 2A protease. *PLoS One* **6**, e25699 (2011)

31. J. P. White, L. C. Reineke, R. E. Lloyd, Poliovirus Switches to an eIF2-Independent Mode of Translation during Infection. *J. Virol.* **85**, 8884-93 (2011)

32. Y. Yang, *et al.*, The structural and accessory proteins M, ORF 4a, ORF 4b, and ORF 5 of Middle East respiratory syndrome coronavirus (MERS-CoV) are potent interferon antagonists. *Protein Cell* **4**, 951–961 (2013)

33. K.-L. Siu, *et al.*, Middle east respiratory syndrome coronavirus 4a protein is a double-stranded RNA-binding protein that suppresses PACT-induced activation of RIG-I and MDA5 in the innate antiviral response. *J. Virol.* **88**, 4866–76 (2014)

34. K. Nakagawa, K. Narayanan, M. Wada, S. Makino, Inhibition of Stress Granule Formation by Middle East Respiratory Syndrome Coronavirus 4a Accessory Protein Facilitates Viral Translation, Leading to Efficient Virus Replication. *J. Virol.* **92**, pii: e00902-18 (2018)

35. J. M. Thornbrough, *et al.*, Middle East Respiratory Syndrome Coronavirus NS4b Protein Inhibits Host RNase L Activation. *MBio* **7**, e00258-16 (2016)

36. J. Il Kim, S. Park, J. Y. Bae, M. S. Park, Evolutionary relationship analysis of Middle East respiratory syndrome coronavirus 4a and 4b protein coding sequences. *J. Vet. Sci.* **20**, e1 (2019)

37. C. E. Comar, *et al.*, Antagonism of dsRNA-induced innate immune pathways by NS4a and NS4b accessory proteins during MERS coronavirus infection. *MBio* **10**, pii: e00319-19 (2019)

38. E. Kindler, *et al.*, Early endonuclease-mediated evasion of RNA sensing ensures efficient coronavirus replication. *PLoS Pathog.* **13**, e1006195 (2017)

39. M. M. Lamers, *et al.*, Deletion Variants of Middle East Respiratory Syndrome Coronavirus from Humans, Jordan, 2015. *Emerg. Infect. Dis.* **22,** 716-9 (2016)

40. K. Kashiwagi, *et al.*, Crystal structure of eukaryotic translation initiation factor 2B. *Nature* **531**, 122–5 (2016)

41. L. R. Kenner, *et al.*, eIF2B-catalyzed nucleotide exchange and phosphoregulation by the integrated stress response. *Science.* **364**, 491-495 (2019)

42. K. Kashiwagi, *et al.*, Structural basis for eIF2B inhibition in integrated stress response. *Science.* **364**, 495-499 (2019)

43. Y. Gordiyenko, J. L. Llácer, V. Ramakrishnan, Structural basis for the inhibition of translation through eIF2α phosphorylation. *Nat. Commun.* **10**, 2640 (2019)

44. T. Adomavicius, *et al.*, The structural basis of translational control by eIF2 phosphorylation. *Nat. Commun.* **10**, 2136 (2019)

45. V. Beilsten-Edmands, *et al.*, EIF2 interactions with initiator tRNA and eIF2B are regulated by post-translational modifications and conformational dynamics. *Cell Discov.* **1**, 15020 (2015)

46. K. A. Mihindukulasuriya, G. Wu, J. St. Leger, R. W. Nordhausen, D. Wang, Identification of a Novel Coronavirus from a Beluga Whale by Using a Panviral Microarray. *J. Virol.* **82**, 5084-8 (2008)

47. J. Sasaki, S. Nagashima, K. Taniguchi, Aichi Virus Leader Protein Is Involved in Viral RNA Replication and Encapsidation. *J. Virol.* **77**, 10799-807 (2003)

48. M. V. Lourenco, S. T. Ferreira, F. G. De Felice, Neuronal stress signaling and eIF2α phosphorylation as molecular

links between Alzheimer's disease and diabetes. *Prog. Neurobiol.* **129**, 37–57 (2015)

49. J. J. M. Hoozemans, *et al.*, Activation of the unfolded protein response in Parkinson's disease. *Biochem. Biophys. Res. Commun.* **354**, 707–711 (2007)

50. J. A. Moreno, *et al.*, Sustained translational repression by eIF2α-P mediates prion neurodegeneration. *Nature* **485**, 507–511 (2012)

51. A. L. Peel, D. E. Bredesen, Activation of the cell stress kinase PKR in Alzheimer's disease and human amyloid precursor protein transgenic mice. *Neurobiol. Dis.* **14**, 52-62 (2003)

52. W. Li, X. Wang, M. S. van der Knaap, C. G. Proud, Mutations Linked to Leukoencephalopathy with Vanishing White Matter Impair the Function of the Eukaryotic Initiation Factor 2B Complex in Diverse Ways. *Mol. Cell. Biol.* **24**, 3295-306 (2004)

53. S. L. Moon, R. Parker, EIF2B2 mutations in vanishing white matter disease hypersuppress translation and delay recovery during the integrated stress response. *RNA* **24**, 841-852 (2018)

54. G. Mercado, *et al.*, Targeting PERK signaling with the small molecule GSK2606414 prevents neurodegeneration in a model of Parkinson's disease. *Neurobiol. Dis.* **112**, 136-148 (2018)

55. H. Radford, J. A. Moreno, N. Verity, M. Halliday, G. R. Mallucci, PERK inhibition prevents tau-mediated neurodegeneration in a mouse model of frontotemporal dementia. *Acta Neuropathol.* **130**, 633-42 (2015)

56. J. A. Moreno, *et al.*, Oral treatment targeting the unfolded protein response prevents neurodegeneration and clinical disease in prion-infected mice. *Sci. Transl. Med.* **5**, 206ra138 (2013)

57. Y. Kim, *et al.*, PKR is activated by cellular dsRNAs during mitosis and acts as a mitotic regulator. *Genes Dev.* **28**, 1310–1322 (2014)

Chapter 7

Addendum

Nederlandse Samenvatting

Dankwoord

Curriculum Vitae

List of Publications

List of Abbreviations

Nederlandse samenvatting

Virussen zijn voor hun vermenigvuldiging afhankelijk van hun gastheercellen. Ze bevatten genetisch materiaal (RNA of DNA) wat de gastheercel ertoe aanzet om meer virusdeeltjes te maken. Dit proces is over het algemeen schadelijk voor de gastheercel en leidt vaak tot celdood. Om zich te beschermen tegen infecties met virussen, is iedere cel uitgerust met afweermechanismen die in werking treden op het moment dat een virus herkend wordt. Een van die afweermechanismen is de zogenaamde Integrated Stress Response (ISR), die kan worden aangezet als reactie op veel verschillende stress situaties, waarvan virus infectie slechts een voorbeeld is. Het belangrijkste gevolg van een geactiveerde ISR is dat de cel (tijdelijk) stopt met translatie, het aanmaken van nieuwe eiwitten. Hiermee wordt veel energie bespaart en krijgt de cel tijd om de stress situatie op te lossen. Wanneer de balans weer is hersteld wordt de ISR uitgezet en kan de cel de normale processen hervatten. Eventueel kan de ISR ook leiden tot celdood in gevallen van chronische stress die niet verholpen kan worden. In virus-geïnfecteerde cellen voorkomt de ISR dat virale eiwitten worden gemaakt, en daarmee wordt de aanmaak van nieuwe virusdeeltjes tegengegaan. Bovendien zal een chronisch actieve ISR uiteindelijk de gastheercel doden, en daarmee definitief voorkomen dat er meer virusdeeltjes gemaakt kunnen worden.

Naast de belangrijke rol van de ISR als afweermechanisme tegen virussen, is de ISR van cruciaal belang bij meerdere andere cellulaire processen, van correcte eiwitvouwing tot celdeling. Daarom is ontregelde ISR activiteit betrokken bij een veelheid aan ziektebeelden. Met name neurologische aandoeningen, bijvoorbeeld de ziekte van Parkinson, ziekte van Alzheimer, en Amyotrofische Laterale Sclerose (ALS), zijn vaak gecorreleerd aan problemen met de ISR. Om die reden is het van groot belang om te weten te komen hoe de ISR precies werkt, en hoe de activiteit van de ISR beïnvloed kan worden. Gedurende miljoenen jaren evolutie hebben virussen allerlei manieren ontwikkeld om zich te beschermen tegen de antivirale effecten van de ISR. Door te onderzoeken hoe virussen dit doen kunnen we de meest effectieve methoden ontdekken om de ISR te beïnvloeden. Zo zijn er voorbeelden bekend van virale eiwitten die ervoor zorgen dat het virus niet herkend kan worden, waardoor de ISR nooit aangeschakeld wordt. Andere virale eiwitten voorkomen dat de nodige signalen doorgegeven kunnen worden, waardoor translatie niet afgesloten wordt ondanks een actieve ISR. Deze zogenaamde “ISR antagonisten” komen voor in (bijna) alle virus families, waaruit blijkt hoe belangrijk ze zijn voor vermenigvuldiging van virussen.

In deze scriptie beschrijven we ons onderzoek naar de manieren waarop virussen de ISR tegenwerken. We identificeren drie virale eiwitten als ISR antagonisten, en beschrijven via welke mechanismen ze deze functie vervullen.

In **hoofdstuk 2** hebben we onderzoek gedaan naar Middle-East Respiratory Syndrome coronavirus (MERS-CoV). Er zijn tientallen verschillende coronavirussen beschreven, die zijn onderverdeeld in vier groepen: Alfa-, bèta-, gamma-, en delta-coronavirussen. Ieder van deze virussen is gespecialiseerd in het infecteren van een bepaalde diersoort, in veel gevallen een zoogdier of vogel. Van tijd tot tijd springen coronavirussen vanuit de ene diersoort over naar een andere. In 2002 sprong Severe Acute Respiratory Syndrome (SARS) coronavirus over op mensen waarschijnlijk vanuit civet katten. Ongeveer een decennium later verscheen Middle-East Respiratory Syndrome (MERS) coronavirus in de menselijke populatie na een transmissie vanuit dromedarissen. Beide virussen kunnen zeer ernstige luchtweginfecties veroorzaken waaraan mensen overlijden in ongeveer 10% van de gevallen

voor SARS-CoV, en zelfs in 30% van de gevallen voor MERS-CoV. MERS-CoV verspreid zich echter zeer inefficiënt tussen mensen, waardoor er weinig infectiegevallen optreden. In hoofdstuk 2 laten we zien dat MERS-CoV, net als veel andere virussen, een afweermechanisme heeft ontwikkeld tegen de ISR. We laten zien dat deze functie wordt vervuld door het virale eiwit p4a. p4a voorkomt activatie van de ISR door zijn binding aan dubbelstrengs RNA (dsRNA). RNA is aanwezig in grote hoeveelheden in iedere cel, maar komt onder normale omstandigheden vrijwel altijd voor in enkelstrengs vorm en bijna nooit in dubbelstrengs vorm. Aangezien de meeste virussen bij de productie van virale RNAs onvermijdelijk grote hoeveelheden dsRNA maken in de cel, wordt dsRNA door de cel herkend als een gevarensignaal dat een virale infectie aanduidt. Tijdens MERS-CoV infectie bindt het p4a de gevormde dsRNA moleculen, die daardoor afgeschermd zijn en niet door de cel herkend kunnen worden. Op deze manier voorkomt p4a dat de ISR geactiveerd raakt in geïnfecteerde cellen, waardoor productie van virale eiwitten ongehinderd door kan gaan en het virus zich kan vermenigvuldigen.

In **hoofdstuk 3** doen we onderzoek naar een molecuul dat de ISR kan onderdrukken. In dit geval gaat het niet om een (viraal) eiwit, maar om een chemicalie genaamd ISRIB ("ISR Inhibitor") die in 2013 is ontwikkeld. Zoals eerder beschreven in deze samenvatting is de ISR van belang bij vele normale cellulaire processen, en een ontregelde ISR leidt tot allerlei complicaties. Vooral neurologische aandoeningen zijn gecorreleerd met een ontregelde ISR, vaak met een overactieve ISR. ISRIB is als ISR onderdrukker gebruikt in meerdere muismodellen voor neurologische aandoeningen. Veel van deze experimenten hebben aangetoond dat ISRIB zeer veelbelovende effecten lijkt te hebben: ISRIB voorkomt celdood in neuronen als gevolg van prion ziekte, het voorkomt lange-termijn hersenschade na fysiek hoofdletsel, en het voorkomt de symptomen van Vanishing White Matter (VWM) ziekte. Vergelijkbare effecten zijn al eerder gezien met andere chemicaliën die de ISR onderdrukken, maar dit ging altijd gepaard met bijwerkingen, terwijl dit bij een ISRIB behandeling niet zo is. Logischerwijs is het van groot belang om te begrijpen hoe de ISR werkt en gereguleerd kan worden op een manier die niet tot zware bijwerkingen leidt. In hoofdstuk 3 geven we een potentiele verklaring waarom ISRIB geen bijwerkingen lijkt te geven. Dit heeft te maken met ISRIB's moleculaire werkingsmechanisme. ISRIB blokkeert de ISR door de binden aan eIF2B. eIF2B is essentieel bij de recycling van de translatiefactor eIF2, en zonder de activiteit van eIF2B ontstaat er snel een gebrek aan eIF2 waardoor translatie vastloopt. De ISR verstoort dit recyclingproces door grootschalige onderdrukking van eIF2B. ISRIB vervult een brugfunctie tussen de afzonderlijke bouwstenen van het eIF2B eiwitcomplex, met als gevolg dat ISRIB de opbouw van eIF2B stimuleert. Hiermee vergroot ISRIB de beschikbare hoeveelheid eIF2B, wat het onderdrukkende effect van de ISR op eIF2B tegenwerkt. We tonen we aan dat ISRIB's functie afhankelijk is van hoe sterk de ISR geactiveerd wordt. Anders gezegd, ISRIB blokkeert zwakke ISR signalering zeer efficiënt, maar heeft geen enkel effect op een sterk geactiveerde ISR. Dit komt omdat de opbouw van eIF2B niet ongelimiteerd gestimuleerd kan worden, en wanneer de ISR actief genoeg is om alle eIF2B te remmen heeft ISRIB geen effect meer. Als gevolg hiervan voorkomt ISRIB schadelijke, langdurige ISR activiteit in neuronen, terwijl de ISR toch intact blijft om te reageren op stress situaties. Het vinden van de juiste balans tussen het blokkeren van schadelijke ISR signalering en het behouden van gezonde ISR activiteit zal cruciaal zijn voor het ontwikkelen van therapieën die zich richten op de ISR.

In **hoofdstuk 4** beschrijven we de onderdrukking van ISR activiteit door een eiwit van een exotisch coronavirus (beluga whale coronavirus, Bw-CoV) dat infecteert in witte dolfijnen en tuimelaars. Dit coronavirus is aangetroffen in een klein aantal in gevangenschap levende dieren en het is nooit in

een laboratorium opgegroeid. De volledige sequentie van het genetisch materiaal van dit virus is in kaart gebracht waardoor we kunnen achterhalen welke virale eiwitten dit virus heeft. Het eiwit dat we beschrijven in hoofdstuk 4, genaamd AcP10, is een ISR antagonist die werkt op een volledig andere manier dan MERS p4a. In cellen die AcP10 bevatten kan de ISR ongehinderd geactiveerd worden, maar de daarop volgende signalen worden niet op de normale manier doorgegeven. Net als ISRIB, werkt AcP10 via een directe interactie met eIF2B. Echter, deze interactie heeft geen effect op de functie of de opbouw van eIF2B, maar voorkomt dat eIF2B kan wordt geremd door de ISR. Op die manier blijft eIF2B actief, ongeacht de activiteit van de ISR, en zal translatie op het normale niveau doorgaan. Dit moleculaire mechanisme waarmee AcP10 de ISR tegenwerkt is niet eerder beschreven voor andere virale of cellulaire eiwitten. AcP10 is daarmee het eerste eiwit waarvan bekend is dat het de meest centrale stap van de ISR blokkeert: de remming van eIF2B. Naast zijn functie als ISR antagonist heeft AcP10 een tweede functie als uridine kinase. Uridine kinases zijn eiwitten die voorkomen in vrijwel iedere levende cel en helpen bij de aanmaak van nucleotiden, de bouwstenen van RNA en DNA. De uridine-kinasefunctie en de ISR-antagonistfunctie zijn niet van elkaar afhankelijk en kunnen afzonderlijk uitgeschakeld worden door kleine aanpassingen te maken in het eiwit. AcP10's gelijkenis met uridine kinases demonstreert dat AcP10 ooit is opgepikt door een "recombinatie" waarbij een (deel van een) cellulair RNA terecht is gekomen in het virale genetisch materiaal. Vanaf dat moment hebben willekeurige mutaties en natuurlijke selectie het eiwit geoptimaliseerd om virus replicatie te ondersteunen. Tijdens dat proces is waarschijnlijk de ISR antagonist functie ontstaan.

In **hoofdstuk 5** doen we onderzoek naar Aichivirus. Dit virus is in 1991 voor het eerst beschreven als de oorzaak van darminfecties in het Japanse district Aichi. Aichivirus behoort tot de familie van picornavirussen, relatief kleine RNA-bevattende virussen. De picornavirus familie omvat grote hoeveelheden verschillende virussen waaronder ook bekende pathogenen voor mens (bijv. poliovirus) en dier (bijv. FDMV; mond-en-klauwzeer). Alle picornavirussen hebben een zeer vergelijkbare set eiwitten die nodig zijn voor de vermenigvuldiging van het virale RNA en het maken van virusdeeltjes. Een aantal picornavirussen hebben hiernaast ook een extra eiwit genaamd Leader (L). De picornavirus L eiwitten zijn zeer variabel; alleen de L-eiwitten van nauw verwante picornavirussen vertonen enige overeenkomst met elkaar. In hoofdstuk 4 beschrijven we het L-eiwit van Aichivirus (AiVL) en zijn functie als onderdrukker van de ISR. Naast het AiVL eiwit is alleen het meeste verwante L eiwit (dat van mouse kobuvirus [M-KoV]) in staat de ISR te blokkeren, terwijl alle andere geteste L eiwitten van verwante virussen deze functie missen. Dit suggereert dat de functie als ISR antagonist recent is ontstaan in AiVL's evolutionaire geschiedenis. Nader onderzoek naar het moleculaire mechanisme waarmee AiVL de ISR onderdrukt leerde ons dat AiVL op zeer vergelijkbare manier werkt als AcP10. Beide eiwitten hebben de directe interactie van het eIF2B eiwitcomplex, en deze interactie voorkomt het onderdrukkende effect van de ISR op eIF2B's functie. Deze overeenkomst tussen AcP10 en AiVL was verrassend, aangezien geen enkele van de vele eerder beschreven ISR antagonisten dit werkingsmechanisme heeft. Bovendien hebben AiVL en AcP10 geen detecteerbare overeenkomsten met elkaar. Het ontstaan van een zeer vergelijkbare strategie om de ISR te blokkeren in twee niet-verwante eiwitten is een voorbeeld van convergente evolutie.

Dankwoord

Graag wil ik iedereen bedanken die een bijdrage heeft geleverd, klein of groot, tijdens mijn verblijf op het virologielab. Om te beginnen natuurlijk mijn promotor en begeleider Frank van Kuppeveld, die mijn PhD mogelijk heeft gemaakt. Gedurende mijn PhD was je altijd beschikbaar en bereid om te overleggen, uitleg te geven, of op andere manieren input te leveren. Ik heb dan ook zeker veel van je geleerd, zowel over de experimentele kant als over het schrijven en het maken van presentaties. Hetzelfde geldt ook voor mijn copromotor Raoul de Groot, die gedurende mijn hele PhD wekelijks bij de werkbesprekingen aanwezig was. Jullie keken vaak op verschillende manieren naar experimentele data, en zelfs naar volledige projecten, wat voor mij deze werkbesprekingen alleen maar interessanter en leerzamer maakte. Bovendien zal ik niet snel de gezamenlijke schrijfsessies vergeten die een groot deel van hoofdstuk 4 hebben opgeleverd! Daarnaast heb ik ook veel plezier gehad bij de gesprekken die we af en toe hadden op willekeurige momenten in de gang of in je kantoor. Die waren steevast zeer nuttig als ze over werk gingen, of anders totaal nutteloos als ze gingen over een onderwerp als Donald Trump.

Verder wil ik mijn andere copromotor bedanken, Martijn Langereis, die vooral gedurende de eerste helft van mijn PhD een grote invloed heeft gehad. Van jou heb ik alle ins-and-outs geleerd over de experimentele kant van het werk op een virologielab. Deze samenwerking heb ik altijd erg positief ervaren! Zelfs nadat je van baan gewisseld was, kwam je nog een aantal keren per jaar langs op de afdeling bij mij, Frank, en Linda voor eten, om te praten over projecten en gewoon voor de gezelligheid.

Linda, erg bedankt voor de samenwerking die we jarenlang gehad hebben. Het is altijd prettig om bij iemand binnen te kunnen komen lopen om over iets willekeurigs te discussiëren. Bovendien is het verrassend gezellig om samen teleurgesteld te zijn over data die zojuist uit een machine is komen rollen. En wat misschien nog wel gezelliger is, zijn natuurlijk de uitstapjes richting de bioscoop die we af en toe deden samen met Lisa, Floor, Dan en Malte. Ik heb jullie allemaal gedurende de periode dat jullie erbij waren erg gewaardeerd. Ik geloof bovendien dat ik Lisa en Floor, vooral Floor, nog eens speciaal moet bedanken. Zonder jullie waren er waarschijnlijk veel experimenten niet doorgegaan wegens een gebrek aan cellen. Jullie waren gelukkig altijd bereid om wat extra beschikbaar te houden voor het geval ik op het laatste moment opeens een experiment wilde doen maar niks had voorbereid.

Ik wil ook een aantal anderen bedanken die direct bijgedragen hebben aan mijn projecten: De masterstudenten die door de jaren heen langsgekomen zijn. Om te beginnen Tim, die bereid was om mee te werken aan een project over Beluga Whales. Ik heb je positieve insteek en enthousiasme ondanks, of misschien wel dankzij, je moeilijke project altijd erg gewaardeerd. Ik hoop dat de periode op de Utrechtse virologieafdeling leerzaam voor je is geweest, en ik heb er vertrouwen in dat je huidige PhD succesvol zal zijn. De tweede student was Jesus. Ook jou wil ik bedanken voor je inzet, en je erg veel succes wensen bij je recent begonnen PhD. Het kortst geleden was de stage van Jose. Je was altijd een gezellige aanwezigheid op het lab, en dat het nuttig was blijkt wel uit het feit dat je voor veel van de figuren in hoofdstuk 5 de data hebt aangeleverd. Ik heb dan ook in alle opzichten positieve herinneringen aan de tijd van jouw stage. Tot slot wil ik ook nog Kyra bedanken. Aangezien je eigenlijk student was bij de celbiologieafdeling onder begeleiding van Susanne, was ik alleen onofficieel begeleider voor het werk dat je op de virologieafdeling deed, en daarbij was jij de ideale

onofficiële student. Voor zover ik sowieso iets moest uitleggen was dat altijd maar een enkele keer. Ik vind het dan ook erg leuk dat je later besloot om een PhD te gaan doen bij celbiologie om je projecten voort te zetten. Alle succes gewenst!

Susanne, van alle tot nu toe genoemde mensen ken ik jou veruit het langst. Of het nou gerelateerd was ons PhD werk of niet, het is altijd fijn om met jou om te gaan. Bovendien kan ik eerlijk zeggen dat het virus-project waaraan jij samen met Kyra werkte altijd een favoriet van me geweest is. Ik hoop echt dat je verder richting de virologie zal gaan in de toekomst. Misschien kunnen we nog wel eens een gezamenlijk project doen.

Nu ik (bijna) iedereen heb genoemd die rechtstreeks betrokken is geweest bij mijn werk, wil ik twee mensen nog even speciaal bedanken: Qian en Arno. Qian vanwege haar hulp gedurende de eerste maanden van mijn PhD toen zij nog aanwezig was bij Virologie, en Arno vanwege zijn hulp in de laatste periode bij het afmaken van de projecten die niet afgekomen zijn. Natuurlijk is Arno als vaste kracht bij de afdeling sowieso onmisbaar, voor iedereen, en bovendien een erg gezellige collega om te hebben.

De virologieafdeling bestaat natuurlijk niet alleen maar uit mensen die direct meegeholpen hebben met mijn werk, maar ook uit veel mensen die het een goede werkomgeving maken. Ik wil op zijn minst de mensen bedanken die in het (recente) verleden kamergenoten zijn geweest, en daarmee het dagelijkse werk gezellig hebben gemaakt. Erion, dankzij jou kan ik nu (zoals Jim dat zei) in het Koreaans zeggen welke dieren ik wil drinken, en hebben Jim en ik nu een soort geschreven geheimtaal gebaseerd op onze waardeloze spelling van het Koreaans. Van alles wat ik geleerd heb in deze jaren is dit misschien toch wel het nuttigst. Ieva, fijn dat ik me door jou zo welkom voel telkens als ik op het lab kom. Ook de kamergenoten van iets langer geleden wil ik niet overslaan: Hilde, Hendrik, Ruben, jullie waren stuk voor stuk goede kamergenoten om te hebben, en jullie werden gemist toen jullie uiteindelijk vertrokken.

Ik denk dat ik dit dankwoord ga afsluiten door iedereen te bedanken die de jaren op de virologieafdeling zo mooi hebben gemaakt. Ik vrees dat ik veel mensen te kort doe door ze zo vluchtig te noemen, maar anders komt er nooit een eind aan dit stuk. Bedankt Erik, Nancy, Xander, Lucian, Oliver, Floor (Peters), Huihui, Matthijn, Anja, Wentao, Peter, Ruisong, Fiona, Maartje, Berend Jan, Inge-Marie, Christine, Vera, Cristina, Tengfeng, Tom, Maryam (…), Jeroen, Yifei, Olga, Ivy, Herman, Brenda, Mark, Jojanneke, Meiling, Clasien, Jos, Hongbo, Laura, Erhard, Wenjuan, Esther, Shan, en last-but-not-least Alan!

Als allerlaatste wil ik nog familie en vrienden bedanken. Hopelijk hebben jullie allemaal na het (kort) bekijken van dit boekje in ieder geval een idee waar deze hele PhD om ging. Met name bedank ik mijn naaste familie, bij wie ik gedurende al deze jaren altijd terecht kon; mijn ouders, mijn broer, mijn oom en tante, en natuurlijk mijn neefje en nichtje!

Curriculum Vitae

Huib Rabouw was born on May 14, 1990 in Gouda. He attended the Willem de Zwijger high school in Schoonhoven, from which he graduated in 2008. That year, he started his bachelor's Biomedical Sciences at the Utrecht University, which was followed up by a master in Immunity and Infection, also at Utrecht University. During this master, he did an internship at the department of immunology under the supervision of Kiki Tesselaar, and an internship at the Utrecht University virology division under the supervision of Erik de Vries. Afterwards, he continued in the field of virology working as a PhD student in the group of Frank van Kuppeveld. His project mostly encompassed the strategies employed by viruses to prevent antiviral responses, and the results of this work are described in this thesis. In april 2019, Huib began his post-doctoral work at the Hubrecht institute, on the topic of live imaging of virus replication kinetics.

List of publications

1. Visser LJ, Langereis MA, **Rabouw HH**, Wahedi M, Muntjewerff EM, de Groot RJ, van Kuppeveld FJM. Essential Role of Enterovirus 2A Protease in Counteracting Stress Granule Formation and the Induction of Type I Interferon. *J Virol.* **93**, pii: e00222-19 (2019)
doi: 10.1128/JVI.00222-19.

2. van der Grein SG, Defourny KAY, **Rabouw HH**, Galiveti CR, Langereis MA, Wauben MHM, Arkesteijn GJA, van Kuppeveld FJM, Nolte-'t Hoen ENM. Picornavirus infection induces temporal release of multiple extracellular vesicle subsets that differ in molecular composition and infectious potential. *PLoS Pathog.* **15**, e1007594 (2019)
doi: 10.1371/journal.ppat.1007594.

3. Lyoo H, van der Schaar HM, Dorobantu CM, **Rabouw HH**, Strating JRPM, van Kuppeveld FJM. ACBD3 Is an Essential Pan-enterovirus Host Factor That Mediates the Interaction between Viral 3A Protein and Cellular Protein PI4KB. *MBio.* **10**, pii: e02742-18 (2019)
doi: 10.1128/mBio.02742-18.

4. **Rabouw HH**, Langereis MA, Anand AA, Visser LJ, de Groot RJ, Walter P, van Kuppeveld FJM. Small molecule ISRIB suppresses the integrated stress response within a defined window of activation. *PNAS*. **116**, 2097-2102 (2019)
doi: 10.1073/pnas.1815767116.

5. Visser LJ, Medina GN, **Rabouw HH**, de Groot RJ, Langereis MA, de Los Santos T, van Kuppeveld FJM. Foot-and-Mouth Disease Virus Leader Protease Cleaves G3BP1 and G3BP2 and Inhibits Stress Granule Formation. *J Virol.* **93**, pii: e00922-18 (2019)
doi: 10.1128/JVI.00922-18.

6. Guo H, **Rabouw HH**, Slomp A, Dai M, van der Vegt F, van Lent JWM, McBride R, Paulson JC, de Groot RJ, van Kuppeveld FJM, de Vries E, de Haan CAM. Kinetic analysis of the influenza A virus HA/NA balance reveals contribution of NA to virus-receptor binding and NA-dependent rolling on receptor-containing surfaces. *PLoS Pathog.* **14**, e1007233 (2018)
doi: 10.1371/journal.ppat.1007233.

7. Veel E, Westera L, van Gent R, Bont L, Otto S, Ruijsink B, **Rabouw HH**, Mudrikova T, Wensing A, Hoepelman AIM, Borghans JAM, Tesselaar K. Impact of Aging, Cytomegalovirus Infection, and Long-Term Treatment for Human Immunodeficiency Virus on CD8(+) T-Cell Subsets. *Front Immunol.* **9**, 572 (2018)
doi: 10.3389/fimmu.2018.00572.

8. Kindler E, Gil-Cruz C, Spanier J, Li Y, Wilhelm J, **Rabouw HH**, Züst R, Hwang M, V'kovski P, Stalder H, Marti S, Habjan M, Cervantes-Barragan L, Elliot R, Karl N, Gaughan C, van Kuppeveld FJ, Silverman RH, Keller M, Ludewig B, Bergmann CC, Ziebuhr J, Weiss SR, Kalinke U, Thiel V. Early endonuclease-mediated evasion of RNA sensing ensures efficient coronavirus replication. *PLoS Pathog.* **13**, e1006195 (2017)
doi: 10.1371/journal.ppat.1006195.

9. **Rabouw HH**, Langereis MA, Knaap RC, Dalebout TJ, Canton J, Sola I, Enjuanes L, Bredenbeek PJ, Kikkert M, de Groot RJ, van Kuppeveld FJ. Middle East Respiratory Coronavirus Accessory Protein 4a Inhibits PKR-Mediated Antiviral Stress Responses. *PLoS Pathog.* **12**, e1005982 (2016)
doi: 10.1371/journal.ppat.1005982.

10. Langereis MA, **Rabouw HH**, Holwerda M, Visser LJ, van Kuppeveld FJ. Knockout of cGAS and STING Rescues Virus Infection of Plasmid DNA-Transfected Cells. *J Virol.* **89**, 11169-73 (2015)
doi: 10.1128/JVI.01781-15.

List of abbreviations

AcP10	Accessory Protein 10
ADAR1	Double-stranded RNA-specific adenosine deaminase 1
AiV	Aichivirus
AiVL	Aichivirus Leader
ANOVA	Analysis of varience
ATF4	Activating Transcription Factor 4
ATF6	Activating Transcription Factor 6
ATP	Adenosine Triphosphate
BCA	Bicinchoninic
BiP	Binding immunoglobulin protein
BSA	Bovine Serum Albumin
Bw-CoV	Beluga Whale Coronavirus
cDNA	Copy DNA
CHOP	C/EBP homologous protein
CoV	Coronavirus
CPE	Cytopathic effect
CRISPR	Clustered Regularly Interspaced Short Palindromic Repeats
CrPV	Cricket Paralysis Virus
Cryo-EM	Cryo Electron Microscopy
CVB3	Coxsackievirus B3
Cys	Cysteine
DAPI	4',6-diamidino-2-fenylindool
DLP	Downstream Loop
DNA	Deoxyribonucleic acid
dsRBD	Double-stranded RNA Binding Domain
dsRNA	Double-stranded RNA
DSSO	Disuccinimidyl Sulfoxide
DTT	Dithiothreitol
E	Envelope Protein
EDTA	Ethylenediaminetetraacetic acid
EGFP	Enhanced Green Fluorescent Protein
eIF2	Eukaryotic Translation Initiation Factor 2
eIF2B	Eukaryotic Translation Initiation Factor 2B
eIF3	Eukaryotic Translation Initiation Factor 3
EMCV	Encephalomyocarditis Virus
ER	Endoplasmatic Reticulum
EV	Empty Vector
FA	Formic Acid
FACS	Fluorescence-activated Cell Sorting
FCS	Fetal Calf Serum
FDR	False Discovery Rate
FECV	Feline Enteric Coronavirus
FMDV	Foot and Mouth Disease Virus
G3BP1	Ras GTPase-activating protein-binding protein 1
G3BP2	Ras GTPase-activating protein-binding protein 2
GADD34	Growth arrest and DNA damage-inducible protein 34
GCN2	General control nonderepressible 2
GDP	Guanine Diphosphate
GEF	Guanin Exchange Factor
GTP	Guanine Triphosphate

HCMV	Human Cytomegalovirus
HIV	Human Immunodeficiency Virus
HRI	Heme-regulated Inhibitor
HRV	Human Rhinovirus
HSV	Herpes Simplex Virus
IAV	Influenza A Virus
IBV	Avian infectious bronchitis virus
IFA	Immunofluorescence Assay
IFN	Interferon
IP	Immunoprecipitation
IRE1	Inositol-requiring enzyme 1
IRES	Internal Ribosomal Entry Site
ISG	Interferon-stimulated Gene
ISR	Integrated Stress Response
ISRIB	Integrated Stress Response Inhibitor
Kb	Kilobase
KoV	Kobuvirus
L	Leader
Lpro	Leader Protease
LSB	Laemmli Sample Buffer
M	Membrane Protein
MDA5	melanoma differentiation-associated protein 5
MeOH	Methanol
MERS-CoV	Middle-East Respiratory Syndrome Coronavirus
Met	Methionine
MFI	Mean Fluorescent Intensity
MHV	Murine Hepatitis Virus
MOI	Multiplicity of Infection
mRNA	Messenger RNA
MS	Mass Spectrometry
N	Nucleocapsid Protein
NaDOC	Sodium deoxycholate
NP-40	nonyl phenoxypolyethoxylethanol
Nsp	Non-structural Protein
NTD	N-terminal Domain
ORF	Open Reading Frame
TC	Ternary Complex
tRNA	Transfer RNA
p4a	Accessory protein 4a
PACT	Protein ACTivator of the interferon-induced protein kinase
PAMP	Pathogen-associated Molecular Patern
PANK	Panthothenate Kinase
Pat. A	Pateamine A
PCR	Polymerase Chain Reaction
p-eIF2	Phosphorylated Eukaryotic Translation Initiation Factor 2
PERK	PKR-like endoplasmic reticulum kinase
PFA	Paraformaldehyde
PKR	Protein Kinase R
PP1	Protein Phosphatase 1
PSM	Peptide-Spectrum Match
RFP	Red Fluorescent Protein
RIG-I	retinoic acid-inducible gene I

RLR	RIG-I-like Receptor
Rluc	Renilla Luciferase
RNA	Ribonucleic Acid
RT-PCR	Reverse-Transcription PCR
RVFV	Rift Valley Fever Virus
S	Spike Protein
SARS-CoV	Severe Acute Respiratory Syndrome Coronavirus
SCX	Strong Cation Exchange
SDS-PAGE	Sodium Dodecyl Sulphate Polyacrylamide Gel Electrophoresis
SEM	Standard Error of the Mean
SG	Stress Granule
TAP	Tandem Affinity Purification
TGEV	Transmissible Gastroenteritis Virus
TIA-1	T-cell-restricted intracellular antigen-1
U	Uridine
UCK	Uridine-Cytidine Kinase
UHPLC	Ultra High Performance Liquid Chromatography
UMP	Uridine Monophosphate
uORF	Upstream Open Reading Frame
UPR	Unfolded Protein Response
VWMD	Vanishing White Matter Disease